Shear Behaviour of Continuous Concrete Beams Reinforced with GFRP Bars

by

KARAM ABDOU AWAD MAHMOUD

A Thesis submitted to the Faculty of Graduate Studies of

The University of Manitoba

in partial fulfillment of the requirements of the degree of

DOCTOR OF PHILOSOPHY

Department of Civil Engineering

University of Manitoba

Winnipeg, Manitoba, Canada

ABSTRACT

Continuous beams represent main structural elements in most reinforced concrete (RC) structures such as parking garages and overpass bridges. Deterioration of such structures due to corrosion of steel reinforcement is common in North America. To overcome the corrosion problems, the use of fiber-reinforced polymer (FRP) bars and stirrups becomes a viable alternative to steel reinforcement. However, to date, the shear behaviour of FRP-RC continuous beams has not been explored yet. As such, the objective of this study is to investigate the shear behaviour of such beams.

In this study, twenty four full-scale continuous concrete beams were constructed and tested. The test beams had rectangular cross section with 200-mm width and a height of 300, 550 or 850 mm and were continuous over two equal spans. The main investigated parameters were concrete strength, type and ratio of longitudinal reinforcement, type and ratio of transverse reinforcement and beam effective depth. Moreover, a 3-D nonlinear finite element model (FEM) was constructed to simulate the behaviour of FRP-RC continuous beams. The model was verified against the experimental results and validated against test results from previous studies. Then, the verified/validated model was used to conduct a parametric study to investigate the effect of a wide range of the parameters on the shear behaviour of GFRP-RC beams.

The experimental and FEM results showed that shear-critical GFRP-RC continuous beams exhibited moment redistribution. Also, it was observed that increasing the concrete strength and the longitudinal reinforcement ratio increased the shear strength significantly. Moreover, the presence of GFRP stirrups significantly enhanced the shear strength of the tested beams. Regarding the size effect, test results showed that there was adverse or no size effect on the shear

strength of GFRP-RC continuous beams when they failed in the interior shear span while beams failed in the exterior shear span exhibited clear size effect. Furthermore, a comparison between the test results and the provisions of the available models and FRP standards and design guidelines in North America revealed that these design provisions can be safely applied to continuous beams.

ACKNOWLEDGMENTS

All thanks are due to the Almighty ***ALLAH***, the Most-Gracious, and the Most-Merciful. Without his guidance and help, I would not be able to complete this work.

I would like to express my sincere appreciation and indebtedness to Dr. Ehab El-Salakawy, Ph.D., P. Eng., Professor and Canada Research Chair in Durability and Modernization of Civil Structures, Department of Civil Engineering, University of Manitoba, for his kind supervision and constant encouragement during the course of this work. His valuable suggestions and opinions at all steps of the research work were very remarkable.

I would also like to thank all my colleagues for their continuous support and help during construction and testing of the test specimens. Moreover, the assistance received from the technical staff at the W. R. McQuade structures laboratory at the University of Manitoba, Chad Klowak, P. Eng., Brenden Pachal and Grant Whiteside, is greatly appreciated.

The financial support provided by the Natural Science and Engineering Research Council of Canada (NSERC) through Discovery and Canada Research Chair programs as well as the University of Manitoba Graduate Fellowship are gratefully acknowledged.

At last, but not least, I would like to express my humble thanks to my family for their patience, support and love. Your prayers gave me the strength to continue working hard to achieve my gaols. Without you in my life, I would not be able to reach this point. May Allah reward you All.

Karam Abdou Awad Mahmoud, August 2015

TABLE OF CONTENTS

LIST OF FIGURES

LIST OF TABLES

NOTATIONS

The following symbols are used in this thesis

A_f = Area of longitudinal FRP reinforcement, mm^2

A_s = Area of longitudinal steel reinforcement, mm^2

A_{fv} = Area of transverse reinforcement,mm^2

$A_{fv,\,min}$ = Minimum area of FRP shear reinforcement, mm^2

b_w = Beam width, *mm*

c = Depth of the neutral axis, *mm*

d = Effective depth of the cross-section, *mm*

d_v = Distance from extreme tension fibres to the centroid of outer reinforcement layer, *mm*

d_b = Bar diameter, *mm*

E = Modulus of elasticity, *GPa*

E_f = Modulus of elasticity of the FRP bars, *GPa*

E_{fv} = Modulus of elasticity of the FRP shear reinforcement, *GPa*

E_c = Concrete modulus of elasticity, *GPa*

f = Stress at any strain, *MPa*

f_c' = Concrete compressive strength, *MPa*

f_r = Concrete modulus of rupture, *MPa*

f_{bend} = Strength of bend portion of FRP bar, *MPa*

f_y = Yielding stress of steel, *MPa*

h = Height of beam, *mm*

h_1 = Distance from centroid of outer layer of reinforcement to neutral axis, *mm*

h_2 = Distance from extreme tension fibres to neutral axis, *mm*

I_{cr}	=	Cracked moment of inertia, mm^4
I_e	=	Effective moment of inertia, mm^4
I_g	=	Gross (un-cracked) moment of inertia, mm^4
k	=	Ratio of depth of neutral axis to reinforcement depth at service condition
M_f	=	Factored moment at a section, *N.mm*
M_{cr}	=	Cracking moment, *kN.m*
n_f	=	Modular ratio which is the ratio of modulus of elasticity of FRP reinforcing bars to that of concrete
r_b	=	Internal bend radius of the FRP stirrup, mm
s	=	Spacing of transverse reinforcement, *mm*
s_{max}	=	Maximum spacing of transverse reinforcement, *mm*
s_z	=	Crack spacing parameter
s_{ze}	=	Equivalent crack spacing parameter; shall not be taken less than 0.85 s_z
V_c	=	Factored shear resistance provided by concrete, *N*
V_f	=	Factored shear force at a section, *N*
V_{FRP}	=	Factored shear resistance provided by FRP shear reinforcement, *N*
ε	=	Strain at stress *f*
ε_{avg}	=	The average strain between cracks in reinforcement
ε_c	=	Concrete crushing strain
ε_{peak}	=	Peak tensile strain in reinforcement at the crack location
ε_t	=	Net tensile strain in reinforcement
ε_{frpu}	=	Ultimate strain of FRP bars
ε_{fv}	=	Strain in an FRP stirrup
ε_o	=	Strain at maximum concrete compressive strength

ε_y	=	Yielding strain of steel
ε_x	=	Longitudinal strain at mid-height of cross section
θ	=	Angle of inclination of principal diagonal compressive stress (in degrees)
λ	=	Factor to account for concrete density
ϕ_c	=	Resistance factor for concrete
ρ	=	Reinforcement ratio
ρ_b	=	Balancing reinforcement ratio
ρ_v	=	Transverse reinforcement ratio
σ	=	Applied stress, *MPa*
τ	=	Bond stress between reinforcement bar and the surrounding concrete, *MPa*
τ_{max}	=	Maximum bond strength, *MPa*

CHAPTER 1: INTRODUCTION

1.1 GENERAL

In North America, many types of reinforced concrete (RC) structures such as parking garages, bridges, and other civil infrastructure are exposed to harsh environmental conditions. These sever conditions cause corrosion of the internal steel reinforcement which, in turn, leads to an increase in the maintenance cost and a decrease in the life-span of these structures. To avoid the consequences of steel corrosion, Fiber-Reinforced Polymers (FRP) bars are now used in lieu of steel bars. The FRP bars have been used as reinforcement because of their favorable characteristics such as corrosion resistance, high tensile strength, light weight, and durable nature. On the other hand, FRP bars have different characteristics from those of steel such as low modulus of elasticity, linear stress-strain relationship until failure, and small resistance in the transverse direction.

In the last two decades, intensive research has been conducted on the use of FRP as reinforcement in new concrete structures as well as strengthening and retrofitting of existing ones. The main objectives of previous research were to compare the behaviour of structural elements reinforced/retrofitted with FRP bars with their counterparts reinforced with steel and to propose expressions for the design taking into account the difference in the mechanical and physical properties of FRP materials. The researchers have focused mainly on simple structures, usually simply-supported beams and one-way slabs. However, in most structural applications, RC beams are either continuous or a part of rigid frames. Using FRP reinforcement in more complicated concrete structures, such as indeterminate structures, is still very limited. Some of the reasons behind that are the limited research conducted on statically indeterminate structures,

the lack of design guidelines and incomplete understanding of the behaviour of FRP-RC statically indeterminate structures.

1.2 PROBLEM DEFINITION

Continuous concrete beams reinforced with conventional steel have the ability to redistribute bending moment between critical sections. This permits portion of negative bending moment peaks that usually form over the interior supports to be shed over positive bending moments at mid-spans. This redistribution of internal forces between critical sections depends on the difference in flexural stiffness after cracking, the rotational capacity and the large deformations provided by the yielding of the steel bars in the cross section. As a result of moment redistribution, shear forces do not follow the elastic distribution and smaller values near the interior supports, critical zones for shear, are induced. This favorable behaviour makes the shear design expressions provided in the different design codes valid for steel-RC continuous beams (Ernst 1958 and Rodriguez et al. 1959). Based on these results, codes and design standards for steel-RC members allow moment redistribution to a certain percentage of the elastic moment. It is also recommended to design for shear in continuous beams in a similar manner to simply-supported ones.

On the other hand, the linear-elastic behaviour of FRP bars with relatively high strains and no yielding plateau up to failure changes the response of continuous beams reinforced with FRP. As such, current FRP design codes and guidelines do not allow for moment redistribution. The elastic distribution of moments and shear forces makes the regions near the interior supports more shear critical than sections in simply-supported beams. Therefore, the adequacy of using expressions provided for FRP-RC simply-supported beams in continuous beams is questionable

and research is needed to investigate the shear behaviour of continuous beams reinforced with FRP bars and stirrups.

1.3 RESEARCH SIGNIFICANCE

The shear behaviour of continuous concrete beams reinforced with steel has been adequately investigated and the behaviour of such beams is well-established. Therefore, shear design provisions provided in codes recommend that continuous beams reinforced with steel could be analyzed in the same way as simply-supported ones. On the other hand, to date, there are no research studies on the shear behaviour of continuous beams with longitudinal and transverse FRP reinforcement. Also, all the FRP design codes and guidelines introduce very limited recommendations for continuous beams, do not allow for moment redistribution and, in the meantime, provide the same shear design provisions. This research program is dedicated to fill in this gap by evaluating the shear behaviour of such beams. In addition, the applicability of the shear design provisions in the current codes and guidelines is examined.

1.4 OBJECTIVES OF THE RESEARCH

The FRP bars are now used as internal reinforcement for many concrete structures. Researchers have been focusing on studying the shear and flexural behaviour of simply-supported beams and one-way slabs. The results of such research provided better understanding of the behaviour of FRP-RC structures. Also, little research has been conducted to investigate the flexural behaviour of continuous beams reinforced with FRP bars. Following this effort, it is intended to study the shear behaviour of statically indeterminate structures reinforced with FRP bars and stirrups. The main objectives of this research are:

- Experimentally investigating the shear behaviour of continuous FRP-RC beams;

- Developing a numerical model simulating the continuity effect on the shear behaviour of continuous FRP-RC beams;
- Conducting a parametric study to further evaluate the shear behaviour of the FRP-RC continuous beams.
- Examining the applicability of the current FRP shear design expressions that are proposed for simply-supported beams to design the continuous beams.

These main objectives can be achieved through a set of more specific ones. The specific objectives include investigating the effect of the different factors known to influence the shear behaviour of continuous FRP-RC beams such as concrete strength, shear span-to-depth ratio, longitudinal reinforcement ratio and transverse reinforcement ratio. In addition, the size effect on the shear strength is investigated in this research.

A numerical model is developed using a finite element specialized software package. This model is verified against the experimental results. The verified model is, then, used to conduct a parametric study to investigate a wide range of the factors affecting the shear behaviour of FRP-RC continuous beams.

1.5 RESEARCH SCOPE

The scope of this study is restricted to two-equal-span continuous concrete beams totally reinforced with glass fiber reinforced polymer (GFRP) reinforcing bars and stirrups. Other types of FRP reinforcing bars, such as carbon and aramid, are not considered in this study. Test specimens are large scale with rectangular cross-sectional areas ranging between 200 × 300 and 200 × 850 mm. The beams are tested under two-point loading system in each span with a

constant shear span-to-depth ratio of 3.0. All test beams have been designed according to the CSA/S806-12 (CSA 2012) design code for FRP-RC building structures.

1.6 METHODOLOGY

To achieve the above mentioned objectives, a research program which includes experimental and numerical phases is proposed. The experimental phase consists of testing large-scale concrete beams continuous over two spans. The proposed beams have rectangular cross sections of 200 mm in width and 300, 550 and 850 mm in height. The beams are reinforced with GFRP bars as longitudinal reinforcement and GFRP stirrups as transverse reinforcement.

The test parameters are:

1. Longitudinal reinforcement ratio;
2. Concrete compressive strength;
3. Transverse reinforcement ratio;
4. Size effect in beams without shear reinforcement; and
5. Shear span-to-depth ratio.

In the numerical phase, a finite element investigation is conducted using ATENA-3D (version 5.0) software (Cervenka et al. 2013). A three-dimensional (3-D) model is constructed to simulate the shear behaviour of continuous beams reinforced with FRP. The model is verified against the experimental results obtained from the experimental phase. The verified model is, then, used to conduct a parametric study to investigate a number of key parameters and assess their influence of the shear behaviour of GFRP-RC beams. The main investigated parameters are the compressive strength of concrete, the longitudinal reinforcement ratio, the amount of transverse reinforcement and the shear span to depth ratio. The analytical results of this parametric

investigation along with the experimental results are used to evaluate the shear strength of GFRP-RC continuous beams and to determine the applicability of the current shear design provisions, which are based on testing simply-supported beams, to the continuous concrete beams.

1.7 OUTLINE OF THE THESIS

This thesis consists of nine chapters. Chapter 1 presents the problem definition, research significance, objectives and scope, and the methodology of achieving the objectives of this research.

Chapter 2 presents the review of the previous work that identifies pertinent experimental investigations and establishes the main factors that affect the shear behaviour of steel- or FRP-RC beams. There is no research that investigated the shear behaviour of continuous concrete beams reinforced with FRP bras and stirrups. This led to the development of the current research program to study the shear behaviour of such beams.

The experimental program is described in Chapter 3. In this chapter, the cross section dimensions and details of a total of 20 continuous concrete beams reinforced with GFRP bars and stirrups are described. Also, the reinforcement details for each beam are illustrated. Moreover, the properties of the used materials, details of instrumentations, test setup and procedure are provided in this chapter.

Chapters 4, 5 and 6 include analysis and discussion of the obtained experimental data. Also, a comparison between behaviour of the tested beams and the simply-supported beams is included to highlight the effect of the continuity on the shear strength of continuous beams. Moreover, the

experimental results are compared to the predictions of the current shear design provisions to determine their applicability to the GFRP-reinforced continuous beams.

In Chapter 7 of the thesis, the construction of the finite element model and its verification against test results are presented.

Chapter 8 presents the parametric analysis, in which a wide range of the parameters are studied and the effect of new parameters is examined.

Chapter 9 contains a summary of the major findings of the program and the important conclusions. Recommendations for future work are included as well.

Flexural and shear design provisions in current codes and guidelines are reviewed in Appendix A. Moreover, the design of test beams is given in Appendix B.

CHAPTER 2: LITURATURE REVIEW

2.1 INTRODUCTION

In this chapter, a review of main findings and conclusions of the available literature is presented. The review includes the shear behaviour of steel-RC elements that has been extensively studied. These steel-RC elements were either simple structures such as simply-supported beams and one-way slabs or indeterminate structures such as continuous beams. Also, the results of recent research carried out to investigate the shear behaviour of simple structures reinforced with FRP bars are included in this chapter. Moreover, the main findings and conclusions of investigations on the flexural behaviour and moment redistribution in continuous beams reinforced with FRP bars are discussed.

2.2 SHEAR BEHAVIOUR OF SIMPLY-SUPPORTED STEEL-RC BEAMS

Before shear failure, the state of stress in the web of a cracked RC member differs considerably from what is predicted by the theory of linear elasticity. Therefore, the question of how a cracked concrete member transmits shear (combined with axial load and bending moment) should be considered. The Joint ASCE-ACI Committee 445 (ASCE-ACI Committee 445 1999) identified the following five mechanisms of shear transfer, as shown in Fig. 2.1:

1) Shear stresses in un-cracked concrete, that is, the flexural compression zone (V_{cz});
2) Interface shear transfer, often called aggregate interlock or crack friction (V_a);
3) Dowel action of the longitudinal reinforcing bars (V_d);
4) Arch action; and
5) Residual tensile stresses transmitted directly across cracks.

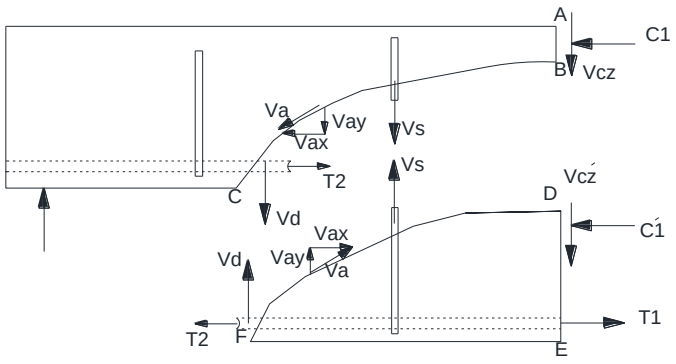

Figure 2.1: Failure surface showing the internal forces (Reproduced from Wight and MacGregor 2011)

According to the Joint ASCE-ACI Committee 445 (ASCE-ACI Committee 445 1999), the five mechanisms for shear transfer can be explained as follows:

Before the occurrence of cracks in a beam, the shear force is transferred by inclined principal tensile and compressive stresses. After formation of cracks, this state of stress is still valid in the un-cracked compression zone. The shear force carried by this un-cracked compression zone can be calculated by the integration of the shear stresses over the depth of the compression zone, which is sometimes thought to be the explanation for the concrete contribution.

In normal strength concrete, aggregate interlock results from the resistance to relative slip between two rough interlocking surfaces of the crack, much like frictional resistance. As long as the crack is not too wide, this action can be significant. In high strength concrete, the cracks tend to pass through, rather than around, the aggregate; hence, the aggregate interlock contribution to the shear strength is lower for beams made of high strength concrete. Significant progress has

been made toward understanding this mechanism, which involves the relationships between four parameters: crack interface shear stress, normal stress, crack width, and crack slip.

In members without transverse reinforcement, dowel action is not very significant. The reason behind that is the maximum shear in a dowel is limited by the tensile strength of the concrete cover supporting the dowel. Dowel action may be significant in members with large amounts of longitudinal reinforcement, particularly when the longitudinal reinforcement is distributed in more than one layer.

Dowel strength across a shear plane can be developed by three mechanisms: the flexure of the reinforcing bars, the shear strength across the bars, and the kinking of the reinforcement. These mechanisms are illustrated in Fig. 2.2.

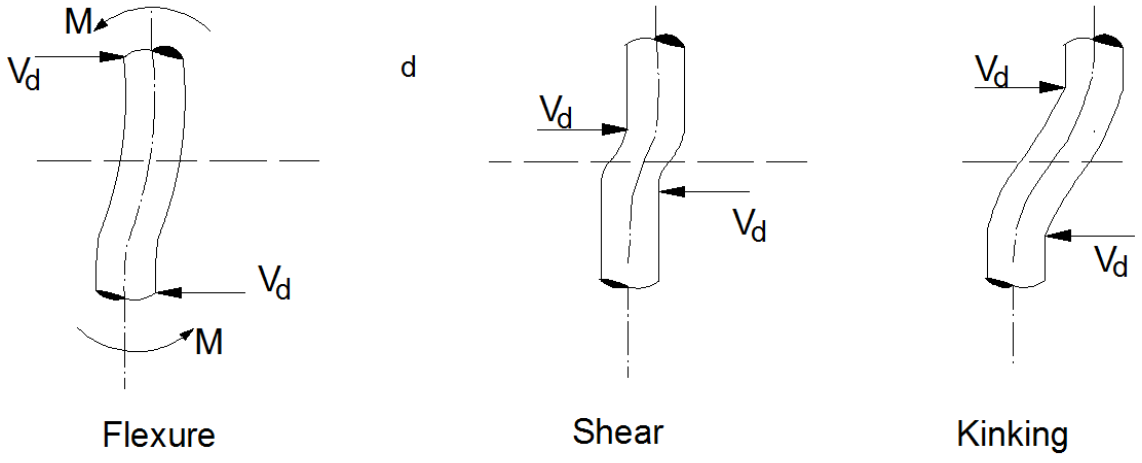

Figure 2.2: The mechanism of dowel action across a shear interface (Reproduced from Park and Pauly 1975)

The residual tensile stresses can be explained as follows. When the crack in the concrete beam forms, a clean break does not occur. Small pieces of concrete bridge the crack and continue to transmit tensile force up to crack widths in the range of 0.05 to 0.15 mm.

Figure 2.3 shows the arching action mechanism which occurs in deep members or in members in which the shear span-to-depth ratio (a/d) is less than 2.5. In these beams, most of the vertical loads are transmitted to the support through the concrete compression struts while the longitudinal reinforcement acts as a tie for the arch. This mechanism is not considered a shear transfer mechanism where it does not transmit a tangential force to a nearby parallel plane.

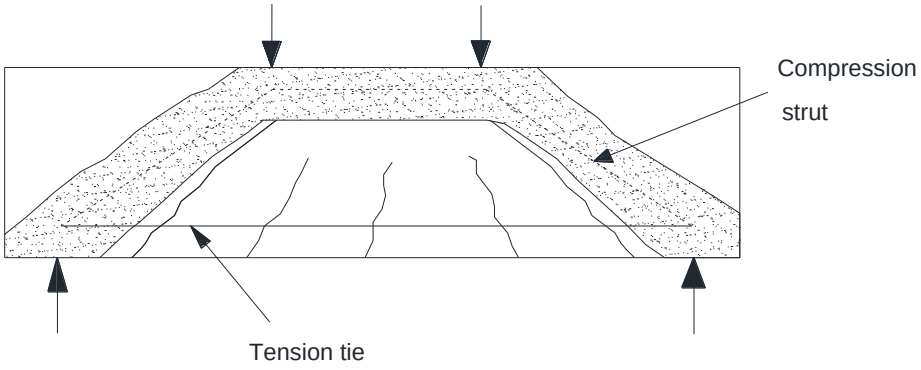

Figure 2.3: Arch mechanism in deep beams (Reproduced from Wight and MacGregor 2011)

Following the formation of inclined cracks, a portion of the shear is carried by the web reinforcement (V_s). When the shear carried by the web reinforcement can no longer increase due to its yielding, any additional shear must be carried by the un-cracked zone, dowel action, and aggregate interlock. As the inclined crack widens, the aggregate interlock shear decreases forcing the un-cracked zone and the dowel action to increase at an accelerated rate until splitting fails due to combined shear and compression. In case of beams without stirrups, beam failure may be caused by the breakdown of any of the components of the force transfer across the section with

different mechanisms dominating in beams of different types. It is possible to see dowel splitting at the tension steel level before the beam collapses and in other cases, dowel failure and beam collapse occur simultaneously. Whereas, it is also possible to see spalling from the sides of inclined cracks before beam failure, indicating that failure of the interlock mechanism is imminent.

2.2.1 Inclined Cracks of RC Beams

Wight and MacGregor (2011) stated that shear failure of beams are characterized by the occurrence of inclined cracks. In some cases, the inclined cracks are immediately followed by member failure and in other cases, the inclined cracks stabilized and substantially more shear force may be applied before the member fails. There are two types of inclined cracking that occur in RC beams, web-shear crack and flexural-shear crack. These two types of inclined cracks are shown in Fig. 2.4.

(a) Web shear crack (b) Flexural shear crack

Figure 2.4: Types of Inclined Cracks (Reproduced from Wight and MacGregor 2011)

Web-shear cracking: It is characterized by an inclined crack forming in the web, at the location of the neutral axis, before flexural cracks develop in its vicinity. This is attributed to the principle tensile stresses that exceed the tensile strength of concrete. Because web-shear crack is initiated before flexural cracks can develop in its vicinity, the principle stresses computed in the web of

an un-cracked section will approximate, with reasonable accuracy, the state of stresses at the time of initial cracking. However, the constantly changing combinations of shearing stress, flexural stress, and the bearing stress, which occurs near the loads and reactions, make it tedious to determine the location and magnitude of the maximum principle tensile stress in a beam at the time of inclined cracking. Web-shear cracking often develops in thin-webbed pre-stressed beams, because of the pre-stressing, which reduces the maximum flexural tension. On the contrary, the pre-stressing is less effective in reducing the maximum diagonal tension in web.

Flexural- shear cracking: It is initiated by flexural cracking. After the formation of the flexural crack, the shear stress in the concrete at the tip of the crack increases. The flexural-shear crack develops when the combined shear and tensile flexural stresses cause a principle tensile stress exceeding the tensile strength of concrete. Flexural-shear cracking occurs when a concrete beam is loaded to its ultimate capacity.

2.2.2 Factors Affecting the Shear Strength of RC Beams

The factors influencing the behaviour and the strength of concrete beams failing in shear are numerous and complex. The main factors are as follows (Wight and MacGregor 2011):

- Shear span-to-depth ratio (*a/d*),
- Concrete compressive strength,
- Longitudinal reinforcement ratio,
- Transverse reinforcement ratio, and
- Depth of the member (size effect).

2.2.2.1 Effect of shear span-to-depth ratio

The shear strength of concrete beams decreases as *a*/*d* ratio increases assuming no change in the other variables. In beams with small *a/d* ratio, part of the load is transmitted directly to supports by diagonal compression. In this case, there is no shear transfer mechanism, in the sense that it does not transmit a tangential force to a nearby parallel plane, but permits the transfer of a vertical concentrated force to the reaction and thereby reduces the demand on other types of load transfer (Wight and MacGregor 2011).

For the same applied load, larger *a/d* ratio means larger bending moment in the shear span; thus the depth of penetration of flexural cracks increases, and hence the flexural stresses near the crack tip increase. By increasing *a/d* ratio, the probability that a flexural crack will develop into an inclined one becomes higher. However, the effect of increasing *a/d* ratio on the shear strength was independent on longitudinal steel ratio. For low longitudinal reinforcement ratio, yielding of longitudinal reinforcement takes place close to failure, which permits the crack to increase in both length and width, and also adversely affects the dowel action. As shown in Fig. 2.5, three ranges of *a/d* ratios can be considered as follows:

Short beams: $1 > a/d > 0.0$ – in this range of shear span-to-depth ratios, flexural stresses are less important than shearing stresses and vertical normal stresses. Significant principal compression and tension, respectively, exist along and across the line joining the load and the reaction, and inclined cracks occur immediately inside the reaction plates. In some cases the cracks appear to be initiated by flexural cracks originating in this region; and in other cases, by principal tensions across the line joining the load and reaction, in a manner similar to an indirect tension test.

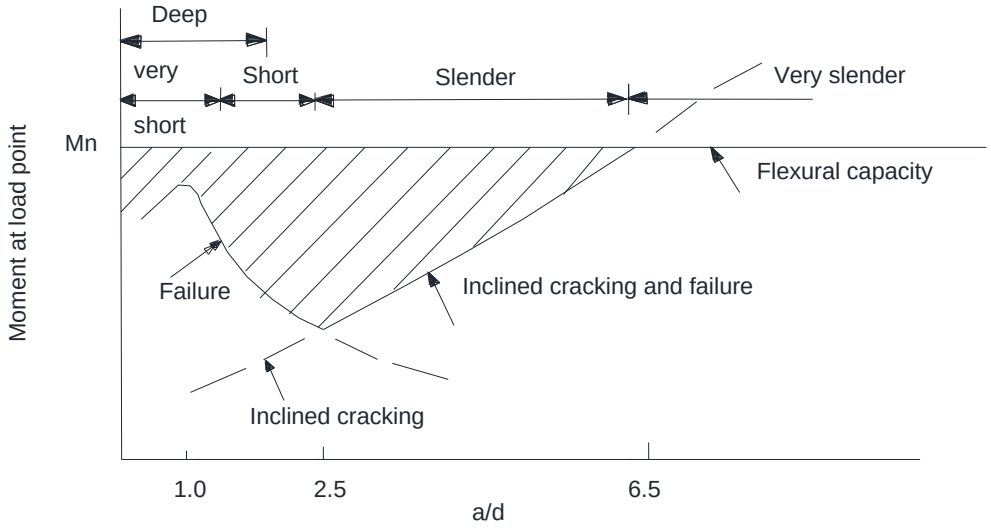

Figure 2.5: Variation in shear capacity with *a/d* for rectangular beams (Reproduced from Wight and MacGregor 2011)

After inclined cracking occurs, the beam transforms almost immediately into a tied-arch which can fail in a number of ways. The number in Fig. 2.6 corresponds to the following modes of failure:

1- Anchorage failure of the tension reinforcement.

2- Crushing failure of concrete at reactions.

3- Flexural failure; either of steel reinforcement caused by yielding or fracture, or in the crown of the arch when the compression exceeds the concrete strength.

4- Tension failure of the arch-rib by cracking over the support, followed by crushing along the crack at point 5. This is a result of the eccentricity of the thrust, which essentially acts along the inclined crack.

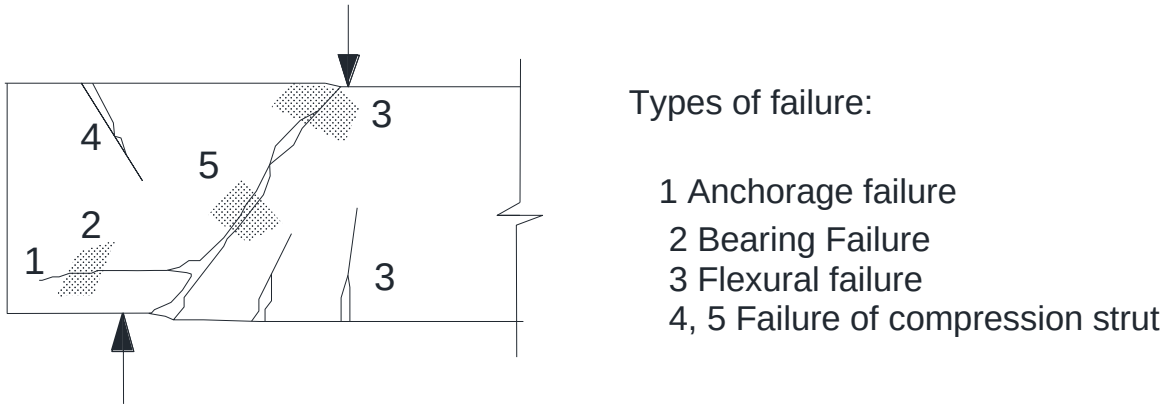

Figure 2.6: Modes of failure in deep beams (Reproduced from Wight and MacGregor 2011)

Medium beams: $2.5 > a/d > 1.0$ – in this range of shear span-to-depth ratios, an inclined crack is generally the result of a flexural crack which extend vertically from the tension surface of the beam to just above the reinforcement and becomes inclined and progresses toward the nearest concentrated load. The major primary inclined crack at about the center of the shear span.

With an increase in load, the inclined part of the crack generally propagates downward to meet the reinforcement at an angle of approximately 45^{o} forming a secondary crack which extends along the reinforcement for a short distance towards the support. This horizontal crack may be associated with either slip or dowel action of reinforcement.

After inclined cracking develops, failure may occur in one of the following two principal ways, as shown in Fig. 2.7.

a- Anchorage failure of the tension reinforcement; sometimes referred to as shear-tension failure,

b- Crushing failure in concrete over the upper end of the inclined crack; sometimes referred to as shear-compression failure.

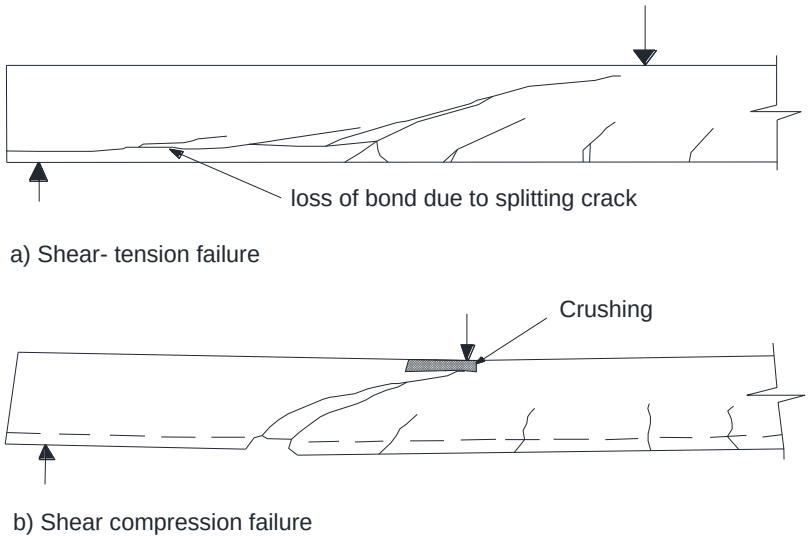

Figure 2.7: Typical shear failures in short beams (Reproduced from Wight and MacGregor 2011)

Normal and Long beams: $a/d > 2.5$ - Beyond a certain value of *a/d*, inclined cracks is not developed before the beam fails in flexural. The limiting value of *a/d*, corresponding to change in mode of failure from shear to flexure, is a function of beam characteristics such as amount of longitudinal reinforcement, yield strength of reinforcing steel, and strength of concrete. In the range of *a/d* values greater than 3, several flexural cracks develop and the beam segments between these inclined cracks form teeth. The vertical tooth between two flexural cracks acts as a cantilever, which begins to break off with increase in load; forming an inclined propagation of flexural cracks.

For *a/d* values greater than 2.5, the inclined cracking load exceeds the shear-compression failure load. With the formation of the inclined crack, a beam without web reinforcement becomes unstable and fails. Although the actual material failure occurs in the shear-compression zone, this type of failure is usually called diagonal-tension failure, recognizing the important role the

inclined cracking plays in the failure mechanism. With a small amount of web reinforcement added to beams in this *a/d* range, shear-compression or flexural failures develop.

2.2.2.2 Effect of concrete compressive strength

Form the tests carried out on RC beams, it was suggested that the most significant variables affecting the cracking shear is the tensile strength of concrete, which is proportional to $\sqrt[n]{f_c^{'}}$, where $f_c^{'}$ is the concrete compressive strength (Arslan 2008).

Yoon et al. (1996) concluded that failure of beams without stirrups is brittle and the failure occurs on the formation of significant shear cracking despite the concrete strength of the beam. Also, the authors observed that the main feature of high-strength concrete (HSC) that affects the structural response is the tendency for cracks to pass through, instead of around, the aggregates. This creates smoother crack surfaces, reduces the aggregate interlock and hence, reduces the shear carried by concrete. Because of the reduced aggregate interlock, higher dowel forces occur in the longitudinal reinforcing bars. These higher dowel forces, together with the highly concentrated bond stresses in higher strength concrete beams, result in higher bond-splitting stresses where the shear cracks cross the longitudinal tension bars.

Rebeiz et al. (2001) studied the effect of the concrete compressive strength on the shear strength. The analysis was carried out using extensive shear strength data retrieved from existing literature for both normal strength and high strength concrete members. It was concluded that compressive strength affected both the cracking and ultimate shear strengths of concrete regardless of the situation (long or short beams, light or heavy reinforcement ratios) when other variables are kept relatively constant.

Cladera and Mari (2005) studied experimentally the behaviour of high strength concrete beams failing in shear. The authors reported that the mode of failure for beams without stirrups was sudden. The tested beams failed with the appearance of a single shear crack and there was a slight increase in failure shear strength as the concrete compressive strength increased. On the other hand, beams containing stirrups presented a more ductile response. After the formation of the first shear crack, stirrups started to work and further shear cracks developed.

Arslan (2008) investigated the cracking shear strength of RC slender beams without stirrups. The main objective of this study was to present alternative equation to predict the cracking shear strength of beams. The author used more than 80 data points obtained from previous shear tests covering a wide range of beam properties and test schemes to verify the proposed cracking shear strength equations. The author reported that from previous work, it is generally accepted that the shear failure of RC members without stirrups initiates, when the principal tensile stress within the shear span exceeds the tensile strength of concrete and a diagonal crack propagates through the beam web. Therefore, the diagonal tensile cracking strength depends directly on the tensile strength of concrete which is a function of the concrete compressive strength.

2.2.2.3 Effect of longitudinal reinforcement ratio

The longitudinal reinforcement ratio has a pronounced effect on the basic shear transfer mechanisms.

1- An important factor that affects the rate at which a flexural crack develops into an inclined one is the magnitude of shear stresses near the tip of that crack. The intensity of principal stresses above the flexural crack depends on the depth of penetration of the crack. The greater the value of the longitudinal reinforcement, the less the penetration of the flexural

crack, and consequently the less the principal stresses that will result in diagonal tension cracking.

2- Increasing the longitudinal reinforcement ratio increases the dowel capacity of the member by increasing the dowel area and hence decreasing the tensile stresses included in the surrounding concrete.

3- Increasing the longitudinal reinforcement ratio, also affects the aggregate interlock capacity. Beams with low longitudinal reinforcement ratio will have wide and long cracks in contrast to the shorter and narrow cracks found in beams with high longitudinal reinforcement ratio. Since the aggregate interlock mechanism depends on the crack width, an increase in the aggregate interlock force is to be expected with an increase in the longitudinal reinforcement ratio.

Ghannoum (1998) stated that increasing the amount of longitudinal steel reinforcement increases the shear stress at failure in both the normal-strength and high-strength concrete beams. The influence of the longitudinal steel ratio is found to attenuate with greater specimen depth. This is due to the reduced effectiveness of the longitudinal steel in controlling crack widths in the deeper elements.

Rebeiz et al. (2001) concluded that the tensile reinforcement ratio correlated better with the cracking shear strength than with the ultimate shear strength in the case of long beams (a/d > 2.5). The effect of the tensile reinforcement ratio on the cracking shear strength is negligible in the case of short beams. In addition, the nature of the relationship between the tensile reinforcement ratio and the cracking shear strength was similar to that between this ratio and ultimate shear strength for the same range of values for a/d and concrete strength.

Khaldoun et al. (2004) studied the effect of the longitudinal reinforcement on the shear behaviour of high strength concrete**.** It was concluded that the longitudinal steel reinforcement affected the performance of the different levels of transverse steel reinforcement. The behaviour of members with larger longitudinal steel was more favorable. Cracking pattern for beams with higher amount of longitudinal reinforcement was more favorable than that for beams with lower amount of longitudinal reinforcement.

Lee and Kim (2008) investigated experimentally the effect of longitudinal tensile reinforcement on the shear strength of simply-supported concrete beams. Test results indicated that the reserve strength and deflection increase as the longitudinal reinforcement ratio increases. It was suggested that the amount of minimum shear reinforcement needs to increase as the longitudinal reinforcement ratio decreases to achieve uniform reserve strength and deflection.

2.2.2.4 Effect of shear reinforcement

Shear reinforcement has three primary functions contributing to the shear strength of a beam;

1- It carries part of the shear force.

2- It restricts the growth of the diagonal tension crack.

3- It holds the longitudinal bars and increases their dowel capacity.

In addition to these functions, stirrups tend to enhance the strength of the compression zone by confining the concrete. From previous tests, the researchers stated that the stirrups had no effect on the diagonal cracking load. Stirrup strains measured during testing were negligible up to diagonal cracking load, after which they increased rapidly. At failure, all stirrups crossing the critical diagonal crack were at yield.

Yoon et al. (1996) carried out a research to evaluate minimum shear reinforcement requirements in normal, medium and high strength RC beams. The authors reported that the provision of even small amounts of shear reinforcement significantly improved the ductility and increased the shear strength. Specimens without stirrups failed in a brittle manner on the formation of significant shear cracking despite the concrete strength of the beam. For a given load level, smaller crack widths were observed in specimens with higher amounts of shear reinforcement.

Ozcebe et al. (1999) performed an evaluation on the minimum shear reinforcement requirements given in the ACI, Canadian, and Turkish codes for high-strength concrete. The authors concluded that the ACI 318-83 requirements for minimum shear reinforcement are not satisfactory when high-strength concrete is used. It gave less reserve strength and a wider crack width at the stage of fully developed diagonal crack as compared to other codes. It also underestimated the concrete contribution in beams having high shear reinforcement index. The minimum shear reinforcement required by TS500- 83 was satisfactory for high-strength concrete.

Khaldoun et al. (2004) studied the effect of the minimum shear reinforcement in beams of high strength concrete. It was concluded that the existence of larger amounts of transverse reinforcement improved the number of cracks. Beam that had no stirrups showed an adequate cracking pattern and this referred to the influence of longitudinal reinforcement on crack control. Test results showed that in beams with smaller amounts of longitudinal steel, increasing the amount of transverse reinforcement from the ACI 318-83 minimum to the ACI 318-02 and CSA/A23.3-94 minimum did not provide the expected improvement in post-cracking reserve strength and in crack control behaviour.

Wight and MacGregor (2011) reported that prior to the formation of inclined cracks; the strain in the stirrups is equal to the corresponding strain of the concrete. Because concrete cracks at a very small strain, the stress in the stirrups prior to inclined cracking will not exceed 3 to 6 ksi (20.7 to 41.4 MPa). Thus, stirrups do not prevent inclined cracks from forming; they come into play only after the cracks form. The shear transferred by tension in the stirrups does not disappear when the crack opens wider, so there will always be a compression force and a shear force acting on the part of the beam below the crack.

2.2.2.5 Effect of the member depth (size effect)

Extensive experimental investigations have been done to study the size effect in shear (Kani 1967, Shoyia et al. 1987 and Collins and Kuchma 1999). The results revealed that the shear stress at failure decreases, as the member depth increases and as the maximum aggregate size decreases. The simplest explanation of the size effect in shear is that the larger crack widths that occur in larger members reduce the aggregate interlock. Crack width increases almost linearly with the tensile strain in the longitudinal reinforcement and with the spacing between cracks. For the same longitudinal reinforcement strain, doubling the depth of the beam will double the crack widths at mid-depth (Shoyia et al. 1987).

Larger members have widely spaced cracks and hence are predicted to fail in shear at lower shear stresses. The failure shear is also related to the roughness of the shear crack which, for normal strength concrete, is influenced by the aggregate size. In members made of high strength concrete, cracks pass through rather than around the aggregate and hence maximum aggregate size does not have the same effect on crack roughness. Therefore, beams made of high strength concrete are more sensitive to size effect in shear (Collins and Kuchma 1999).

Bažant and Kazemi (1991) studied the size effect on diagonal shear failure of beams without stirrups. The authors concluded that the diagonal shear failure exhibited a strong size effect of fracture mechanics type, due to differences in the stored energy that can be released to drive the failure propagation. Also, prevention of bond slip of bars by providing an anchorage at the ends increased the brittleness number.

Ghannoum (1998) tested twelve beam specimens to evaluate the size effect on shear strength of RC beams. From the test results, it was found out that the size effect is very evident in both normal-strength and high-strength concrete beams. The shallower specimens were consistently able to resist higher shear stresses than the deeper ones. High-strength and normal-strength concrete specimens of the same size and same reinforcement ratios had almost equal shear stresses at failure, showing no significant gain in shear strength with increased concrete compressive strength.

Collins and Kuchma (1999) conducted an extensive experimental investigation that aimed at evaluating the significant parameters that influence the magnitude of the size effect in shear. The authors recommended some modifications to the ACI 318-95 shear provisions. These modifications resulted in a more consistent level of safety across the possible range of concrete strengths and member sizes. The results of the changes on the maximum shear forces that would be permitted for beams and one-way slabs of different depths showed that for members without stirrups, the proposed changes would permit somewhat higher shears for most beams but would substantially reduce the maximum shear force permitted for very thick slabs.

Also, the authors tested twelve continuous concrete beams. The test results showed that the shear stresses at failure reduced as the member size increased. The high-strength concrete series

indicated somewhat greater reduction. Beams that contained equally spaced layers of crack control reinforcement, showed no reduction in failure shear stress as the member size increased. For beams which contained stirrups, the shear stress at failure actually increased as the member size increased.

Lubell et al. (2004) discussed the test results of large, wide beams. The test results were in a good agreement with the previous conclusions that are related to the size effect in shear. The shear strength of the wide beams is directly proportional to the width of the beam. Because of this, it was concluded that the experimental results from narrow beams could be used to investigate the safety of wide beams. Also the authors stated that there was a significant size effect in shear. Moreover, beams made of high strength concrete are more sensitive to the size effect in shear. This was attributed to the cracks in high-strength concrete beams that pass through the aggregate rather than around it as in normal strength concrete.

Sneed et al. (2010) investigated the influence of the effective depth on the shear strength of concrete beams; they tested eight simply supported RC beams without shear reinforcement. Test results showed a reduction in shear strength with increasing effective depth; however, significant differences in behaviour were observed between the smaller specimens and the larger specimens in terms of amount of flexural cracking, crack progression, load-displacement, and load-strain measurements despite holding other traditionally considered influential parameters constant. These differences suggest that the reduction was influenced not only by the effective depth parameter, but also by factors that influenced the difference in behaviour and mode of shear transfer. In other words, the effective depth parameter was not entirely isolated; thus, the observed reduction in shear strength was not entirely due to a size effect.

2.2.3 Shear Behaviour of FRP-RC Beams

The shear behaviour of FRP-RC beams is different compared to their counterparts reinforced with traditional steel reinforcement. This is because of the different mechanical behaviour between the two types of reinforcements. FRP bars exhibit linear stress-strain behaviour up to failure without any yielding. Also, compared to steel, FRP has relatively low modulus of elasticity and less resistance in the transverse direction. These different characteristics affect the shear behaviour of FRP- RC beams.

Due to the relatively low modulus of elasticity of FRP composite material, concrete members reinforced with FRP bars develop wider and deeper cracks than members reinforced with similar amounts of steel. Deeper cracks decrease the contribution to shear strength from the un-cracked concrete due to the lower depth of concrete in compression. Wider cracks, in turn, decrease the contributions from aggregate interlock and residual tensile stresses. Additionally, due to the relatively small transverse strength of FRP bars and relatively wider cracks, the contribution of dowel action can be very small compared to that of steel. As such, it is expected that the overall shear capacity of concrete members reinforced with FRP bars as flexural reinforcement is lower than their counterparts reinforced with steel bars.

2.2.3.1 Effect of longitudinal FRP reinforcement

Tureyen and Frosch (2002), Tureyen and Frosch (2003), Maurizio et al. (2006) and El-Sayed et al. (2006a) studied the shear strength of beams with FRP longitudinal reinforcement. They also investigated the effect of differences in the modulus of elasticity of FRP and steel reinforcement on the concrete contribution to shear strength of slender beams. The main objective was to determine the applicability of the shear design methods to members reinforced with FRP bars.

The tested variables of these investigations were the reinforcement type and the longitudinal reinforcement ratio.

The experiments indicated that the flexural concrete members reinforced with FRP bars in the longitudinal direction failed in shear at loads considerably lower than those reinforced by an equivalent area of steel bars. The reduction in shear strength was found to be a function of the axial stiffness of the main tensile reinforcement

Maurizio et al. (2006) also reported that the development of critical shear stresses was indicated clearly by the earlier formation of inclined cracks in the shear spans of the beams with a/d =2.2 and 3.3. This could be attributed to the different distribution of internal stresses due to the lower axial stiffness of the flexural reinforcement. The stiffness of the flexural reinforcement also had a direct effect on the overall cracking behaviour of the tested beams.

El-Sayed et al. (2006a) found out that the average ratio between the post-cracking flexural stiffness of the steel-RC beams and the GFRP-RC beams and that between the steel-RC beams and the CFRP-RC beams were approximately the same as the ratios of the modulus of elasticity of steel/GFRP and that for steel/CFRP, respectively. Consequently, it was concluded that the post-cracking flexural stiffness of the FRP-RC beams to that of the steel-RC beams is the same as the ratio of the axial stiffness of FRP reinforcing bars to the axial stiffness of steel bars.

The increase in shear strength due to increasing the flexural reinforcement ratio is attributed to the improvement in the shear transfer mechanisms. Increasing the reinforcement ratio decreases the penetration depth and width of the shear crack. This, in turn, increases the contribution of aggregate interlock as well as the contribution of un-cracked concrete by increasing the area of concrete in compression. In addition, increasing the reinforcement ratio increases the dowel

capacity of the member by increasing the dowel area, thereby decreasing the tensile stresses induced in the surrounding concrete.

El-Sayed et al. (2006b) examined the effect of the amount of the longitudinal reinforcement on the shear strength of FRP-RC beams made of high strength concrete. It was noted that the load-deflection response of the high strength concrete beams that had the same concrete strength but with a different reinforcement ratio showed that the lower the reinforcement ratio or the modulus of elasticity, the lower the post-cracking flexural stiffness of the tested beams. Also, increasing the amount of reinforcement, for the same type of reinforcing material, increased the post-cracking flexural stiffness.

2.2.3.2 Effect of FRP shear reinforcement

Whitehead and Ibell (2005) studied the shear behaviour of FRP-reinforced and FRP-prestressed concrete beams containing continuous FRP helical transverse reinforcement. The results showed that full-depth un-bonded rectangular helical transverse reinforcement was more effective than un-bonded circular helical transverse reinforcement for equal quantities of material. A fully-bonded full-depth helix system, combined with a fully bonded compression-zone circular helix system, led to considerable deformability and ductility. It is suggested that this configuration produces high shear capacity and genuine plastic-based ductility during shear collapse. Comparing the test results with ACI 440.1R-03 predictions for the FRP-reinforced specimens, it was found out that the ACI 440.1R-03 is more conservative.

Maurizio et al. (2006) concluded that the principle of strain control adopted by the current FRP design recommendations is recognized as a valid approach but it is recommended that the maximum allowable strain for both flexural and shear reinforcement should be increased to

0.0045 to account for structural performance, serviceability, and economic viability. At these levels of strain, cracking is effectively controlled, the shear resisting mechanisms offered by both concrete and shear reinforcement are effectively mobilized, and their contribution can be added together to estimate the total resistance.

El-Sayed et al. (2007) carried out an experimental investigation to develop new carbon fiber reinforced polymer (CFRP) stirrups as shear reinforcement for concrete members. To simulate the performance mechanism of stirrups in concrete beams, the CFRP stirrup was embedded in two concrete blocks and tested in tension by pushing the concrete blocks away from each other. In addition, two full-scale concrete beams reinforced with CFRP stirrups as shear reinforcement were constructed and tested to failure.

Test results of the concrete blocks indicated that the strength at the bend of the newly developed CFRP stirrups was adequate and fulfilled the design requirements of different codes and design guides. Furthermore, the tail length was found to be not less than six times the bar diameter to develop the stirrup capacity. The performance of the stirrups in the beam tests was appropriate until reaching the failure of the beams in flexure.

Ahmed et al. (2010) conducted an experimental investigation to evaluate the shear strength of concrete beams reinforced with GFRP stirrups. The significance of that research was to evaluate the shear performance and strength of large-scale RC beams reinforced with GFRP stirrups considering different shear reinforcement ratios. The authors concluded that the presence of GFRP stirrups in the beam specimens, similar to steel stirrups, enhances the concrete contribution after the formation of the first shear crack. The lesser the spacing of the GFRP stirrups, the higher the shear resistance enhancement due to the confinement, which controls the

shear cracks and improves the aggregate interlocking. Also, at shear failure, the inclination angle of the shear crack in concrete beams reinforced with GFRP stirrups was in good agreement with the traditional 45-degree truss model. An important finding was that using FRP stirrups with a strength ratio of bend-to-straight portion ≥ 0.6 enabled using the capacity of the straight portions of the FRP stirrups. Lower ratios will cause the bend strength to govern the stirrup regardless of the tensile strength of the straight portion.

2.2.3.3 Size effect in shear strength of FRP-RC beams

Bentz et al. (2010) investigated the shear strength of large beams reinforced with FRP bars. It was reported that all members without stirrups failed in shear after formation of a diagonal crack. For the lightly reinforced members, the largest beam failed in shear at only 51% of the shear stress at which the smallest beam failed in shear. For the heavily reinforced members, the largest beam failed at a shear stress of 69% of that of the smallest beam. Test results demonstrated a significant size effect and also demonstrated that the extent of this size effect depended on the amount of longitudinal reinforcement and was not simply a function of size alone.

Razaqpur et al. (2011) studied the shear strength of FRP-RC beams subject to unsymmetrical loading. One of the tested parameters was the beam depth. The authors reported that there was a size effect of the tested beams because the calculated shear strength significantly decreased with the increase in beam depth. A reduction of approximately 60% occurred when the beam depth increased from 200–500 mm.

Alam and Hussien (2012 and 2013) examined the effect of depth on the shear strength and behaviour of normal and high-strength concrete beams reinforced with GFRP and CFRP bars in the longitudinal direction only without stirrups. It was concluded that the shear strength of both

GFRP- and CFRP-RC beams decreases as the depth of the beams increases. This reveals the size effect in high-strength FRP-RC beams. They added that the observed size effect corresponds well with Bažant law of size effect. Moreover, the normalized shear strength of both GFRP- and CFRP-RC beams increased almost linearly with the inverse of the cubic root of the effective depth of the beams. Furthermore, Matta et al. (2013) concluded that there is a strong effect of the member depth on the shear strength of FRP-RC large beams. This effect was more significant in beams with small longitudinal reinforcement ratio.

2.3 MOMENT AND SHEAR REDISTRIBUTION IN STEEL-RC CONTINUOUS BEAMS

Ernst (1958) tested twenty four, two-span, steel-RC continuous beams to determine the manner and degree of moment and shear redistribution after yielding of the first critical section. The quantity and spacing of transverse reinforcement was designed to take the full shear at plastic collapse.

Results showed that the redistribution of moments and shear was initiated by the beginning of steel yield at the first critical section. Yielding of steel reinforcement at the last critical section indicated that the redistribution was essentially complete. The moment and shear redistribution happened in the same way for all tested beams, regardless of the differences in steel ratios and length of the top bars. It was concluded that designing the transverse reinforcement to take the shear at plastic collapse ensured against the diagonal tension failures and that the spread of steel yield was in a good agreement with the findings of the previous studies.

Mattock (1959) studied experimentally the redistribution of design bending moments in RC continuous beams. This work was concerned with the influence of arbitrary redistribution of

design bending moments on the performance of continuous RC beams at design load. The tests continued until failure in order to accumulate additional evidence of the elasto-plastic behaviour of RC. Test results showed that the redistribution of moment occurred even though the steel stresses were well below the yield-point stress. It was observed that there was an actual redistribution of bending moments at working load amounting to slightly more than one quarter of the arbitrary amount of redistribution of bending moment assumed in design. This redistribution occurred because the moment/rotation relation for a RC section is not linear for low loads.

At working loads cracking and deflection of the beams for which the design moments had been redistributed was no more severe than that of the beam designed for the elastic-theory distribution of moments.

Rodriguez et al. (1959) carried out experimental tests on fifty-two continuous beams with steel reinforcement in order to determine the effect of continuity on the shear strength of statically indeterminate members, contribution of web reinforcement to shear strength, and to establish the minimum amount of web reinforcement required to prevent shear failures. The research significance lies in the need to verify the applicability of design formulas and equations developed using simply supported beams to design continuous beams, hence study whether the continuity has any effect on shear behaviour. The included variables of the test were cutoff or the extended longitudinal steel, percentage and spacing of the transverse reinforcement, type of loading, and grade of longitudinal reinforcement. The tested beams had four different failure modes. These modes were diagonal tension, flexural, shear compression and splitting failure. It was found out that the manner of diagonal crack formation and the modes of failure of two span continuous beams failing due to shear were similar to those observed in tests of simple beams.

However, continuity had a marked effect on redistribution of stresses in the beam. Also, tests showed that beams may fail simultaneously with the formation of a diagonal tension crack in a region in which no web reinforcement is provided.

Based on the analysis of the test results, the authors concluded that the analysis for diagonal tension cracking used for simple beams is applicable for continuous beams. Also, it is possible to have a shear failure in a beam even after yielding of the longitudinal reinforcement has occurred at a particular section.

Bryant et al. (1962) studied the shear strength of two-span continuous concrete beams with multiple points loading. The authors noted that the overall cracking pattern in a two span continuous beams was uniform enough to keep the beam reactions in a good agreement with the elastic theory before yielding of the longitudinal reinforcement occurred. However, a small variation of the middle support reaction which could affect the moment at the critical sections was observed. Beams which were designed to determine the adequacy of the web reinforcement to prevent shear failures failed in flexure. In these beams, stirrups either yielded or were near yielding.

Lin and Chien (2000) conducted analytical and experimental investigation to study the effect of the section ductility on moment redistribution of continuous RC beams. The main objectives of this study were to evaluate the influence of the volumetric ratio of the transverse reinforcement on the moment redistribution and to obtain more reasonable equations for moment redistribution. The results obtained from the tested specimens showed that higher steel ratio decreases the ductility. Larger amounts of transverse reinforcement increase the ductility significantly. Also higher concrete strength leads to higher ductility, but its effect is not prominent as transverse

reinforcement. It was concluded that the hinging region provided in the ACI code, which is twice the member depth, was in a reasonable agreement with the results. Also, provisions on moment redistribution of continuous beams as specified by ACI code are conservative.

2.4 MOMENT AND SHEAR REDISTRIBUTION IN FRP-RC CONTINUOUS BEAMS

According to the North America Codes and design guidelines for FRP-RC structures, the redistribution of moment and shear in indeterminate structures is not allowed. The reason behind that is the linear-elastic behaviour of the FRP reinforced structures. However, research has been done to examine the moment redistribution in continuous beams reinforced with FRP bars. In this section, the important conclusions regarding the moment redistribution in FRP-reinforced continuous concrete beams are presented.

Tezuka et al. (1995) conducted an experimental study on moment redistribution of continuous concrete beams reinforced or pre-tensioned with fiber reinforced plastic to make clear the behaviour of the moment redistribution. Also a simple non-linear analysis based on beam theory is performed considering non-linearity of stress-strain relationship of materials to predict the moment redistribution of continuous beams. Test results showed that moment redistribution occurred where a decrease up to 29.7% in the hogging moment and increase in the sagging moment up to 22.6% were reported. The experimental ratios of the moment redistribution of reinforced specimens were remarkably greater than computed ones. The reason behind that is the development of diagonal shear cracks near the middle support. On the other hand, experimental and computed ratios of the moment redistribution agreed relatively well in prestressed beams. This could be due to that the prestress contributed to control the diagonal shear crack; consequently, flexural cracks became predominant.

Grace et al. (1998) studied the behaviour and ductility of simple and continuous FRP-reinforced concrete beams. The test variables were the type of both longitudinal reinforcement (steel, CFRP and GFRP) and the type of stirrups (steel, CFRP and GFRP). It was reported that modes of failure of continuous concrete beams were flexural failure in beams with steel bars and GFRP or steel stirrups, shear failure in beams with GFRP bars and GFRP or steel stirrups and in case of using CFRP bars any mode of failure is possible, depending on the type of stirrups used.

Regarding the failure loads, the continuous beams failed at different load capacities. Beams reinforced with steel bars and steel stirrups had the largest load while beams with GFRP bars and stirrups had the lower value of failure loads. This was attributed to the weak dowel effect of the GFRP bars and the low shear capacity of the GFRP stirrups. Beams reinforced with CFRP bars and stirrups sustained a larger failure loads than that of the GFRP reinforced beams. The difference in failure loads was attributed to the difference in dowel effect between the CFRP and the GFRP bars. Studying the ductility of the tested beams, it was found out that continuous beams failed in more ductile fashion than did simple beams. This was attributed to the moment redistribution in continuous beams.

Razaqpur and Mostofinejad (1999) conducted an experimental investigation to study the behaviour of continuous beams reinforced with carbon fiber reinforced polymer. The main aims were to study the shear strength of continuous beams reinforced with CFRP and to investigate the feasibility of using FRP grids as shear reinforcement. The results indicated that FRP stirrups can undergo larger strain without adverse effect on the behaviour of the beam. The measured strain in steel stirrup was less than that in CFRP grids. Based on the observed behaviour of the tested beams, the authors concluded that using CFRP grids as shear reinforcement is possible. Despite of the lower modulus of elasticity of the CFRP grid, and the lower shear reinforcement

ratio of the grid used in the study, the beams failed at a much higher load than their counterparts reinforced with steel stirrups.

Habeeb and Ashour (2008) investigated the flexural behaviour of continuous GFRP-RC beams. In this study, the authors tested two simply and three continuously supported beams reinforced with GFRP and one beam reinforced with conventional steel. The authors tested only one parameter which was the amount of the longitudinal reinforcement. Over and under GFRP reinforcement ratios were provided in both simply and continuously supported beams.

Four different failure modes were reported throughout the experimental tests. These failure modes were bar rupture in under-reinforced beams, concrete crushing in over-reinforced beams, concrete crushing combined with shear failure and ductile flexural failure in steel reinforced beams. Regarding the mid-span deflection and cracks, GFRP reinforced beams exhibited higher mid-span deflections and wider cracks than that reinforced with steel.

It was concluded that continuously supported GFRP-RC beams did not demonstrate any remarkable load redistribution. Moreover, Comparisons between experimental results and those obtained from simplified methods proposed by the ACI 440 Committee showed that ACI 440.1R-06 equations could reasonably predict the load capacity and deflection of the simply and continuously supported GFRP-RC beams tested.

El-Mogy et al. (2010 and 2011) investigated experimentally the flexural behaviour of continuous FRP-RC beams. The studied parameters were the type and amount of longitudinal reinforcement at the critical sections. The main objective was to investigate the range of moment redistribution that could be achieved by GFRP- and CFRP-RC continuous beams and their flexural behaviour with different reinforcement configurations. Regarding to the cracking pattern, it was observed

that beams demonstrated uniform crack distribution in both positive and negative moment regions. Beams reinforced with either GFRP or CFRP exhibited a wider and deeper cracks. This could be attributed to the low axial stiffness of the FRP reinforcement compared to that of steel reinforcement.

Test results showed that in steel reinforced continuous concrete beam, moment redistribution began before yielding of tensile reinforcement at the middle support. Also, it was found out that in beam reinforced with FRP moment redistribution from the middle support section to mid-span section occurred similar to that reinforced with steel but with different percentages. Moreover, using a reinforcement configuration that allows for moment redistribution in GFRP-RC continuous beams had a positive effect on deflection reduction while maintaining the load-carrying capacity as reinforcement configuration satisfying the elastic moment distribution. Continuous beams reinforced with FRP bars showed ample warning in the form of large deflections and wide cracks prior to failure.

The authors also studied the effect of transverse reinforcement on the flexural behaviour of continuous beams reinforced with FRP. The included parameters in this study were the material, spacing and amount of transverse reinforcement. On the basis of the results of this investigation, the authors concluded that the performance of the GFRP-reinforced beam provided with GFRP stirrups was similar to its counterpart reinforced with steel stirrups. Also, increasing the transverse reinforcement in GFRP-reinforced continuous beams without increasing the longitudinal reinforcement reduced deflection and improved moment redistribution. Moreover, reducing the spacing of the stirrups increased the capability of the beam to deform and allowed for more moment redistribution.

Santos et al. (2013) conducted experimental and numerical investigations on the flexural behaviour of GFRP-RC continuous beams focusing on their capacity to redistribute internal forces. The authors tested seven small-scale, two-span continuous beams with T cross-section. The studied parameters were the GFRP reinforcement ratio and the confinement level at the critical zones of the beams, namely at the middle support. The numerical investigations included the development of non-linear finite element (FE) models for all tested beams. After calibration with the test data, a comprehensive parametric study was performed, in which the effects of the span, the cross-section geometry, and the longitudinal GFRP reinforcement ratio on the moment redistribution capacity of full-scale continuous beams were evaluated. The results showed that moment redistribution occurs and that elastic analyses are considerably conservative. The confinement of the concrete at critical cross sections may be a good solution to enhance the plastic hinge ductility and consequently, the moment redistribution in GFRP-RC beams.

Also, Kara and Ashour (2013) studied the moment redistribution in continuous concrete beams reinforced with FRP bars. The authors developed a numerical technique based on equilibrium of forces and full compatibility of strains to evaluate the moment-curvature relationships and moment capacities of FRP- and steel-RC sections. It was reported that the curvature of under reinforced FRP sections was large at FRP rupture but failure was sudden, that would not allow any moment redistribution. On the other hand, FRP over-reinforced sections experienced higher curvature at failure than steel over-reinforced sections because of the lower FRP modulus of elasticity.

CHAPTER 3: EXPERIMENTAL PROGRAM

3.1 GENERAL

Based on the literature review presented earlier, it is evident that the shear strength of concrete beams, in general, depends mainly on concrete strength, shear span-to-depth ratio, longitudinal reinforcement ratio and transverse reinforcement ratio. Also, the well-documented moment and shear redistribution in steel-RC indeterminate structures made it possible to use the same shear design provisions for both simple and indeterminate structures. Moreover, recent research proved that the moment redistribution in FRP-RC continuous beams is possible. Therefore, investigating the shear behaviour of continuous FRP-RC beams is needed to examine whether or not these members behave similar to their counterparts reinforced with conventional steel. The objectives of this research program are to study the effect of the above mentioned variables and the moment redistribution on the shear behaviour of such indeterminate beams. Moreover, this study includes testing of beams having variable depth to investigate the size effect on the shear strength of continuous beams.

3.2 TEST BEAMS

A total of twenty four large-scale continuous concrete beams reinforced with either GFRP or steel bars were constructed and tested to failure. Sixteen beams had a 200 × 300 mm rectangular cross-section with an overall length of 6,000 mm. These sixteen beams were continuous over two equal spans of 2,800 mm with a 200 mm overhang at each end to provide adequate anchorage for longitudinal bars. The shear-to-depth ratio, *a/d*, ratio for those beams was 3.0. The remaining eight beams had different spans and cross-section depths to investigate the size effect. The difference in length of the eight specimens was a result of keeping a constant *a/d* ratio of 3.0,

similar to all other test beams. The effective depth was chosen to be twice and three times that of the above mentioned sixteen beams. As a result, the effective depth was 500 mm for four beams and 750 for the remaining four beams. Beams having an effective depth of 500 mm were continuous over two equal spans of 3,750 mm with an overall length of 8,100 mm, while beams having an effective depth of 750 mm were continuous over two equal spans of 5,250 mm with an overall length of 11,300 mm.

The test beams were labeled based on the different parameters in this study. The label of each beam can be explained as follows. The first letter refers to the type of the longitudinal reinforcement ("S" for steel and "G" for GFRP). The second letter indicates the grade of concrete ("N" for NSC and "H" for HSC). The third number is the ratio of the longitudinal reinforcement at both the hogging and sagging moment regions. The fourth number refers to the transverse reinforcement ratio. The last letter refers to the depth of the beam where *d* equals to 250 mm ("2*d*" and "3*d*" for beams having a depth of 500 and 750 mm, respectively).

For example, specimen "GN-1.2-0.48-*d*" is reinforced with GFRP bars, made of normal strength concrete, has a longitudinal reinforcement ratio of 1.2%, and has a transverse reinforcement ratio of 0.48 with a depth of 250 mm.

3.3 DESIGN CONCEPT

The beams were designed according to the applicable design codes to satisfy both flexural and shear strength requirement. The Canadian standard CSA/S806-12 (CSA 2012) was used to design the GFRP-RC beams, while CSA/A23.3-04 (CSA 2004) was used to design the steel-RC beams. The flexural and shear design provisions in the current codes and guidelines are documented in Appendix A. It should be noted that all beams were designed to fail in shear

before reaching their flexural capacity. As such, the reinforcement for both flexure and shear were selected to lead the specimens to the desired mode of failure. Also, the longitudinal reinforcement arrangement was selected to satisfy assumed 20% moment redistribution from hogging to sagging moment region. Detailed design calculations of all tested beams can be found in Appendix B. It is worth mentioning that, after casting all test beams, a new version of the CSA/A23.3 standard was recently published in 2014 (CSA 2014); however, there are no changes in the design provisions used to design the beams in the current study.

3.4 MATERIALS

To construct the specimens in this research program, different materials such as concrete, GFRP bars and stirrups, and steel bars and stirrups were used. All specimens in this research program were constructed in the structures laboratory at the University of Manitoba. Due to the large quantities and different required characteristic strength, ready-mix normal-weight concrete was used. As concrete strength is one of the studied parameters, two compressive strengths of 35 and 70 MPa were targeted. The nominal maximum aggregate size was 19 mm in all the used concrete. Also, slump was measured in the laboratory and it ranged from 80 to 100 mm for normal strength concrete and from 180 to 220 mm for high strength concrete. Twenty four standard cylinders 100×200 mm and ten standard cylinders 150×300 mm were cast from each batch and tested to determine the concrete actual compressive and tensile strength at 7, 14 and 28 days and at the day of test of each beam.

Sand coated GFRP pultruded bars were used as main longitudinal reinforcement and sand coated GFRP stirrups were used as shear reinforcement as well. Also, steel bars and stirrups were used to reinforce the reference beams. Standard characteristics tests were conducted in the laboratory

to obtain the actual mechanical properties of the used reinforcement as applicable. Determination of the cross-sectional area of the used GFRP bars including the sand coating was obtained using the specified method in CSA/S806-12, Annex A. Also, the tensile strength, modulus of elasticity and ultimate strain of the used GFRP bars and stirrups were calculated according to CSA/S806-12, Annexes C and D, respectively. The mechanical properties of the used reinforcement are listed in Table 3.1. Figure 3.1 shows photos for the used reinforcement.

Table 3.1: Mechanical properties of the longitudinal and transverse reinforcement

Bar type	Diameter (mm)	Area (mm^2)		Tensile strength (MPa)	Modulus of Elasticity (GPa)	Ultimate Strain (%)
		Nominal	CSA/S806-12 Annex A			
GFRP Bars	15.9	198	282.7	1,442	67	2.1
	19.1	285	396.6	1,383	53	2.6
GFRP Stirrups	6.3*	32*	44.0*	1,383*	53*	2.6*
	9.5*	72*	84.7*	1,195*	45*	2.7*
	12.7*	127*	145.7*	1,328*	53*	2.5*
Steel bars	16.0	200	-	f_y = 430	200	ε_y = 0.23
Steel Stirrups	4.8	18.1	-	f_y = 460	200	ε_y = 0.23

* Provided values are for the straight portion of the stirrups

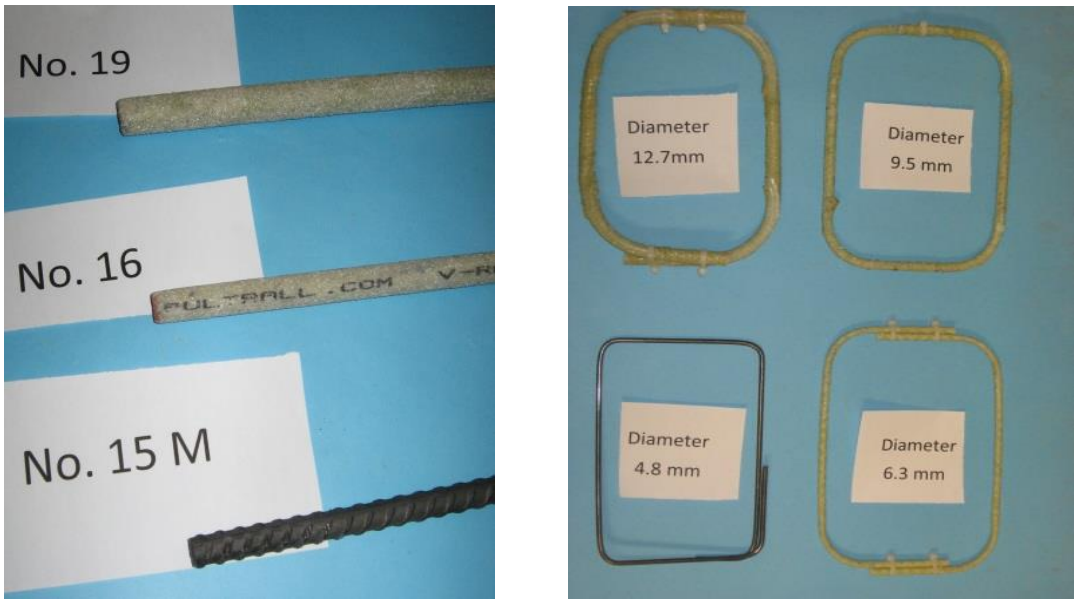

Figure 3.1: Reinforcing bars and stirrups

3.5 DETAILS OF TEST BEAMS

The test beams were divided into three series based on the objective of each one. Series I consisted of seven beams without transverse reinforcement. All test beams in this series had a rectangular cross section of 300 mm height and 200 mm width. One beam was reinforced with conventional steel to serve as reference, while the other six beams were reinforced with GFRP bars. The main aim of this series was to evaluate the concrete contribution to the shear strength of GFRP-RC continuous beams. The test variables were type and ratio of the longitudinal reinforcement and the concrete strength. The longitudinal reinforcement ratio ranged between 0.8% and 1.6%. The details of test beams in Series I are listed in Table 3.2.

Series II included a total of twelve beams, eight new beams and four beams from Series I. The objective of this series was to investigate the size effect on the shear strength of GFRP-RC continuous beams without transverse reinforcement. The variables in this series included, in

addition to the varied effective depth, the longitudinal reinforcement ratio and the concrete strength. Table 3.3 summarizes the details of beams in Series II.

The third series, Series III, was dedicated to investigate the effect of the transverse reinforcement ratio on the shear strength of GFRP-RC continuous beams. This series included nine beams with transverse reinforcement. The test variables were the type and ratio of the longitudinal reinforcement, the type and ratio of the transverse reinforcement and the concrete strength. One reference beam was reinforced longitudinally and transversely with steel bars and stirrups, while the other eight specimens were reinforced with GFRP bars and stirrups. The shear reinforcement, in the steel-RC beam, was the minimum area specified in the Canadian standards CSA/A23.3-04 (CSA 2004). In GFRP-RC continuous beams, the transverse reinforcement varied form the minimum shear reinforcement specified in the CSA/S806-12 (CSA 2012), in four beams, to half that minimum, in two beams, to twice that minimum in the remaining two beams. To eliminate the effect of stirrup spacing and at the same time achieve the different shear reinforcement ratios, the stirrup spacing were kept constant (150 mm for NSC beams and 115 mm for HSC beams), while different stirrup size was used. The details of the test beams in Series III are shown in Table 3.4. Moreover, the dimensions, geometry and reinforcement of the test specimens are shown in Figs. 3.2 to 3.4. As described later, the strain gauge locations in the longitudinal and transverse reinforcement are shown in these figures as well.

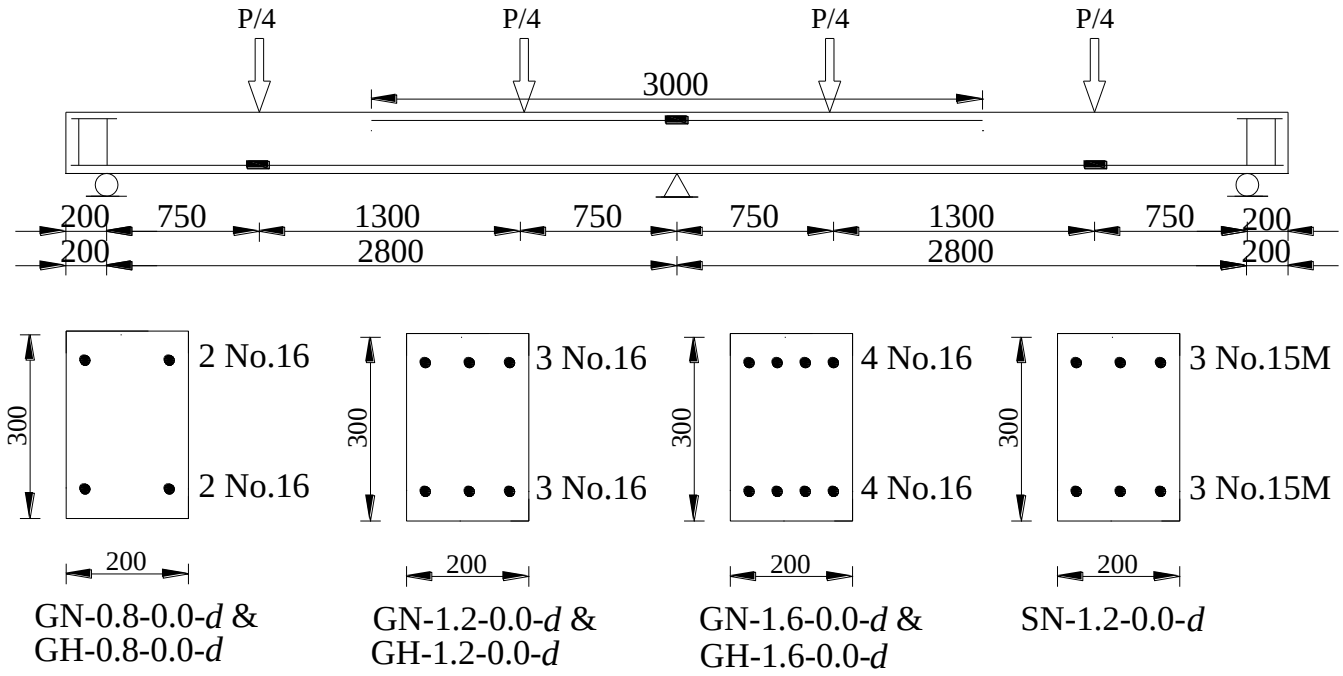

Figure 3.2: Details of beams without stirrups and having an effective depth of 250 mm

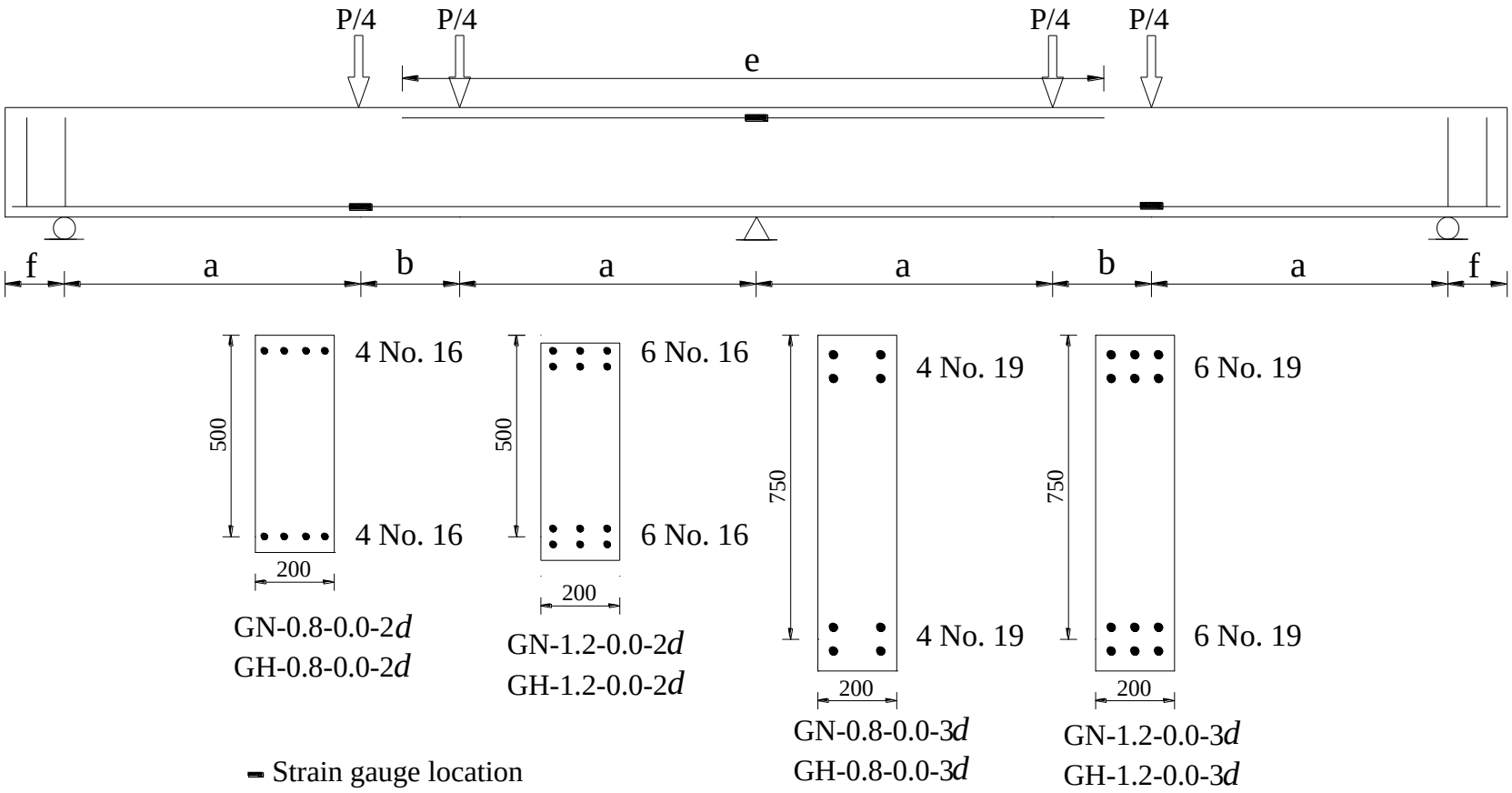

Beam	a	b	e	f
Beams having an effective depth of 500 mm	1500	750	3750	300
Beams having an effective depth of 750 mm	2250	750	5250	400

Figure 3.3: Details of beams without stirrups and having an effective depth of 500 and 750 mm

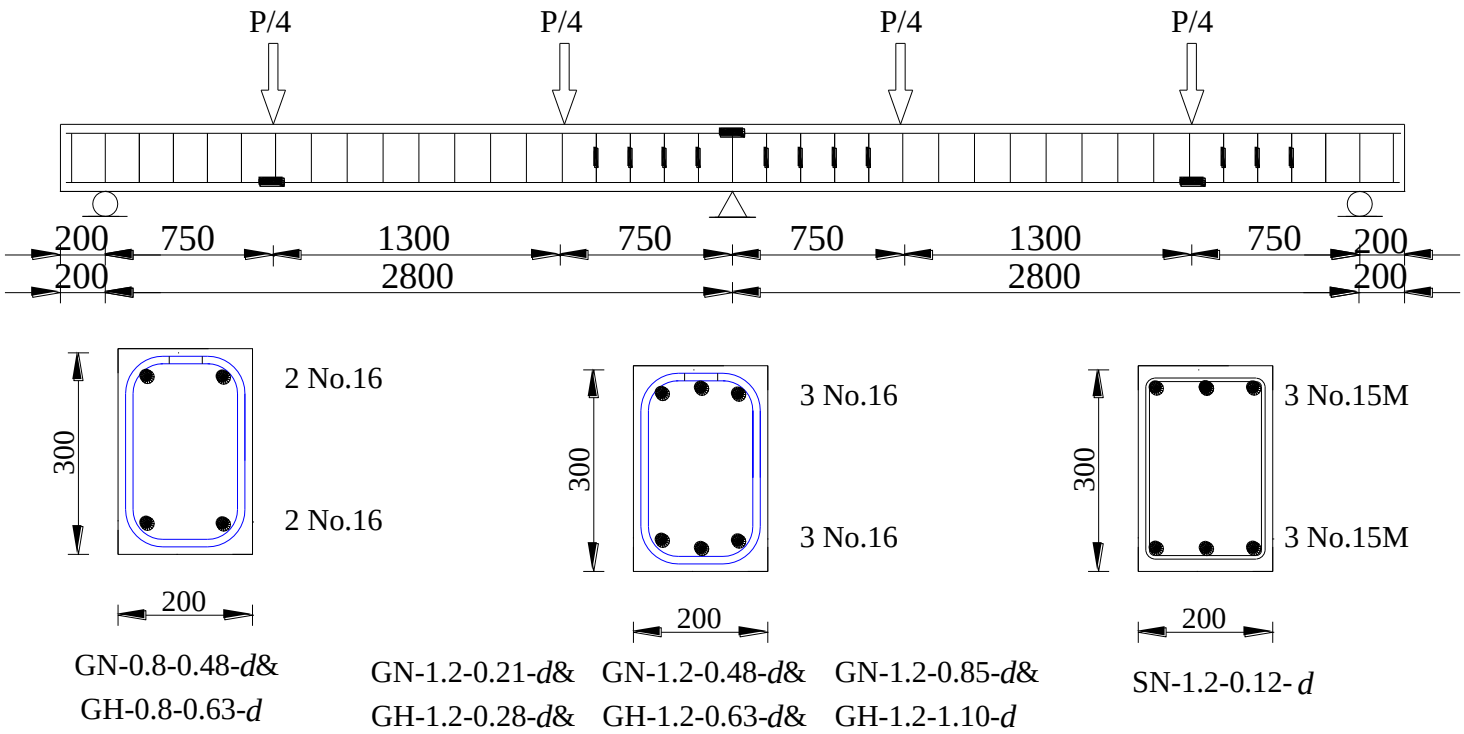

Figure 3.4: Details of Series III beams

Table 3.2: Details of test specimens in Series I

Beam	$f_c^{'}$ (MPa)	Depth (mm).	Flexural reinforcement		Shear reinforcement		
			ρ (%)	$\frac{\rho}{\rho_{bal}}$	ρ_v (%)	Stirrup spacing (mm)	Stirrup diameter (mm)
SN-1.2-0.0-*d*	35	250	1.2	0.32	NA	NA	NA
GN-0.8-0.0-*d*			0.8	3.22			
GN-1.2-0.0-*d*			1.2	4.83			
GN-1.6-0.0-*d*			1.6	6.44			
GH-0.8-0.0-*d*	70	250	0.8	1.91	NA	NA	NA
GH-1.2-0.0-*d*			1.2	2.86			
GH-1.6-0.0-*d*			1.6	3.82			

Table 3.3: Details of test specimens in Series II

Beam	$f_c^{'}$ (MPa)	Depth (mm).	Flexural reinforcement		Shear reinforcement		
			ρ (%)	$\frac{\rho}{\rho_{bal}}$	ρ_v (%)	Stirrup spacing (mm)	Stirrup diameter (mm)
GN-0.8-0.0-*d**	39	250	0.8	3.22	NA	NA	NA
GN-1.2-0.0-*d**	39		1.2	4.83			
GN-0.8-0.0-2*d*	39	500	0.8	3.20			
GN-1.2-0.0-2*d*	44		1.2	4.41			
GN-0.8-0.0-3*d*	39	750	0.8	3.22			
GN-1.2-0.0-3*d*	39		1.2	4.83			
GH-0.8-0.0-*d**	72	250	0.8	1.91	NA	NA	NA
GH-1.2-0.0-*d**	72		1.2	2.86			
GH-0.8-0.0-2*d*	70	500	0.8	1.90			
GH-1.2-0.0-2*d*	70		1.2	2.61			
GH-0.8-0.0-3*d*	77	750	0.8	1.91			
GH-1.2-0.0-3*d*	71		1.2	2.87			

*Beams from Series I

Table 3.4: Details of tested specimens in series III

Beam	f_c' (MPa)	Depth (mm).	Flexural reinforcement		Shear reinforcement		
			ρ (%)	$\frac{\rho}{\rho_{bal}}$	ρ_v (%)	Stirrup spacing (mm)	Stirrup diameter (mm)
SN-1.2-0.12-*d*	45	250	1.2	0.32	0.12*	150	4.8
GN-0.8-0.48-*d*	43		0.8	3.22	0.48†	150	9.5
GN-1.2-0.48-*d*	43		1.2	4.83			
GN-1.2-0.21-*d*	42				0.21		6.3
GN-1.2-0.85-*d*	43				0.85		12.7
GH-0.8-0.63-*d*	81	250	0.8	1.91	0.63†	115	9.5
GH-1.2-0.63-*d*	80		1.2	2.86			
GH-1.2-0.28-*d*	81				0.28		6.3
GH-1.2-1.10-*d*	80				1.10		12.7

*Minimum transverse reinforcement ratio specified by CSA/A23.3-14
†Minimum transverse reinforcement ratio specified by CSA/S806-12

3.6 CONSTRUCTION OF TEST BEAMS

The construction of the test beams started with building formworks using plywood sheets. The second step was to prepare the reinforcement bars to be assembled to form the cage. The bar surface were prepared and cleaned to receive the strain gauges; then, the strain gauges were attached to the bars at the designated locations using special glue specifically designed for this purpose. To protect the strain gauges against moisture, impact or damage during casting, they were covered with a thin layer of silicone coating throughout the gauge length. The reinforcement cage was assembled and very carefully placed in the plywood forms after brushing the insides with oil to facilitate the beam removal after casting and curing of the concrete. The reinforcement cage rested on plastic chairs to maintain the required clear concrete cover.

The concrete was poured in the forms while properly vibrated using electrical vibrator. The reinforcement cage was carefully maintained in the center of the forms to keep the side-cover uniform and equal. Moreover, extreme care was dedicated to the strain gauges and the attached wires not to be damaged in the process. The surface of the concrete was finished after casting to a smooth surface and then covered with a plastic sheet. Twenty four 100×150 mm cylinders and ten 150×300 mm cylinders were prepared by casting concrete in plastic molds. The cylinders were filled with concrete over three layers while tamping each layer with the standard steel rod for 25 times. The curing process for the constructed beams and the concrete cylinders started the next day and the concrete surface was kept wet for seven days.

After 28 days, all beams were prepared for testing by painting beam sides in white and marking the surface with a grid in order to trace the crack pattern during the test. Figure 3.5 shows some of the construction stages of the test beams.

a) Beams without stirrups (d = 250 mm)

b) Beam with stirrups (d = 250 mm)

c) Beam without stirrups (d =750 mm)

d) Steel-RC Beams (d = 250 mm)

e) After casting and finishing

f) Beams and cylinders in curing

Figure 3.5: Construction stages of test specimens

3.7 TEST SET-UP AND INSTRUMENTATION

The test beams were continuous over two equal spans and were supported on one hinged support at the middle and two roller supports at both ends. The beams were tested under a two-point loading system in each span with a constant shear span-to-depth ratio of 3.0. For beams having 300 mm height, a 1000-kN MTS machine was used to apply a monotonic concentrated load that was transmitted to the beam through a rigid system of spreader beams. For beams having 500 and 750 mm effective depth, the 1000-kN MTS machine and a 1000-kN MTS hydraulic actuator were used to apply the load to the beam through spreader beams. In all tests, a load-controlled rate of 10 kN/min was used to apply equal loads to the two spans. After the formation of the first flexural crack, the loading was put on-hold every 25 kN to visually inspect the beam and to mark the cracks, if any.

Two load cells were used to measure the reactions at the end supports. Also, deflection was measured, using linear variable displacement transducers (LVDTs), at three different locations in each span, at mid-span and at each loading point in the span. To measure the actual strains at critical locations, a number of strain gauges were installed on the reinforcement and on the concrete surface to monitor their strain during loading. Four strain gauges were installed on the longitudinal reinforcement in each beam. Moreover, three strain gauges were attached to the concrete side surface in the compression zone of critical sections at 10 mm from the beam top and bottom surface, as appropriate, to measure the corresponding compressive strains in concrete. In addition, 200-mm long PI gauges were also attached to the concrete side surface at the mid-height of the cross section to measure the width of the diagonal cracks in the critical shear zones. The applied load, exterior reactions, displacements, crack widths, and strain readings were electronically recorded during the test using a data acquisition system monitored

by a computer. Figures 3.6 to 3.8 show the test setup and instrumentations of test beams. Also, Fig. 3.8 shows photos for the test setup for beams with different depths.

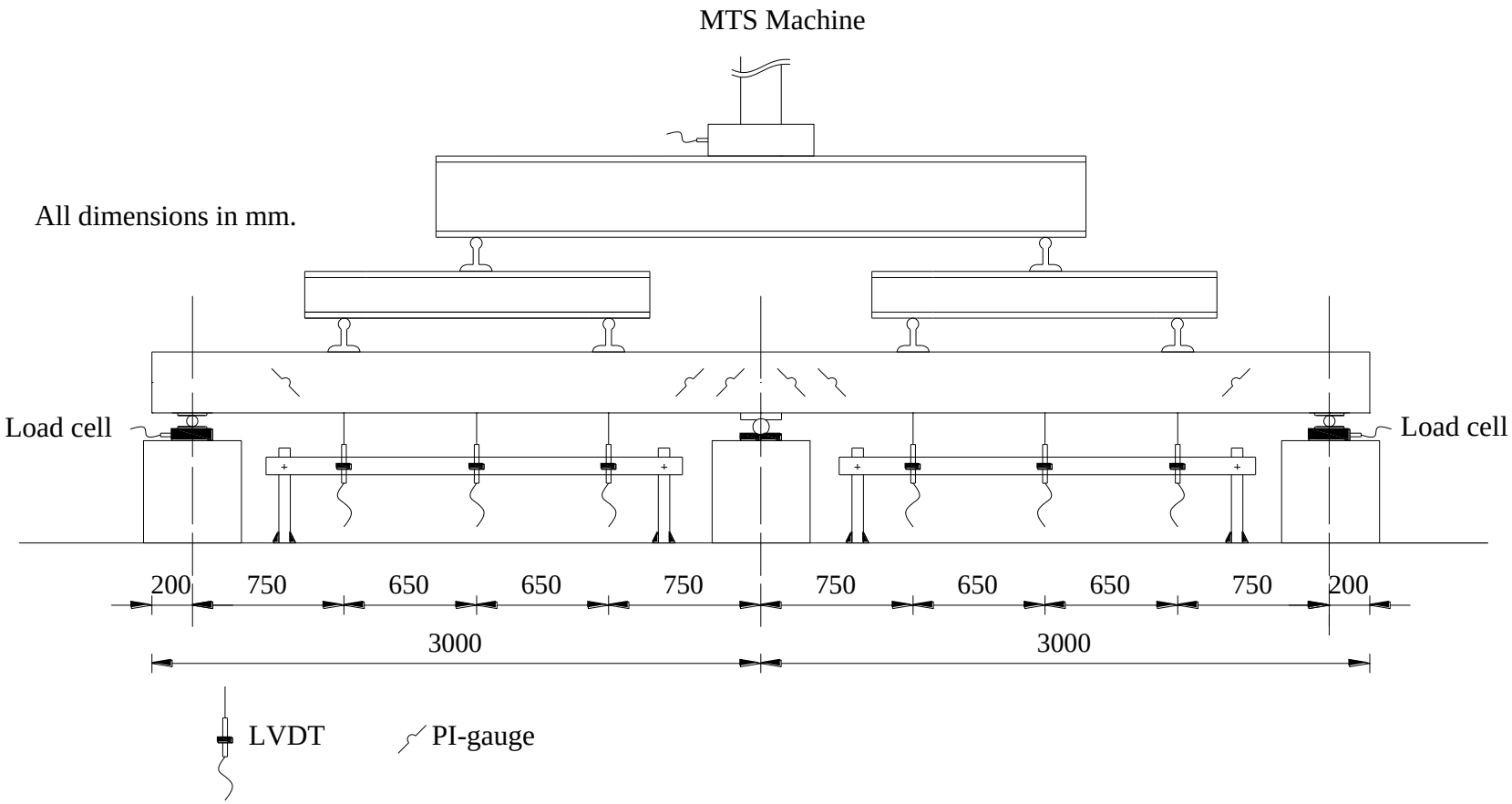

Figure 3.6: Test setup and instrumentations of test beams with 250 mm effective depth

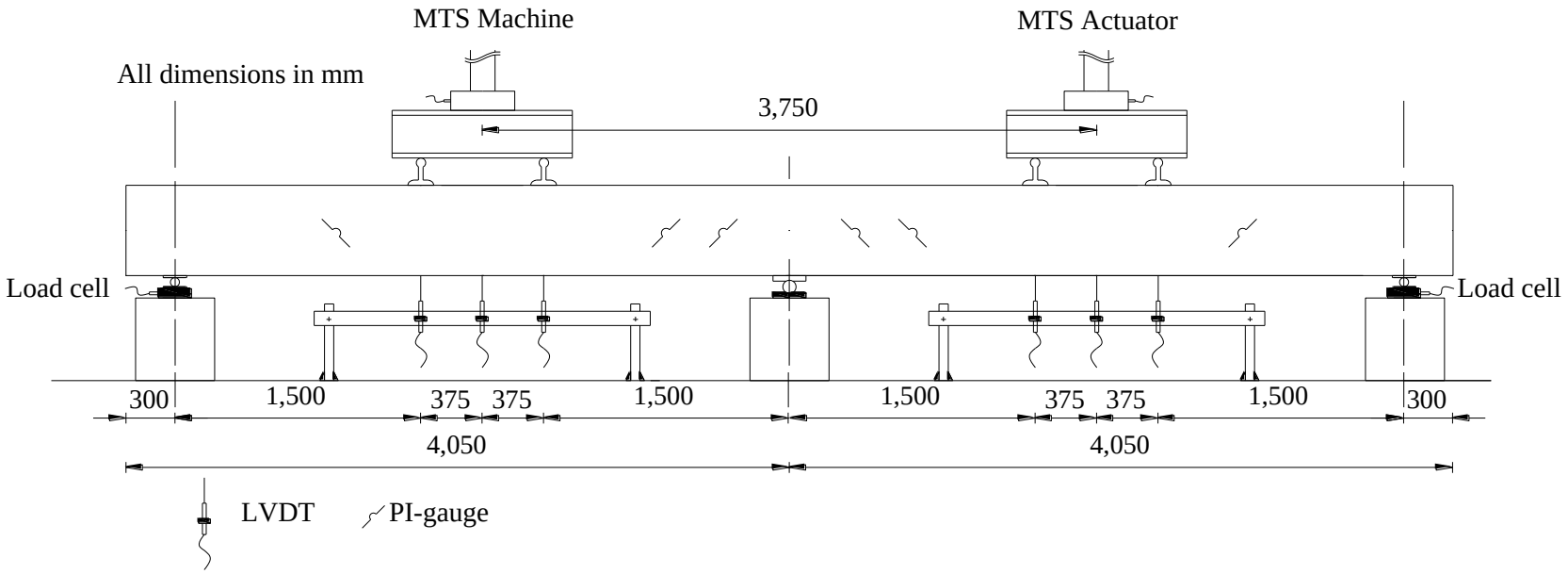

Figure 3.7: Test setup and instrumentations of test beams with 500 mm effective depth

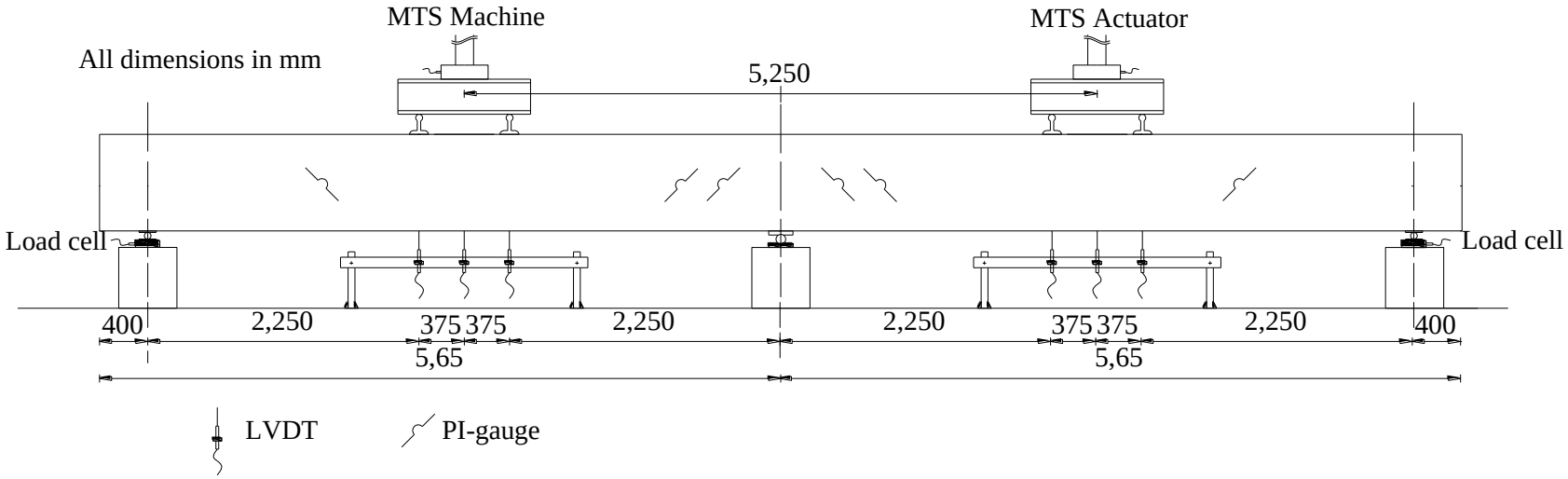

Figure 3.8: Test setup and instrumentations of test beams with 750 mm effective depth

(a) Beam with 250 mm depth

(b) Beam with 500 mm depth

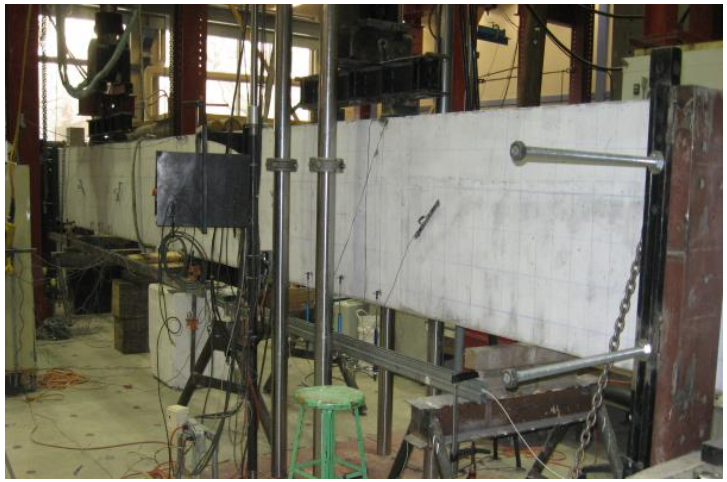

(c) Beam with 750 mm depth

Figure 3.9: Photos of test setup and instrumentation of beams with different effective depth

CHAPTER 4: RESULTS AND DISCUSSIONS OF SERIES I

4.1 GENERAL

This chapter presents the analysis and discussion of the experimental results of the test beams in Series I. As stated in Chapter 3, this series includes seven large-scale two-span continuous RC beams. All beams were tested under a two-point loading arrangement in each span with a shear span-to-depth ratio of 3.0. The test variables included the type and ratio of the longitudinal reinforcement and the concrete strength. The main objectives of this series were to evaluate the shear strength of GFRP-RC continuous beams without shear reinforcement and to examine the capability of such beams (shear-critical beams) to redistribute moments between the critical sections. The behaviour of the test beams was carefully monitored during the test. The recorded data were the deflections at three different locations in each span, the strains in both reinforcement and concrete at the critical sections, the reactions at the exterior supports, and crack width in the exterior and interior shear spans. The complete behaviour of the test beams, in terms of cracking patterns, load-deflection curves, and strain variations in the reinforcement bars and concrete surface, is described in this chapter. Moreover, moment redistribution and shear capacity of the test beams are also discussed. Furthermore, a comparison between the experimental and predicted shear strength by CSA/S806-12 (CSA 2012), CSA/S6-06 (CSA 2009) and ACI 440.1R-06 is also presented in this chapter. It should be noted that a new version of the ACI 440.1R design guidelines was recently published in 2015 (ACI Committee 440 2015); however, there was no change in the shear design provisions that were used for the comparison purposes.

4.2 GENERAL BEHAVIOUR, CRACKING AND MODE OF FAILURE

At early loading stages, the internal forces followed the elastic distribution; therefore, the first crack was a vertical flexural crack in the hogging moment region over the middle support followed by similar cracks in the sagging moment regions. The first flexural crack in the test beams was developed at a load of 110, 50, 65, 60, 90, 95 and 90 kN in beams SN-1.2-0.0-*d*, GN-0.8-0.0-*d*, GN-1.2-0.0-*d*, GN-1.6-0.0-*d*, GH-0.8-0.0-*d*, GH-1.2-0.0-*d* and GH-1.6-0.0-*d*, respectively. With increasing the load, new flexural cracks formed in both the hogging and sagging moment regions. The vertical flexural cracks in the vicinity of the middle support propagated diagonally towards the support. A similar behaviour was observed in the exterior shear span, but the cracks propagated diagonally towards the loading point. The formed cracks grew wider and deeper with further increase in the load. In beam GN-0.8-0.0-*d*, two new diagonal cracks initiated simultaneously at the mid-height of the beam in both interior and exterior shear spans leading to the failure of the beam. Beams GN-1.2-0.0-*d*, GH-0.8-0.0-*d* and GH-1.2-0.0-*d* failed after the formation of a diagonal crack at the interior shear span. In contrary, beams SN-1.2-0.0-*d*, GN-1.6-0.0-*d* and GH-1.6-0.0-*d* failed due to a diagonal crack formed in the exterior shear span. Figure 4.1 shows photos for all Series I test beams at failure.

Schematic drawings of the cracking patterns of Series I test beams at failure are shown in Fig. 4.2. Similar crack pattern was observed in all test beams. It was noted that beams made of HSC had more cracks at both hogging and sagging moment regions than their counterparts made of NSC. Moreover, it was observed that the cracks were deeper in beams with 0.8% longitudinal reinforcement ratio than that in beams with 1.2% longitudinal reinforcement ratio. The same behaviour was observed with increasing the longitudinal reinforcement ratio from 1.2 to 1.6%. Also, it was noted that angle of inclination of the diagonal cracks that led to failure of the test specimens depends on the failure location.

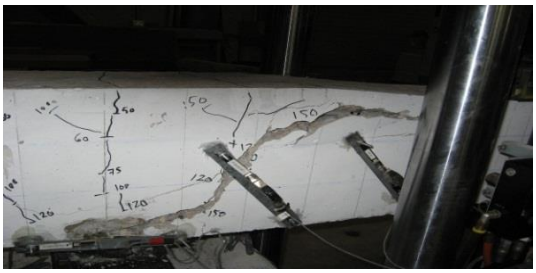

(a) GN-0.8-0.0-*d*, interior shear span

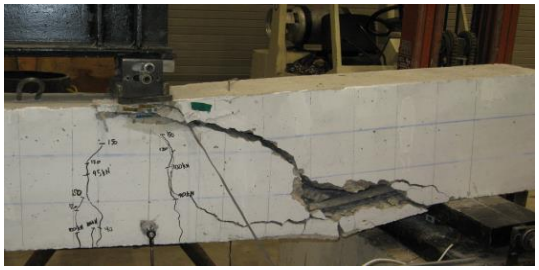

(b) GN-0.8-0.0-*d*, exterior shear span

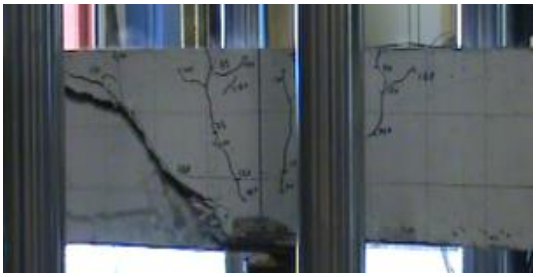

(c) GN-1.2-0.0-*d*, interior shear span

(d) GN-1.6-0.0-*d*, outer shear span

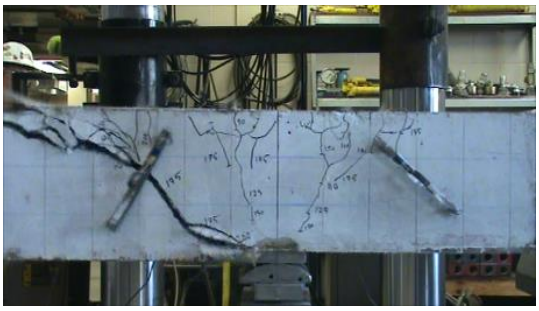

(e) GH-0.8-0.0-*d*, interior shear span

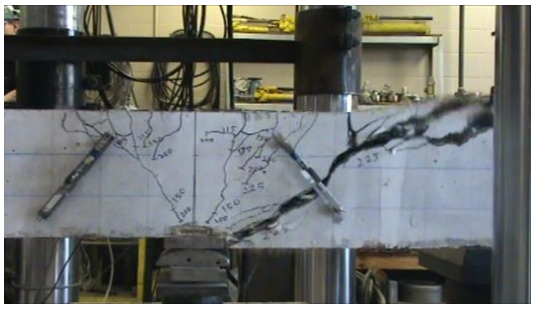

(f) GH-1.2-0.0-*d*, interior shear span

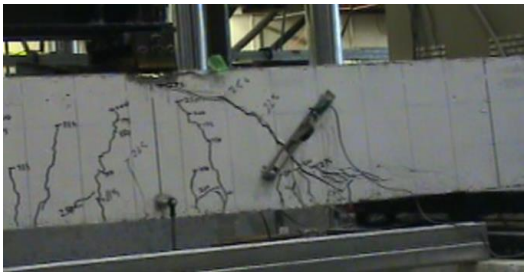

(g) GH-1.6-0.0-*d*, exterior shear span

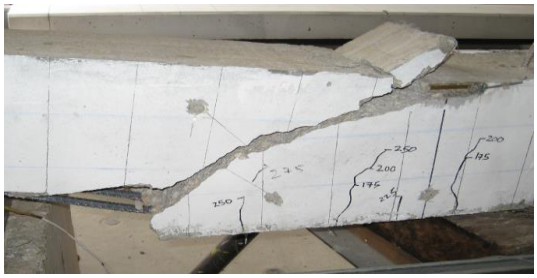

(h) SN-1.2-0.0-*d*, exterior shear span

Figure 4.1: Mode of failure for test beams of Series I

The diagonal cracks in the interior shear span were steeper than those in the exterior shear span. This is can be attributed to the fact that bending moment and shear force distribution in the

exterior shear span is close to that of simply-supported beams, while the continuity affects the angle of inclination of the diagonal cracks in the interior shear span. The effect of the continuity on the angle of the diagonal crack was clear in beam GN-0.8-0.0-*d* where the angle in the interior and exterior shear span was 51^o and 39^o, respectively. In beams SN-1.2-0.0-*d*, GN-1.6-0.0-*d*, GH-1.6-0.0-*d*, which failed in the exterior shear span, the angle of inclination of the failure plane was 42^o, 40^o and 41^o, respectively. In beams GN-1.2-0.0-*d*, GH-0.8-0.0-*d* and GH-1.2-0.0-*d*, the angle of inclination of the failure plane was 52^o, 50^o and 43^o, respectively. The average angle of inclination in the interior shear span was approximately $49^{o,}$ while it was 41^o in the exterior shear span. Moreover, the angle of inclination of the failure crack was close to what was observed in simply-supported beams reinforced with FRP bars where the average crack inclination was 44^o with the longitudinal axis (Ahmed et al. 2010).

4.3 MID-SPAN DEFLECTION

Figure 4.3 shows the load-mid-span deflection relationship for all test beams of Series I in the span where failure took place. Generally, the typical load-deflection curve can be divided into two distinct stages, pre-cracking and post-cracking. In the first stage, there was insignificant deflection; however, the deflection increased after the formation of the first flexural crack in the beam. Since the slope of the load-deflection curve in the second stage depends on the axial stiffness of the flexural reinforcing bars of the test beams, beam SN-1.2-0.0-*d* showed the steepest post-cracking curve.

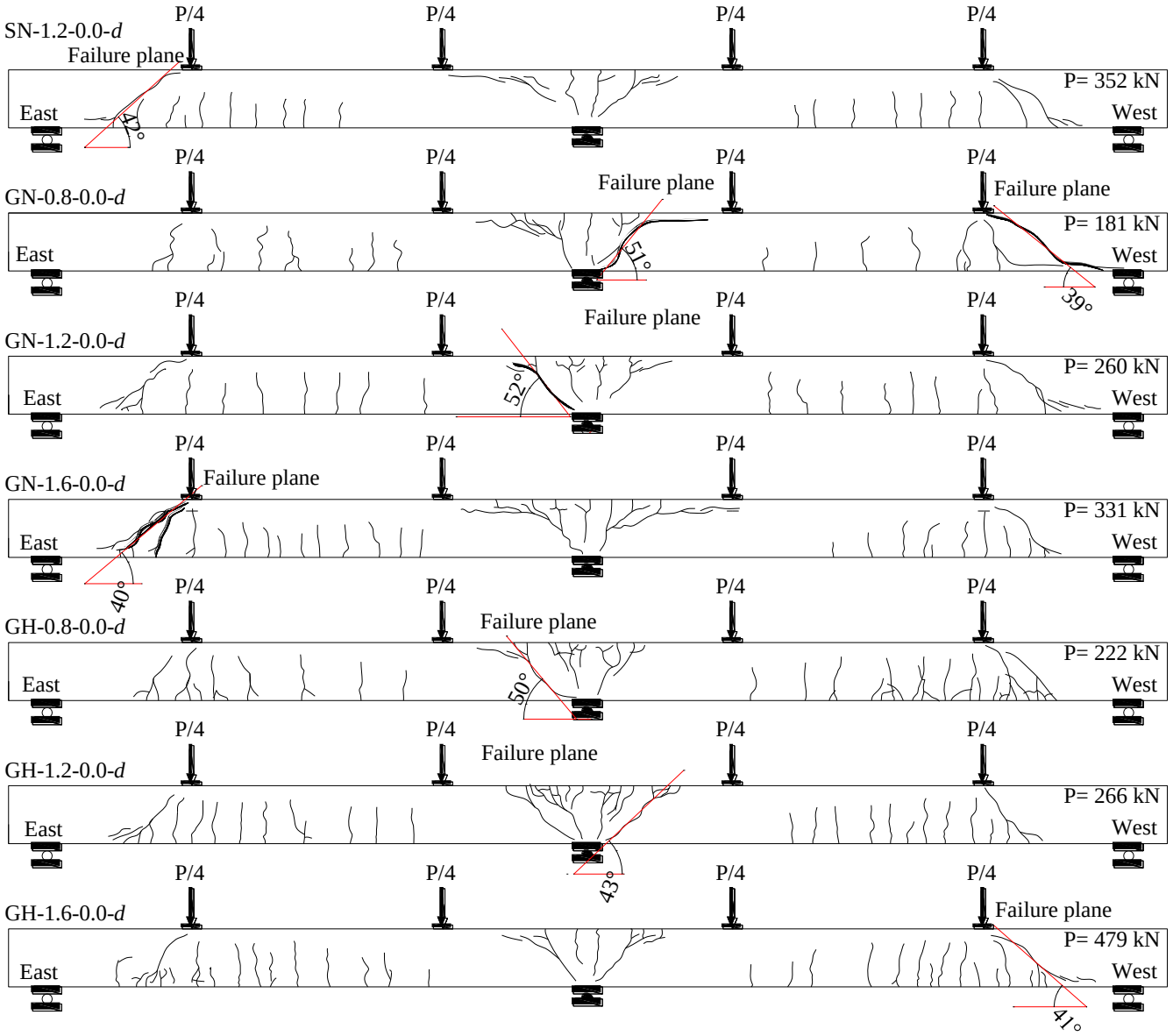

Figure 4.2: Cracking pattern at failure of beams of Series I

The NSC beams reinforced with GFRP bars followed the same trend where beam GN-1.6-0.0-*d* with higher axial stiffness showed steeper post-cracking curve than GN-1.2-0.0-*d* which, in turn, showed steeper curve than beam GN-0.8-0.0-*d*. The HSC beams exhibited similar behaviour compared to their NSC counterparts; however, the effect of increasing the concrete strength on the deflection was more pronounced. The slope of the load-deflection curve for the HSC beams was slightly steeper than that of their NSC counterparts.

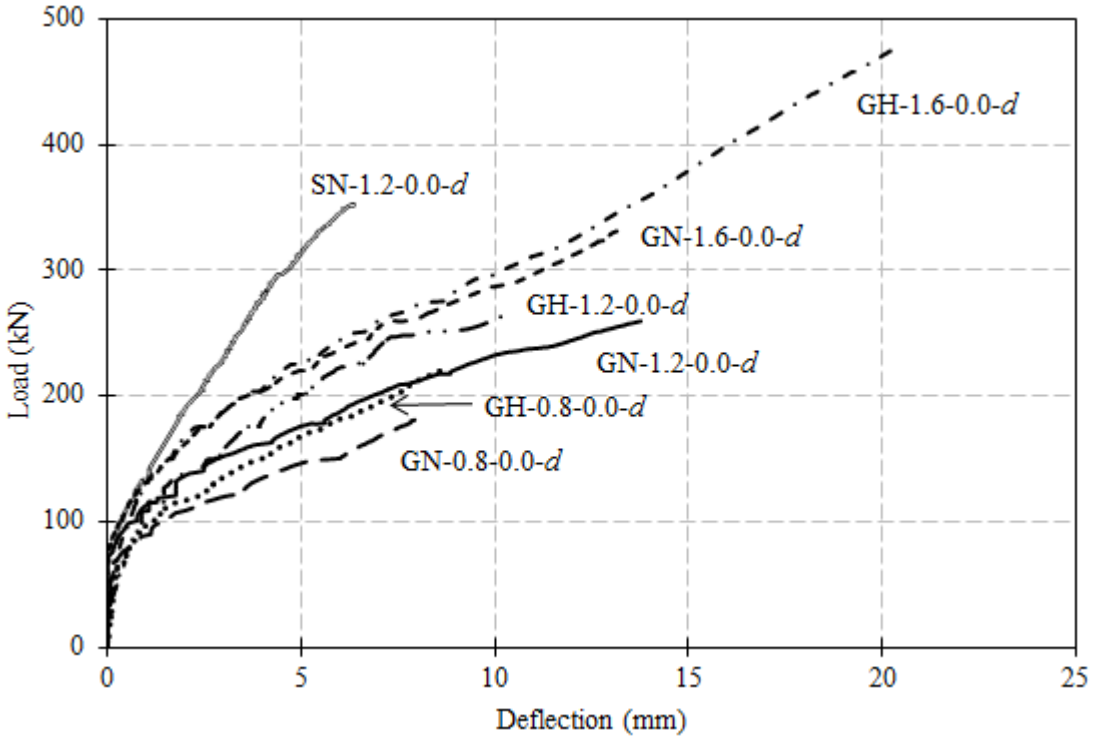

Figure 4.3: Load-deflection relationship at mid-span of beams of Series I

4.4 STRAIN IN LONGITUDINAL REINFORCEMENT AND CONCRETE

The measured tensile strains in GFRP bars and the compressive strains in concrete at the hogging and sagging moment sections, where failure took place, are shown in Figs. 4.4 and 4.5. It can be noticed that the tensile strains in the steel reinforcing bars of beam SN-1.2-0.0-*d*, in both hogging

and sagging moment sections, were less than the yield strain of the bars. The strains in the hogging and the sagging moment sections were 1,740 and 1,380 $\mu\varepsilon$, respectively. This was expected since the beam was designed to fail in shear. Similar strains in the hogging and sagging moment sections were reported in steel-RC continuous beams without transverse reinforcement where no yielding observed at the critical sections (Rodriguez et al. 1959).

In all Series I test beams reinforced with GFRP bars, the maximum recorded compressive strains in the concrete neither reached the specified crushing strain of 0.0035 by the CSA standards nor 0.003 by the ACI code. The maximum compressive strain in concrete, measured at the middle support section, was less than 2,000 $\mu\varepsilon$ in beam GH-1.6-0.0-*d*. Also, in the same beam, the compressive strain at the middle support section started to decrease at approximately 94% of the failure load. This might be attributed to the formation of a diagonal crack that was very close to the strain gauge location.

Regarding tensile strains, the figures show that the strains in FRP bars increased suddenly after concrete cracking. The value of the maximum measured strains in the longitudinal reinforcement in the hogging and sagging moment regions in each beam are listed in Table 4.1. The values measured in the hogging moment region were approximately 15, 10, 12, 16.5, 13 and 17% of the rupture strain of the used GFRP bars in beams GN-0.8-0.0-*d*, GN-1.2-0.0-*d*, GN-1.6-0.0-*d*, GH-0.8-0.0-*d*, GH-1.2-0.0-*d* and GH-1.6-0.0-*d*, respectively.

Furthermore, the strains in the longitudinal reinforcement and concrete over the middle support were greater than those at the sagging moment region. This can be attributed to the early formation and high intensity of flexural cracks over the middle support, which led to high tensile and compressive stresses in GFRP reinforcement and concrete, respectively.

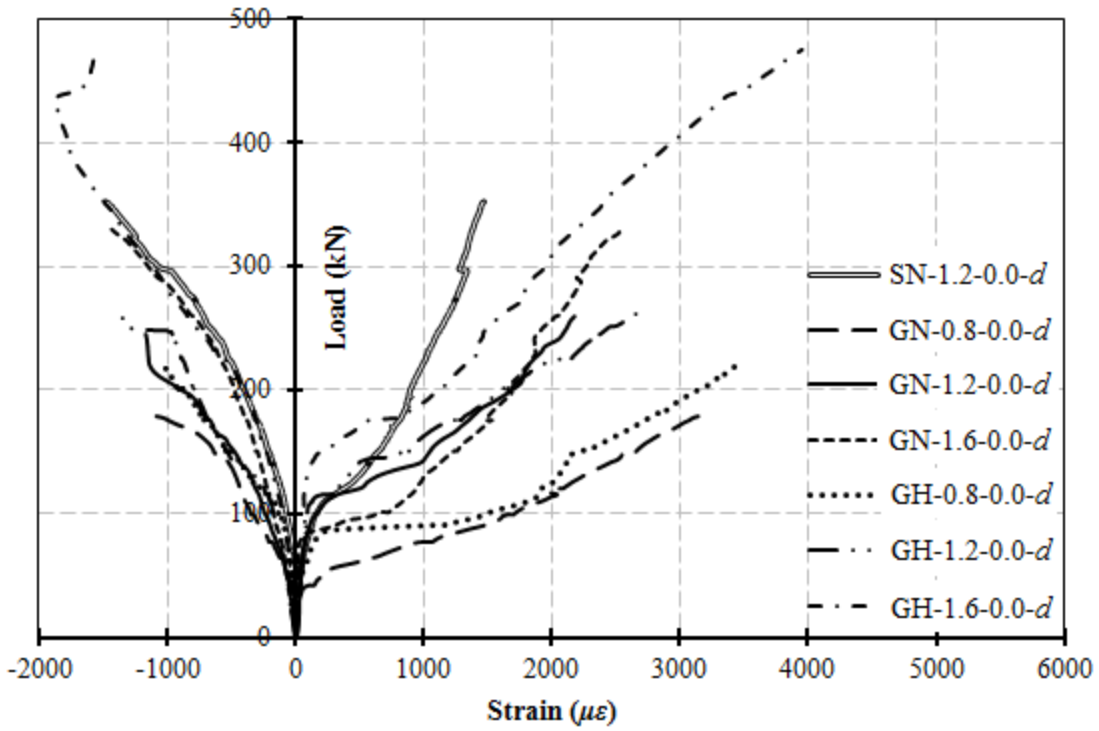

Figure 4.4: Load-strain relationship at the hogging moment section of beams of Series I

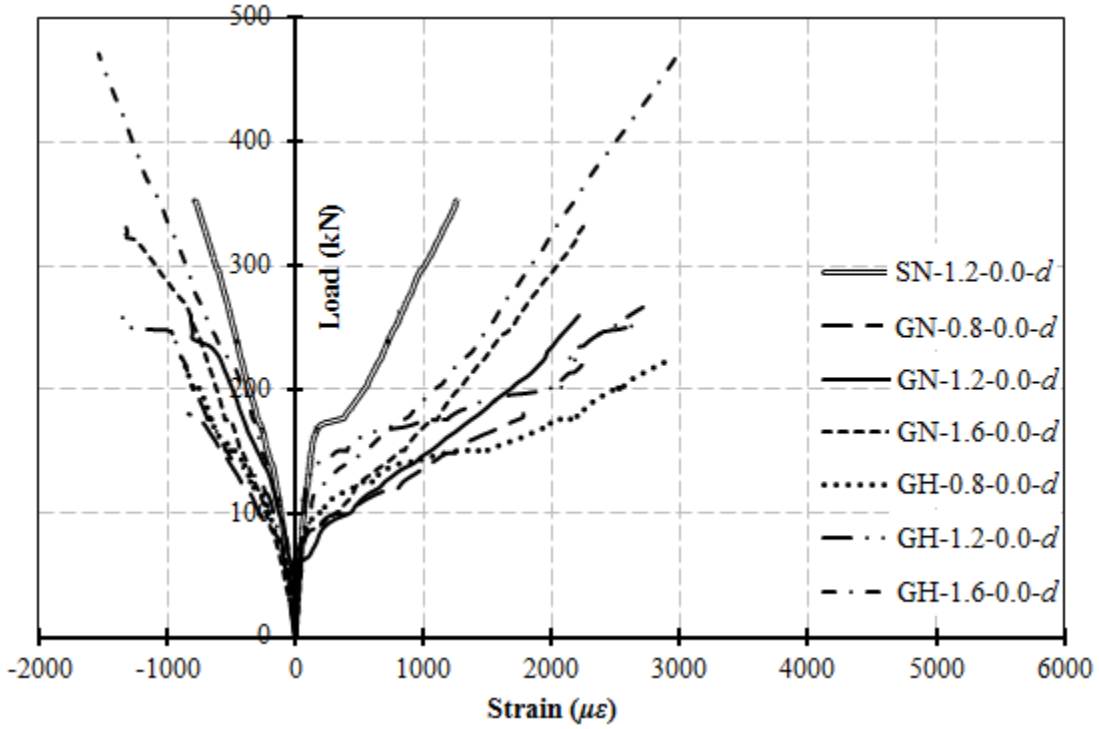

Figure 4.5: Load-strain relationship at the sagging moment section of beams of series I

Table 4.1: Cracking load and moments, strains and moment redistribution at failure

Beam	Cracking load (kN)	Failure moment (kN.m)		Concrete strains ($\mu\varepsilon$)		Reinforcement strains ($\mu\varepsilon$)		MR (%)
		Hogg.	Sagg.	Hogg.	Sagg.	Hogg.	Sagg.	
SN-1.2-0.0-*d*	110	51.9	52.1	1,480	790	1,470	1,250	28.3
GN-0.8-0.0-*d*	50	25.6	26.8	1,190	820	3,210	1,770	31.0
GN-1.2-0.0-*d*	65	37.7	38.6	1,170	810	2,180	2,210	29.4
GN-1.6-0.0-*d*	60	47.2	49.5	1,460	1,350	2,580	2,250	30.8
GH-0.8-0.0-*d*	90	36.4	31.9	1,050	870	3,470	2,880	20.8
GH-1.2-0.0-*d*	95	45.6	37.7	1,080	1,350	2,730	2,710	16.7
GH-1.6-0.0-*d*	90	73.3	70.2	1,880	1,530	3,530	2,990	25.5

4.5 REACTIONS AND MOMENT REDISTRIBUTION

In all test beams, the measured exterior reactions were used to calculate the bending moments and shear forces along the beam length. It was found out that the exterior reactions followed the elastic distribution at early stages of loading. After the formation of flexural cracks at the middle support region, the measured reactions started to have higher values than those obtained by the elastic distribution. These higher values continued until the failure of the beam as can be seen in Fig. 4.6. All NSC beams showed normal redistribution of bending moment from the hogging to the sagging moments regions of more than the assumed 20%. The percentage of moment redistribution of beams SN-1.2-0.0-*d*, GN-0.8-0.0-*d*, GN-1.2-0.0-*d* and GN-1.6-0.0-*d* were approximately 28, 31, 29 and 31%, respectively. On the other hand, the HSC beams exhibited smaller moment redistribution percentages than their NSC counterparts, which is in good agreement with previous studies (El-Mogy et al. 2013). The smaller moment redistribution

percentages in HSC beams could be attributed to the brittleness of the HSC compared to NSC. The moment redistribution percentage in beams GH-0.8-0.0-*d*, GH-1.2-0.0-*d* and GH-1.6-0.0-*d* was 20.8, 16.7 and 25.5%, respectively. The moments at the hogging moment section, sagging moment section and the moment redistribution percentages at failure are shown in Table 4.1. Again, for steel-RC continuous beams without shear reinforcement, Rodrigues et al. (1959) reported that the recorded middle support reaction slightly deviated from the elastic one. However, they added that only 1% change in the middle support reaction resulted in significant moment redistribution, 4%, from the hogging to the sagging moment region. This agrees well with the test results reported herein.

Regarding the carrying capacity of the test beams, the capacity can be attributed to two distinct factors. The first factor is related to the used materials, namely type and amount of longitudinal reinforcement and concrete compressive strength. The second factor is the percentage of moment redistribution in each beam. It is well-documented that beams with ability to redistribute higher moment percentages can carry more loads before failure. In the NSC beams, the increase in the longitudinal reinforcement ratio resulted in the majority of, if not all, the increase in the capacity of the beams since they all achieved similar moment redistribution percentages. In the HSC beams, however, the increase in the loading capacity was due to both the increase in the longitudinal reinforcement ratio and the high moment redistribution. Beam GH-1.6-0.0-*d*, which achieved 25.5% moment redistribution, showed an 80% increase in the loading capacity when compared to beam GH-1.2-0.0-*d* that exhibited 16.7% moment redistribution. However, this increase in the load carrying capacity was only 20% when beam GH-0.8-0.0-*d*, with 20.8% moment redistribution, was compared to beam GH-1.2-0.0-*d* with lower moment redistribution (16.7%).

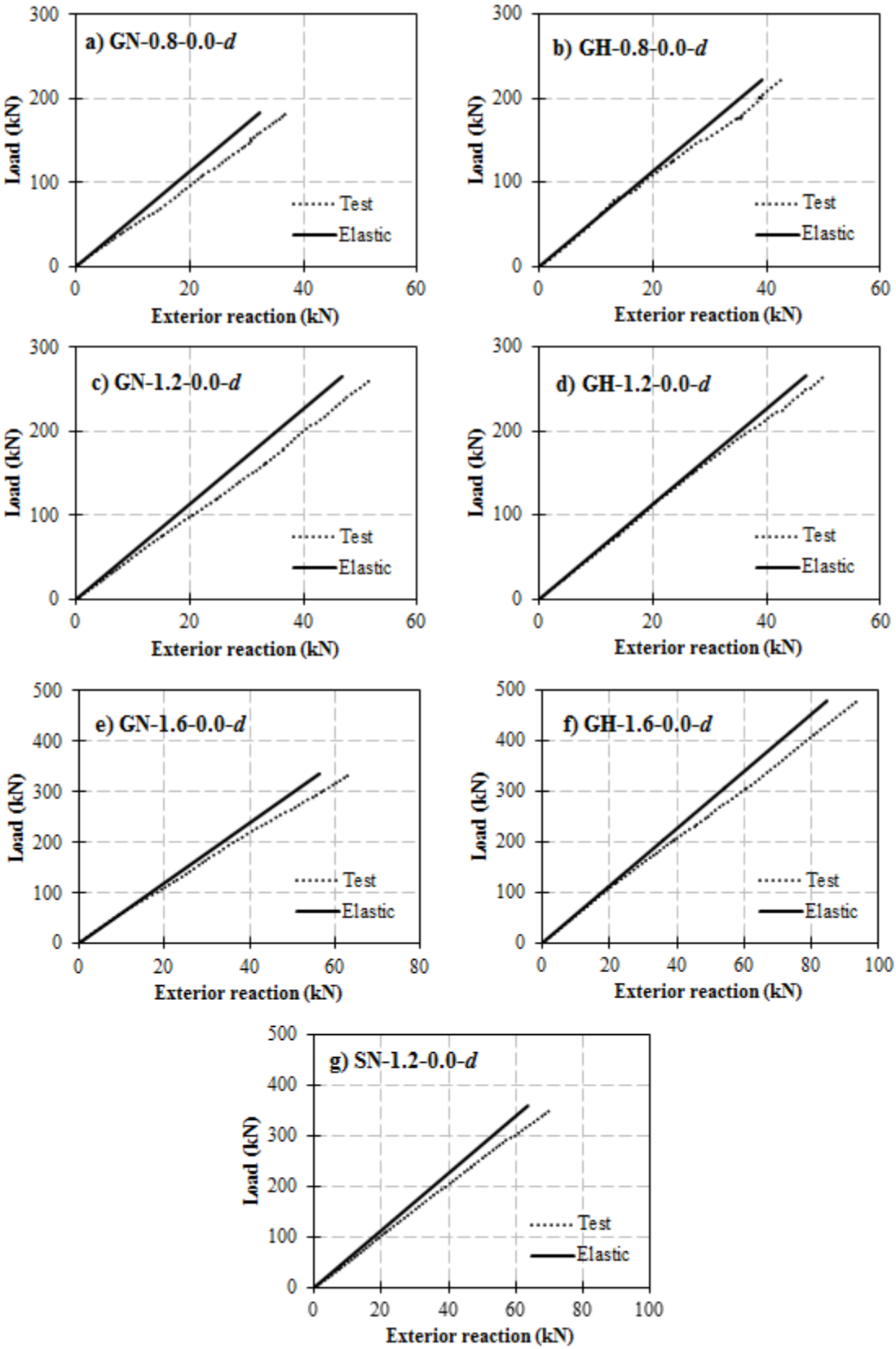

Figure 4.6: Load-exterior reaction relationship of beams of Series I

4.6 SHEAR CAPACITY

It is well-established that cracking of RC beams occurs when the principal stresses exceed the tensile strength of concrete. Also, the principal stresses, at any location along the beam, depend on the magnitude of the shear force and the bending moment at that location. Therefore, in addition to the factors that affect the shear strength of simple beams, the percentage of moment redistribution is a key factor for the shear strength of continuous beams. As a result, discussing the shear strength of continuous beams cannot be separated from the bending moments at the critical sections, which depend on the moment redistribution percentage.

In the control beam SN-1.2-0.0-*d*, the shear force in the interior shear span was 107 kN, which is 53% greater than that in the exterior shear span (70 kN). However, failure occurred in the exterior shear span. This can be attributed to the bending moment at the critical section in the exterior shear span, which was 70% higher than that in the interior one. This reflects the significant effect of the bending moment on the shear strength of RC beams. Similarly, beams GN-1.6-0.0-*d* and GH-1.6-0.0-*d* failed in the exterior shear span after significant moment redistribution. For these beams (SN-1.2-0.0-*d*, GN-1.2-0.0-*d* and GH-1.6-0.0-*d*), the moment-to-shear ratio (*M/V*) in the interior shear span at the critical section was smaller than that in beams failed in the interior shear span. In beam GN-0.8-0.0-*d*, the failure occurred simultaneously in the interior and exterior shear spans. This may be attributed to the high percentage of moment redistribution that resulted in a significant increase in the bending moment at the shear-critical section in the exterior shear span. The moment-to-shear ratio in both exterior and interior shear spans for all beams of Series I at failure is listed in Table 4.2. This ratio is constant for the exterior shear span (*M/V*= 0.474), while it varies in the interior shear span based on the moment redistribution percentage. The remaining beams, namely GN-1.2-0.0-*d*, GH-0.8-0.0-*d* and GH-

1.2-0.0-*d*, failed due to diagonal tension cracks in the interior shear span only. This is due to the high shear force and bending moment ratios at the shear-critical sections in the interior shear span that resulted in high *M/V* ratio.

Regarding the effect of the GFRP longitudinal reinforcement ratio, it was found out that the shear capacity increased by 42% (from 55 to 78.3 kN) when the longitudinal reinforcement ratio increased by 50% in NSC beams. Also, in HSC beams (GH-0.8-0.0-*d* and GH-1.2-0.0-*d*), the shear capacity increased by 20% for the same increase in the longitudinal reinforcement ratio. Moreover, increasing the longitudinal reinforcement ratio by 100% resulted in a 95% increase in the shear capacity of NSC beams (from 35.4 kN in beam GN-0.8-0.0-*d* to 69.1 kN in beam GN-1.6-0.0-*d*), considering the shear capacity in the exterior shear span. The same increase in the longitudinal reinforcement ratio in HSC beams, with high moment redistribution percentage (beam GH-1.6-0.0-*d*), changed the failure location as mentioned earlier. However, the shear force in the interior and exterior shear spans of beam GH-1.6-0.0-*d* were 2.1 and 2.2 times that in beam GH-0.8-0.0-*d*. Furthermore, the effect of the type of the reinforcing bars can be realized by comparing beams SN-1.2-0.0-*d* and GN-1.2-0.0-*d*, where replacing the steel bars with similar area of GFRP bars changed the failure location. Also, the load capacity of the steel-reinforced beam (SN-1.2-0.0-*d*) was approximately 35% higher than that of beam GN-1.2-0.0-*d*.

Moreover, the concrete strength had a pronounced effect on the shear strength of the test beams where increasing the concrete strength from 39 to 70 MPa, resulted in an increase in the shear capacity of approximately 25% and 33% in beams with 0.8% and 1.6% longitudinal reinforcement ratio, respectively. The same increase in the concrete strength, in beams with 1.2% longitudinal reinforcement ratio resulted in a slight increase of the shear capacity by approximately 5.7%. This can be attributed to the high moment redistribution in beam GN-1.2-

0.0-*d* (29%) compared to the moment redistribution in beam GH-1.2-0.0-*d* (16.7%). The highest increase in shear capacity was in beams having longitudinal reinforcement ratio of 1.6% that exhibited similar percentages of moment redistribution. Therefore, the increase in the shear capacity would be higher in beams with lower longitudinal reinforcement ratios, if they achieve similar moment redistribution percentages.

Table 4.2: Shear and bending moment at the critical shear sections at failure of Series I

Beam	f_c' (MPa)	Shear, V_{test}, (kN)		Moment, M_{test}, (kN.m)		Moment-to-shear ratio, M/V, (m)	
		Int.	Ext.	Int.	Ext.	Int.	Ext.
SN-1.2-0.0-*d*	45	107.4	70.2	19.7	33.3	0.183	0.474
GN-0.8-0.0-*d*	39	55.0	35.4	9.1	16.8	0.165	0.474
GN-1.2-0.0-*d*	39	78.3	51.4	14.2	24.4	0.181	0.474
GN-1.6-0.0-*d*	39	102.8	69.1	16.4	32.8	0.160	0.474
GH-0.8-0.0-*d*	72	69.0	42.5	15.7	20.2	0.228	0.474
GH-1.2-0.0-*d*	72	82.8	50.2	20.8	23.85	0.251	0.474
GH-1.6-0.0-*d*	70	144.8	92.3	29.9	43.8	0.206	0.474

4.7 COMPARISION BETWEEN EXPERIMENTAL AND PREDICTED SHEAR STRENGTH

The ACI 318-14 (ACI Committee 318 2014) was used to predict the shear strength of the control beam SN-1.2-0.0-*d*. It was found out that the experimental-to-predicted shear strength ratio was approximately 1.25. This ratio for a large number of shear tests conducted on simply-supported beams was 1.4 (Bentz et al. 2006). This slight reduction of the experimental-to-predicted shear strength can be attributed to the continuity effect and this agrees with the conclusions of Rodrigues et al. (1959). Also, the CSA/A23.3-14 (CSA 2014) underestimated the shear strength of beam SN-1.2-0.0-*d*, where the experimental-to-predicted shear strength ratio was 1.35.

Table 4.3 shows the experimental shear strength of the GFRP–RC test beams at failure locations and the predicted shear strength by the ACI 440.1R-06, CSA/S806-02, CSA/S806-12 and CSA/S6-06. The experimental shear capacity of each beam is the shear force in the shear span where the beam failed. The Canadian standards CSA/S806-12 predicted well the experimental shear strength, where the ratio of experimental-to-predicted capacity is 1.03. This ratio is 1.16 on average for simply-supported beams (Yost et al. 2001; Razaqpur et al. 2004; El-Sayed et al. 2005; El-Sayed et al. 2006a &b; Alam and Hussein 2012). This means that continuity has a significant effect on the shear strength of such beams. Moreover, it can be noted that the CSA/S806-12 overestimated the shear capacity of beams with 0.8% longitudinal reinforcement ratio (GN-0.8-0.0-*d* and GH-0.8-0.0-*d*). The opposite can be noted in beams GN-1.2-0.0-*d*, GN-1.6-0.0-*d* and GH-1.6-0.0-*d*.

Regarding the previous version of the CSA/S806 (CSA 2002), it was found out that the ratio of the experimental-to-predicted shear capacity is 1.28, which is close to that of simply-supported

beams, 1.21 (Yost et al. 2001). This might be attributed to the fact that the shear equation in CSA/S806-02 accounts for the straining actions at the section in terms of the square root while in CSA/S806-12 it is a function of the cubic root which, in turn, resulted in a higher shear capacity.

Furthermore, the CSA/S6-06 (2009) and the second-order expression for shear proposed by Hoult et al. (2008) were also used to calculate the shear strength of the test beams. The predicted shear capacities according to the CSA/S6-06 (2009) were conservative where the ratio of the experimental-to-predicted capacity was 1.66. This ratio was reduced to 1.28 when Hoult et al.'s expression for shear was used. However, this ratio was 1.38 and 1.15 for the results of 146 simply-supported beams (Hoult et al. 2008) using the CSA/S6-06 (2009) and the second-order expression, respectively.

The ACI 440.1R-06 yields very conservative predictions of concrete contribution to the shear strength where the ratio of the experimental-to-predicted capacity is 2.37 which is less than that of simply-supported beams (3.06) reported by Yost et al. (2001).This reduction in the margin of safety from 3.06 to 2.23 can be attributed to the fact that the shear design equation in the ACI 440.1R-06 design guidelines does not account for the straining actions at the critical section.

Table 4.3: Comparison of experimental and predicted shear strength of beams of series I

Beam	Shear Capacity, V_{test}, (kN)	Predicted shear capacity							
		ACI 440.1R-06		CSA/S806-02		CSA/S806-12		CSA/S6-06	
		V_{pred} (kN)	$\frac{V_{test}}{V_{pred}}$	V_{pred} (kN)	$\frac{V_{test}}{V_{pred}}$	V_{pred} (kN)	$\frac{V_{test}}{V_{pred}}$	V_{pred} (kN)	$\frac{V_{test}}{V_{pred}}$
GN-0.8-0.0-*d*	55.0*	21.6	2.55	48.5	1.13	62.3	0.88	38.0	1.45
	35.4†	21.6	1.64	39.1	0.91	50.8	0.70	31.8	1.11
GN-1.2-0.0-*d*	78.3*	25.9	1.98	55.5	1.41	62.3	1.26	44.6	1.75
GN-1.6-0.0-*d*	69.1†	29.4	2.35	49.3	1.40	62.3	1.11	42.3	1.63
GH-0.8-0.0-*d*	69.0*	25.2	2.7	55.9	1.23	77.3	0.89	39.3	1.76
GH-1.2-0.0-*d*	82.8*	30.3	2.73	64.0	1.29	77.3	1.07	46.2	1.79
GH-1.6-0.0-*d*	92.3†	34.6	2.67	56.9	1.62	72.2	1.27	44.2	2.1
Mean			2.37		1.28		1.03		1.66
COV (%)			17.6		17.7		20.6		18.7

* shear capacity in the interior shear span at failure;

† shear capacity in the exterior shear span at failure;

§ Shear capacity according to the ACI 440.1R-06 is the same for interior and exterior shear spans

CHAPTER 5: RESULTS AND DISCUSSIONS OF SERIES II

5.1 GENERAL

This series investigates the size effect on the shear strength of GFRP-RC continuous beams. To achieve this purpose, the test results of four beams from Series I and eight new beams of large size are presented. The test variables are the effective depth of the beam, the longitudinal reinforcement ratio and the concrete strength. The main aim of this series is to evaluate the size effect on the shear strength of GFRP-RC continuous beams without transverse reinforcement as currently there is no data available on this issue. In this series, the monitored data were the deflections at three different locations in each span, the strains in both reinforcement and concrete at critical sections, the reactions at the exterior supports, and the diagonal crack width in the exterior and interior shear spans. The complete behaviour of the test beams, in terms of failure mode, cracking patterns, load-deflection curves, and strains in the reinforcing bars and in concrete surface, moment redistribution and shear strength of the test beams are discussed. Moreover, a comparison between the experimental and predicted shear strength by the relevant design codes and guidelines is presented in this chapter.

5.2 GENERAL BEHAVIOUR, CRACKING AND MODE OF FAILURE

In small and medium size beams, vertical flexural cracks were observed first at the hogging moment region followed by similar flexural cracks at the sagging moment region in both spans. However, for all large size beams, these flexural cracks initiated simultaneously in the hogging and sagging moment regions. As the load increased, these flexural cracks propagated towards the compression zones while new flexural cracks developed in the shear spans. It was observed that the number of flexural cracks in the sagging moment region increased as the effective depth

increased. Further increase in the load resulted in the development of diagonal cracks, extending form flexural crack developed in the shear spans. All test beams of Series II failed in shear due to a main diagonal tension crack developed in the interior, exterior or both shear spans simultaneously. Beams GN-1.2-0.0-*d*, GH-0.8-0.0-*d*, GH-1.2-0.0-*d* and GH-1.2-0.0-3*d* failed in the interior shear span, near the middle support, while beam GN-0.8-0.0-2*d* failed due to a suddenly formed diagonal tension crack in the interior shear span near the loading point. On the other hand, beams GH-0.8-0.0-2*d*, GN-1.2-0.0-3*d* and GH-0.8-0.0-3*d* failed in the exterior shear span. The failure of beams GN-0.8-0.0-*d*, GN-1.2-0.0-2*d*, GH-1.2-0.0-2*d* and GN-0.8-0.0-3*d* was due to two simultaneous diagonal tension cracks, one was in the interior shear span and the other was in the exterior shear span. Photos of all test beams at failure are shown in Fig. 5.1 and 5.2.

Also, schematic drawings of the cracking pattern of all Series II test beams at failure are shown in Figs. 5.3 and 5.4. In beams with 250 mm depth (GN-0.8-0.0-*d*, GN-1.2-0.0-*d*, GH-0.8-0.0-*d* and GH-1.2-0.0-*d*), the majority of cracks were vertical flexural cracks concentrated in the maximum moment regions. Also, there were few diagonal cracks formed near failure of the beams. Similar cracking pattern was observed in medium and large size beams (GN-0.8-0.0-2*d*, GN-1.2-0.0-2*d*, GH-0.8-0.0-2*d*, GH-1.2-0.0-2*d*, GN-0.8-0.0-3*d*, GN-1.2-0.0-3*d*, GH-0.8-0.0-3*d* and GH-1.2-0.0-3*d*); however, flexural cracks formed near the interior loading point and diagonal cracks were observed in the interior shear spans. Also, as the effective depth increases, secondary flexural cracks (shallower than the major flexural cracks developed earlier) initiated in both the hogging and sagging moment regions. Furthermore, with increasing the effective depth, the cracking pattern became similar to that of a simply-supported beam where more flexural and diagonal cracks were observed near the interior loading point.

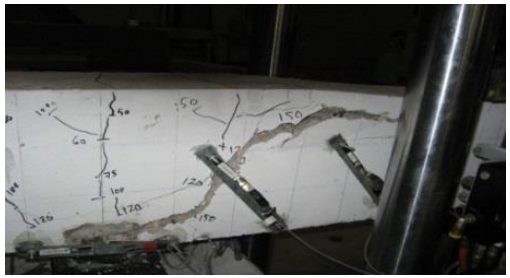

(a) GN-0.8-0.0-*d*, int. shear span

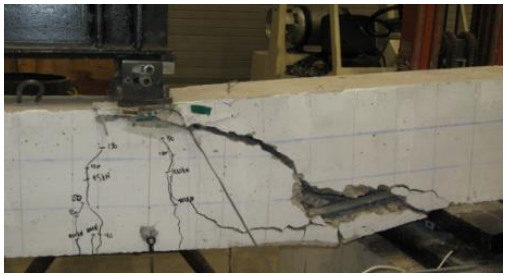

(b) GN-0.8-0.0-*d*, ext. shear span

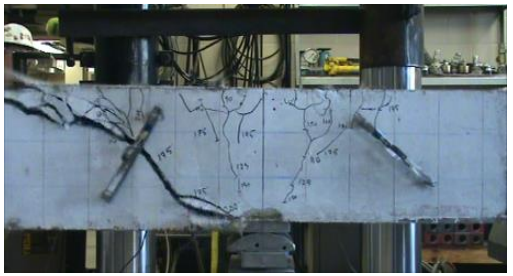

(c) GH-0.8-0.0-*d*, int. shear span

(d) GN-0.8-0.0-2*d*, int. shear span

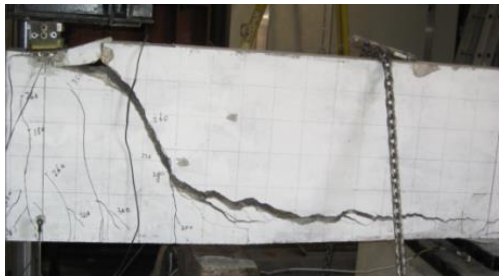

(e) GH-0.8-0.0-2*d*, ext. shear span

(f) GN-0.8-0.0-3*d*, ext. shear span

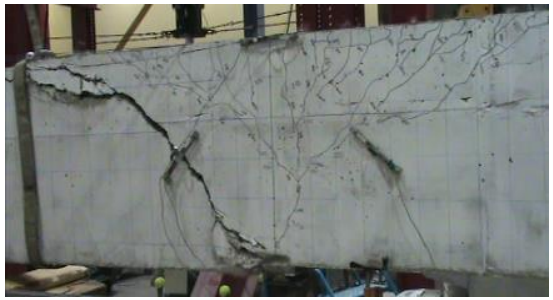

(g) GN-0.8-0.0-3*d*, int. shear span

(h) GH-0.8-0.0-3*d*, ext. shear span

Figure 5.1: Photos for Series II beams with 0.8% reinforcement ratio at failure

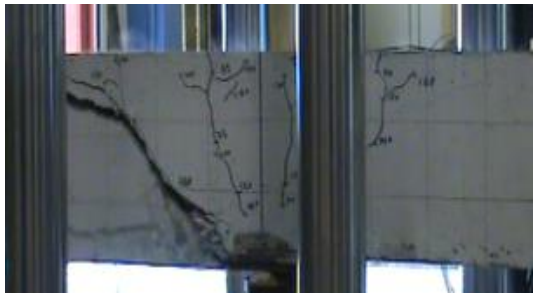

(a) GN-1.2-0.0-*d*, ext. shear span

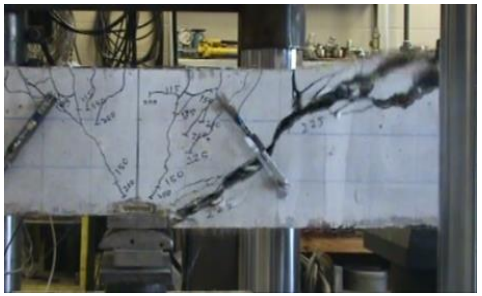

(b) GH-1.2-0.0-*d*, int. shear span

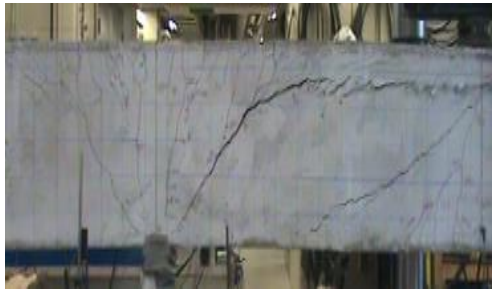

(c) GN-1.2-0.0-2*d*, int. shear span

(d) GN-1.2-0.0-2*d*, ext. shear span

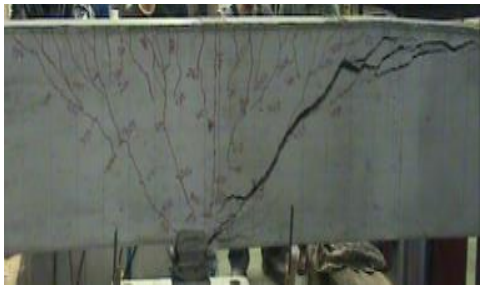

(e) GH-1.2-0.0-2*d*, int. shear span

(f) GH-1.2-0.0-2*d*, ext. shear span

(g) GN-1.2-0.0-3*d*, ext. shear span

(h) GH-1.2-0.0-3*d*, Int. shear span

Figure 5.2: Photos for Series II beams with 1.2% reinforcement ratio at failure

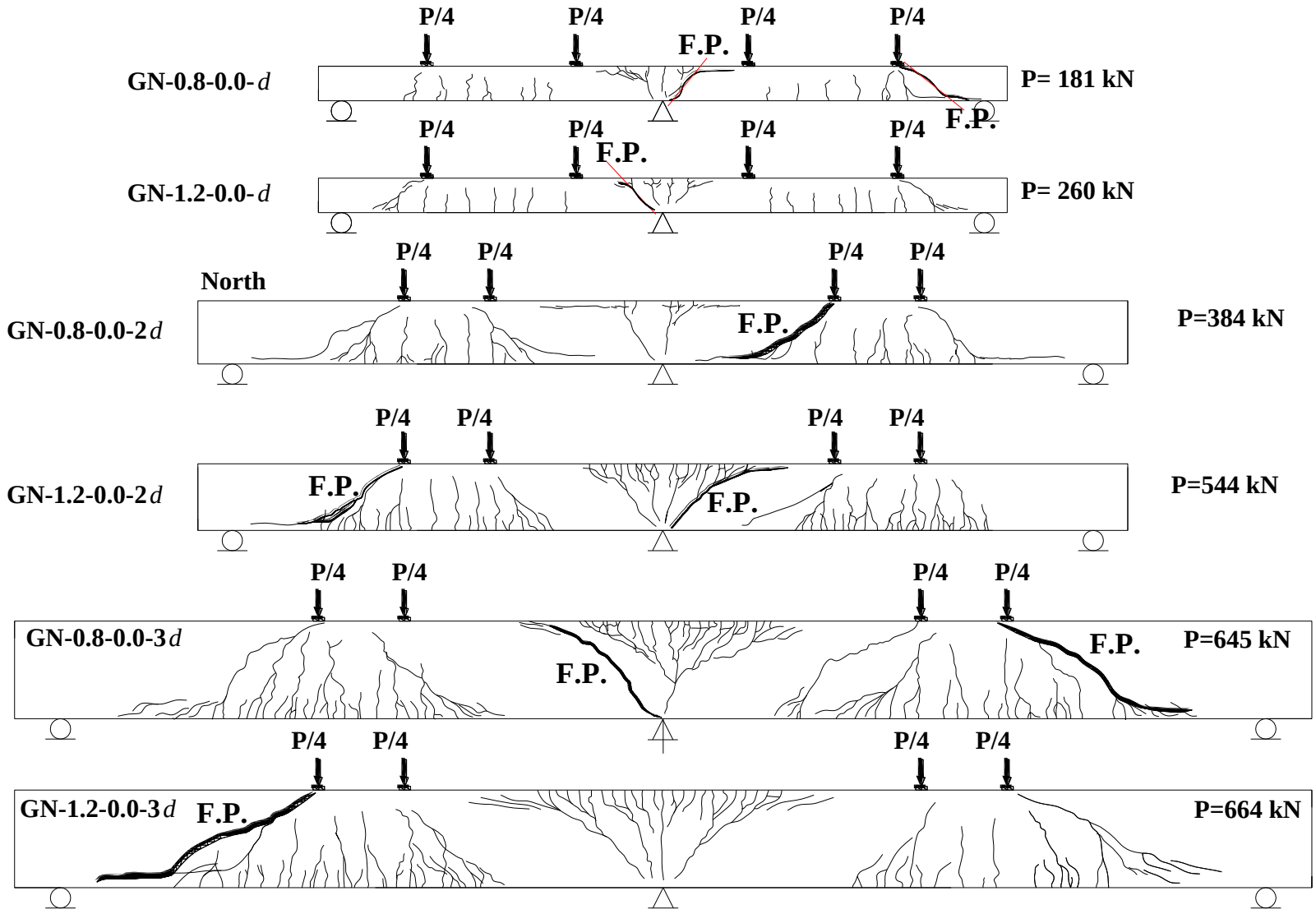

Figure 5.3: Cracking pattern at failure of NSC beams of Series II

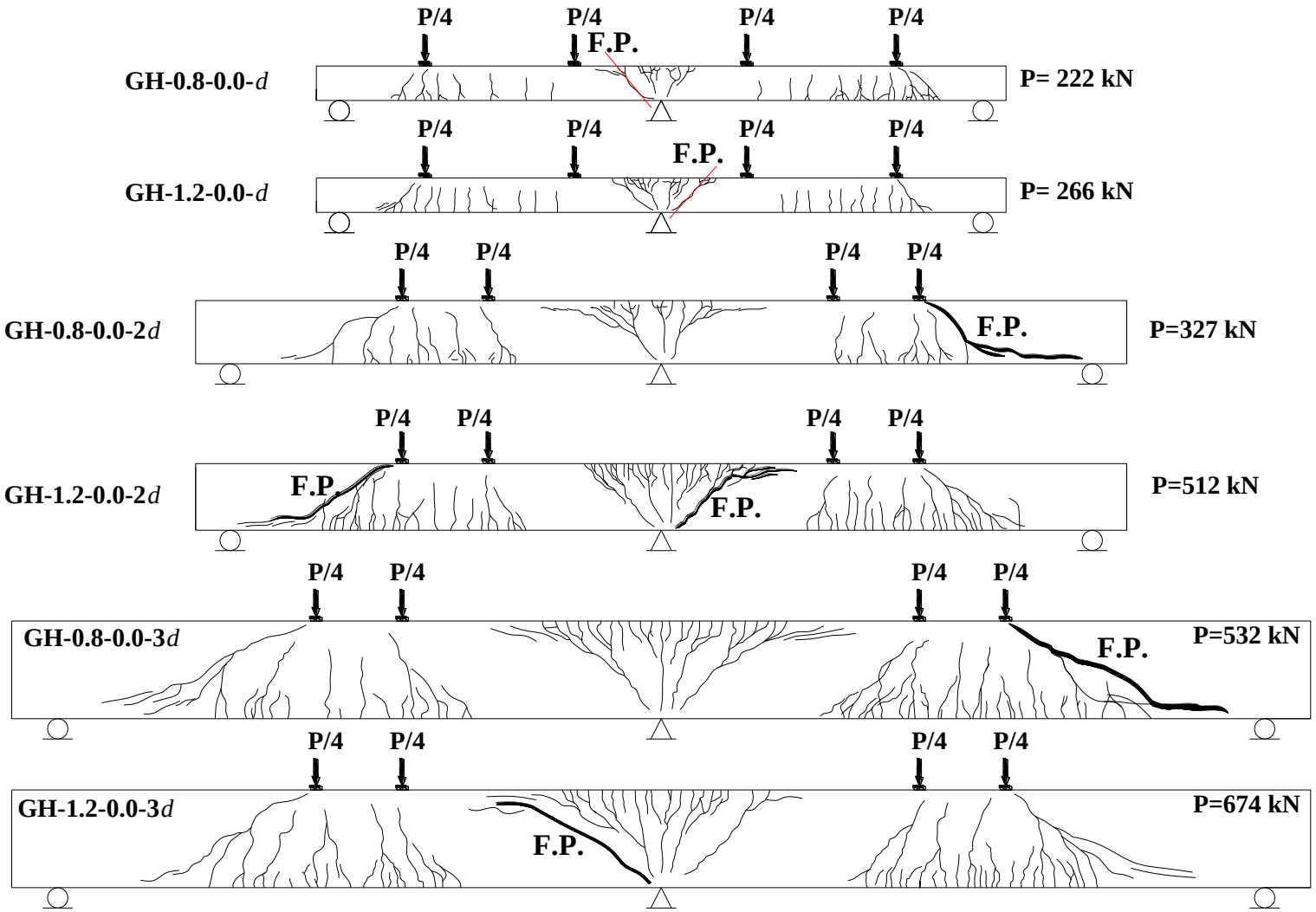

Figure 5.4: Cracking pattern at failure of HSC beams of Series II

5.3 DEFLECTION

Figures 5.5 and 5.6 show the load-deflection relationship at mid-span of all test beams in the span where failure took place. Generally, the typical load-deflection curve can be divided into two distinct stages, pre-cracking and post-cracking. In the pre-cracking stage, the measured deflection was insignificant in all beams; however, the deflection increased after the formation of the first flexural crack in the beam. At the beginning of the post-cracking stage, the development of additional cracks resulted in a decrease in the flexural stiffness of the beams; then, the behaviour of the beams became approximately linear until failure. It can be seen that the size of the beam did not affect the slope of the load-deflection graph in the post-cracking stage which was similar for beams having similar longitudinal reinforcement ratio, until failure. As expected, increasing the longitudinal reinforcement ratio/rigidity and the concrete strength increased the post-cracking flexural stiffness.

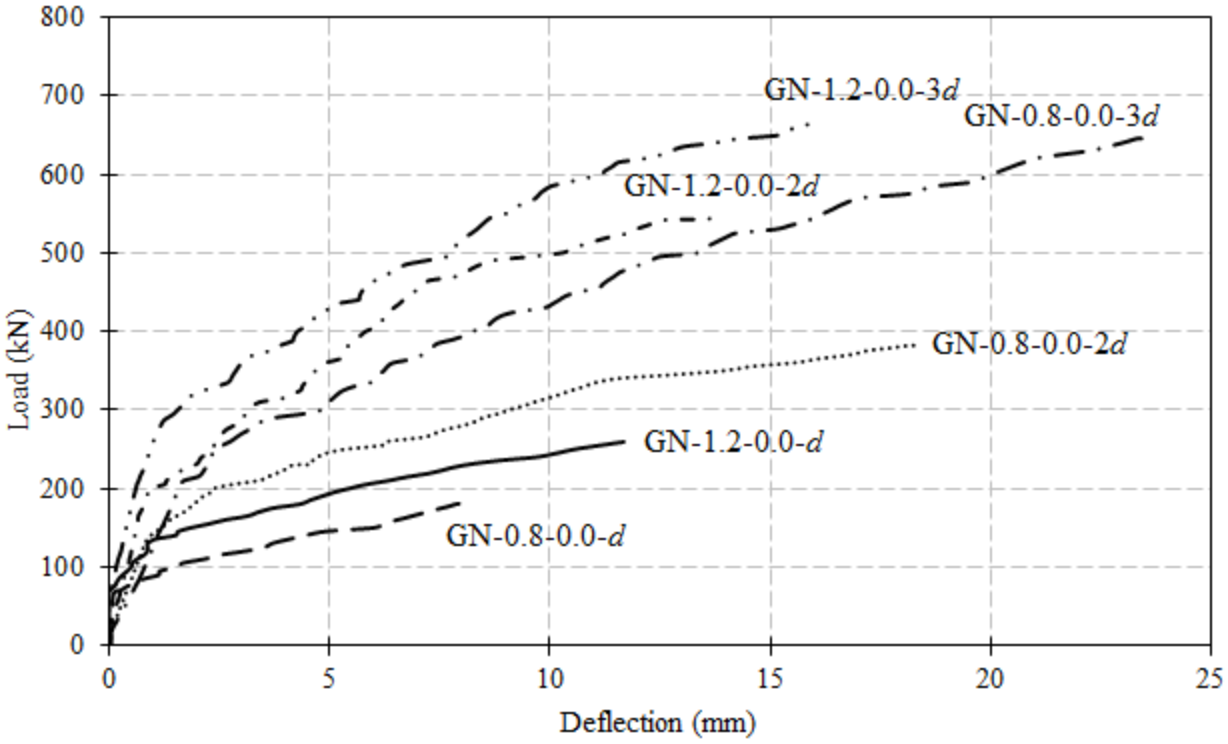

Figure 5.5: Load-deflection relationship at mid-span of NSC beams of Series II

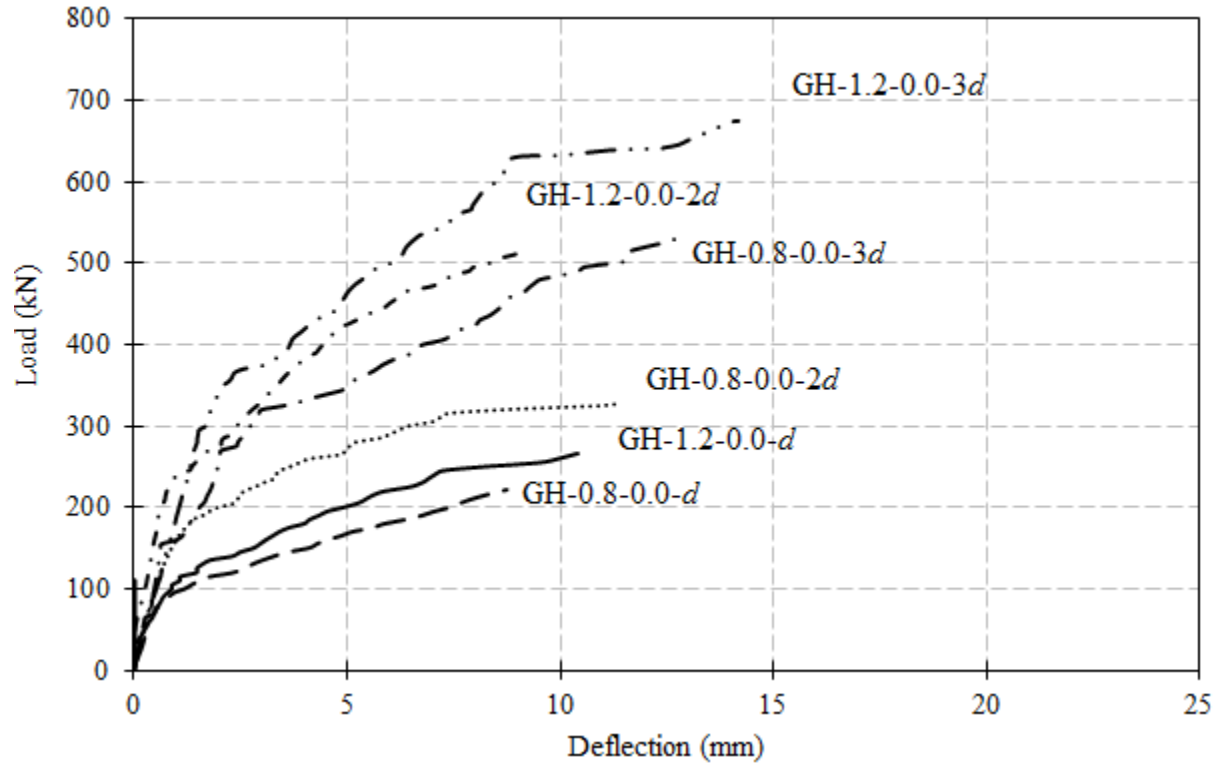

Figure 5.6: Load-deflection relationship at mid-span of HSC beams of Series II

5.4 STRAINS IN LONGITUDINAL REINFORCEMENT AND CONCRETE

The variation of strain in reinforcing bars and concrete at the hogging and sagging moment sections for all Series II test beams are shown in Figs 5.7 to 5.10. At failure, the maximum measured strains in all beams were well below the rupture strain of the used GFRP bars. This was expected since the sections were over-reinforced and the moment at failure was small compared to the flexural capacity of the sections as provided in Table 5.1. A maximum strain of 3,580 $\mu\varepsilon$ was measured in the hogging moment region in beam GH-1.2-0.0-2*d*. This strain represents approximately 17% of the rupture strain of the used GFRP bars. Also, the strains at the hogging moment region were greater than those at the sagging moment region. Moreover, it can be seen that the strains in the HSC beams were greater than those in NSC beams. Furthermore, increasing the effective depth in NSC beams had insignificant effect on the tensile strains at the hogging moment section. On the other hand, the tensile strains at the sagging moment section increased with increasing the depth. This can be attributed to the wide cracks observed in the sagging moment regions in medium and large size beams.

Also, because of the small failure moments compared to the flexural capacity, the compressive strains in concrete at both hogging and sagging moment sections were of small values. In all test beams, the maximum recorded compressive strains in concrete neither reached the specified crushing strain of 0.0035 by the CSA standards nor 0.003 by the ACI code. The maximum compressive strain in concrete was 2,950 $\mu\varepsilon$ measured at the sagging moment section in beam GN-1.2-0.0-2*d*.

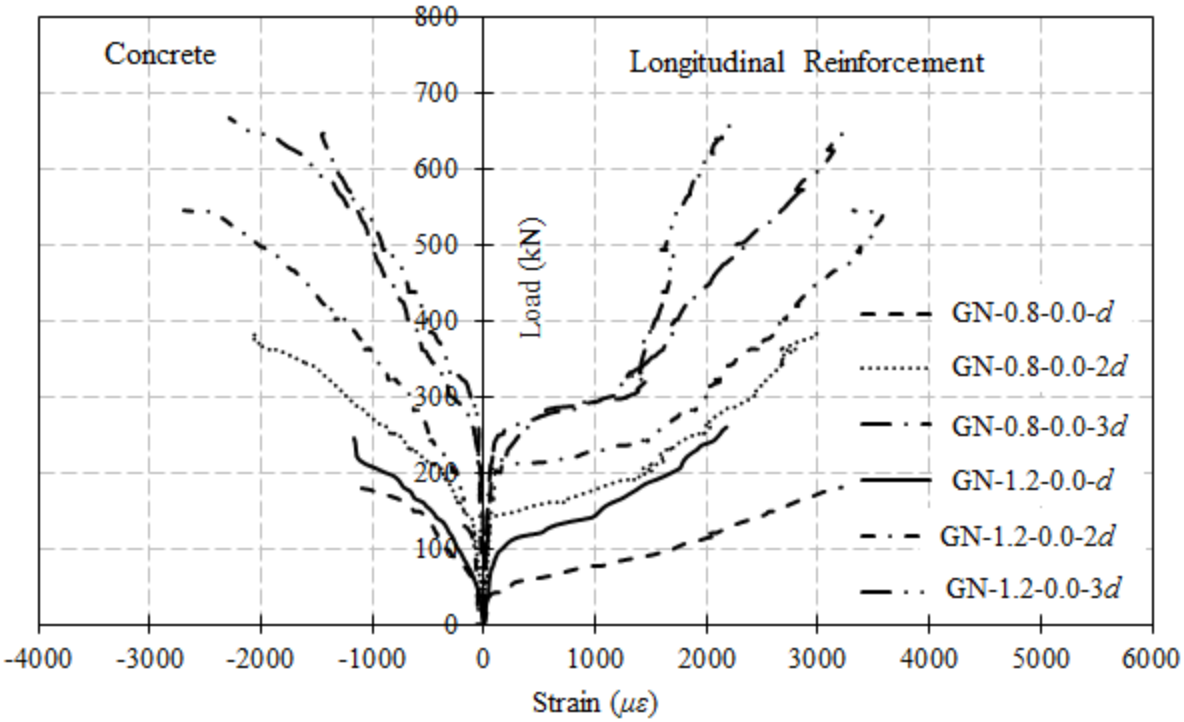

Figure 5.7: Load-strain relationship at the hogging moment section of NSC beams of Series II

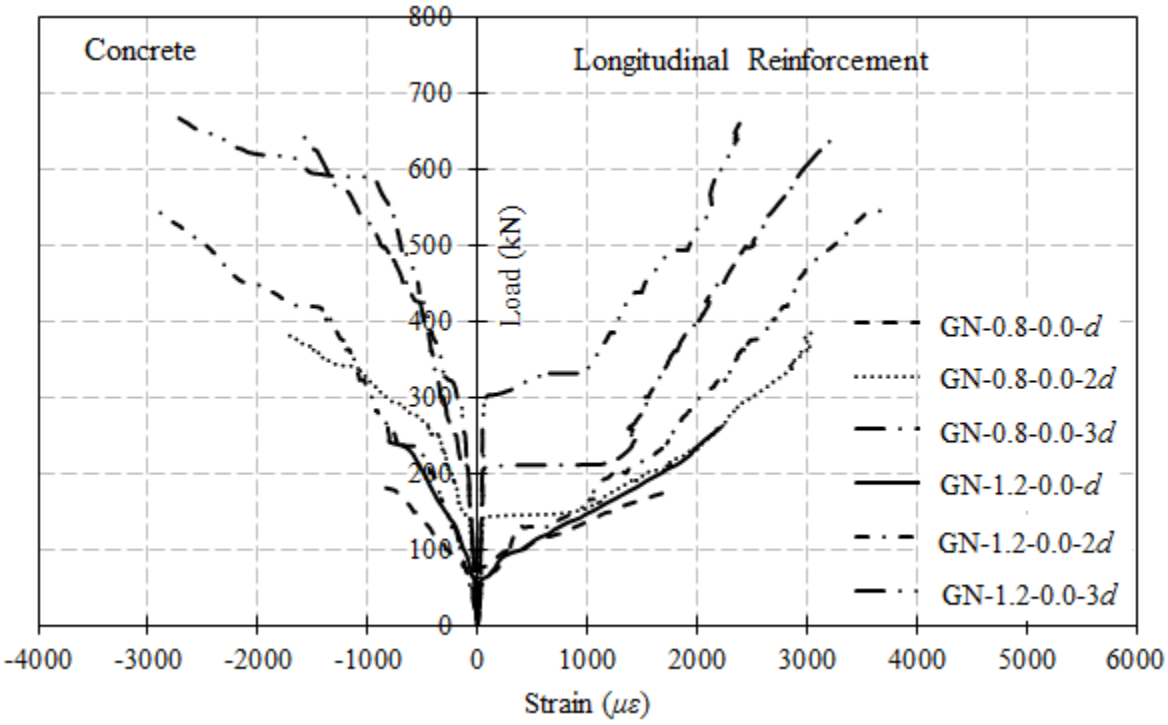

Figure 5.8: Load-strain relationship at the sagging moment section of NSC beams of Series II

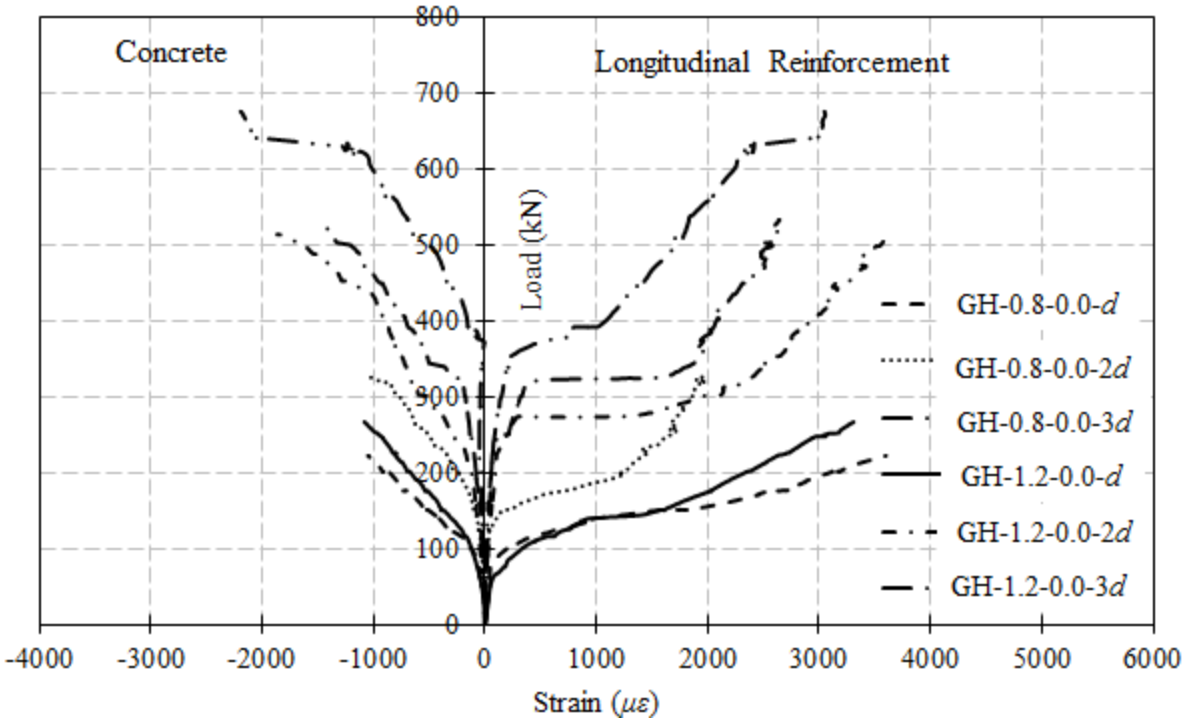

Figure 5.9: Load-strain relationship at the hogging moment section of HSC beams of Series II

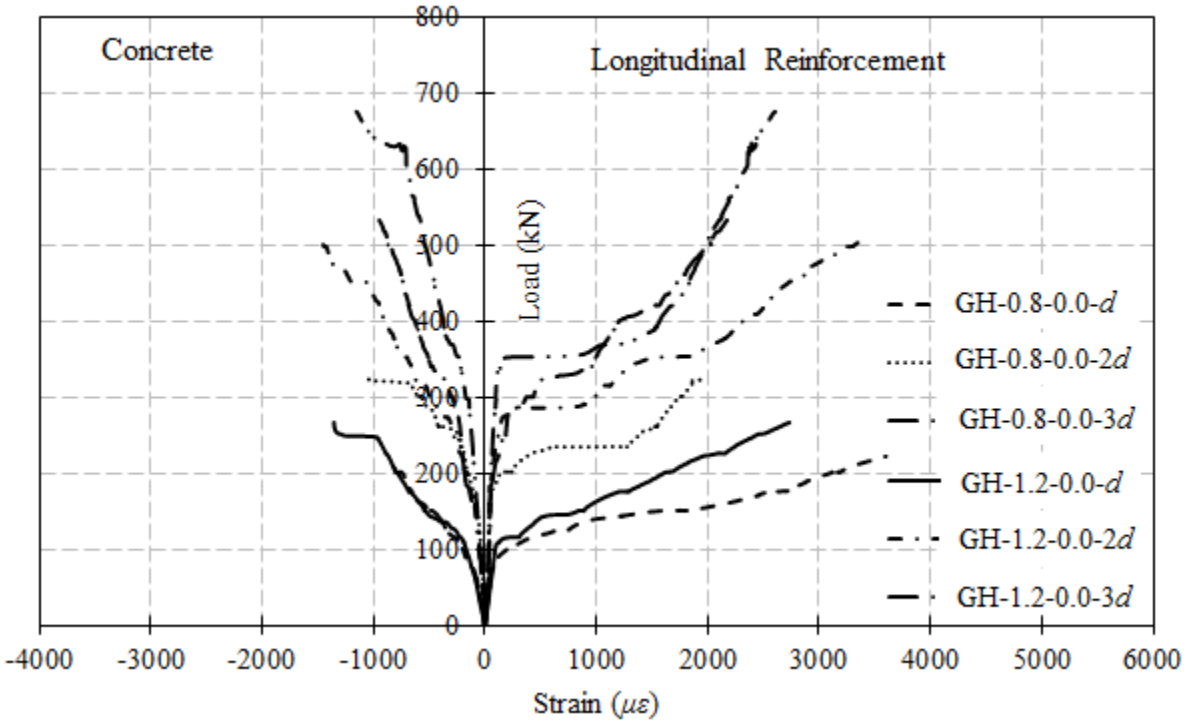

Figure 5.10: Load-strain relationship at the sagging moment section of HSC beams of Series II

5.5 REACTIONS AND MOMENT REDISTRIBUTION

The measured exterior reactions were used to calculate the shear force and bending moment distribution along the beam. The moment redistribution was then calculated based on the actual and theoretical bending moment at failure. In beams having 250 and 500 mm depth, the exterior reaction followed the elastic distribution at early stages of loading. After the formation of flexural cracks at the middle support region, the measured end reactions started to have higher values than those obtained theoretically by the elastic theory. This trend continued until failure of the beam as can be seen in Figs. 5.11 and 5.12. Higher exterior reactions than the elastic ones means normal redistribution of bending moment occurred from hogging to sagging moment regions. The percentage of moment redistribution in beams GN-0.8-0.0-*d*, GN-0.8-0.0-2*d*, GN-1.2-0.0-*d*, GN-1.2-0.0-2*d*, GH-0.8-0.0-*d*, GH-0.8-0.0-2*d*, GH-1.2-0.0-*d* and GH-1.2-0.0-2*d*, from hogging to sagging moment regions, was approximately 31, 6.6, 29.4, 8.1, 20.8, 17.4, 16.7 and 11.0%, respectively. This behaviour agrees well with the findings of the recent research conducted on continuous beams reinforced with FRP bars (Kara and Ashour 2013; El-Mogy et al. 2010 & 2011).

On the other hand, large size beams GN-0.8-0.0-3*d*, GN-1.2-0.0-3*d*, GH-0.8-0.0-3*d* and GH-1.2-0.0-3*d*, showed significantly different behaviour after cracking of critical sections where the exterior reactions were of smaller values compared to those calculated by the elastic theory. This behaviour continued until the failure of the beams resulting in reversed moment redistribution from sagging to hogging moment regions. The percentage of moment redistribution at failure was -7.0, -9.0, -17.0 and -14.3% in beams GN-0.8-0.0-3*d*, GN-1.2-0.0-3*d*, GH-0.8-0.0-3*d* and GH-1.2-0.0-3*d*, respectively. The reversed moment redistribution in these beams can be attributed to the cracking pattern in those large size beams. The first cracks occurred in both

hogging and sagging moment regions simultaneously, followed by extensive flexural cracking in the sagging moment regions while no more cracks formed in the hogging moment region. The moments at hogging and sagging moment sections and moment redistribution percentages at failure are listed in Table 5.1.

Table 5.1: Flexural capacity, failure moments and moment redistribution at failure

Beam	Flexural capacity, $M_{flex.}$, (kN.m)	Failure moment				Moment Redistribution (%)
		Hogging		Sagging		
		M_{test} (kN.m)	$M_{test}/M_{flex.}$	M_{test} (kN.m)	$M_{test}/M_{flex.}$	
GN-0.8-0.0-*d*	79.3	25.6	0.32	26.8	0.34	31.0
GN-0.8-0.0-2*d*	321	120.9	0.38	95.8	0.30	6.6
GN-0.8-0.0-3*d*	613	342.5	0.56	217.2	0.35	-7.0
GN-1.2-0.0-*d*	94.3	37.7	0.40	38.6	0.41	29.4
GN-1.2-0.0-2*d*	610	168.9	0.28	136.7	0.22	8.1
GN-1.2-0.0-3*d*	954	349.5	0.37	223.7	0.23	-9.0
GH-0.8-0.0-*d*	103	36.4	0.36	31.9	0.32	20.8
GH-0.8-0.0-2*d*	375	91.3	0.24	86.0	0.23	17.4
GH-0.8-0.0-3*d*	822	300.3	0.37	170.6	0.21	-17.0
GH-1.2-0.0-*d*	123	45.6	0.38	37.7	0.31	16.7
GH-1.2-0.0-2*d*	765	153.9	0.20	130.7	0.17	11.0
GH-1.2-0.0-3*d*	1,199	363.2	0.30	215.1	0.18	-14.3

It can be noted that increasing the beam depth changed the magnitude and direction of moment redistribution in both NSC and HSC beams. The moment redistribution decreased from 31% in beam GN-0.8-0.0-*d* (*d* = 250 mm) to 6.6% in beam GN-0.8-0.0-2*d* (*d* = 500 mm) and to -7.0% in beam GN-0.8-0.0-3*d* (*d* = 750 mm). Similarly, in beams having longitudinal reinforcement ratio of 1.2%, the moment redistribution decreased form 29.4% in beam GN-1.2-0.0-*d* to 8.1% in beam GN-1.2-0.0-2*d* and to -9.0% in beam GN-1.2-0.0-3*d*. A similar trend was observed in HSC beams. Increasing the effective depth from 250 to 500 mm resulted in a slight decrease in the moment redistribution, from 20.8 to 17.4% in beams GH-0.8-0.0-*d* and GH-0.8-0.0-2*d*, respectively, and from 16.7 to 11.0% in beams GH-1.2-0.0-*d* and GH-1.2-0.0-2*d*, respectively. Further increase in the effective depth to 750 mm resulted in a change in the direction of the moment redistribution, but of similar absolute value of -17% in beam GH-0.8-0.0-3*d* (compared to 17.4% moment redistribution of the beam GH-0.8-0.0-2*d*) and -14.3% in beam GH-1.2-0.0-3*d* (compared to 17.4% moment redistribution of the beam GH-1.2-0.0-2*d*). As discussed above, this could be attributed to the wider and additional cracks developed in the sagging moment regions compared to those in the hogging moment region. This resulted in a relatively weaker sagging moment region which caused the internal forces redirected to the relatively stronger zone (the hogging moment zone).

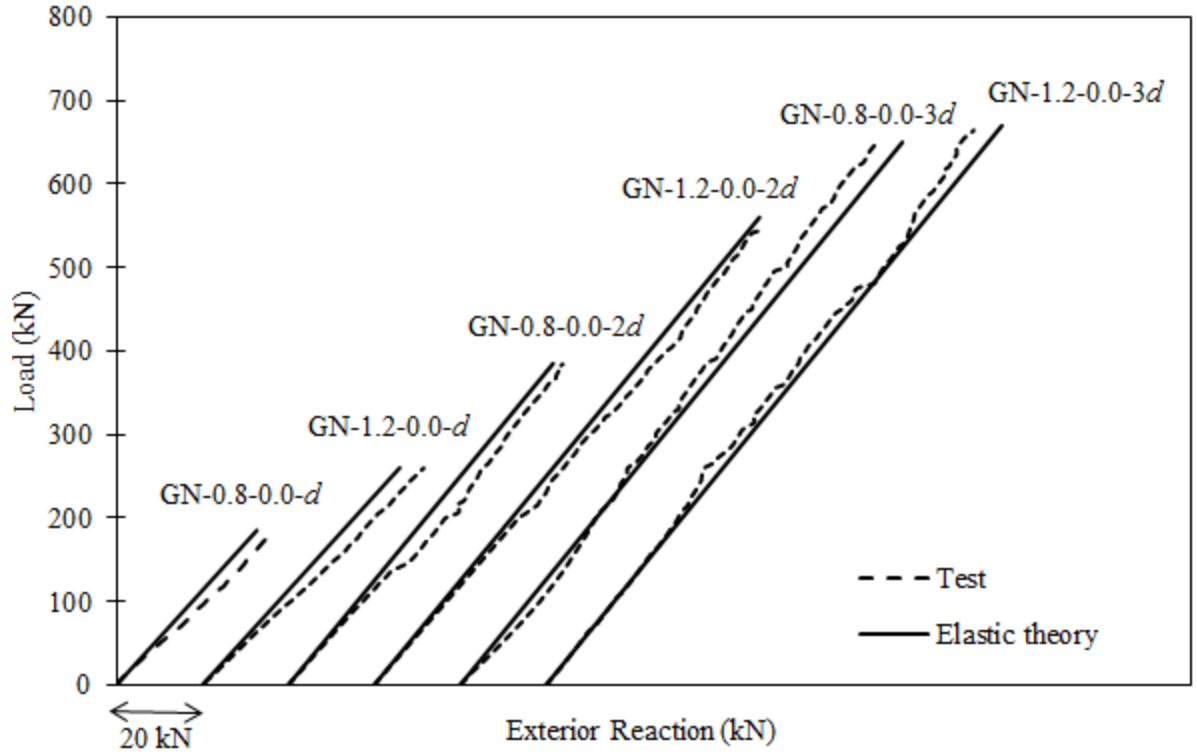

Figure 5.11: Load-exterior reaction relationship for NSC beams of Series II

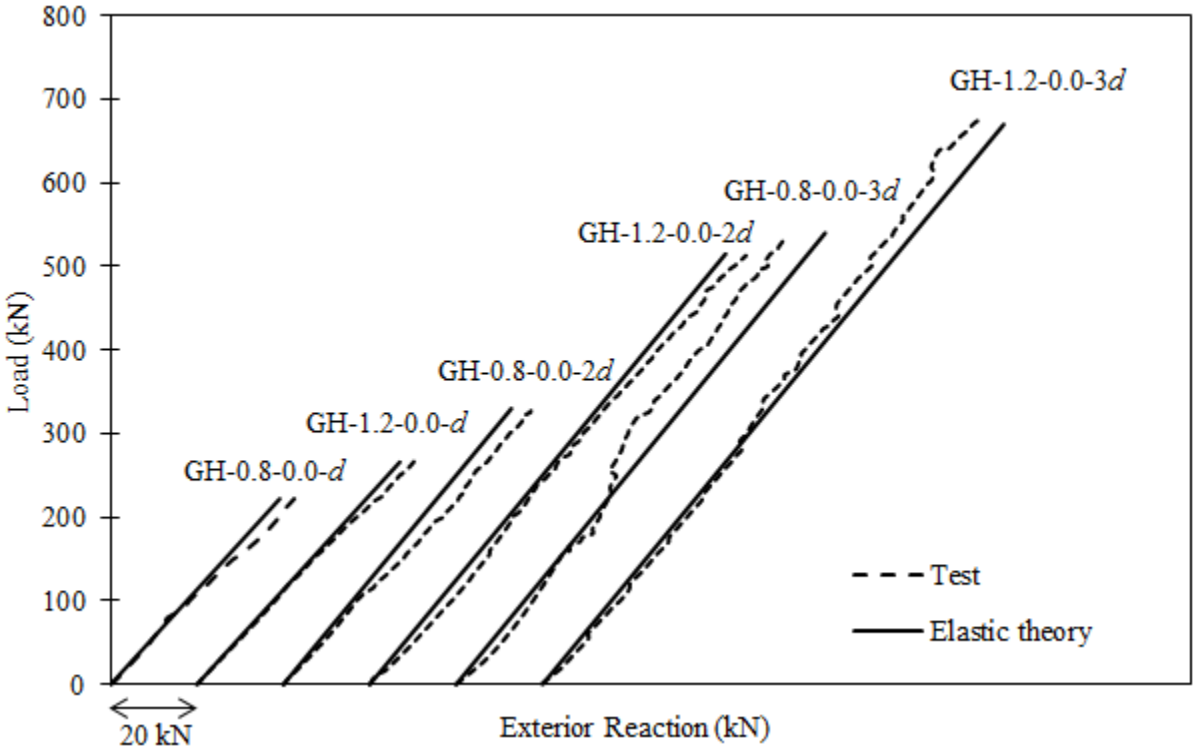

Figure 5.12: Load-exterior reaction relationship for HSC beams of Series II

5.6 SHEAR STRENGTH

The experimental shear stress and normalized shear stress ($V_{test} / b_w d \sqrt{f_c'}$) at failure in both interior and exterior shear spans are listed in Table 5.2. It can be noted that beams failed in the interior shear span exhibited adverse size effect where the shear strength increased as the effective depth increased. In NSC beams with longitudinal reinforcement ratio of 0.8%, the shear strength increased by 20% (from 1.1 to 1.32 MPa) and 10% (from 1.32 to 1.45 MPa) when the effective depth increased from 250 to 500 mm and from 500 to 750 mm, respectively. Also, in beams with a higher longitudinal reinforcement ratio (1.2%), increasing the shear strength from 250 to 500 mm resulted in an increase in the shear strength by 16% (from 1.57 to 1.82 MPa). In HSC beams with longitudinal reinforcement ratio of 1.2%, there was no significant change in the shear strength where beams having 250, 500 and 750 mm failed at similar shear stresses (1.66, 1.7 and 1.68 MPa, respectively). However, this behaviour is contradicting the well-established size effect in simply-supported beams especially that the size effect is more pronounced in HSC beams. On the other hand, the shear strength of the test beams failed in the exterior shear span was strongly affected by the size of the beam. In beams GN-0.8-0.0-*d* and GN-0.8-0.0-3*d*, the shear strength in the exterior shear span decreased by 13% (from 0.71 to 0.62 MPa) when the depth increased from 250 to 750 mm. This ratio was 27% (form 0.91 to 0.66 MPa) when the depth increased from 500 mm in GN-1.2-0.0-2*d* to 750 mm in beam GN-1.2-0.0-3*d*. Moreover, similar behaviour was observed in HSC beams where increasing the depth from 500 mm in beam GH-0.8-0.0-2*d* to 750 mm in GH-0.8-0.0-3*d* resulted in a 13% (from 0.56 to 0.49 MPa) decrease in the shear strength at the exterior shear span as well. Regardless the failure location in the test beams, the shear strength decreased with increasing the depth at the exterior shear span in both NSC and HSC beams. This decrease was greater in the case of HSC beams. This can be

attributed to the width of the diagonal crack where it was observed that the diagonal cracks in the exterior shear span were wider than those in the interior shear span.

Collins and Kuchma (1999) reported similar decrease in the shear strength of continuous concrete beams (overhang beams) reinforced with steel bars where, in NSC beams, increasing the depth from 459 to 920 mm resulted in 14% decrease in the normalized shear strength. Moreover, higher decrease in the shear strength of HSC beams was reported where the same increase in the depth (from 459 to 920 mm) resulted in a reduction of 27% in the normalized shear strength. These results, reported in Collins and Kuchma (1999), show that there is a size effect on the shear strength of steel-RC overhang beams. The GFRP-RC continuous beams exhibited similar size effect when they failed in the exterior shear span while opposite behaviour was observed in beams failed in the interior shear span (Fig. 5.13). This decrease in the shear strength of the steel-RC continuous beams with approximately 1% longitudinal reinforcement ratio was comparable to that occurred in this study (13%) in the case of NSC beams. However, beams made of HSC demonstrated higher reduction in the shear strength than what observed in this study. This might be attributed to the higher compressive strength (100 MPa) compared to that used in this study.

To investigate the continuity effect on the different size beams, test results were compared to simply-supported GFRP-RC beams reported in literature. Bentz et al. (2010) tested six simple beams without shear reinforcement. Three beams had a GFRP longitudinal reinforcement ratio in the range of 0.5 to 0.66 % and a depth in the range of 194 to 938 mm. It was found out that increasing the depth from 194 to 438 mm resulted in a 29% reduction of the normalized shear strength, while increasing the depth from 438 to 938 mm resulted in a decrease of 37% in the normalized shear strength. The other three beams had a higher longitudinal reinforcement ratio

(ranged from 2.23 to 2.54%) demonstrated lower decrease in the shear strength when the depth increased. Increasing the depth from 188 to 405 mm and from 405 to 860 mm resulted in a decrease in the shear strength by 14 and 22%, respectively. Matta et al. (2013) tested beams having depths of 292 and 883 mm. It was reported that the shear strength, in beams having 0.59% longitudinal reinforcement ratio, reduced by 30% when the depth increased from 292 mm to 883 mm. Alam and Hussien (2012 and 2013) reported similar decrease in the shear strength (20%) when the depth increased from 291 to 578 mm in NSC beams with a reinforcement ratio ranging from 0.86 to 0.91%. Higher reduction in the shear strength (38%) occurred when the depth increased from 305 to 734 mm in HSC beams with a reinforcement ratio ranging from 0.87 to 1.37%. These results are presented in Fig. 5.14.

It can be seen that the results of GFRP-RC continuous beams failed in the interior shear span showed opposite behaviour and high shear strength when compared to that of simply-supported ones. On the other hand, continuous beams failed in the exterior shear span have a trend similar to that of the simply-supported beams. This adverse size effect can be attributed to the different moment-to-shear ratio near the middle support compared to that in the exterior shear span (similar to simply-supported beams). Also, the steep angle of inclination of the failure plane in the interior shear span compared to that in the exterior shear span may have contributed to that behaviour. Moreover, the decrease in the shear strength of such simple beams is higher than that in continuous beams failed in the exterior shear span (13%). This might be attributed to the higher reinforcement ratio used in this study, approximately 0.8%, compared to that in the simple beam tests. Also, the modulus of elasticity of the used GFRP bars in this study was approximately 1.75, 1.6 and 1.4 times that of the used bars in Bentz et al. (2010), Matta et al. (2013) and Alam and Hussien (2012 and 2013), respectively. High longitudinal reinforcement

ratio and larger elastic modulus better controlled the crack width and thus the size effect decreased. Therefore, continuous beams failed in the exterior shear span demonstrated a similar size effect to that in simple beams. However, continuous beams failed in the interior shear span showed opposite behaviour where adverse or no size effect was noted.

Table 5.2: Shear strength, normalized shear strength and predicted shear capacity of Series II test beams

Beam	v_{test} (MPa)		$\frac{V_{test}}{\sqrt{f'_c}\, b_w d}$ $(\sqrt{MPa})$		Predicted shear strength (MPa)						
					ACI 440.1R-06 §	CSA/S806-12		CSA/S6-06		Hoult et al. (2008)	
	Int.	Ext.	Int.	Ext.		Int.	Ext.	Int.	Ext.	Int.	Ext.
GN-0.8-0.0-*d*	1.10*	0.71†	0.176	0.114	0.43	1.23	1.0	0.76	0.64	0.78	0.67
GN-0.8-0.0-2*d*	1.32*	0.64	0.211	0.102	0.43	1.12	0.81	0.64	0.40	0.62	0.45
GN-0.8-0.0-3*d*	1.45*	0.62†	0.232	0.099	0.42	0.86	0.61	0.52	0.35	0.51	0.38
GN-1.2-0.0-*d*	1.57*	1.03	0.251	0.165	0.51	1.23	1.14	0.93	0.75	0.89	0.77
GN-1.2-0.0-2*d*	1.82*	0.91†	0.274	0.137	0.53	1.29	0.92	0.78	0.50	0.74	0.54
GN-1.2-0.0-3*d*	1.55	0.66†	0.248	0.106	0.5	0.97	0.68	0.64	0.43	0.61	0.46
GH-0.8-0.0-*d*	1.38*	0.85	0.162	0.100	0.51	1.55	1.17	0.79	0.66	0.82	0.70
GH-0.8-0.0-2*d*	1.06	0.56†	0.127	0.067	0.5	1.27	0.91	0.62	0.39	0.60	0.43
GH-0.8-0.0-3*d*	1.28	0.49†	0.146	0.056	0.5	0.98	0.69	0.50	0.33	0.48	0.36
GH-1.2-0.0-*d*	1.66*	1.0	0.196	0.118	0.61	1.55	1.31	0.92	0.78	0.94	0.81
GH-1.2-0.0-2*d*	1.70*	0.87†	0.203	0.104	0.61	1.43	1.02	0.73	0.47	0.69	0.50
GH-1.2-0.0-3*d*	1.68*	0.67	0.191	0.076	0.59	1.11	0.78	0.57	0.38	0.53	0.41

* shear strength in the interior shear span at failure,
† shear strength in the exterior shear span at failure,
§ Shear strength is the same for interior and exterior shear spans (ACI 440.1R-06)

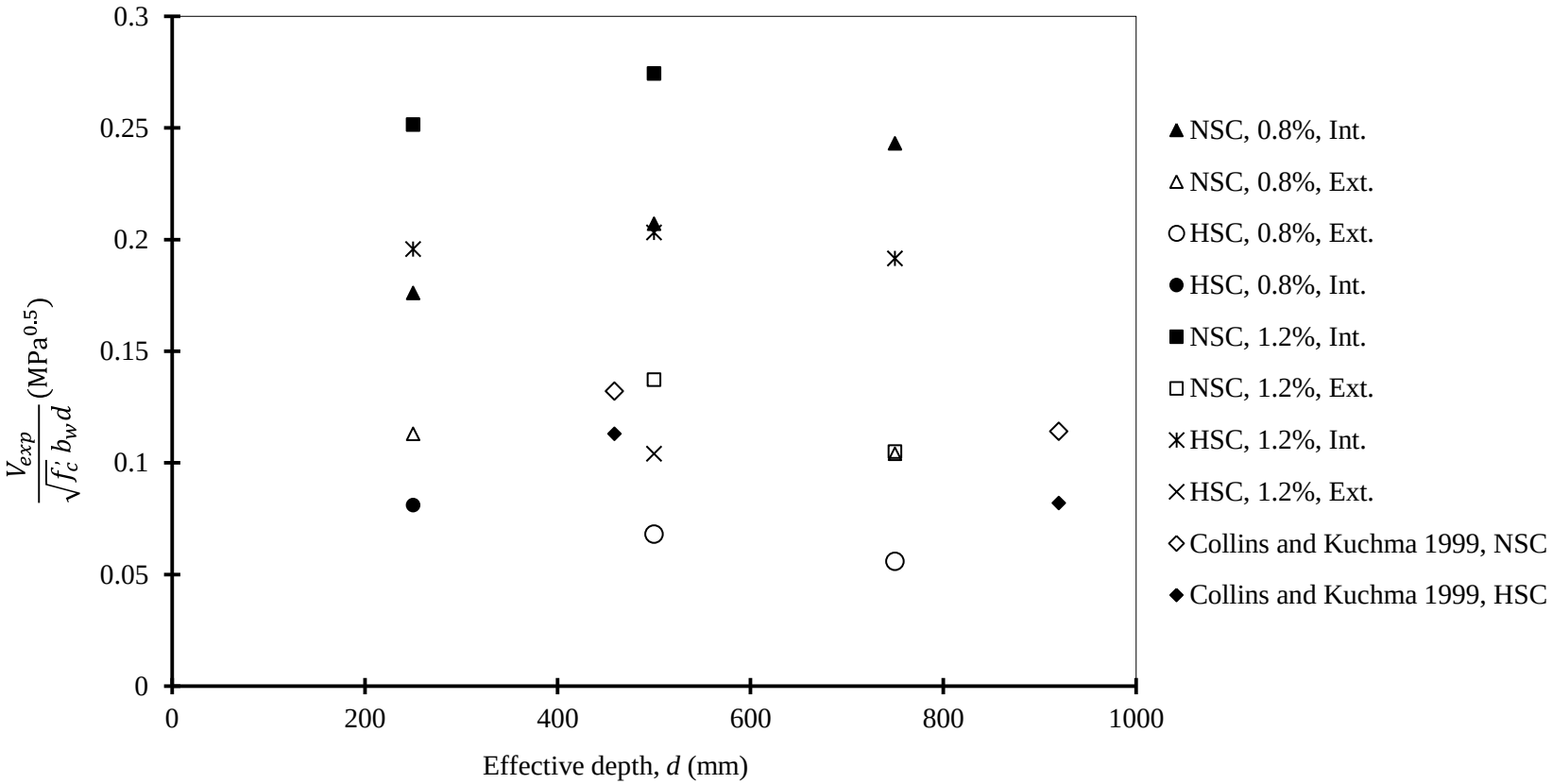

Figure 5.13: Size effect on the normalized shear strength from this study and from steel-RC continuous beams

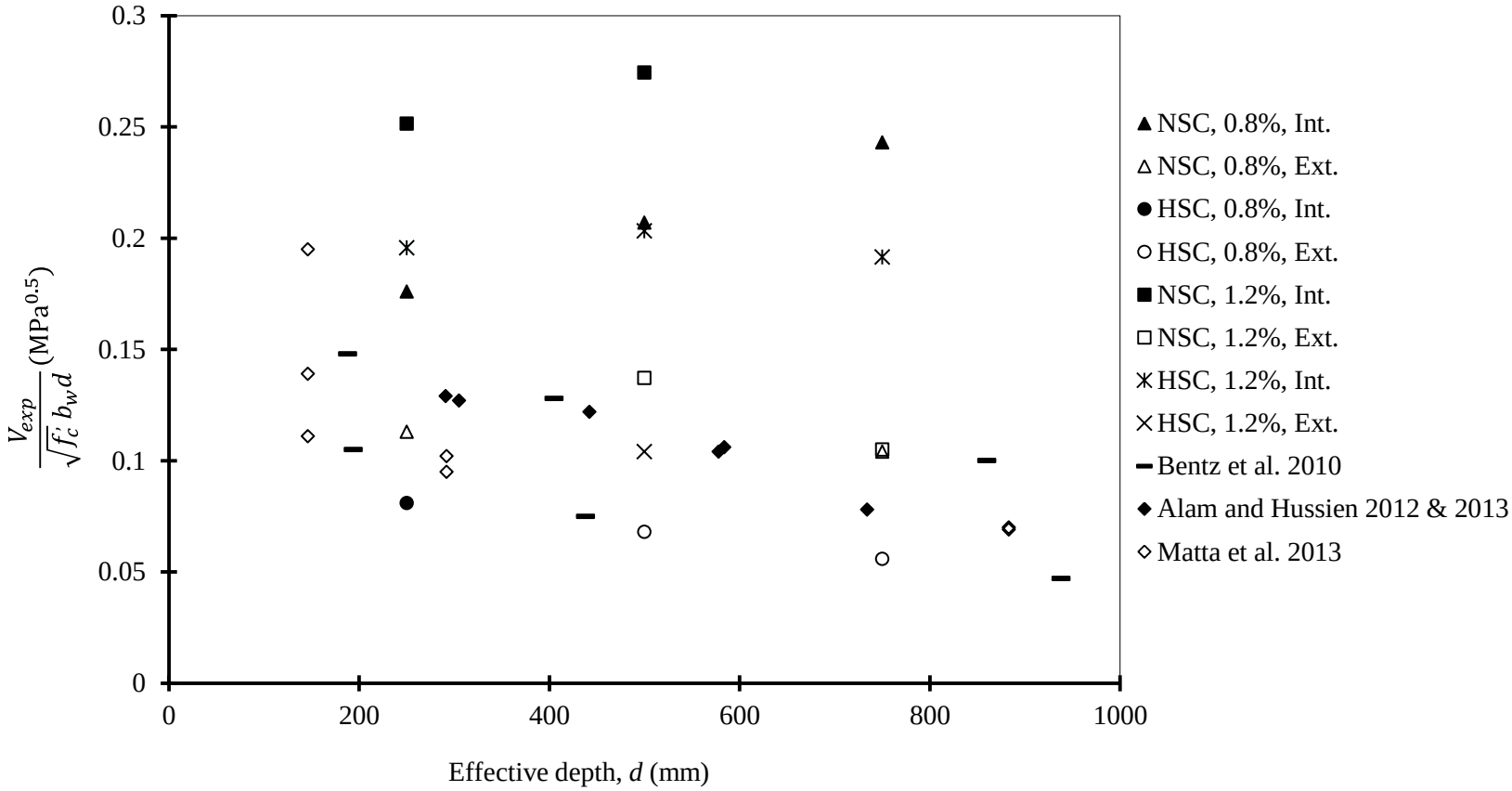

Figure 5.14: Size effect on the normalized shear strength from this study and from FRP-RC simply-supported beams

5.7 COMPARISON BETWEEN EXPERIMENTAL AND PREDICTED SHEAR STRENGTH

Table 5.2 shows the experimental shear strength of the test beams at failure sections and the predicted shear strength by ACI 440.1R-06, CSA/S806-12 and CSA/S6-06. Also, the second order equation ($V_c = \frac{0.3}{0.5+(1500\varepsilon_x+0.15)^{0.7}} \times \frac{1300}{1000+S_{ze}} \sqrt{f_c'} b_w d_v$) proposed by Hoult et al. (2008) was used to predict the capacity of the test beams. It is worth mentioning that all these shear design expressions are based on the test results of simple structures. Therefore, the predicted shear strength expressions proposed by the CSA/S806-12, the CSA/S6-06 and Hoult et al. (2008) decreased with increasing the effective depth. On the contrary, the ACI 440.1R-06 did not account for the size effect where the shear strength was approximately constant as the depth increased. According to these expressions, the critical shear section is at the interior shear span.

Figure 5.15 shows a comparison between the experimental and predicted shear strength of the test beams. Regardless of the failure location, all the investigated shear design expressions obtained conservative predictions. However, the Canadian standards CSA/S806-12 reasonably predicted the shear strength of beams failed in the interior shear span. For beams failed in the exterior shear span, the shear stress in the interior shear span was higher than the predicted one. It can be noted that only small size beams with longitudinal reinforcement ratio of 0.8% failed at shear strength smaller than the predicted one. Considering the shear strength, at failure in the interior shear span, the average experimental-to-predicted shear strength ratio was 1.23 with a coefficient of variation (COV) of 24.0%. This average ratio was 1.1 (COV of 10%) and 1.03 (COV of 12%) on average for simply-supported beams investigated by Bentz et al. (2010) and Alam and Hussein (2012), respectively. On the other hand, the CSA/S806-12 yielded un-

conservative predictions of the shear strength of beams failed in the exterior shear span. The average experimental-to-predicted shear strength was 0.85% (COV = 20%). Comparison between the experimental shear strength at the exterior shear span and that predicted by the shear expressions are shown in Fig. 5.16.

Although it does not account for the size effect, the ACI 440.1R-06 highly underestimated the shear strength of such beams where the average experimental-to-predicted shear strength ratio in the interior shear span was 2.87 (COV = 14.0%). This ratio for simply-supported beams was 1.53, 1.6 and 1.7 as reported in Bentz et al. (2010), Alam and Hussein (2012 & 2013) and Matta et al. (2013), respectively. Similar results were obtained for the CSA/S6-06 where the average experimental-to-predicted shear strength ratio in the interior shear span was 2.16 (COV = 23.0%). This ratio was 1.23, 1.36 and 1.33 in Bentz et al. (2010), Alam and Hussein (2012 & 2013) and Matta et al. (2013), respectively. The second order expression by Hoult et al. (2008) also resulted in conservative predictions to the shear strength of GFRP-RC beams. The average experimental-to-predicted shear strength ratio was 2.24 (COV = 25.5%). This ratio for simple beams reported in Matta et al. (2013) was 1.14 with a COV of 16.9%. Considering beams failed in the exterior shear span, the shear strength was also greater than that predicted by both ACI 440.1R-06 and CSA/S6-06 and the proposed equation by Hoult et al. (2010); however, less conservatism can be noted compared to that in the case of beams failed in the interior shear span, refer to Fig. 5.16.

Generally, the high average ratios in the interior shear span (1.23, 2.87 and 2.16) compared to these of simple beams might be attributed to the fact that the investigated shear design expressions highly underestimated the shear strength of beams failed in the interior shear span that exhibited no or adverse size effect.

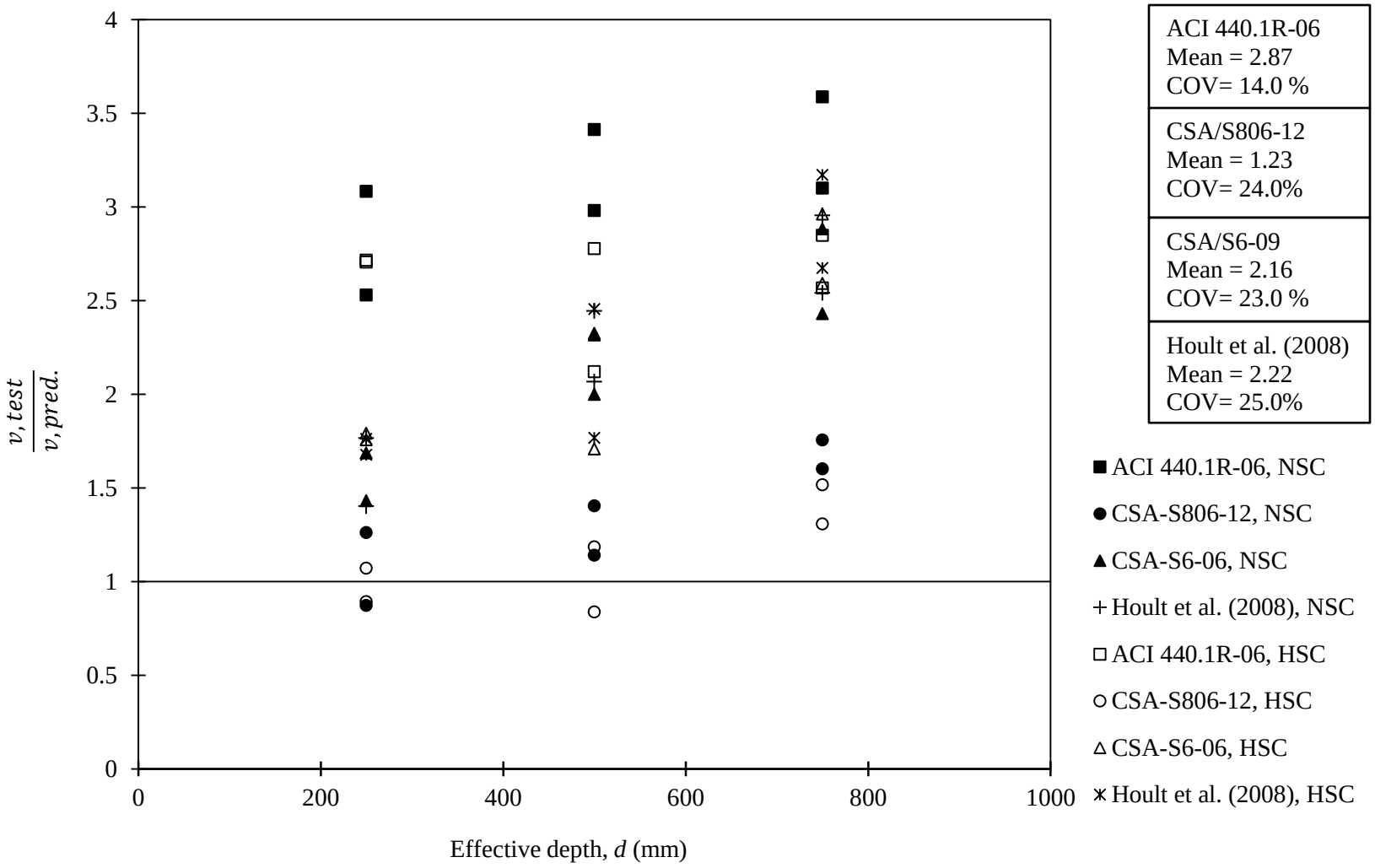

Figure 5.15: Comparison between the experimental and predicted shear strength in the interior shear span

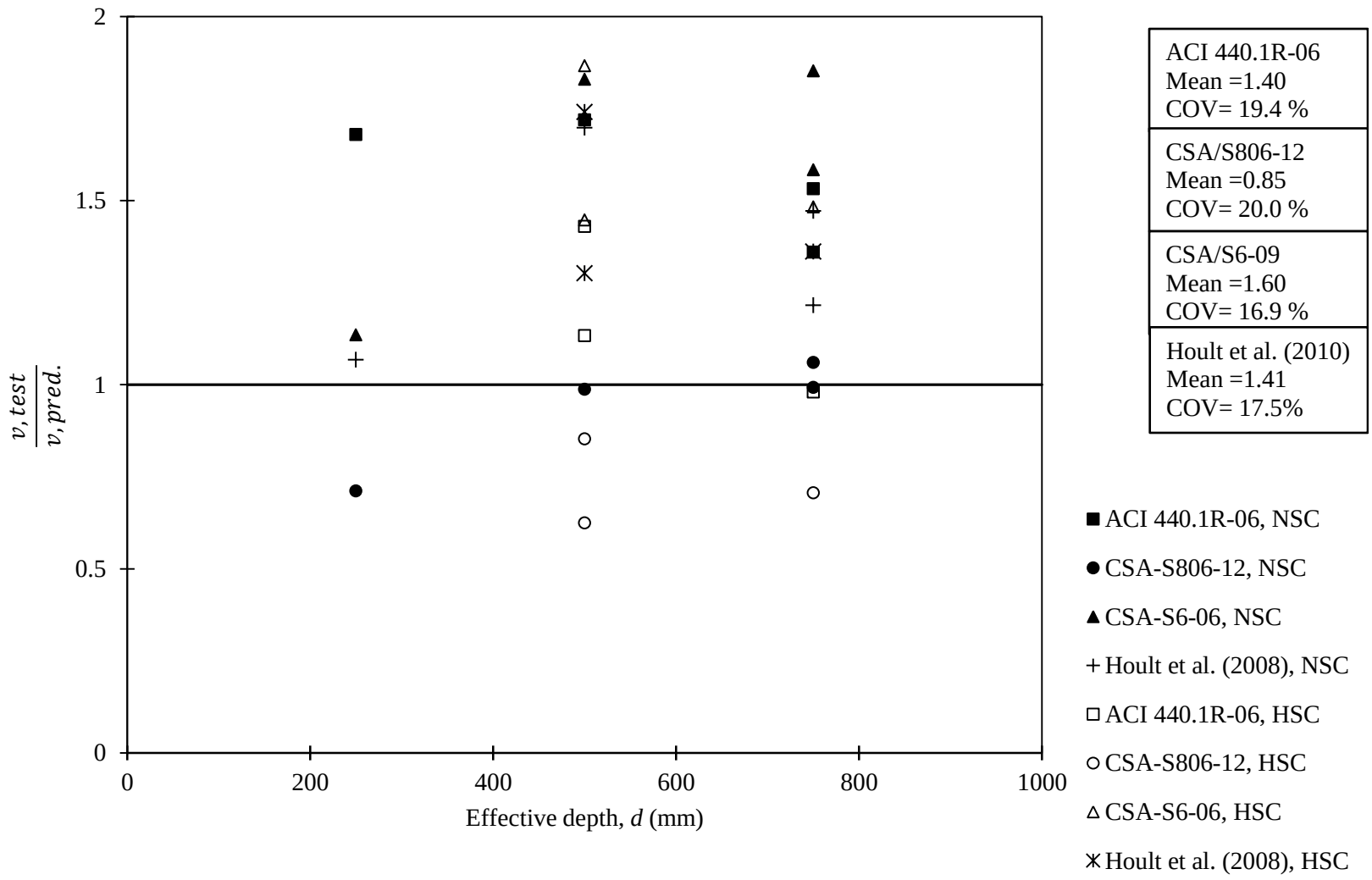

Figure 5.16: Comparison between the experimental and predicted shear strength in the exterior shear span

CHAPTER 6: RESULTS AND DISCUSSIONS OF SERIES III

6.1 GENERAL

This chapter presents the experimental results of nine RC continuous beams with transverse reinforcement. One reference beam was reinforced with steel bars and stirrups (SN-1.2-0.12-*d*) and eight beams were reinforced longitudinally and transversally with GFRP bars (GN-1.2-0.21-*d*, GN-0.8-0.48-*d*, GN-1.2-0.48-*d*, GN-1.2-0.85-*d*, GH-1.2-0.28-*d*, GH-0.8-0.63-*d*, GH-1.2-0.63-*d* and GH-1.2-1.1-*d*). The variables included in this series are the type and ratio of the longitudinal reinforcement, type and ratio of the transverse reinforcement and the concrete strength. The steel-RC beam had the minimum shear reinforcement as specified by the CSA/A23.3-04 standards (CSA 2004). The other eight beams were reinforced with GFRP bars and stirrups. The provided GFRP shear reinforcement (stirrups) was 0.5 $A_{vF,min}$, $A_{vF,min}$ and 2$A_{vF,min}$, where $A_{vF,min}$ is the minimum shear reinforcement as specified by the CSA/S806-12 standards (CSA 2012). This was achieved by using three different stirrup diameters while keeping the spacing constant for each type of concrete.

To evaluate the shear behaviour of the test beams of this series, the deflections at three different locations in each span, the strains in both reinforcement and concrete at critical sections, the reactions at exterior supports, and crack width in both exterior and interior shear spans were monitored. The collected data was used to extensively describe the behaviour of the test beams, in terms of cracking patterns, load-deflection curves, and strain variations in the reinforcement bars and concrete surface. Also, the moment and shear redistribution and the shear capacity of the test beams were discussed. Moreover, the experimental and predicted shear strengths by the relevant codes were compared.

6.2 GENERAL BEHAVIOUR, CRACKING AND MODE OF FAILURE

All Series III test beams demonstrated similar behaviour during the test until failure. The first crack was initiated vertically at the hogging moment region; then, similar vertical cracks initiated later in both sagging moment regions. This agrees with the elastic bending moment distribution in such continuous beams. The first crack at the hogging moment region was visually observed at a load of 100, 85,75, 75, 80, 100, 110, 115 and 95 kN in beams SN-1.2-0.12-*d*, GN-1.2-0.21-*d*, GN-0.8-0.48-*d*, GN-1.2-0.48-*d*, GN-1.2-0.85-*d*, GH-1.2-0.28-*d*, GH-0.8-0.63-*d*, GH-1.2-0.63-*d* and GH-1.2-1.1-*d*, respectively. With increasing the load, more flexural cracks were formed in both hogging and sagging regions. The formed flexural crack in exterior and interior shear span propagated diagonally towards the exterior loading point and the middle support, respectively, with further increase in the load. The diagonal cracks, near the interior support, grew wider and deeper while minor splitting cracks formed horizontally at the top reinforcement level. Finally, the failure in all test beams, took place due to diagonal tension crack at one side only of the middle support. The mode of failure of all Series III test beams is shown in Figs. 6.1 and 6.2.

Schematic drawings of the cracking patterns of the test beams at failure are shown in Fig. 6.3. It was observed that beams made of HSC had more cracks at both hogging and sagging moment regions than their counterparts made of NSC. Dawood and Marzouk (2012) reported that the stirrups act as crack initiator; therefore, HSC beams that had closer stirrup spacing showed more cracks. Also, as expected, the depth of cracks increased as the axial stiffness of the longitudinal reinforcement increased where in beams with the lower longitudinal reinforcement ratio (GN-0.8-0.48-*d*, and GH-0.8-0.63-*d*) were deeper than those in beams having higher ratios (GN-1.2-0.48-*d*, GN-1.2-0.85-*d*, GH-1.2-0.28-*d* and GH-1.2-1.1-*d*). Close to failure, horizontal cracks formed parallel to the top reinforcement. Finally, the failure occurred due to a diagonal tension

crack at one side of the middle support. It was observed that the main diagonal crack intersected with three adjacent stirrups. In beam SN-1.2-0.12-*d*, necking in the stirrup was observed at the intersection of the diagonal crack and the stirrup. In beams with GFRP stirrups, the crack intersected with the middle stirrup at the straight portion near the mid-height of the beam, which resulted in high measured strains in this stirrup. However, it intersected with the other two stirrups near the weak bent portions; which led to rupture of stirrups at these locations.

The diagonal cracks, which led to failure of the test specimens, were steep and close to the middle support. The angle of inclination of the failure plane in beams SN-1.2-0.12-*d*, GN-1.2-0.21-*d*, GN-0.8-0.48-*d*, GN-1.2-0.48-*d*, GN-1.2-0.85-*d*, GH-1.2-0.28-*d*, GH-0.8-0.63-*d*, GH-1.2-0.63-*d* and GH-1.2-1.1-*d* was 44^o, 44^o, 50^o 54^o, 48^o, 50^o, 55^o, 59^o and 52^o with the longitudinal/horizontal beam axis, respectively. NSC beams showed shallower failure planes than HSC beams. The average angle of inclination was approximately 51^o, which is in good agreement with the observations of previous studies (El-Mogy et al. 2010 & 2011). Moreover, the failure crack was steeper than that observed in simply-supported beams reinforced with GFRP bars and stirrups (Ahmed et al. 2010), where the average crack inclination was only 44^o with the longitudinal axis.

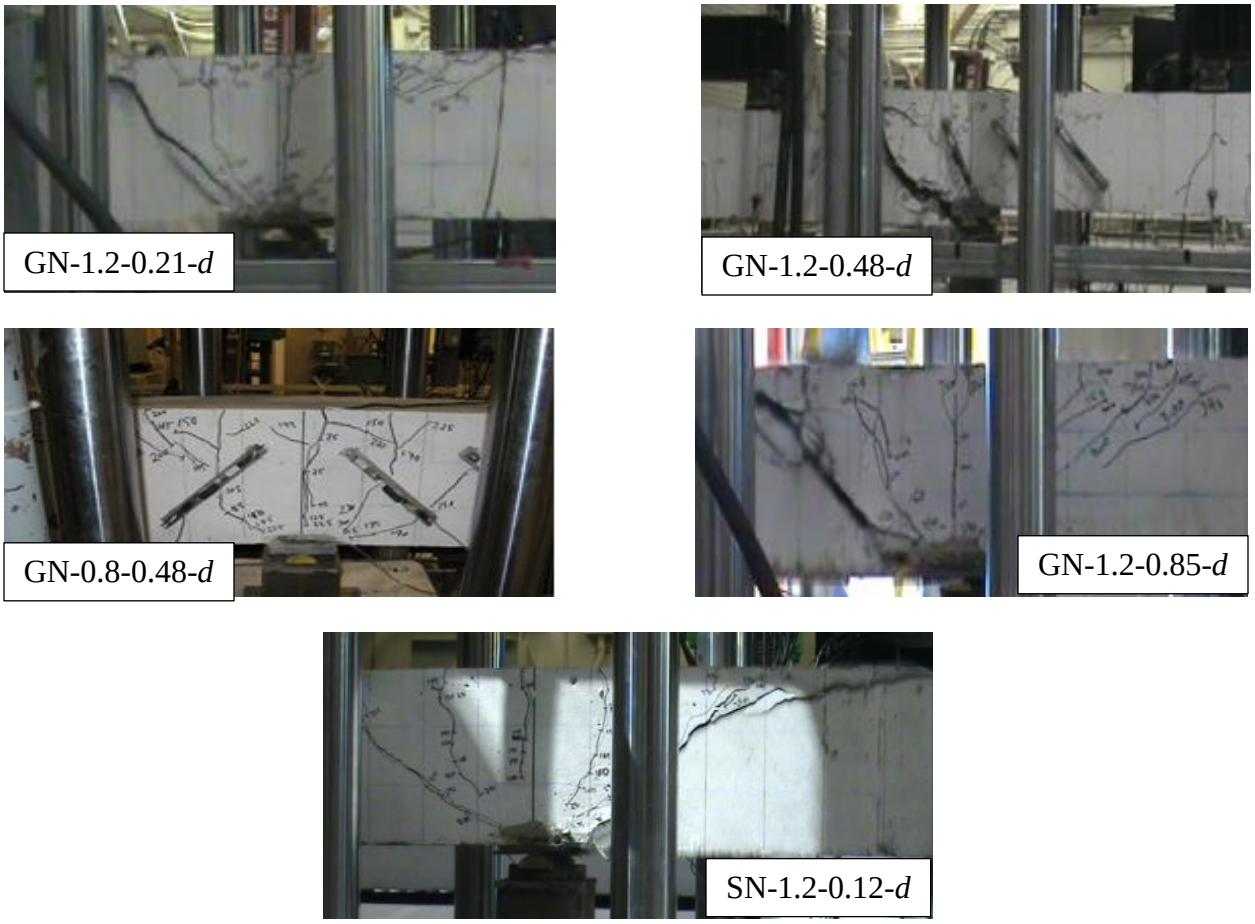

Figure 6.1: Photos of NSC beams of Series III at failure

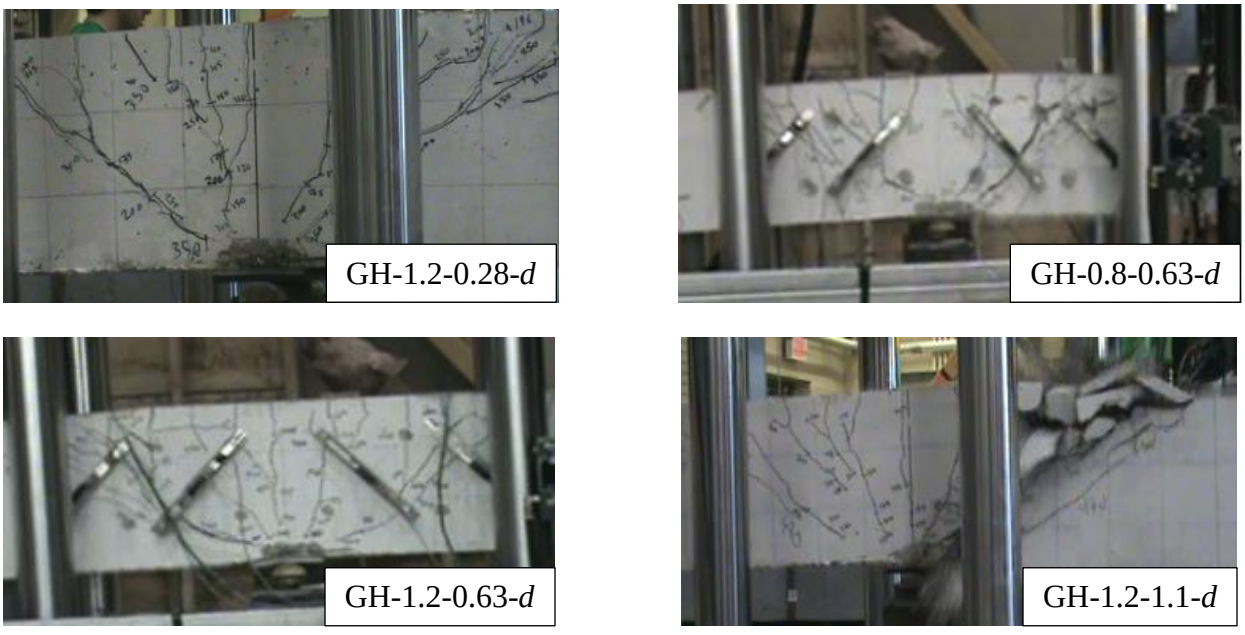

Figure 6.2: Photos of HSC beams of Series III at failure

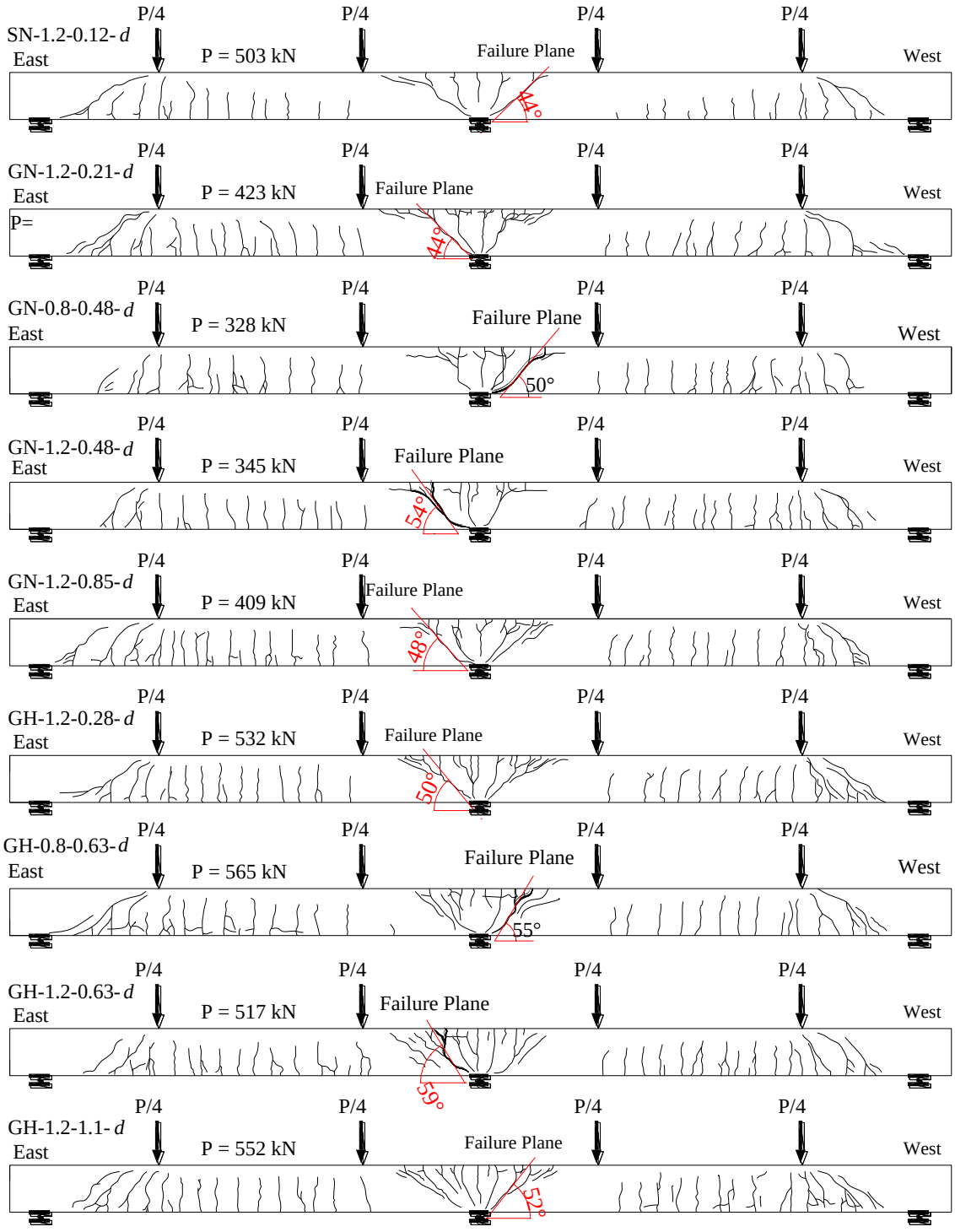

Figure 6.3: Cracking pattern at failure of beams of Series III

6.3 DEFLECTION

For all Series III test beams, the maximum deflection in each span was measured at the mid-span. The relationship between the applied total load and the average recorded deflection at both mid-span points for all test beams is shown in Figs. 6.4 and 6.5. The typical load-deflection curve can be defined by two distinct stages. The first stage is up to flexural cracking where deflection was of small values. The second stage starts at cracking and continues until failure. In this latter stage, the flexural stiffness of the beam is mainly dependent on the axial stiffness of the reinforcing bars. Therefore, it can be seen that, amongst all beams, beam SN-1.2-0.12-*d* demonstrated the highest post-cracking flexural stiffness. Moreover, for GFRP-RC beams, the post-cracking flexural stiffness decreased as the longitudinal reinforcement ratio decreased. At the same load, the measured deflection in beams with 0.8% longitudinal reinforcement ratio was higher than that in beams with 1.2%. Also, since flexural stiffness is a function of the modulus of elasticity of the concrete, beams made of HSC exhibited higher flexural stiffness. Therefore, the deflection graphs for HSC beams were steeper than those of NSC beams.

The measured deflections at service load level of 87 kN in beams GN-0.8-0.48-*d* and GH-0.8-0.63-*d* were 1.1 and 0.7 mm, respectively. At 145 kN, the measured deflections were 2.65, 3.1, 3.2, 2.7, 2.5, 2.2 mm in beams GN-1.2-0.21-*d*, GN-1.2-0.48-*d*, GN-1.2-0.85-*d*, GH-1.2-0.28-*d*, GH-1.2-0.63-*d*, and GH-1.2-1.10-*d*, respectively. In all Series III test beams, the deflections at service load satisfied the requirements of the CSA/S806-12 (CSA 2012), where the allowable deflection is in the range of 6-15 mm (ℓ/480 to ℓ/180 depending on the type and function of the structure). Regarding the steel-RC beam, the safe service load is 215 kN, according to CSA/A23.3-04. At this load level, the deflection was, 3.52 mm, well below the specified limit in the CSA/A23.3-04 (6-15 mm).

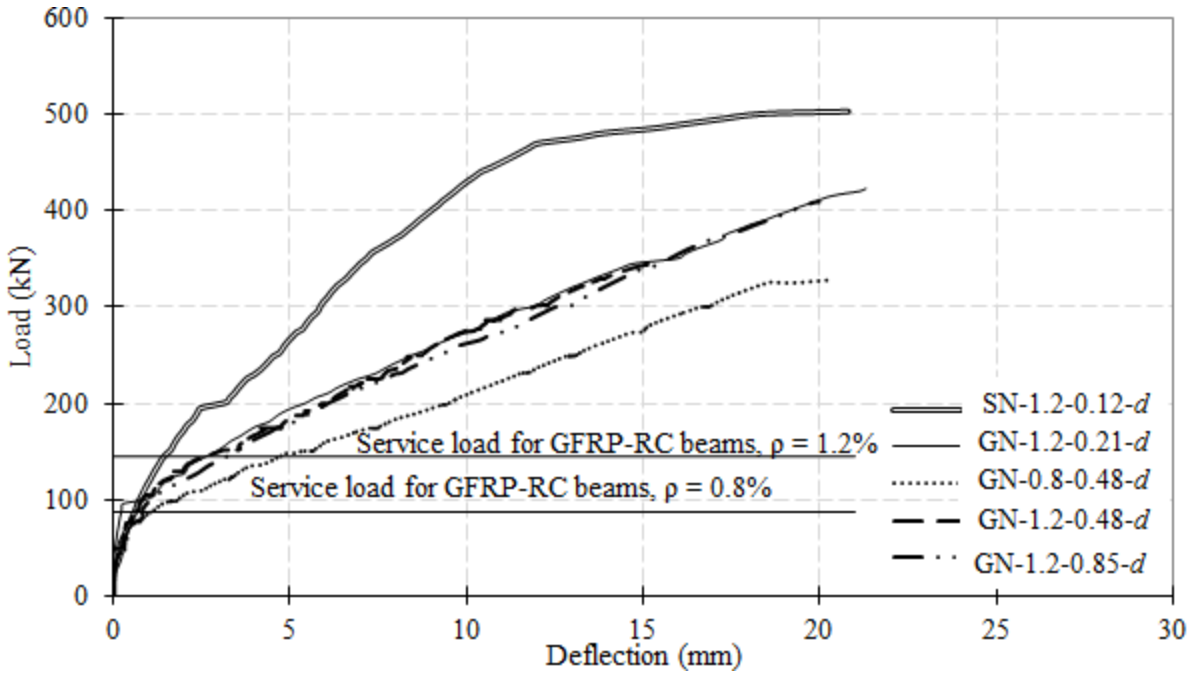

Figure 6.4: Load-deflection relationship at mid-span of NSC beams of Series III

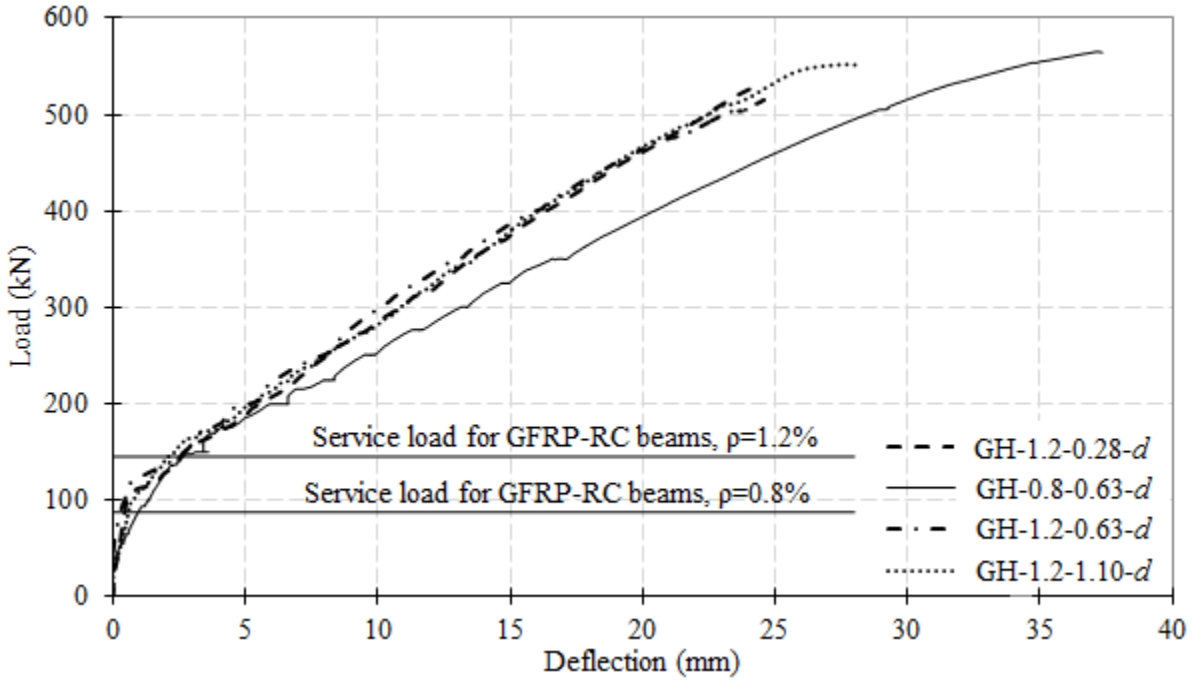

Figure 6.5: Load-deflection relationship at mid-span of HSC beams of Series III

6.4 STRAIN IN LONGITUDINAL REINFORCEMENT AND CONCRETE

Figures 6.6 and 6.7 show the measured tensile strains in GFRP bars at the hogging and sagging moment sections, respectively. The figures also show the maximum measured compressive strains in concrete at the same sections. Except beam GH-1.2- 0.63-*d*, the maximum compressive strains in concrete in all specimens did not reach the crushing strain of 0.0035 specified by the CSA standards. In beam GH-1.2-0.63-*d*, the maximum compressive strain in concrete, measured at the middle support section, was 3,880 $\mu\varepsilon$. Although this value is greater than the specified value by the code, there were no signs of flexural failure because the experimental moment was well below the flexural capacity of the section. Also, in all beams, the compressive strain started to decrease after the diagonal crack completely propagated. This might be attributed to that the diagonal crack was very close to the strain gauge location. Since the ratio of the hogging moment at failure to the flexural capacity in HSC beams (0.72 on average) was greater than that in NSC beams (0.6 on average), it was observed that the compressive strains in NSC beams were smaller than those in HSC beams.

Regarding tensile strains, the figures show that the strains in FRP bars increased suddenly after concrete cracking. The value of the maximum measured strains in the longitudinal reinforcement in the hogging and sagging moment regions in each beam are shown in Table 6.1. The tensile strains measured in the hogging moment region were approximately 22, 25, 16, 25, 28, 33, 31, and 30% of the rupture strain of the used GFRP bars in beams GN-1.2-0.21-*d*, GN-0.8-0.21-*d*, GN-1.2-0.48-*d*, GN-1.2-0.85-*d*, GH-1.2-0.28-*d*, GH-0.8-0.63-*d*, GH-1.2-0.63-*d*, and GH-1.2-1.10-*d*, respectively. As expected, beams having 0.8% longitudinal reinforcement ratio experienced higher strains than those having 1.2% longitudinal reinforcement ratio. In beam SN-1.2-0.12-*d*, the tensile strain was smaller than that in GFRP bars until the steel reached

yielding point; then, the strain increased rapidly forming the yielding plateau. The strain at failure was 13,040 and 10,380 $\mu\varepsilon$ at the hogging and sagging moment section, respectively. It can be seen the measured reinforcement strains showed good correlation with the experimental moments (Table 6.1). However, unlike all other beams that showed tensile strains at the sagging moment sections less than those at the hogging moment sections, beam GN-1.2-0.48-*d* had similar moments and strains at both hogging and sagging section.

Table 6.1: Moments and strains at failure of test beams

Beam	Failure Moments (kN.m)		Strain in longitudinal reinforcement ($\mu\varepsilon$)		Strains in Concrete ($\mu\varepsilon$)	
	Hogging	Sagging	Hogging	Sagging	Hogging	Sagging
SN-1.2-0.12-*d*	78.4	73.4	13,040	10,380	2,730	2,630
GN-1.2-0.21-*d*	70.0	60.5	4,600	3,960	2,460	2,180
GN-0.8-0.48-*d*	54.3	48.9	5,210	4,260	1,510	1,040
GN-1.2-0.48-*d*	53.6	52.0	3,380	3,370	2,030	1,140
GN-1.2-0.85-*d*	65.5	59.2	5,300	4,290	1,320	1,420
GH-1.2-0.28-*d*	87.6	76.4	5,860	4,820	1,310	1,880
GH-0.8-0.63-*d*	86.1	82.9	6,990†	7,710	1,610	2,460
GH-1.2-0.63-*d*	82.3	74.9	6,490	4,090	2,170	1,740
GH-1.2-1.10-*d*	85.8	80.4	6,330	4,580	1,120	2,090

†At 93% of the failure load.

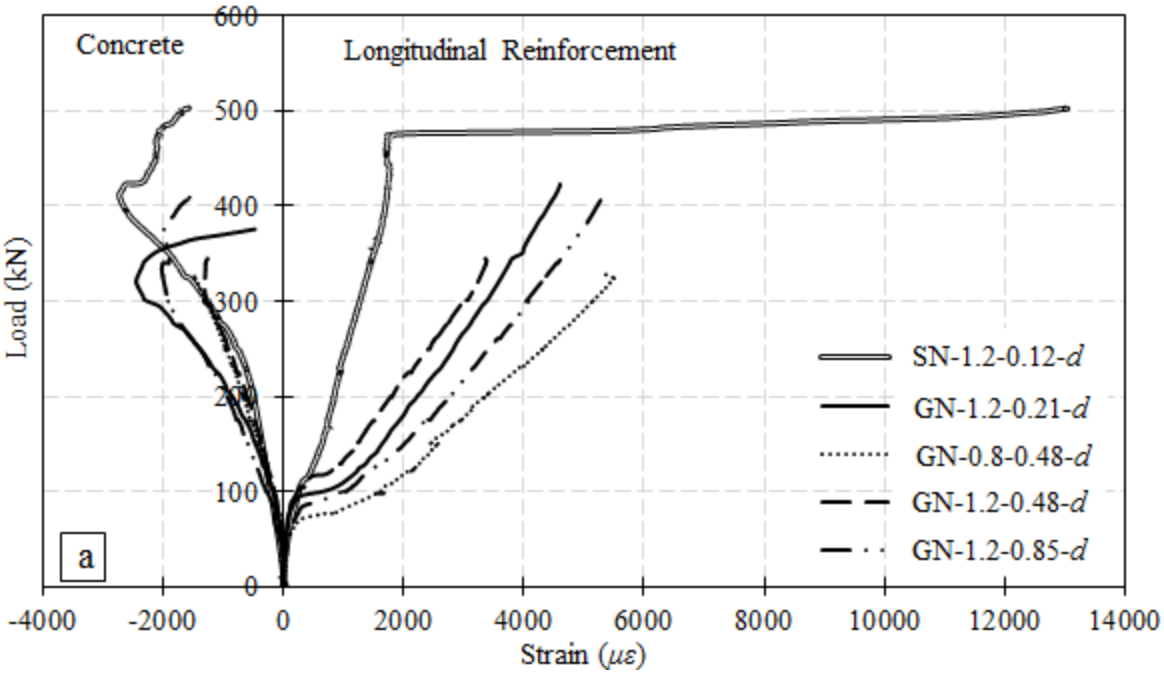

(a) The hogging moment section

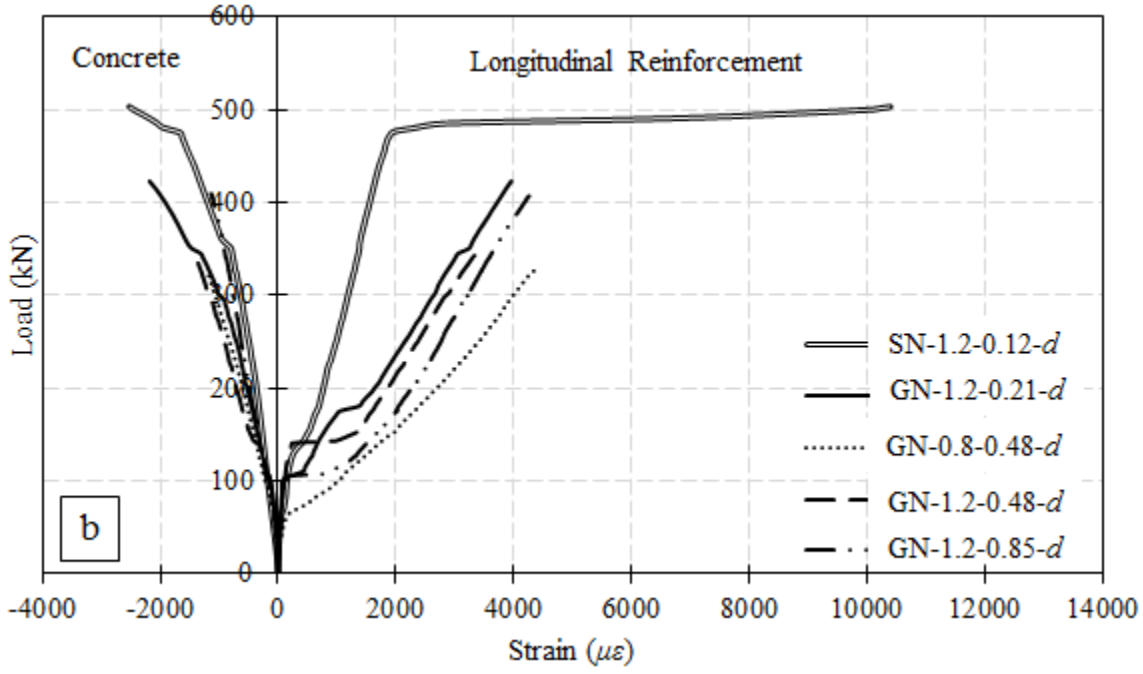

(b) The sagging moment section

Figure 6.6: Load-strain relationship for NSC beams of Series III

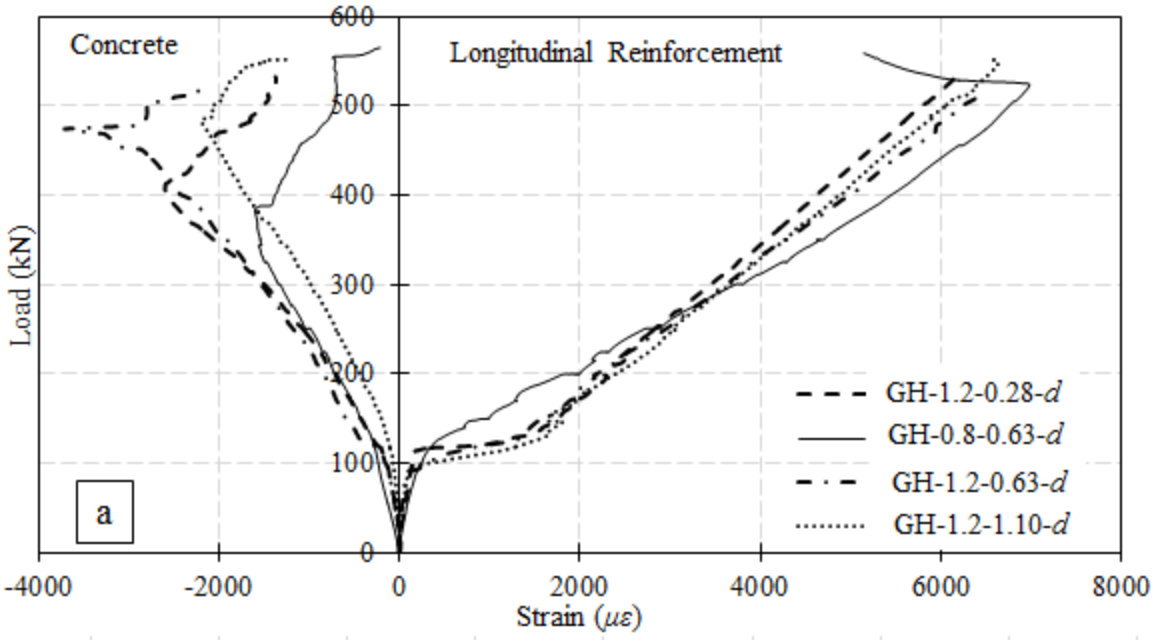

(a) The hogging moment section

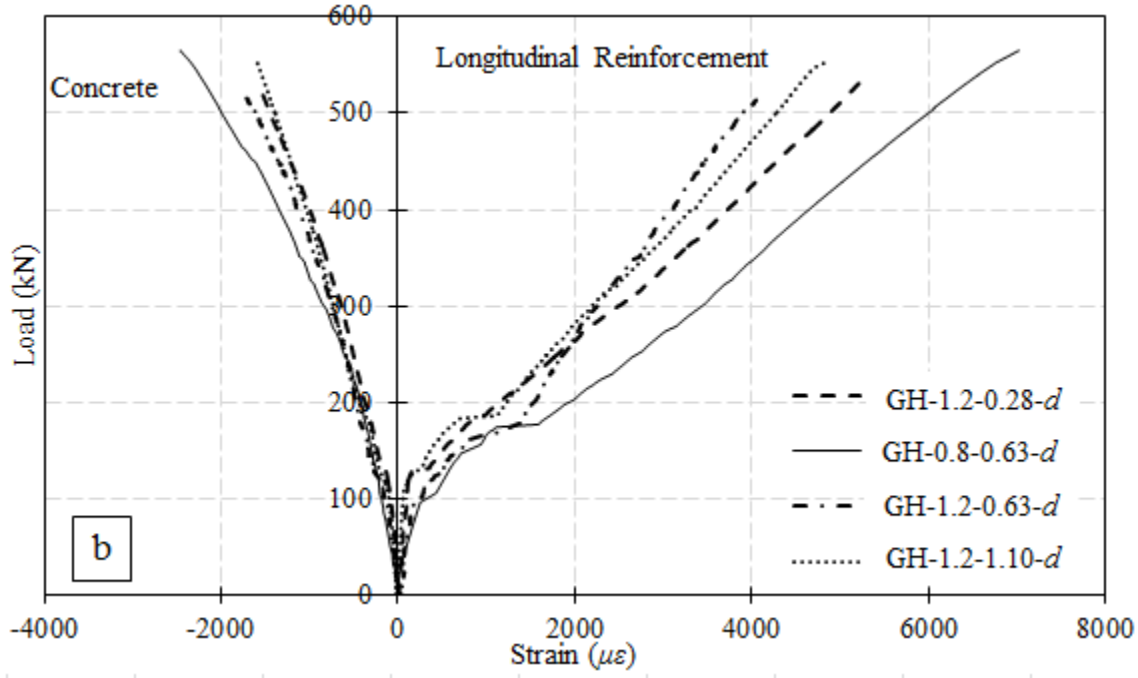

(b) The sagging moment section

Figure 6.7: Load-strain relationship for HSC beams of Series III

At service load level, the tensile strength in the longitudinal reinforcement should be less than one-quarter the ultimate tensile strength; according to CSA/S806-12 (CSA 2012). The corresponding strain at that limit of the used bars is 5,250 $\mu\varepsilon$. In all the GFRP-reinforced beams, the longitudinal tensile strains were well below that limit at both the hogging and sagging moment sections. The strain at the hogging moment section was 1,590, 1,020, 1,180, 1,940, 1,690, 200, 1,500 and 1,580 $\mu\varepsilon$ in beams GN-1.2-0.21-*d*, GN-0.8-0.21-*d*, GN-1.2-0.48-*d*, GN-1.2-0.85-*d*, GH-1.2-0.28-*d*, GH-0.8-0.63-*d*, GH-1.2-0.63-*d*, and GH-1.2-1.10-*d*, respectively. It can be seen that the strain in beam GH-0.8-0.63-*d* was very small compared to the other beams. At the theoretical service load (87 kN) in that beam (GH-0.8-0.63-*d*), there were no flexural cracks at the hogging moment section. In beam SN-1.2-0.12-*d*, the strain at the hogging moment section at the service load was approximately 900 $\mu\varepsilon$. This value represents 75% of the specified limit in the CSA/A23.3-04 (1,200 $\mu\varepsilon$).

6.5 STRAINS IN STIRRUPS

In general, the stirrup strains in the interior shear span were very small until the formation of the diagonal crack; then, strains increased rapidly until failure. Similar behaviour was observed for the stirrups in the exterior shear span; however, the strains started to increase at higher load levels when the diagonal cracks in the exterior shear span developed. Also, the maximum measured stirrup strain in the exterior shear span was less than that in the interior shear span in which failure took place. The strains in the steel stirrups showed similar behaviour until the yielding point; then, very high strains (15,500 $\mu\varepsilon$) were measured. As expected, for both NSC and HSC GFRP-RC beams, the stirrups having small diameters experienced higher strains compared to those having large diameters. The maximum stirrup strain measured in all beams for both interior and exterior shear spans is presented in Table 6.2. When failure occurred in the

interior shear span, the maximum measured strains in the straight portion of the GFRP stirrups were 6,620, 8,940 and 7,640 $\mu\varepsilon$ in beams GN-1.2-0.63-*d*, GH-1.2-0.26-*d* and GH-1.2-1.10-*d*, respectively. These values represent approximately 25, 34 and 28% of the ultimate tensile strains of the used stirrups. However, the failure was due to the rupture of the stirrups at the bent portion that has low tensile strength and consequently ultimate strain compared to the straight portion. In beams GN-1.2-0.85-*d* and GH-1.2-1.10-*d*, failed due to the crushing of concrete web, the maximum stirrup strain was 2,600 and 3,160 $\mu\varepsilon$, respectively, which represents approximately 11 and 13% of the ultimate strain of the used stirrup (12.7-mm diameter).

Table 6.2: Maximum and average stirrup strain in test beams

Beam	Maximum measured stirrup strain ($\mu\varepsilon$)		Average stirrup strain ($\mu\varepsilon$)	
	Interior shear span	Exterior shear span	Interior shear span	Exterior shear span
SN-1.2-0.12-*d*	20,220	7,160	15,480	6,950
GN-1.2-0.21-*d*	-	5,240	-	2,470
GN-0.8-0.48-*d*	3,430	2,290	1,590	1,150
GN-1.2-0.48-*d*	6,620	2,910	2,350	1,450
GN-1.2-0.85-*d*	2,600	2,360	1,900	2,150
GH-1.2-0.28-*d*	8,940	7,600	5,090	2,700
GH-0.8-0.63-*d*	2,900	4,250	2,350	2,150
GH-1.2-0.63-*d*	7,640	1,950	4,100	1,790
GH-1.2-1.10-*d*	3,160	2,680	2,550	1,910

Moreover, the average of the measured strains in the stirrups intersected by the diagonal cracks in the interior shear spans is shown in Fig. 6.8. The higher the shear reinforcement ratio, the lower the average strain in both interior and exterior shear spans. This can be attributed to the axial stiffness (E_{fy} A_{fy}) of the stirrups. The HSC beams showed higher maximum and average strain values than their NSC counterparts. This can be attributed to the smooth crack surface in HSC beams that led to a reduction in the contribution of the aggregate interlock. This reduced contribution of the aggregate interlock resulted in an increase in the share of the load carried by the stirrups (Johnson and Ramirez 1989).

The measured stirrup strains in beams GN-1.2-0.48-*d*, GH-1.2-0.28-*d* and GH-1.2-0.63-*d* (stirrups with 6.3 and 9.5-mm diameter) exceeded the strain limits specified in both CSA/S806-12 (5,000 $\mu\varepsilon$) and ACI 440.1R-06 (4,000 $\mu\varepsilon$). The maximum measured stirrup strains, in the interior shear span, in beams GN-1.2-0.48-*d*, GH-1.2-0.28-*d* and GH-1.2-0.63-*d* were approximately 1.32, 1.8 and 1.53 times the CSA/S806-12 limit, respectively. These values were approximately 1.66, 2.24 and 1.91 times the ACI 440.1R-06 limit, respectively. Also, the maximum measured stirrup strains in the exterior shear span in beams GN-1.2-0.21-*d* and GH-1.2-0.28-*d*, reported in Table 6.2, exceeded these limits without reaching failure. The maximum stirrup strains in beams GN-1.2-0.85-*d* and GH-1.2-1.10-*d*, on the other hand, were well below the limits since failure was due to the crushing of the concrete in the web.

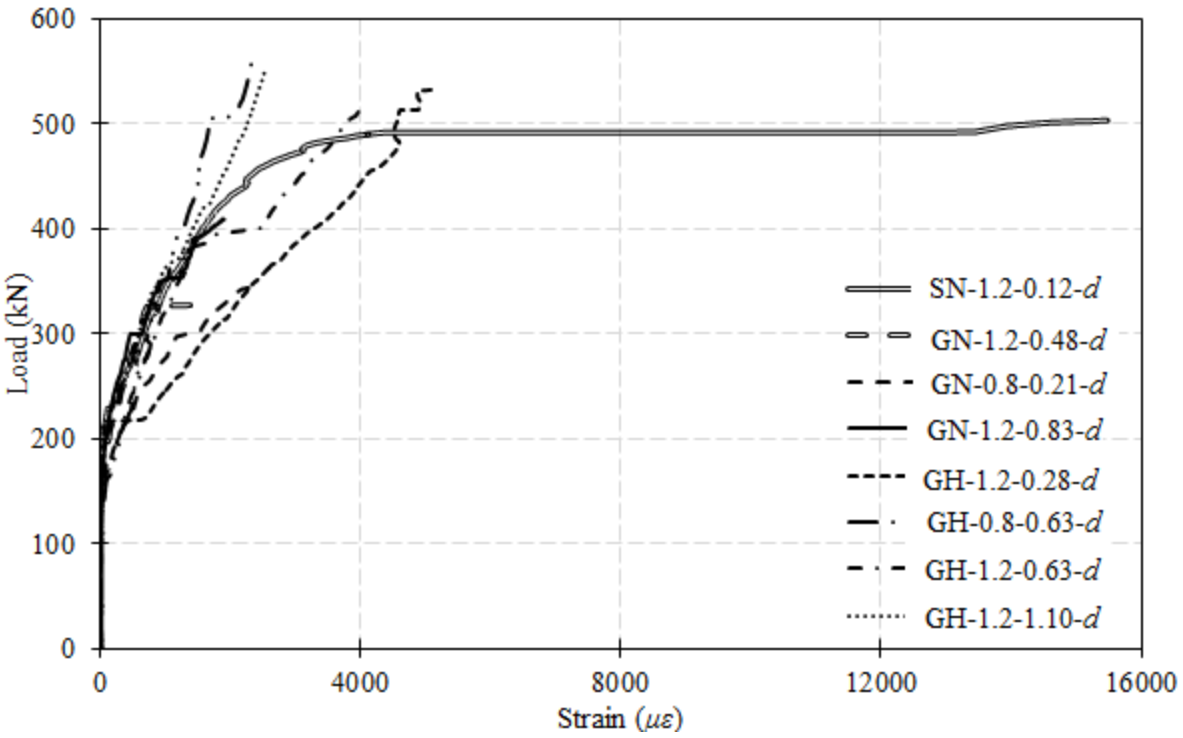

Figure 6.8: Load-average stirrup strain relationship in the interior shear span

6.6 REACTIONS AND MOMENT REDISTRIBUTION

The measured exterior-support reactions were used to calculate the actual internal forces, mainly bending moments and shearing forces, at any location along the length of the beam. The variation of the exterior reaction versus the total applied load, for all test beams of Series III, is shown in Figs. 6.9 and 6.10. The moment redistribution percentage can be obtained by comparing the actual and elastic bending moments. It can be seen that the forces and internal stresses followed the elastic distribution at the early stage of loading. After the formation of cracks at the hogging moment region, the exterior reaction and consequently the internal stresses began to diverge from the elastic values. The moment redistribution was from the hogging moment to the sagging moment regions, allowing the beam to resist higher loads than expected. At failure, the percentages of moment redistribution were approximately 29.0, 19.6, 20.0, 24.0,

22.2, 20.0, 26.0, 23.0 and 24.0% in specimens SN-1.2-0.12-*d*, GN-1.2-0.21-*d*, GN-0.8-0.48-*d*, GN-1.2-0.48-*d*, GN-1.2-0.85-*d*, GH-1.2-0.28-*d*, GH-0.8-0.63-*d*, GH-1.2-0.63-*d* and GH-1.2-1.10-*d*, respectively. The experimental and elastic bending moment the hogging and sagging sections at failure are presented in Table 6.3.

It can be noted that moment redistribution percentages in HSC beams were higher than those in NSC beams. This might be attributed to the higher amount of minimum shear reinforcement provided in the HSC beams as required by the CSA/S806-12 standard. The higher the transverse reinforcement ratio, the better the confinement of the concrete is. As the confinement increased, the ability of the beam to redistribute the moments increased. This is in a good agreement with the findings of El-Mogy et al. (2011). Moreover, it was found out that the curvature at the middle-support section in HSC beams is greater than that in NSC beams. In addition, this curvature was affected by the longitudinal reinforcement ratio where the curvature in beams with 0.8% longitudinal reinforcement ratio is greater than that in beams with higher ratio of 1.2%. It is well established that the higher rotation (or curvature) of the beam at the middle support results in higher amount of redistribution of the internal stresses. The calculated curvatures at the hogging and sagging moment sections in the test specimens are given in Table 6.3.

Increasing the shear reinforcement ratio by increasing the size of the stirrups seems to have a little effect on the moment redistribution. The moment redistribution increased with increasing the stirrup size in both the NSC and HSC beams, except beams GN-1.2-0.48-*d* and GH-0.8-0.48-*d*. Beams GN-1.2-0.48-*d* and GH-0.8-0.48-*d* exhibited the highest moment redistribution compared to other beams made of NSC and HSC beams, respectively. This might be attributed to the fact that beams GN-1.2-0.48-*d* and GH-0.8-0.48-*d* had more minor flexural cracks at the hogging moment region compared with the other beams. These minor cracks enhanced the

ability of beams GN-1.2-0.48-*d* and GH-0.8-0.48-*d* to exhibit more rotation at the middle support and, consequently, redistribute more bending moment from the hogging to the sagging moment region. A similar observation was reported by El-Mogy et al. (2011).

Table 6.3: Bending moments, elastic moments, curvature and moment redistribution at failure

Beam	Experimental Moment (kN.m)		Elastic Moment (kN.m)		Curvature × 10-6		MR (%)
	Hogging	Sagging	Hogging	Sagging	Hogging	Sagging	
SN-1.2-0.12-*d*	78.4	73.4	103.6	66.6	58	52	29.0
GN-1.2-0.21-*d*	70.0	60.5	87.0	55.9	19	23	19.6
GN-0.8-0.48-*d*	54.3	48.9	71.2	45.8	28	24	20.0
GN-1.2-0.48-*d*	53.6	52.0	73.5	47.3	19	20	24.0
GN-1.2-0.85-*d*	65.5	59.2	84.2	54.2	27	22	22.2
GH-1.2-0.28-*d*	87.6	76.4	109.5	70.5	29	25	20.0
GH-0.8-0.63-*d*	86.1	82.9	116.7	75.0	23	40	26.0
GH-1.2-0.63-*d*	82.3	74.9	105.0	67.5	36	24	23.0
GH-1.2-1.10-*d*	85.8	80.4	113.7	73.1	29	26	24.0

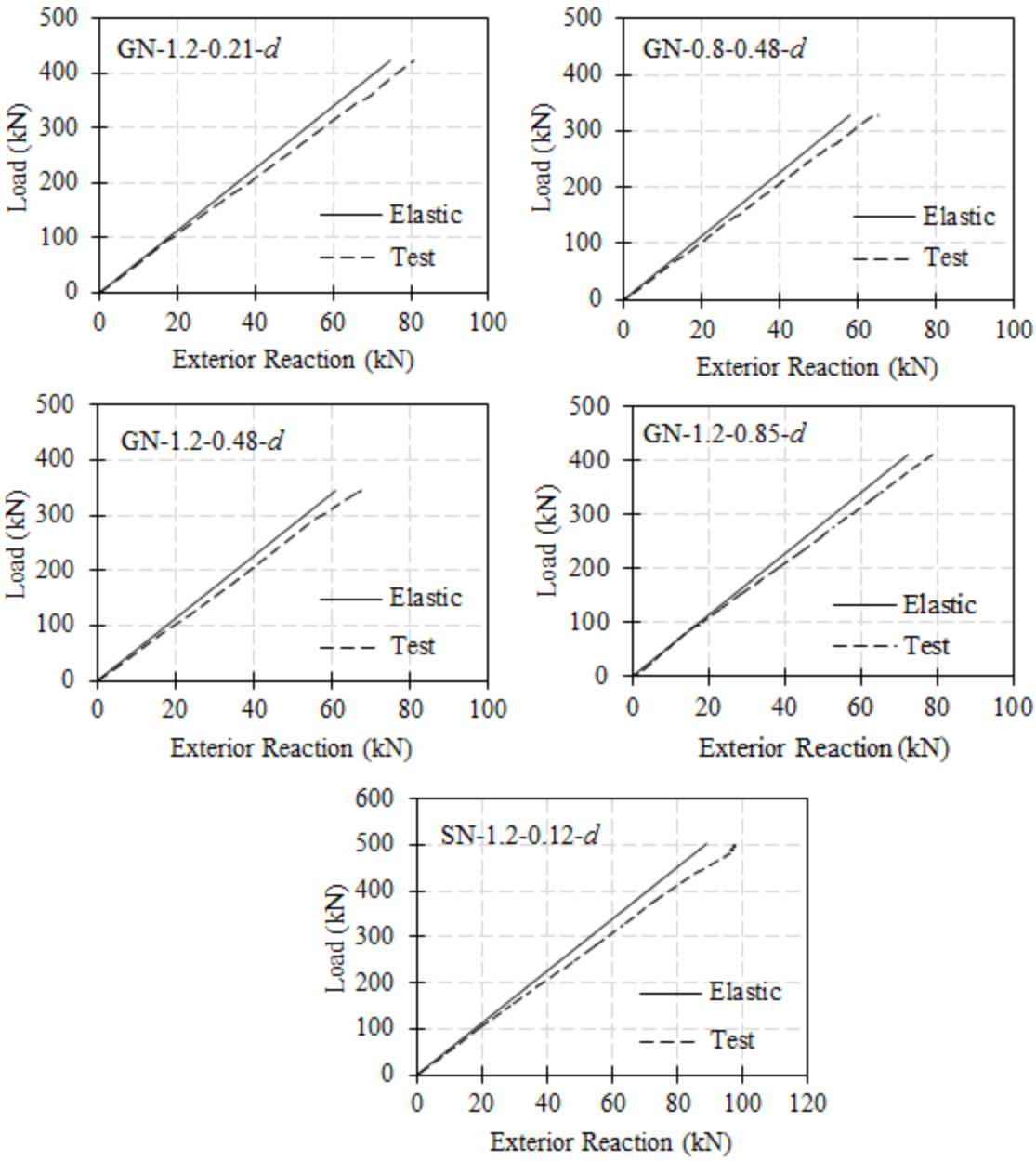

Figure 6.9: Load-exterior reaction relationship for NSC beams of Series III

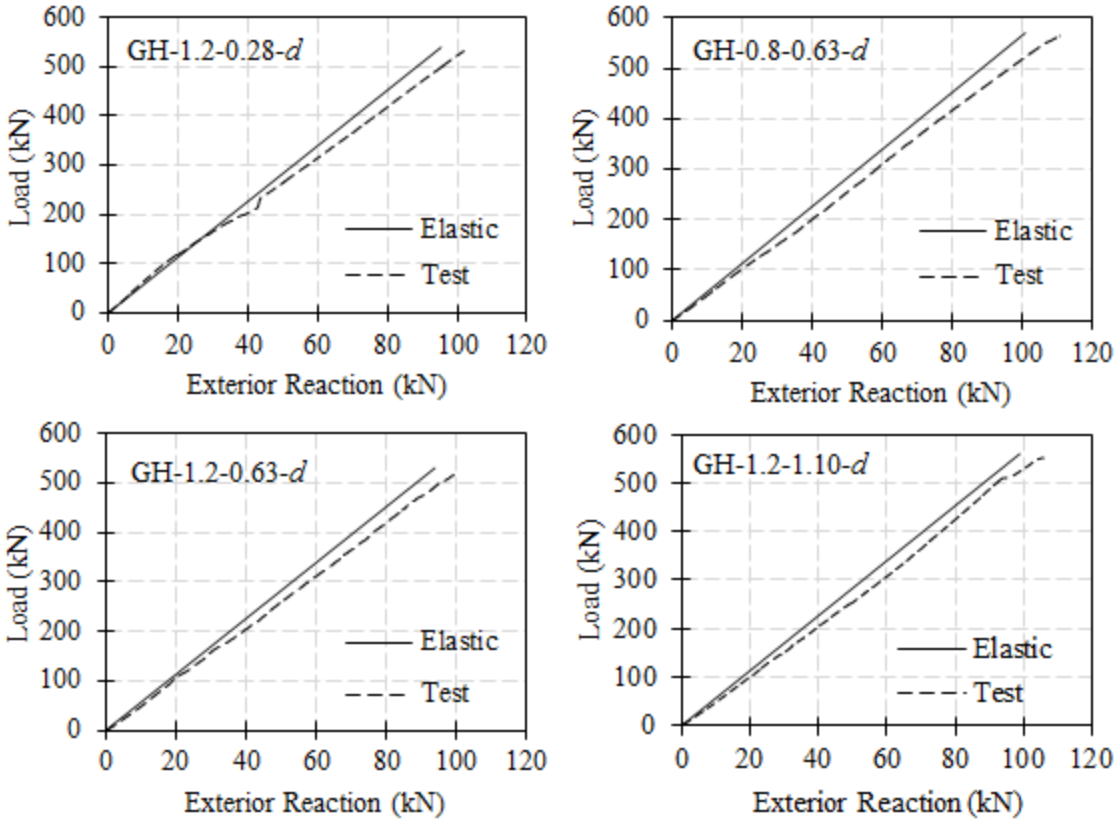

Figure 6.10: Load-exterior reaction relationship for HSC beams of Series III

6.7 SHEAR STRENGTH

Based on measured support reactions, the calculated shear forces followed the elastic distribution along the beam until moment redistribution began. Afterwards, for all beams, the shear force in the interior shear spans started to have lower values than those of the elastic distribution until failure. Comparison between measured and elastic shear force at the same load, in the interior and exterior shear spans, is documented in Table 6.4. It is well-known that the principal tensile stresses, that cause diagonal cracking at any location near the interior support, depend on the values of bending moments and shear forces at that location. Therefore, beams that experienced higher moment redistribution were capable of resisting higher loads before failure.

In GFRP-RC beams, the shear capacity in the interior shear span was 130.0, 104.0, 107.0, 126.0, 164.0, 172.0, 160.0 and 169.0 kN. In beams GN-1.2-0.12-*d*, GN-0.8-0.48-*d*, GN-1.2-0.48-*d*, GN-1.2-0.85-*d*, GH-1.2-0.28-*d*, GH-0.8-0.63-*d*, GH-1.2-0.63-*d* and GH-1.2-1.10-*d*, respectively. The ratio of the shear force in the exterior shear span to that in the interior shear span was approximately 0.63 on average. Beams with half the minimum shear reinforcement (GN-1.2-0.21-*d* and GH-1.2-0.28-*d*) achieved higher or similar shear capacity compared to that of beams with the minimum shear reinforcement (GN-1.2-0.48-*d* and GH-1.2-0.63-*d*). This could be attributed to the higher tensile strength of the 6.3-mm diameter stirrups used in GN-1.2-0.21-*d* and GH-1.2-0.28-*d* compared to that of the 9.5-mm diameter stirrups used in GN-1.2-0.48-*d* and GH-1.2-0.63-*d*. This high tensile strength allowed the 6.3-mm diameter stirrups to sustain higher loads before failure compared to those measured in the 9.5-mm diameter ones. Also, the angle of inclination of the diagonal crack contributed to this behaviour where the angle was 44^o and 50^o in GN-1.2-0.21-*d* and GH-1.2-0.28-*d*, respectively, compared to 54^o and 59^o in beams GN-1.2-0.21-*d* and GH-1.2-0.28-*d*, respectively. Steeper diagonal cracks results in lower shear reinforcement contribution.

Twice the minimum shear reinforcement, in both NSC and HSC beams, did not show an increase in the shear capacity compared to beams with lower shear reinforcement. This is due to that the failure was governed by the crushing of the concrete in the web before the stirrups reached their rupture strain.

In beams with minimum shear reinforcement, it can be seen that the shear strength of NSC beams was not significantly affected by the 50% increase in longitudinal reinforcement ratio (from 0.8 to 1.2%). However, for HSC beams, the shear strength decreased by approximately 8% for the same increase in longitudinal reinforcement ratio (50%). This may be attributed to the

higher percentage of moment redistribution that occurred in beam GH-0.8-0.63-*d* compared with beam GH-1.2-0.63-*d*. Higher percentage of moment redistribution results in lower moment at the middle support and consequently more shear force is needed to cause failure. In addition, in beam GH-1.2-0.63-*d*, the angle of inclination of the diagonal shear crack was steeper than that observed in all other test beams. Steeper crack results in less contribution of stirrups.

Test results showed that the concrete strength had a pronounced effect on the shear strength. However, this increase in the shear strength is a result of increasing both the concrete strength and the transverse reinforcement ratio. Increasing the concrete strength from 42 to 80 MPa increased the shear strength by 20 and 28% in beams having half and twice the minimum shear reinforcement, respectively. Moreover, the shear strength in beams with minimum shear reinforcement ratio increased by approximately 64 and 48% when the concrete strength increased from 43 to 81 MPa for beams with longitudinal reinforcement ratio of 0.8 and 1.2%, respectively. Again, this is due to a combination of the effect of the increase in the concrete strength and the higher shear-reinforcement ratio in HSC beams. In addition, the amount of moment redistribution contributes to this increase as explained previously. On the contrary, smaller percentage of moment redistribution results in greater moment near the middle support, which causes higher principal tensile stresses that lead to failure of the beam at a lower shear force.

For beam SN-1.2-0.12-*d*, the shear capacity, in the interior shear span, was 153.75 kN. This represents approximately 1.44 times that of beam GN-1.2-0.48-*d*, with the same longitudinal reinforcement ratio and minimum shear reinforcement ratio. This increase is due to the high axial stiffness of both the longitudinal and transverse reinforcement of beam SN-1.2-0.12-*d*.

Table 6.4: Concrete strength, failure load and experimental and elastic shear forces at failure

Beam	f_c' (MPa)	Failure Load (kN)	Experimental Shear, V_{test}, (kN)		Elastic shear, $V_{elastic}$, (kN)		V_{test} / $V_{elastic}$	
			Int.	Ext.	Int.	Ext.	Int.	Ext.
SN-1.2-0.12-*d*	45	503	153.8	97.8	162.8	88.8	0.95	1.10
GN-1.2-0.21-*d*	43	423	130.0	80.8	136.2	74.6	0.95	1.08
GN-0.8-0.48-*d*	43	328	104.0	65.0	109	61.0	0.96	1.08
GN-1.2-0.48-*d*	43	345	107.0	69.0	110	63.0	0.98	1.10
GN-1.2-0.85-*d*	43	409	126.0	78.9	132.7	72.2	0.95	1.09
GH-1.2-0.28-*d*	80	532	164.0	101.9	172.1	93.9	0.95	1.08
GH-0.8-0.63-*d*	81	565	172.0	111.0	183	100	0.94	1.10
GH-1.2-0.63-*d*	81	517	160.0	100.0	165	90.0	0.95	1.10
GH-1.2-1.10-*d*	80	552	169.0	107.1	178.6	97.4	0.94	1.10

6.8 COMPARISON BETWEEN EXPERIMENTAL AND CODE PREDICTED SHEAR STRENGTH

Table 6.5 presents a comparison between the experimental and predicted shear capacity by the CSA/S806-12 (CSA 2012), the ACI 440.1R-06 (ACI Committee 440 2006) and the CSA/S6-06 (CSA 2009). It can be seen that the CSA/S806-12 yielded conservative predictions of the shear capacity. The average experimental-to-predicted shear capacity ratio is 1.42 with a coefficient of variation of 17.6%. The ACI 440.1R-06 was more conservative and high scatter of the points where the experimental-to-predicted shear capacity ratio was 1.81 and a coefficient of variation of 34.0%. The better prediction by the CSA/S806-12 is mainly due to that the fact that it accounts for the straining actions at the shear critical section. Moreover, the CSA/S6-06 (2009)

gave close predictions to that of the CSA/S806-12 with an average experimental-to-practiced ratio of 1.38. However, the coefficient of variation was 34.0% which is higher than that in the case of the CSA/S806-12. This is because the CSA/S6-06 (2009) overestimated the shear strength of beams having twice the minimum shear reinforcement.

Table 6.5: Experimental and predicted shear strength of test specimens

Beam	Experimental shear capacity, V_{exp}, (kN)	Predicted shear capacity					
		CSA/S806-12		ACI 440.1R-06		CSA/S6-06	
		V_{pred} (kN)	$\frac{V_{exp}}{V_{pred}}$	V_{pred} (kN)	$\frac{V_{exp}}{V_{pred}}$	V_{pred} (kN)	$\frac{V_{exp}}{V_{pred}}$
GN-1.2-0.21-*d*	130.0	76.9	1.69	49.2	2.64	73.3	1.77
GN-0.8-0.48-*d*	104.0	87.1	1.19	65.6	1.60	99.5	1.05
GN-1.2-0.48-*d*	107.0	87.1	1.23	70.0	1.53	99.8	1.07
GN-1.2-0.85-*d*	126.0	111	1.14	117	1.05	157.5	0.80
GH-1.2-0.28-*d*	164.0	92.2	1.77	61.5	2.67	79.0	2.08
GH-0.8-0.63-*d*	172.0	106.6	1.61	83.1	2.07	94.6	1.82
GH-1.2-0.63-*d*	160.0	106.6	1.50	88.5	1.82	107.3	1.49
GH-1.2-1.10-*d*	169.0	136.3	1.24	150	1.13	171.6	0.98
Mean			1.42		1.81		1.38
COV (%)			17.6		34.0		34.0

CHAPTER 7: FINITE ELEMENT MODELING

7.1 GENERAL

A non-linear finite element model (FEM) was constructed to simulate the shear behaviour of continuous concrete beams reinforced with GFRP bars. A specialized finite element analysis software package, ATENA 3D – version 5.0 (Cervenka et al. 2013), was used in this process. To verify the accuracy of the constructed FEM, the experimental results presented earlier were used. Moreover, the model was validated using the test results of previous research done by El-Mogy et al. (2011). In this chapter, the steps to construct the FEM including the elements used in modeling, material types and boundary conditions are explained in details. In addition, the different assumptions made in the finite element modeling process including meshing, constitutive models for concrete and the used solution method are also discussed.

Afterwards, the verified and validated FEM, described in this chapter, was used to conduct a parametric study to investigate the influence of key parameters on the behaviour of FRP-RC continuous concrete beams. The results of this study are presented in the next chapter.

7.2 CONSTITUTIVE MODELS FOR MATERIALS AND ELEMENTS TYPES

7.2.1 Concrete Material

In this study, 8-node brick elements (CCIsoBrick) with three degrees of freedom at each node were used to model the concrete (Fig. 7.1). These are isoparametric elements integrated by Gauss integration.

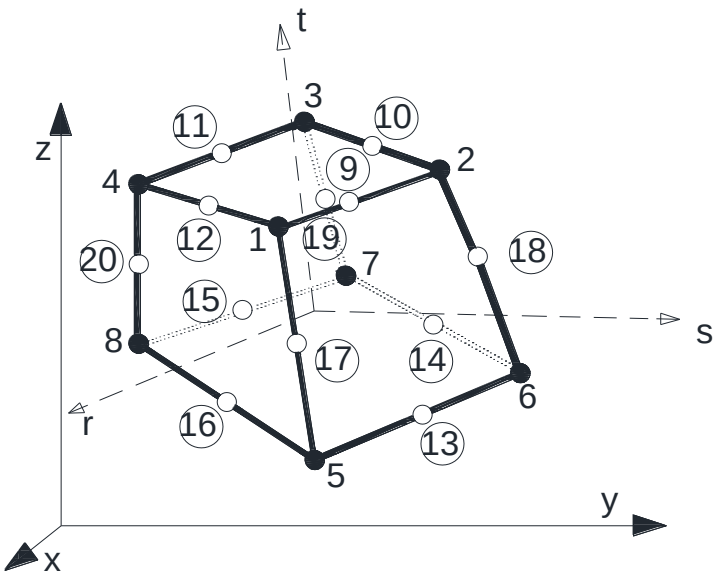

Figure 7.1: Element CCIsoBrick (Cervenka et al. 2013)

ATENA software contains three nonlinear material models. These models are a crack-band model based on fracture energy, a fracture-plastic model with non-associated plasticity and a micro-plane material model. These advanced models account for all the important aspects of the material behaviour in tension and compression. A built-in fracture-plastic material "3D Nonlinear Cementitious 2" is used for concrete in this study. The fracture model is based on the classical orthotropic smeared crack formulation and crack band model. It employs Rankine failure criterion, exponential softening, and it can be used as rotated or fixed angle crack model. The hardening/softening plasticity model is based on Menétrey-Willam failure surface. The model can be used to simulate concrete cracking, crushing under high confinement, and crack closure due to crushing in other material directions. The shear strength of cracked concrete is determined using the Modified Compression Field Theory, proposed by Vecchio and Collins (1986). A reduction of the concrete compressive strength is also considered in the direction parallel to the cracks. Another feature of ATENA's model is its capability to simulate the

contribution of the cracked concrete to the stiffness of the reinforcement, which is defined as tension stiffening.

The nonlinear behaviour of concrete in the biaxial stress state is described by means of the effective stress σ_c^{ef} and the equivalent uniaxial strain ε^{eq}. The effective stress is, in most cases, a principal stress. The equivalent uniaxial strain is introduced in order to eliminate the Poisson's effect in the plane stress state.

$$\varepsilon^{eq} = \frac{\sigma_{ci}}{E_{ci}} \qquad \text{[Eq. 7.1]}$$

The equivalent uniaxial strain can be considered as the strain, that would be produced by the stress σ_{ci} in a uniaxial test with modulus E_{ci} associated with the direction *i*. Within this assumption, the nonlinearity representing damage is caused only by the governing stress σ_{ci}.

The complete equivalent uniaxial stress-strain diagram for concrete is shown in Fig. 7.2. The concrete model incorporates the biaxial failure criterion recommended by Kupfer et al. (1969) as shown in Fig. 7.3.

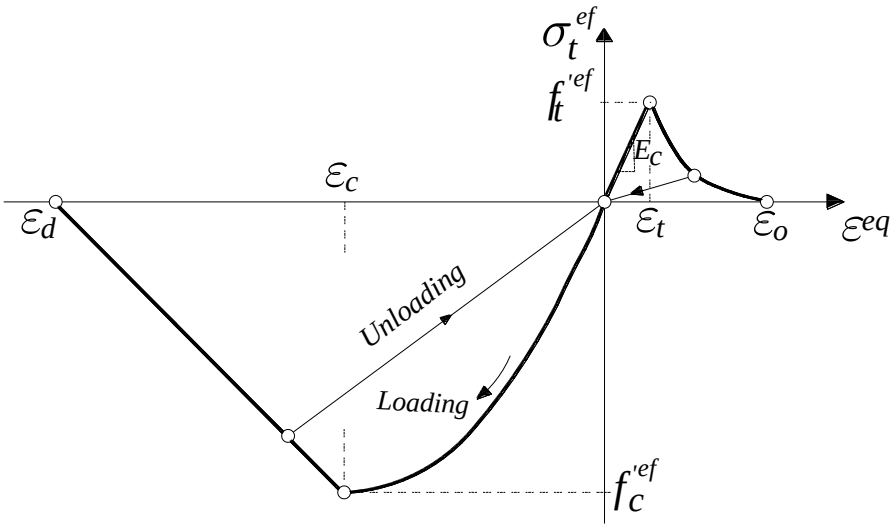

Figure 7.2: Uniaxial stress-strain law for concrete model (Cervenka et al. 2013)

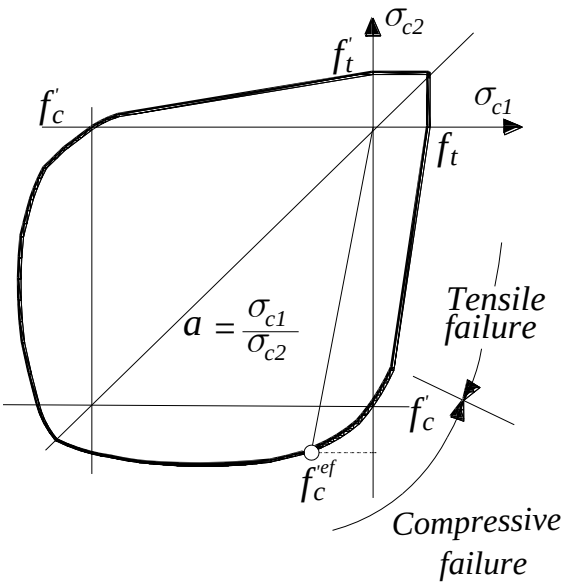

Figure 7.3: Biaxial failure function for concrete (Cervenka et al. 2013)

Fracture energy, G_f, is one of the mechanical characteristics of concrete that is used to define post-peak behaviour of RC in tension, and depends on the concrete strength as well as the aggregate size. The crack model that is used by the finite element program, ATENA, is based on the exponential crack opening law, relating the effective tensile strength, f'_t, to the crack width, *w*, as proposed by Hordijk (1991) and shown in Fig. 7.4.

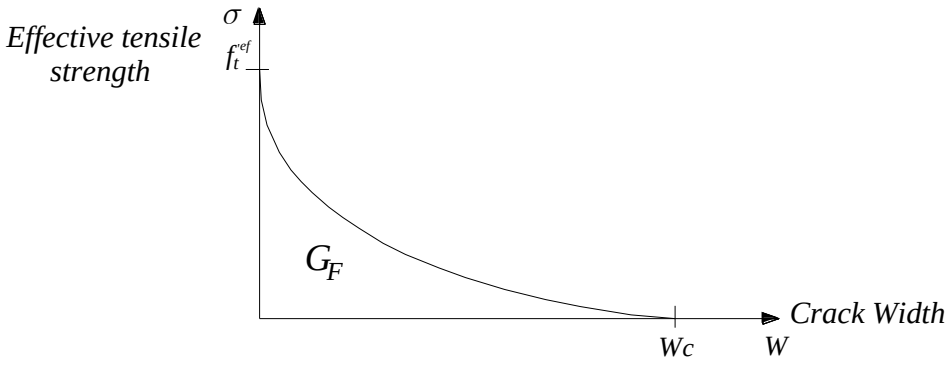

Figure 7.4: Exponential crack opening law (Cervenka et al. 2013).

In this model, the cube strength is entered then the program automatically generates a set of parameters based on codes and recommendations. However, any parameter can be changed based on rational reasons. In this study, some parameters were changed to better simulate the experimental results. The used tensile strength was calculated according to the CSA standards equation ($f_r = 0.6\sqrt{f_c'}$). Also, the modulus of elasticity was changed since the suggested equation gives high values. These high values increased the stiffness of the beam that, in turn, resulted in steeper load-deflection relationship. The used modulus of elasticity was calculated according to the CSA standards where it can be determined as follows:

$$E_c = (3300\sqrt{f_c'} + 6900)(\frac{\gamma_c}{2300})^{1.5} \qquad \text{[Eq. 7.2]}$$

where γ_c is the density of concrete and ranges from 1500 to 2500 kg/m^3

For normal concrete strength with compressive strength between 20 and 40 MPa, the modulus of elasticity may be taken as

$$E_c = 4500\sqrt{f_c'} \qquad \text{[Eq. 7.3]}$$

7.2.2 Reinforcement Materials

The reinforcement materials in this research (longitudinal bars and stirrups) were modeled as truss elements with one node at each end. The finite element "CCIsoTruss" was used for that purpose. These are isoparametric elements integrated by Gauss integration at 1 or 2 integration points for the case of linear or quadratic interpolation, i.e. for elements with 2 or 3 element nodes, respectively. They are suitable for plane 2D as well as 3D analysis problems. Geometry of the elements is depicted in Fig. 7.5.

Steel was defined using bilinear stress-strain relationship with a yielding strength, yielding strain and modulus of elasticity obtained experimentally (Chapter 3). The GFRP reinforcement was defined with linear-elastic stress-strain relationship up to failure. Again, the modulus of elasticity, ultimate strength and strain for GFRP bars, documented in Chapter 3, were used for the reinforcing bars in the program.

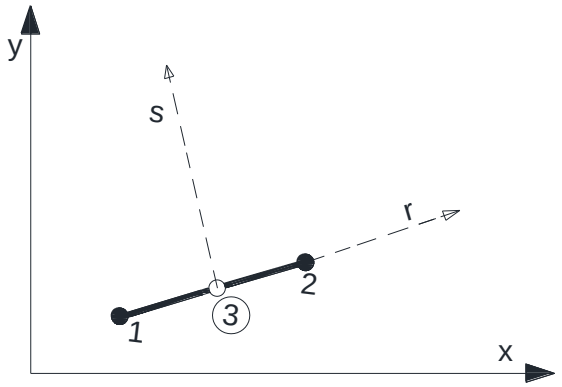

Figure 7.5: CCIsoTruss finite element (Cervenka et al. 2013)

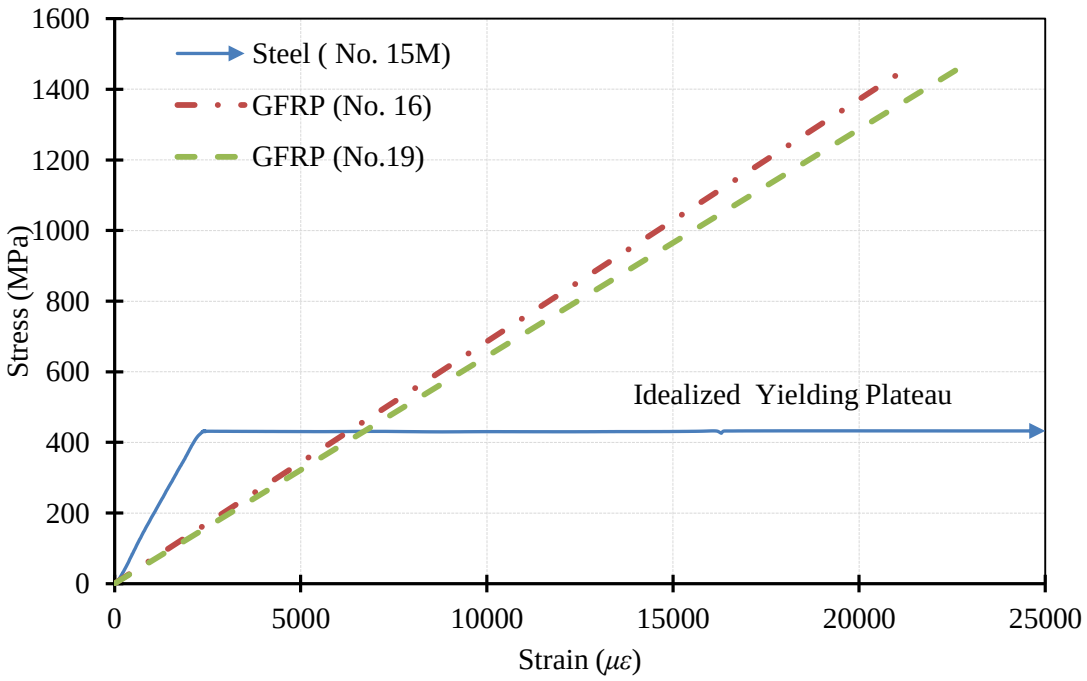

Figure 7.6: Stress-strain relationship for reinforcing bars

7.2.3 Bearing Plates

Steel plates were used at both loading and supporting locations. These plates ensured proper distribution of concentrated stress. Similar to concrete, these plates were modeled using the eight-node brick elements used for concrete. However, the steel bearing plates were defined as linear-elastic material with a modulus of elasticity of 210 GPa and a Poisson's ratio of 0.3.

7.3 BOND-SLIP MODELS FOR REINFORCING BARS

The bond-slip relationship represents a basic property of the reinforcement bond model in finite element modelling. This relationship defines the bond strength depending on the value of current slip between reinforcement and surrounding concrete. In previous studies (Gravina and Smith 2008 and El-Mogy et al. 2010 &2011), it was reported that the bond-slip relationship between FRP bars and the surrounding concrete are one of the factors that affect the overall behaviour of continuous beams. Therefore, different bond-slip relationship was used in this study based on the reinforcing material type. ATENA contains three bond-slip models: 1) according to the CEB-FIB model code 1990, 2) slip law by Bigaj (Bigaj 1999) and, 3) the user defined law. In the first two models, the laws are generated based on the concrete compressive strength, reinforcement diameter and reinforcement type. The important parameters are also the confinement conditions and the quality of concrete casting. Of these models, the CEB-FIB model code 1990 was used for the steel-RC concrete beams. This model consists of ascending curve followed by a descending branch with a steady-constant line at the end of the relationship as shown in Fig. 7.7. The ascending branch of the model follows the formula given in Eq. 7.4 (CEB-FIP 1990).

$$\tau = \tau_{max} \left(\frac{s_l}{0.6}\right)^{0.4} \qquad \text{[Eq. 7.4]}$$

Where τ and s_l are the bond stress and the corresponding slippage, respectively, and τ_{max} is the maximum bond strength of the steel bar embedded in concrete calculated from Eq. 7.5. The relationship was defined by six points on the ascending branch. The descending branch of the model is linear all the way down to a bond stress of $0.15\,\tau_{max}$ followed by a constant stress values for slip more than 1 mm as shown in Fig.7.7.

$$\tau_{max} = 2\sqrt{f_c'} \qquad \text{[Eq. 7.5]}$$

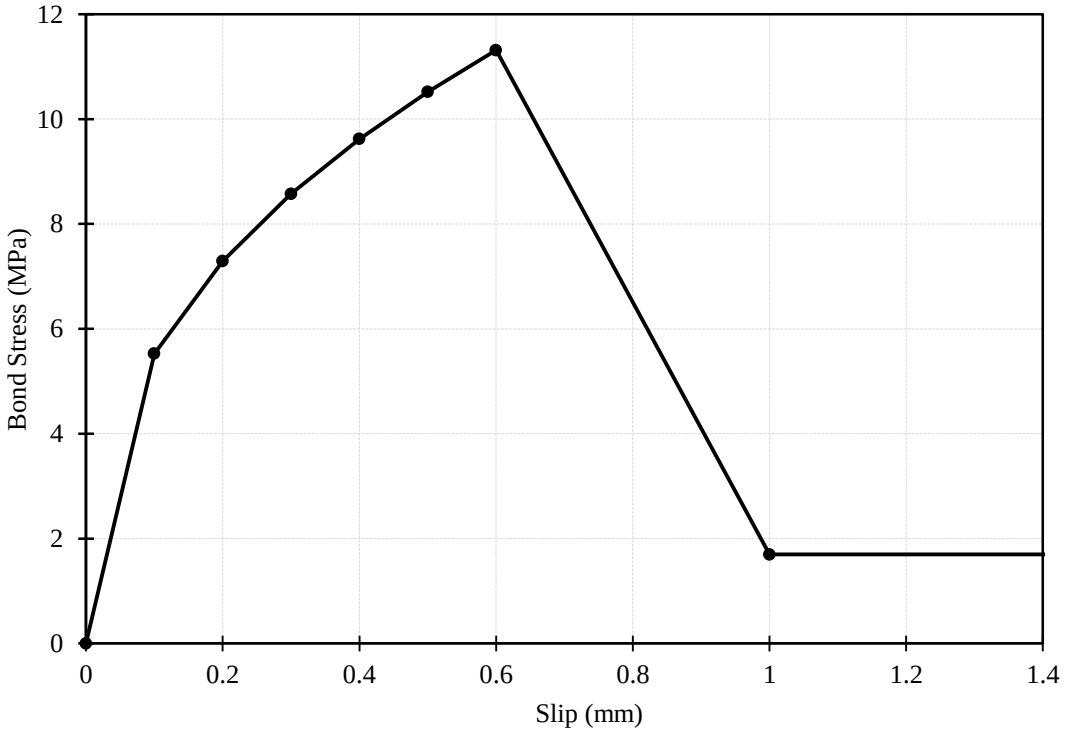

Figure 7.7: Bond-slip relationship for steel bars embedded in concrete (CEB-FIP 1990)

Because the GFRP bars have different surface characteristics, a user defined bond-slip model was used Fig. 7.8. This model was proposed by Alves et al. (2011) at the University of Manitoba. The proposed bond-slip relationship was a result of extensive testing of sand-coated GFRP bars that had similar surface texture to those used in this study.

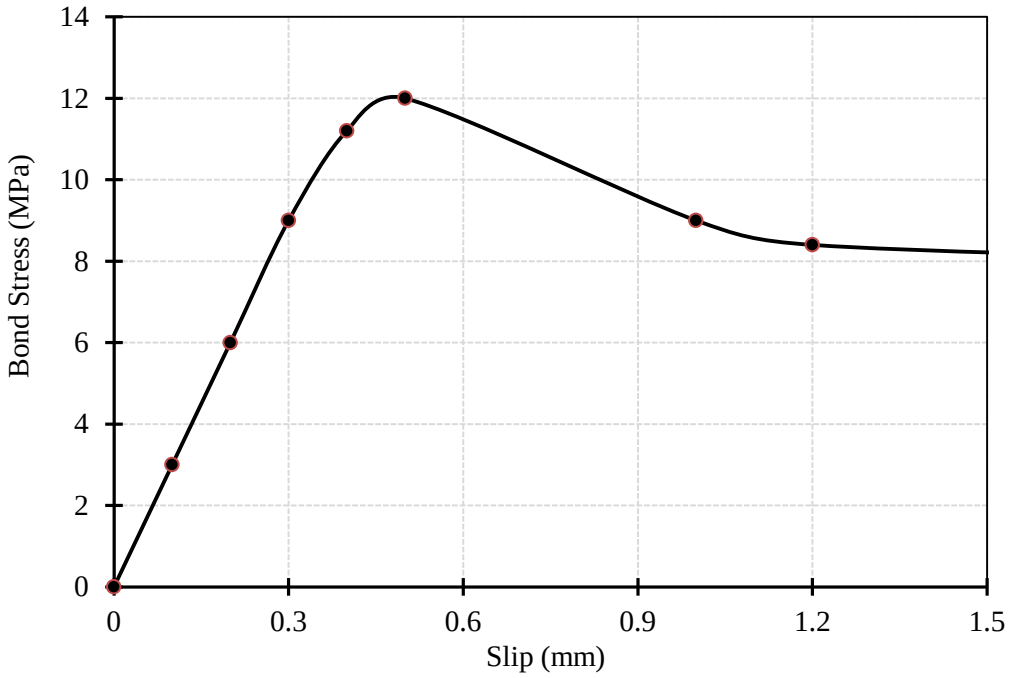

Figure 7.8: Bond-slip relationship for GFRP bars (Alves et al. 2011)

7.4 MODEL GEOMETRY, BOUNDARY CONDITIONS AND MESH SIZE

The tested beams were modeled in full as shown in Fig. 7.9. Similar to the experiments, the translation was restrained in the longitudinal direction at the middle support to simulate the hinge support while the horizontal translation was allowed at the external supports to simulate rollers supports. Moreover, translations at the three external supports were also prevented in the out-of-plan direction.

A preliminarily study was conducted to evaluate the effect of mesh size on the finite element results. The main objective was to find suitable mesh size to achieve a reasonable balance between accuracy of the result and the number of elements in the model which dramatically affects the required computing space and processing time to solve the model. A number of trials were conducted using different mesh size ranging from 50 to 100 mm (element side length). It was found out that there is no significant difference in the results at that range while the model with a 50-mm mesh size required more than double the time in the case of the 100-mm mesh size. Therefore, a mesh size of 100 mm was chosen in the entire study. An isometric view of the geometry and dimensions of the 3-D model is shown in Fig. 7.9. The longitudinal reinforcement and transverse stirrups are illustrated in Fig. 7.10.

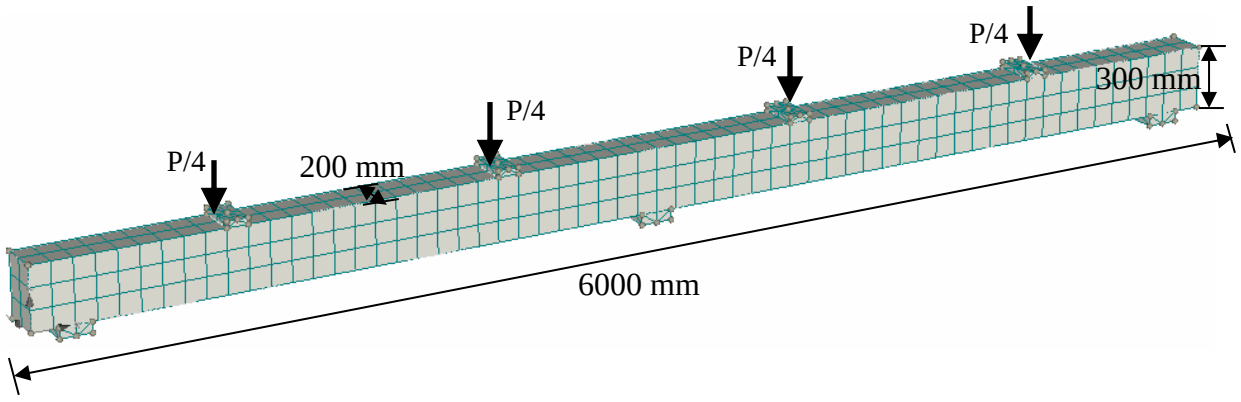

Figure 7.9: Model geometry and concrete elements

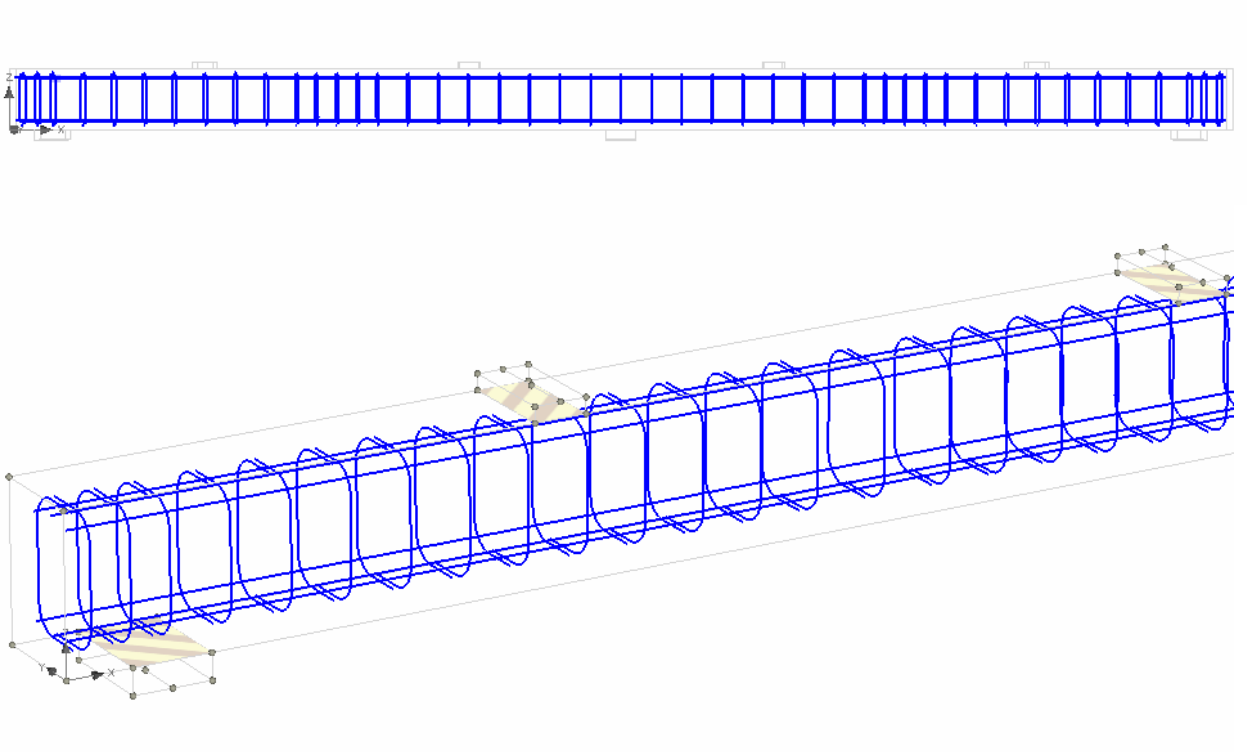

Figure 7.10: Longitudinal and transverse reinforcement configuration

7.5 SOLUTION CONTROL

In finite element analysis, the total applied load was divided into a series of load steps to take the effect of non-linearity into consideration. Each load step was assigned a specific load increment in a certain direction. The stiffness matrix of the model was adjusted at the end of each load step to include the non-linear changes to the stiffness before proceeding to the next step. Newton-Raphson equilibrium iterations technique was selected to update the model stiffness. This technique provides convergence at the end of each load step within a pre-defined tolerance limit. In each step, the program was allowed to run up to 100 iterations until convergence was achieved the tolerance limit. This process of iterations continued until the problem converges (Cervenka et al. 2013).

7.6 MODEL VERIFICATION

7.6.1 Beams without Shear Reinforcement

The developed model described above was verified against the experimental results of the tested beams. Four beams were selected from beams without shear reinforcement (Series I) for the verification process. Those beams are SN-1.2-0.0-*d*, GN-0.8-0.0-*d*, GN-1.2-0.0-*d* and GN-1.6-0.0-*d*. Beam SN-1.2-0.0-*d* was chosen to verify the model against beam with longitudinal steel reinforcement. The other three beams with GFRP reinforcement were chosen to verify the model against different longitudinal reinforcement ratios. The exterior reaction, load-deflection behaviour and the tensile strains in the longitudinal reinforcement at both the hogging and sagging moment sections in each beam were compared to those obtained from the FEM.

Figure 7.11 shows the load-exterior reaction relationship predicted by the model against that obtained experimentally for the above mentioned beams. It can be seen that the model was able to redistribute the internal forces once the first crack initiated. Moreover, the exterior reactions obtained from FEM were in good agreement with the experimentally measured ones.

The shear strength predicted by the FEM was calculated using the measured exterior and interior reactions along with the applied load. The FEM could reasonably predict the experimental shear strength where the ratio of the experimental-to-FEM shear, in the interior shear span at failure, was 1.01, 0.99, 0.95 and 1.0 in SN-1.2-0.0-*d*, GN-0.8-0.0-*d*, GN-1.2-0.0-*d* and GN-1.6-0.0-*d*, respectively. This ratio in the exterior shear span was 1.05, 1.01, 1.02 and 1.09 in SN-1.2-0.0-*d*, GN-0.8-0.0-*d*, GN-1.2-0.0-*d* and GN-1.6-0.0-*d*, respectively

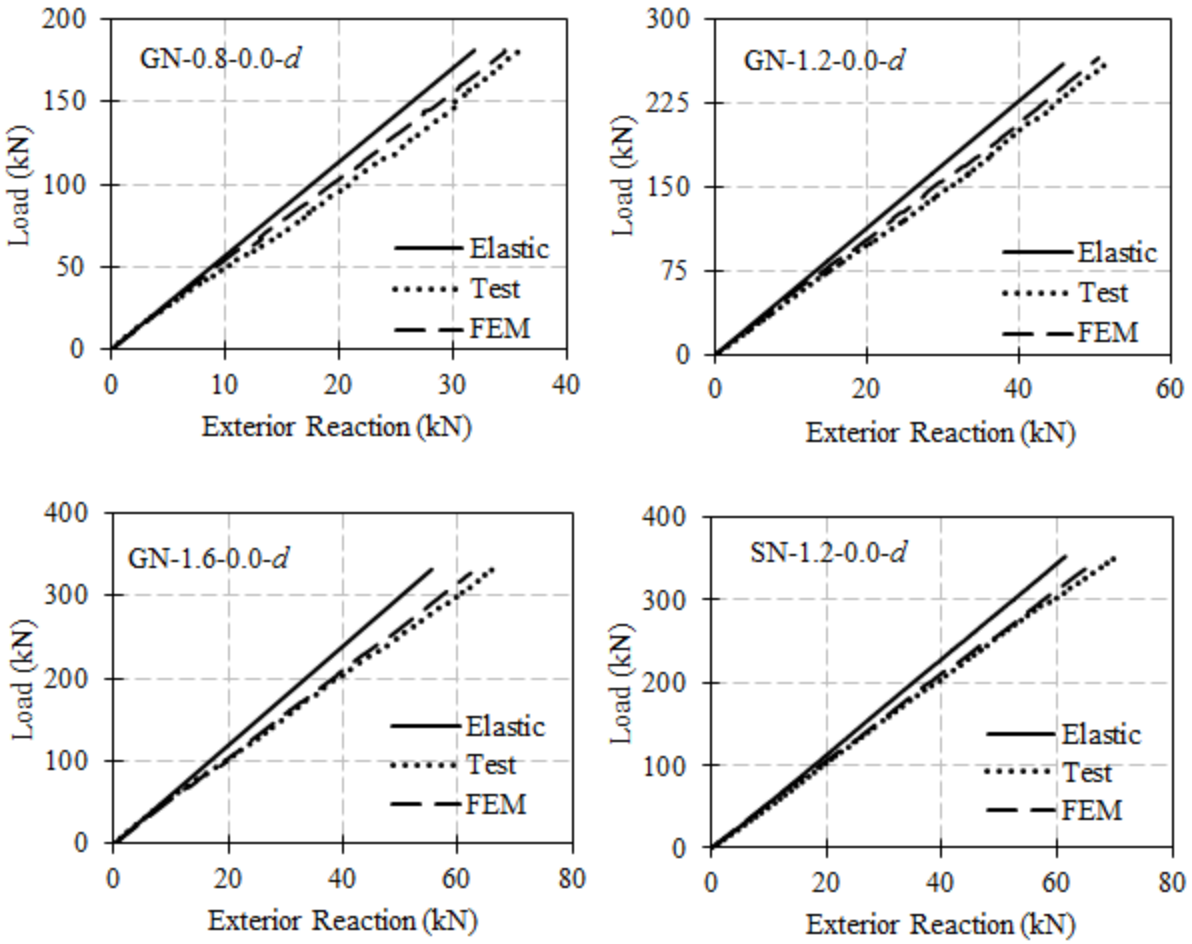

Figure 7.11: Load-exterior reaction relationship

Regarding the load-deflection relationship, it can be seen, in Fig. 7.12, that the FEM showed a very similar behaviour. The load-deflection relationship was linear up to the development of the first crack at the hogging moment section; then, nonlinear behaviour observed until failure. Near failure, there was slight difference between the FEM deflection and the experimental one. The failure load predicted by the FEM was within approximately 5% of the experimental one.

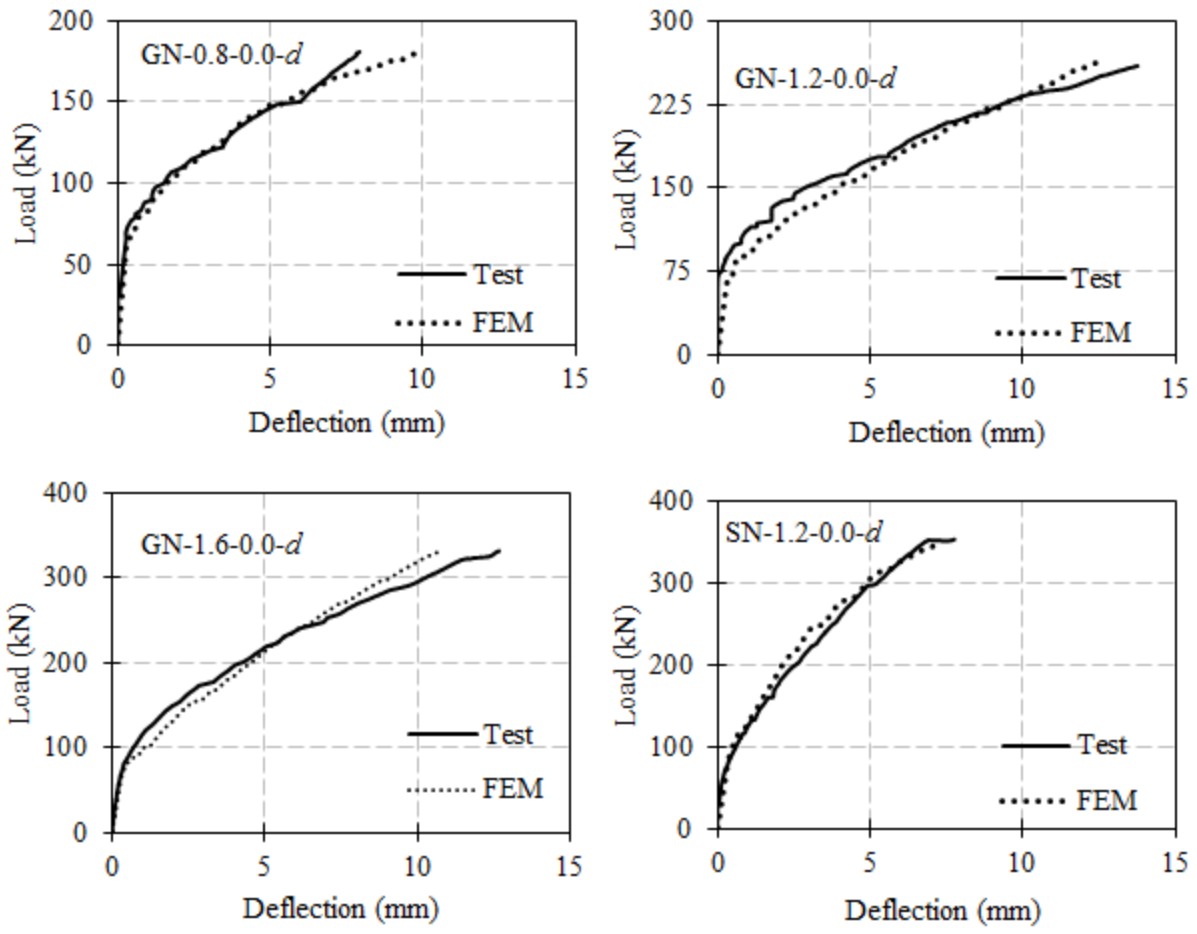

Figure 7.12: Load-deflection relationship at mid span

Figures 7.13 and 7.14 show a comparison between the experimental and the FEM strains at the hogging and sagging moment sections, respectively. The FEM was able to predict similar strains at both sections in beams SN-1.2-0.0-*d*, GN-1.2-0.0-*d* and GN-1.6-0.0-*d*. In model GN-0.8-0.0-*d*, the FEM predicted smaller strain than the experimental one at the hogging moment section; however, the curves were approximately identical near failure. The opposite can be seen at the sagging moment section where the FEM strain was greater than the experimental one all the way up to failure. This might be due to a difference in the cracking load where the flexural cracks at the hogging moment section in the FEM initiated at a higher load than the cracking load in the

experiment, refer to Fig. 7.13. The opposite can be seen in the case of the sagging moment section (Fig. 7.14).

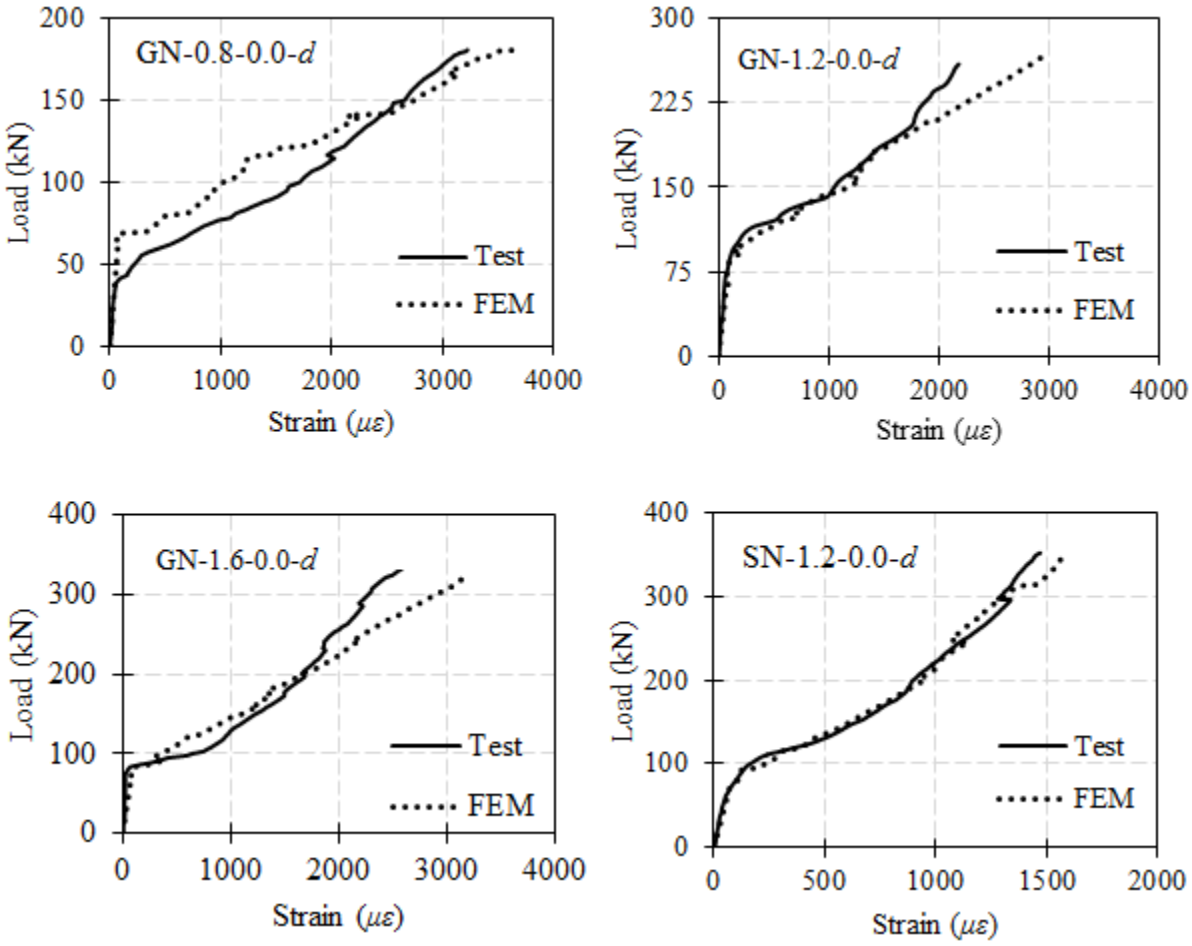

Figure 7.13: Load-strain relationship at the hogging moment section

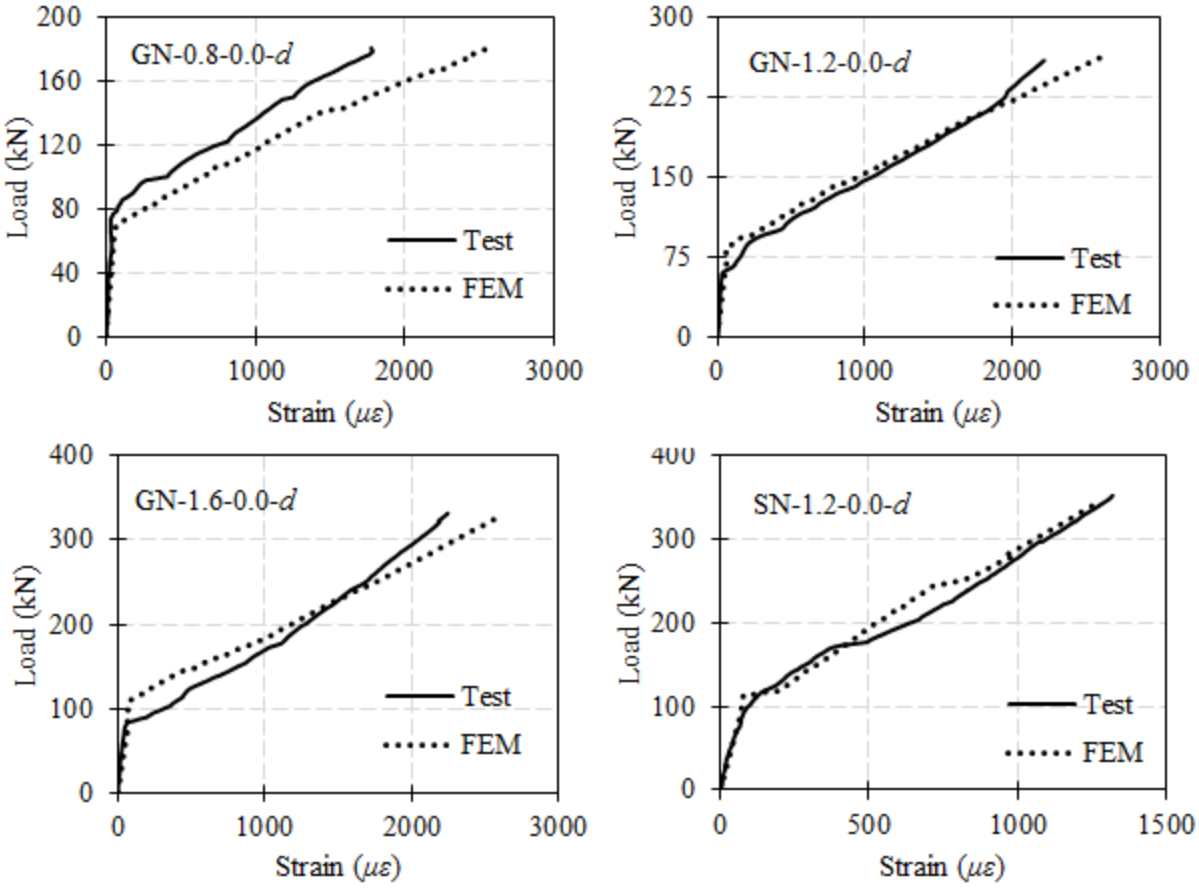

Figure 7.14: Load-strain relationship at the sagging moment section

7.6.2 Beams with Shear Reinforcement

In this section, the verification of the proposed model was conducted against five beams featuring most of the variables tested experimentally such as concrete compressive strength, longitudinal reinforcement type and stirrup diameter. The selected beams were GN-1.2-0.21-*d*, GN-1.2-0.48-*d*, GH-1.2-1.10-*d* and GH-1.2-0.28-*d* and SN-1.2-0.12-*d*. Generally, the model could predict well the failure load for all beams where the loads predicted by the FEM were within 5% of the experimental ones. A comparison between the experimental load-deflection, load-strain at the hogging moment region, load-average stirrup strain in the interior shear span

and load-exterior reaction relationships and those predicted by the FEM analysis are shown in Figs. 7.15 to 7.18.

It can be seen that the FEM was capable of predicting the deflection before and after cracking with a reasonable accuracy (Fig. 7.15). Also, the FEM deflection at failure was approximately equal to the experimentally measured one for all beams. In beam SN-1.2-0.12-*d*, the FEM could predict the three stages of the load-deflection relationship; the pre-cracking, post-cracking and after yielding of the longitudinal reinforcement (as discussed in details in Chapter 6).

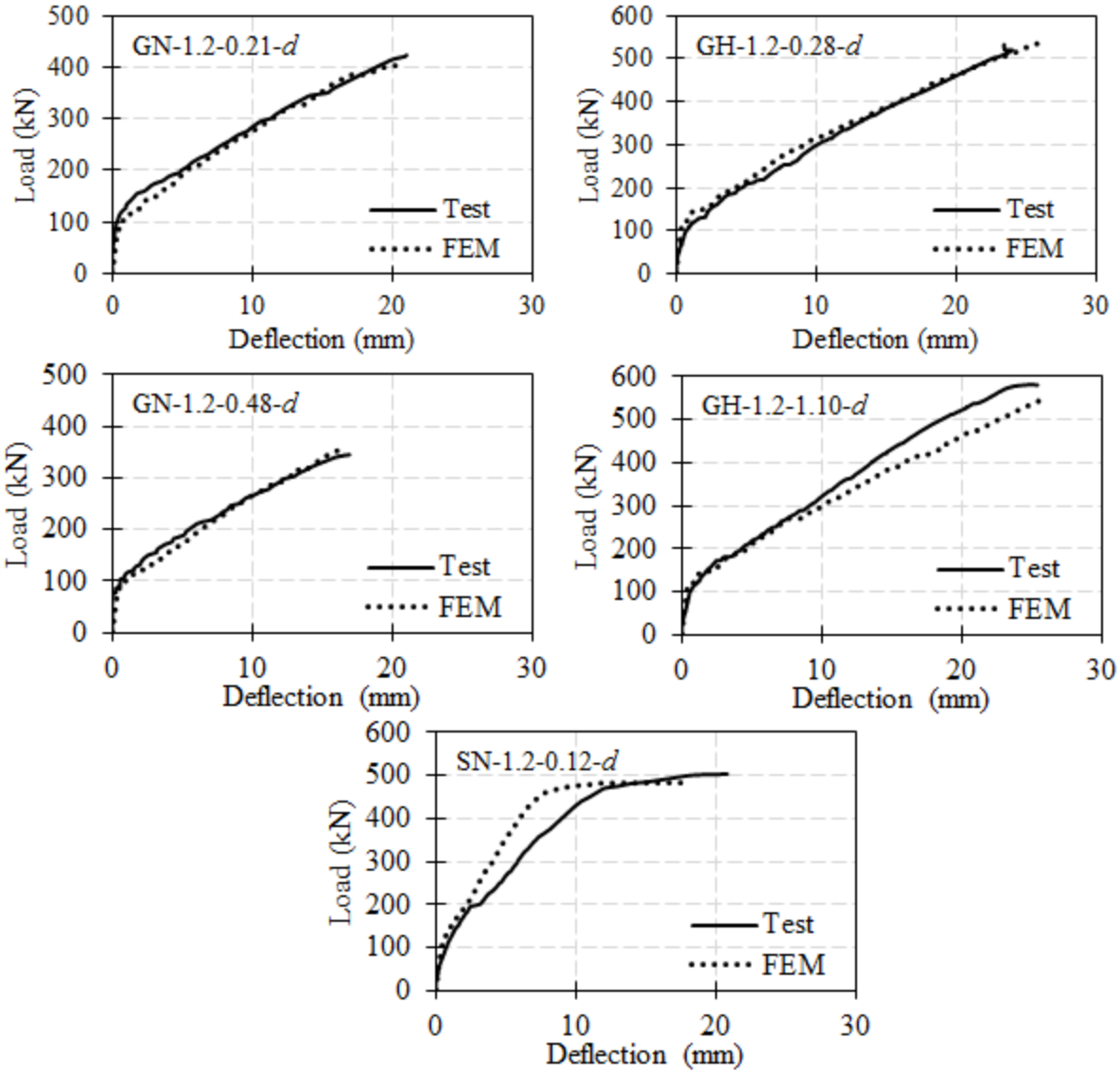

Figure 7.15: FEM versus experimental mid-span deflection

Regarding the strains in the longitudinal reinforcement at the hogging moment section, the FEM was able to predict the tensile strains before cracking. However, the strains in the post-cracking stage were less than the experimentally measured strains up to approximately 80% of the load then the strains were greater than the experimental ones. The strain in the longitudinal reinforcement predicted by the FEM was approximately identical to the experimental one in beam SN-1.2-0.12-*d* (Fig. 7.16). Similar observation can be noted for the average stirrup strain in

the interior shear span where the FEM showed very reasonable predictions for the average stirrups strains as shown in Fig. 7.17.

Moreover, the exterior reaction predicted by the FEM was in good agreement with the experimental one for all beams. Therefore, the model was able to redistribute the internal forces from the hogging to the sagging moment regions. The moment redistribution percentage calculated based on the FEM was very similar to that calculated from the experimental results. Moreover, the shear capacity predicted by the FEM was 121, 112, 156, 170 and 148 kN in beams GN-1.2-0.21-*d*, GN-1.2-0.48-*d*, GH-1.2-1.10-*d*, GH-1.2-0.28-*d* and SN-1.2-0.12-*d*, respectively. This represents 93, 104, 101, 100 and 96% of the experimental shear capacity. Based on the comparison above, it can be concluded that the FEM could reasonably predict the shear capacity of GFRP-RC continuous beams.

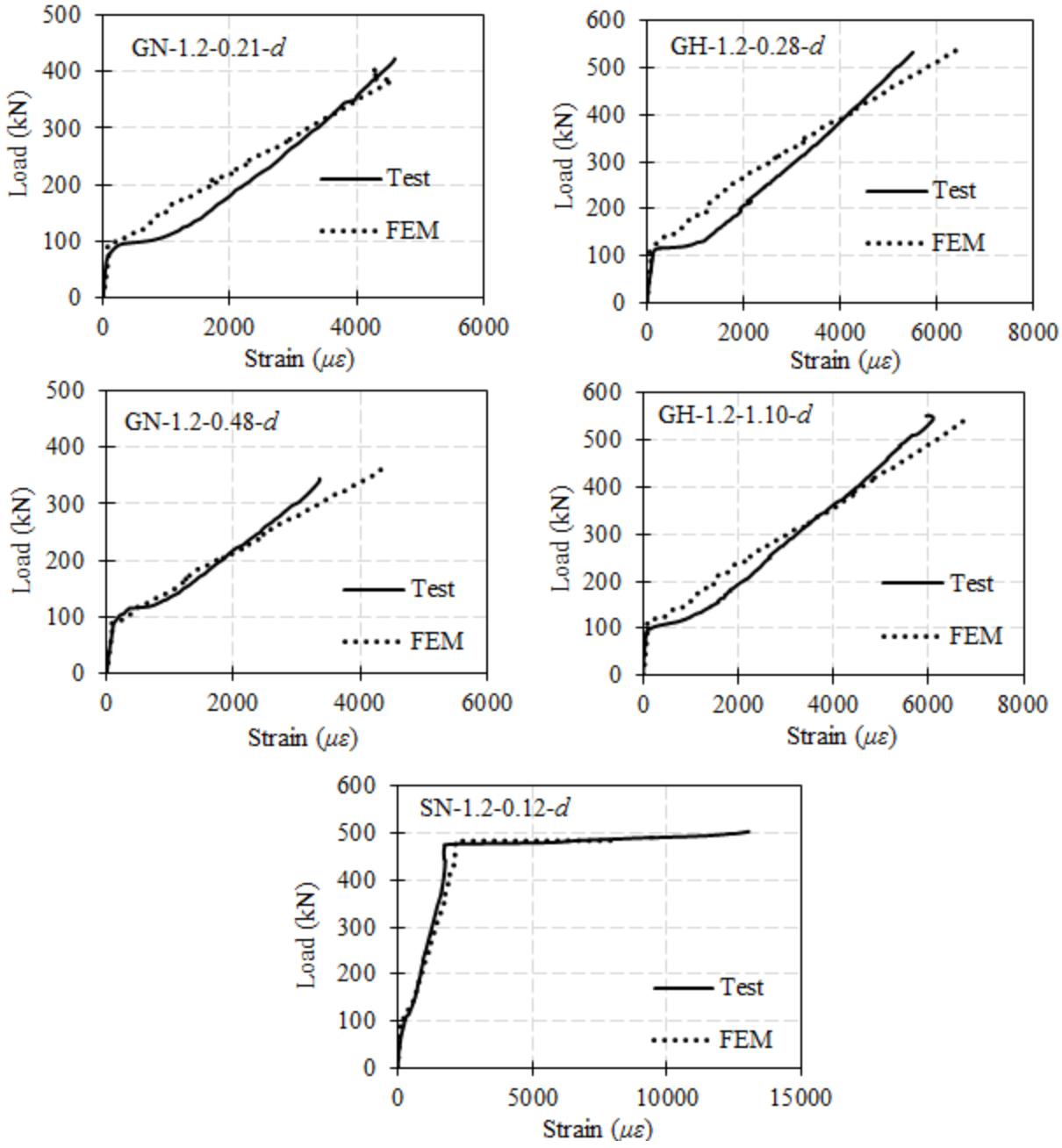

Figure 7.16: FEM versus experimental tensile strain at hogging moment section

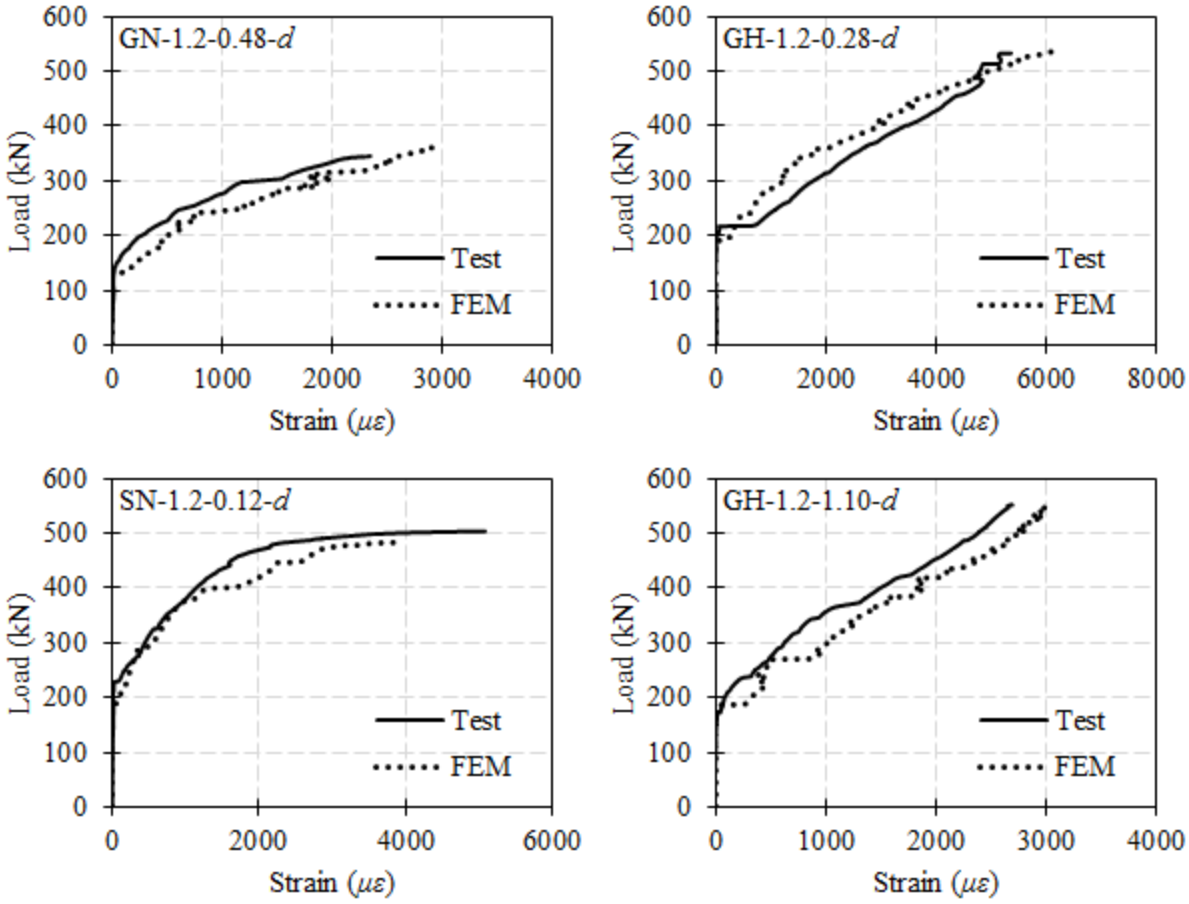

Figure 7.17: FEM versus experimental average stirrup strain in the interior shear span

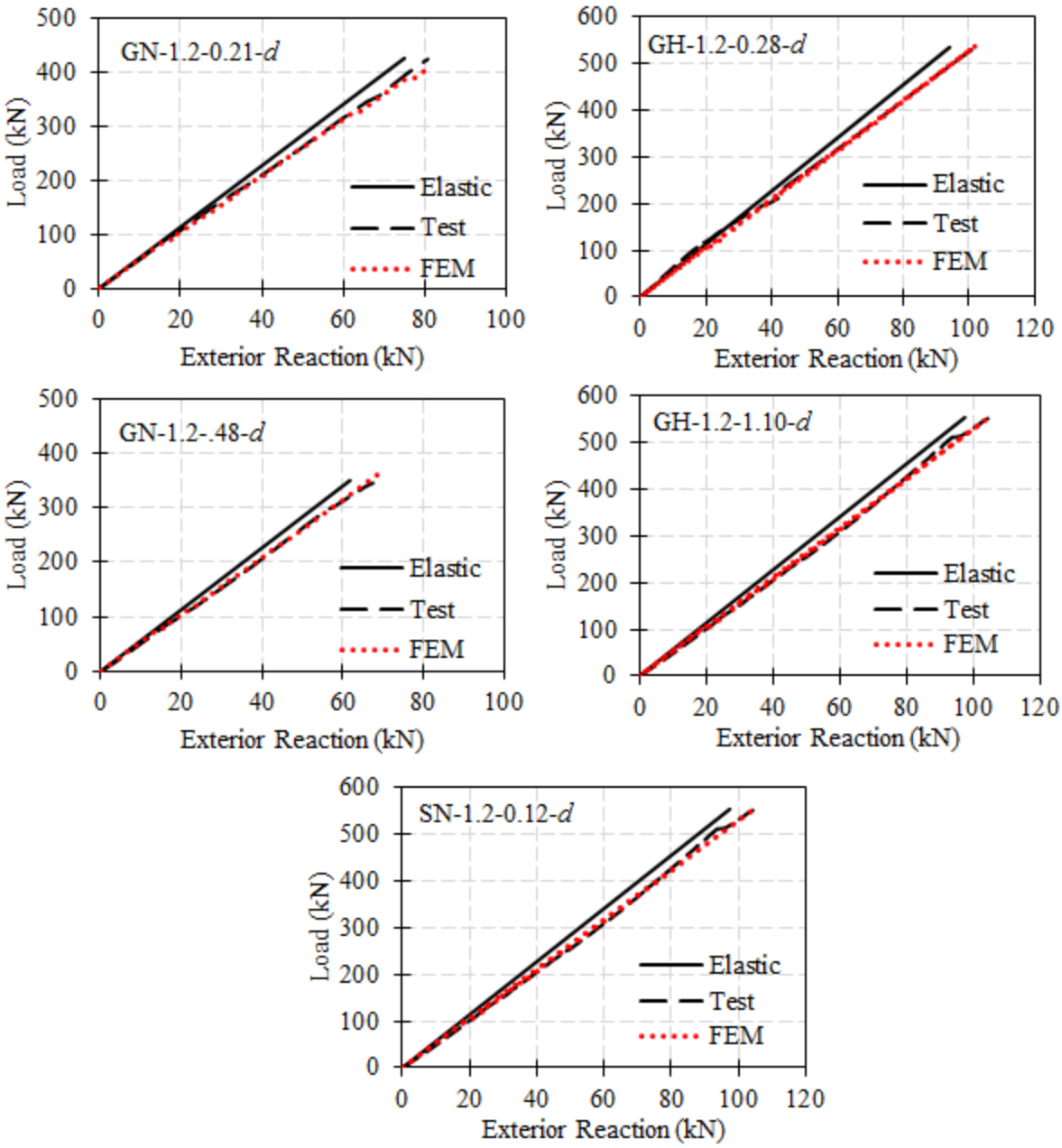

Figure 7.18: FEM versus experimental exterior reaction

7.7 MODEL VALIDATION

The verified model was then validated against two GFRP-RC continuous beams tested by El-Mogy et al. (2011) where it was reported that those two beams failed in shear. Those two beams (GGu-10d/2P and GGu-10d/3P) had 200×300 mm rectangular cross section and have the same

length as beams tested in this study. The top reinforcement was 2 No. 16 GFRP bars while the bottom reinforcement was 3 No.16 GFRP bars. The shear reinforcement was GFRP stirrup having 9.5-mm diameter. The stirrups were spaced at 120 and 80 mm in beams GGu-10d/2P and GGu-10d/3P, respectively. The beams were tested under one point load in each span with a shear span-to-depth ratio of 5.6.

Figure 5.19 shows a comparison between the experimental and the FEM in terms of the load-deflection relationship at the mid-span point. The FEM could reasonably predict the general behaviour, the pre-cracking and the post cracking stages. However, the measured deflection in the FEM was slightly less than the experimental one. This might be due to the different loading scheme and shear span-to-depth ratio.

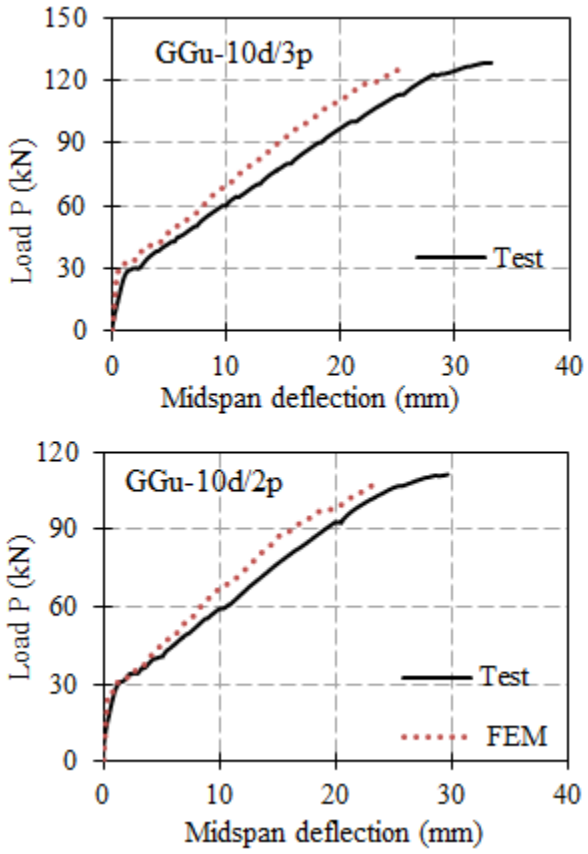

Figure 7.19: Load-deflection relationship at mid-span

The FEM yielded good predictions for the total applied load where the failure load was approximately 96.4% and 99.6% of the experimental failure load in GGu-10d/2P and GGu-10d/3P, respectively.

The FEM and the experimental strains at the hogging moment sections for both beams are shown in Fig. 7.20. It can be seen that the strains were identical until the cracking loads. The experimental cracking load was less than that in the FEM and this resulted in an early start of the increase in the strains at that level. However, the FEM strains became very close to the experimental strains at approximately 40 and 46% of the failure load of GGu-10d/2P and GGu-10d/3P, respectively. Afterwards, the FEM strains were fairly comparable to the experimental ones.

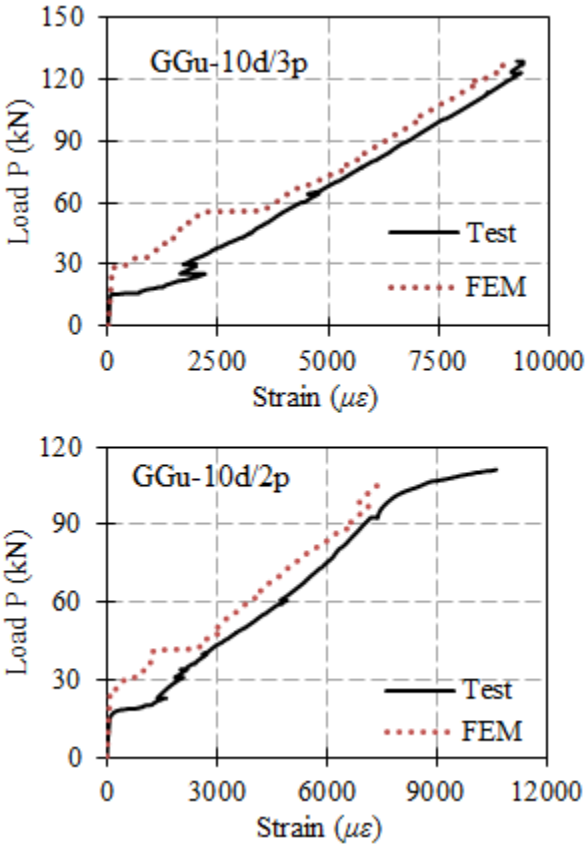

Figure 7.20: Load-strain relationship at the hogging moment region

Regarding the measured exterior reactions, it was found out that, similar to the experimental one, the FEM reaction followed the elastic distribution until cracking; then, it started to have a higher values compared to the elastic reaction. However, the FEM exterior reaction was less than the experimental one especially near failure. The FEM exterior reaction at failure was approximately 91 and 93% of those experimentally measured in beams GGu-10d/2P and GGu-10d/3P, respectively (Fig. 7.21). This also might be attributed to the different loading configuration in these two beams compared to the tested beams in this study.

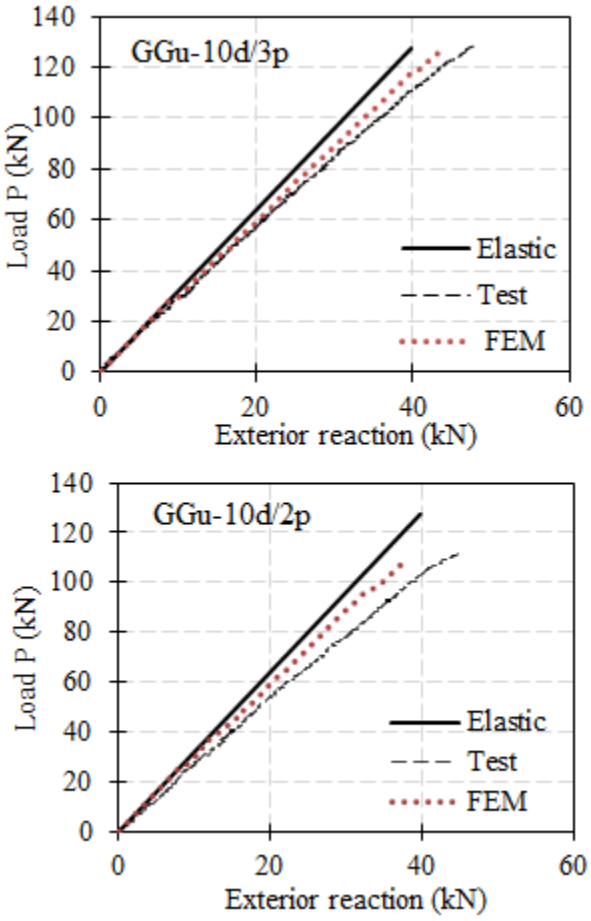

Figure 7.21: Load-exterior reaction relationship

As mentioned earlier, these two beams, GGu-10*d*/2P and GGu-10*d*/3P, failed due to shear in the interior shear span. This exactly was the case in the FEM where the failure took place due to shear in the interior shear span at shear forces that are very similar to the experimental ones. The ratio of the FEM-to-the experimental shear strength at failure was approximately 99.7 and 103.4% of the experimental shear in beams GGu-10d/2P and GGu-10*d*/3P, respectively. This gives a very good creditability for the developed FEM in predicting the shear strength of GFRP-RC continuous beams which is the main focus of this study.

CHAPTER 8: PARAMETRIC STUDY

8.1 GENERAL

The verified and validated FEM, described in Chapter 7, was used to conduct a parametric study. The effect of key parameters on the shear behaviour of GFRP-reinforced continuous beams was investigated. The investigated parameters included concrete compressive strength, longitudinal reinforcement ratio, transverse reinforcement ratio and shear span-to-depth ratio. For each parameter, the studied variable was changed a number of times to cover a wide practical range. The results were compared in terms of the load-deflection response, strains in the longitudinal reinforcement, the strains in stirrups, the moment redistribution at failure and the shear strength. The investigation resulted in a number of important conclusions regarding the effects of studied parameter on the shear behaviour of continuous concrete beams reinforced with GFRP bars. In this chapter, the results of the parametric study are presented and discussed.

8.2 EFFECT OF CONCRETE STRENGTH

The Canadian code for FRP-RC building structures (CSA/S806-12) limits the design concrete strength to 80 MPa. In this study, concrete strength in the range of 30 to 80 MPa was chosen to evaluate the effect of the concrete strength on the shear strength of GFRP-RC continuous beams. In beams without transverse reinforcement, the effect of concrete strength was evaluated for beams with different longitudinal reinforcement ratios (0.8, 1.2 and 1.6%). For beams having transverse reinforcement, the reinforcement ratios were 1.2 and 1.71%. Beams with 1.2% had the minimum shear reinforcement ratio specified in the ACI 440.1R-06 (0.256%) while beams with 1.71% had higher shear reinforcement ratio (1.10%) which represents twice the minimum shear reinforcement ratio. In all models, the concrete strength increased with increments of 10 MPa.

8.2.1 Load-Deflection Response

Figure 8.1 shows the load-deflection relationship for models having varying concrete strength for different longitudinal reinforcement ratio (0.8 and 1.6%). These models were without transverse reinforcement. The general behaviour of the models can be described by two distinct stages. The first stage is pre-cracking in which deflection increases with the load in a linear relationship all the way up to the cracking load. The slope of this portion of the relationship represents the uncracked stiffness of the beam. The second stage is post-cracking that starts immediately after the initiation of flexural cracks. In this stage the response becomes nonlinear until failure. It can be seen also that increasing the concrete compressive strength increased the cracking load due to the increase in concrete tensile strength. Increasing the concrete compressive strength from 30 to 80 MPa increased the cracking load by approximately 85%. Also, in the post-cracking stage, the slop of the curve is significantly reduced due to cracking which resulted in a reduction of the stiffness. Moreover, it was observed that as the concrete strength increases, the nonlinearity of the load-deflection relationship after cracking increased.

The load-deflection relationship for beams with transverse reinforcement is shown in Fig. 8.2. It can be seen that the load-deflection relationship is similar to that of beams without shear reinforcement where the beams exhibited similar behaviour in the pre-cracking and post-cracking stages. However, as expected, beams having transverse reinforcement showed significantly high load and deflections at failure compared to their counterparts without shear reinforcement. Also, as the transverse reinforcement ratio increased, both the post-cracking flexural stiffness and failure load increased as can be seen in Fig. 8.2.

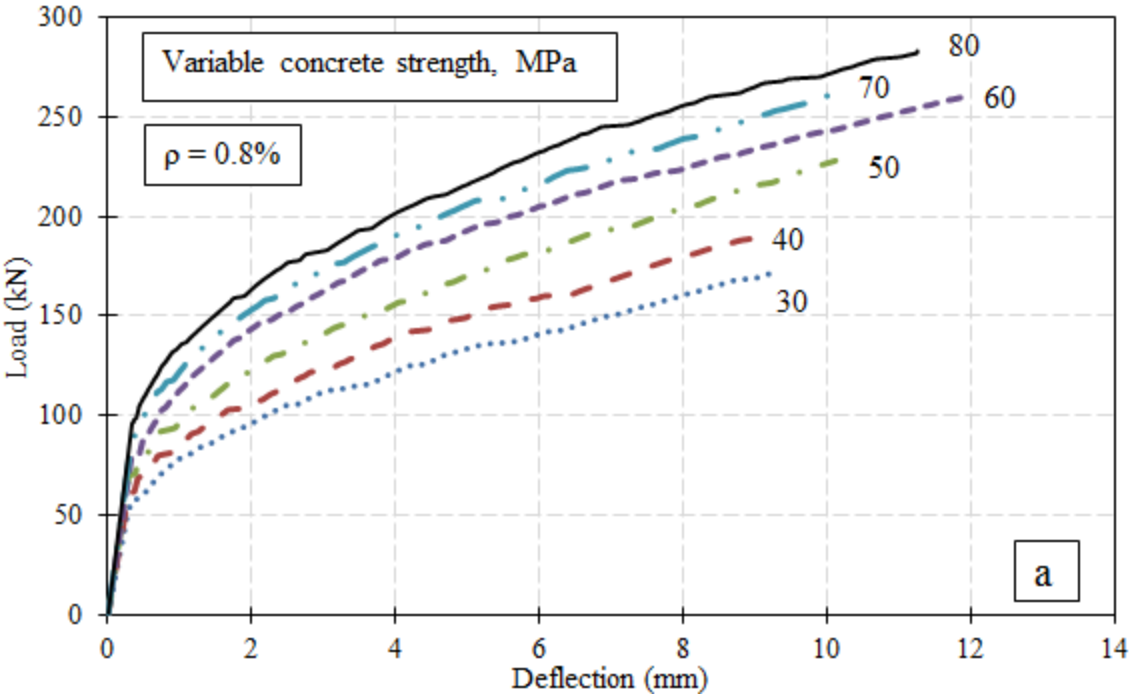

(a) Models with longitudinal reinforcement ratio of 0.8%

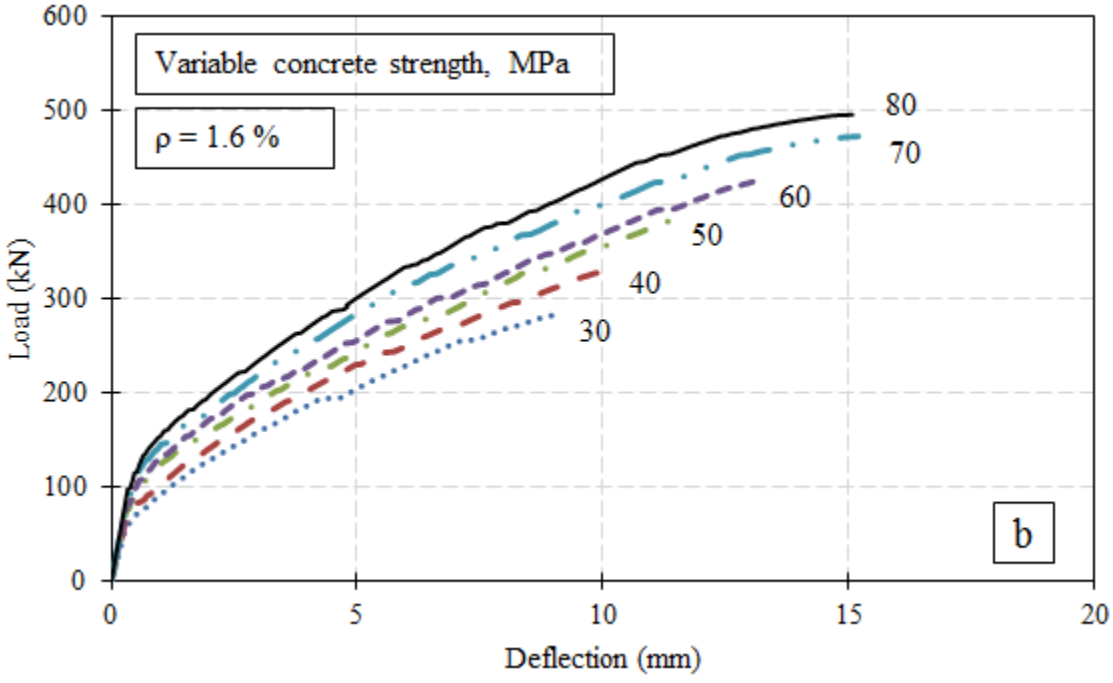

(b) Models with longitudinal reinforcement ratio of 1.6%

Figure 8.1: Load-deflection relationship at mid-span for varying concrete strength in models without shear reinforcement

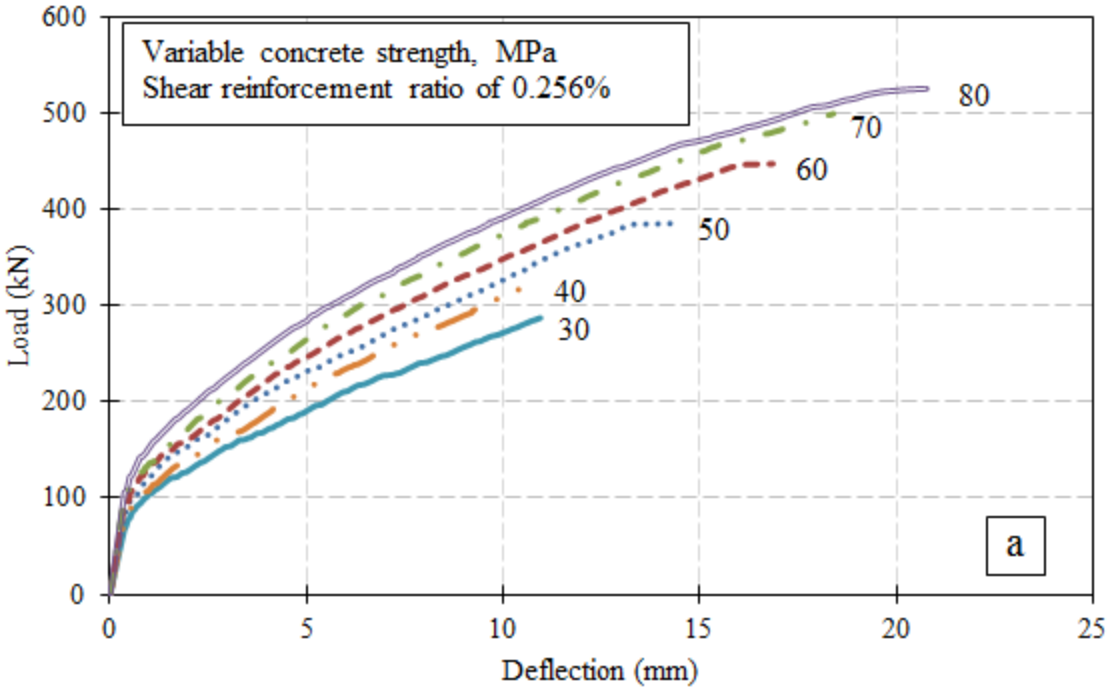

(a) Models with longitudinal reinforcement ratio of 1.2%

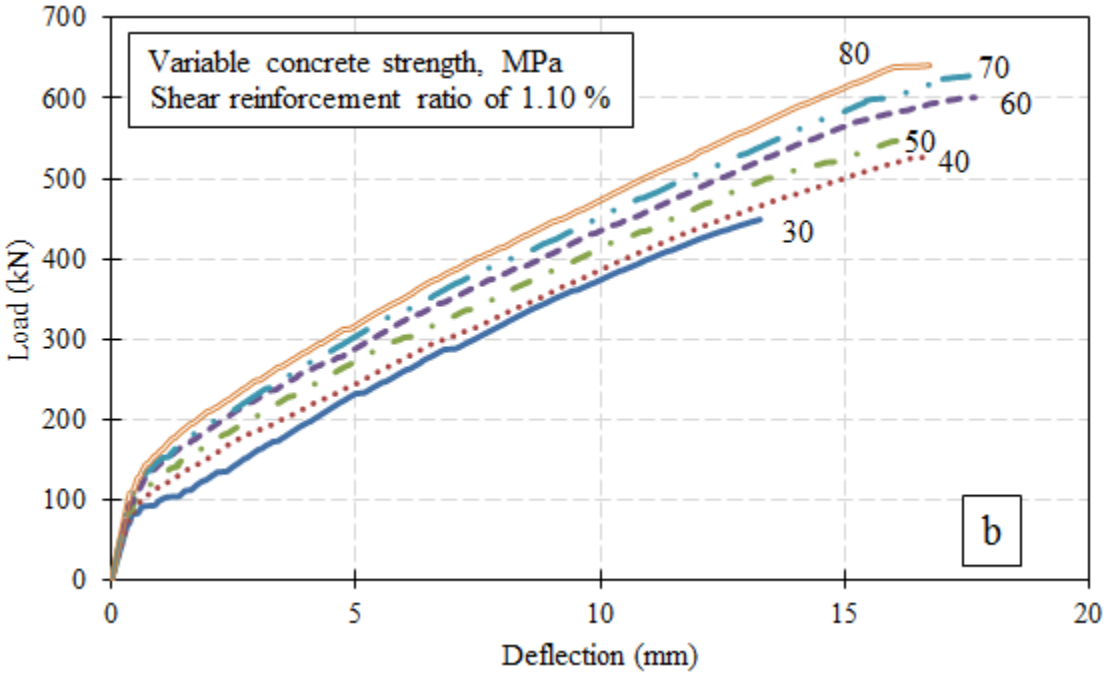

(b) Models with longitudinal reinforcement ratio of 1.71%

Figure 8.2: Load-deflection relationship at mid-span for varying concrete strength for models with shear reinforcement

8.2.2 Moment Redistribution

Similar to the experimental results, the exterior reaction and consequently the bending moment at the middle support section followed the elastic distribution at early loading stages. Once the cracks initiated in the hogging moment section, the exterior reaction diverged from the elastic one and the hogging bending moment started to be less than the elastic one until the model stopped at failure. Figure 8.3 shows the relationship between the elastic and FEM exterior reaction. Moreover, Fig. 8.4 shows the moment redistribution percentage for each model calculated at last step. In general, the effect of changing the concrete strength from 30 to 80 MPa resulted in a change in the moment redistribution. However, there is no consistent trend especially in beams with 0.8%; however, the moment redistribution decreased significantly at high concrete strengths. In beams with a longitudinal reinforcement ratio of 1.2 and 1.6%, the moment redistribution increased as the concrete strength increased from 30 to 40 MPa. Further increase in the concrete strength from 40 up to 80 MPa resulted in insignificant change in the moment redistribution in beams having a longitudinal reinforcement ratio of 1.2%. The same can be noticed in beams with a longitudinal reinforcement ratio of 1.6%. Most of the models achieved the assumed moment redistribution percentage (20%) as can be seen in Fig. 8.4. At the last step, the moment redistribution ranged between 17 and 23.3% in all models.

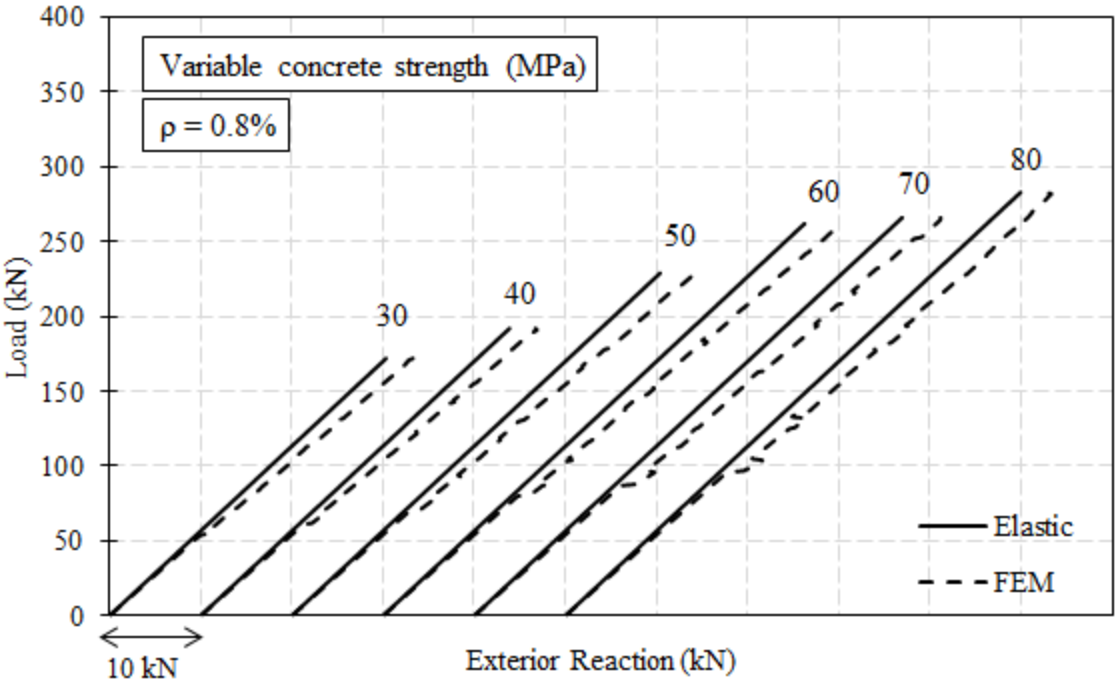

(a) Models with longitudinal reinforcement ratio of 0.8%

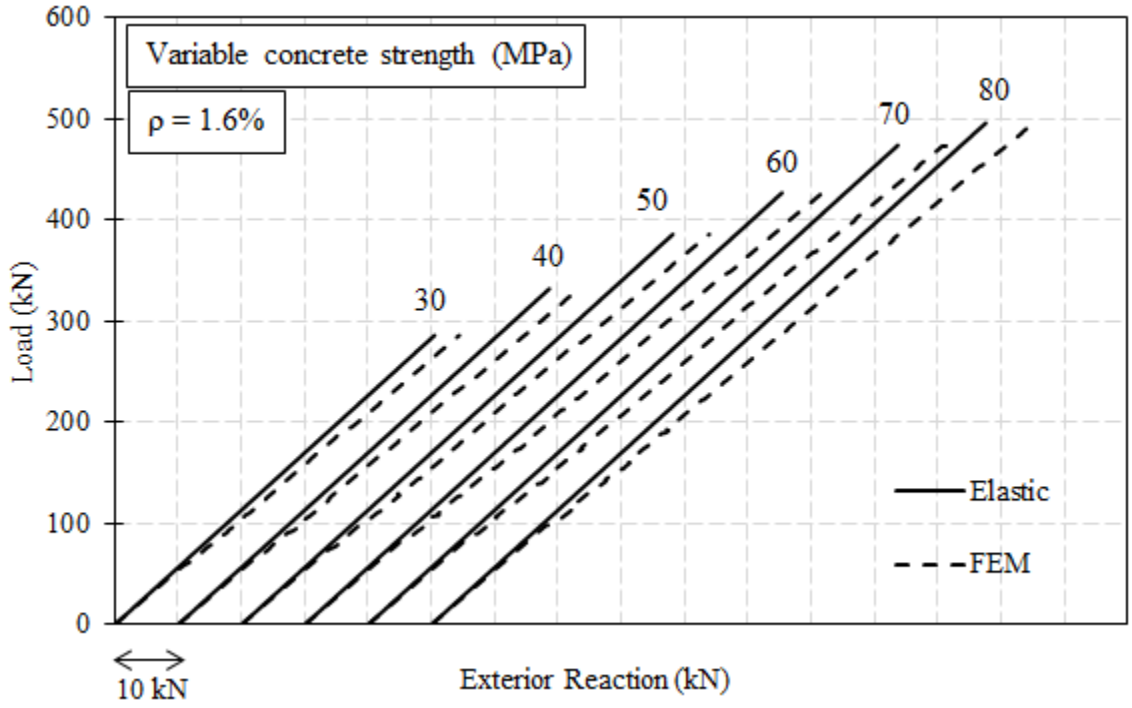

(b) Models with longitudinal reinforcement ratio of 1.6%

Figure 8.3: Load-exterior reaction relationship for beams with varying concrete strength in models without shear reinforcement

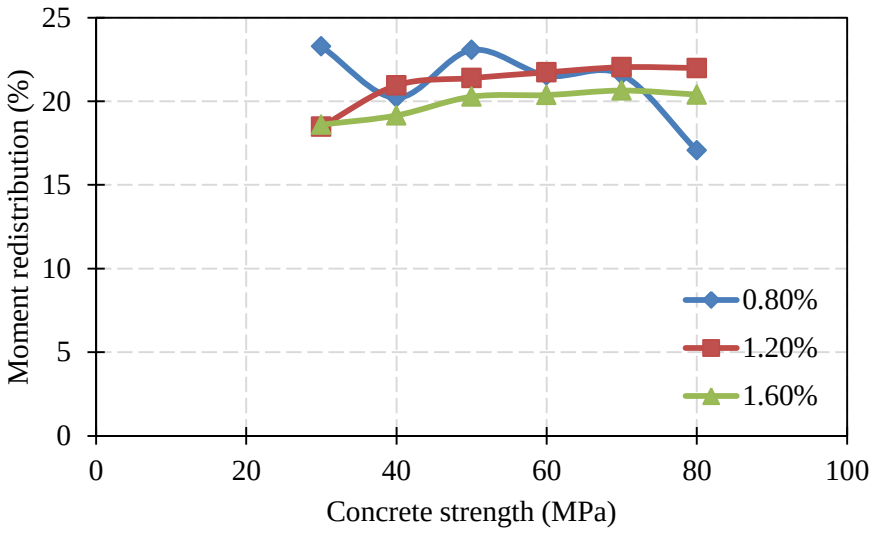

Figure 8.4: Variation of moment redistribution percentage with the concrete strength (beams without shear reinforcement)

Beams having transverse reinforcement showed similar behaviour to that observed in beams without shear reinforcement in terms of the load-exterior reaction relationship (Fig. 8.5). At the last step, the FEM exterior reaction was higher than the elastic one by 7.45% to 10.6% in models with longitudinal reinforcement ratio of 1.2% and by 7.7 to 11.5% in models with a longitudinal reinforcement ratio of 1.71%. Figure 8.7 shows the calculated moment redistribution versus the concrete strength for models with a longitudinal reinforcement ratio of 1.2 and 1.71%. The moment redistribution decreased with increasing the concrete strength in models with longitudinal reinforcement ratio of 1.2%. In models with longitudinal reinforcement ratio of 1.71%, the moment redistribution increased with increasing the concrete strength in the range from 30 to 60 MPa while it decreased significantly when the concrete strength increased from 60 to 70 MPa and from 70 to 80 MPa. Again, most models achieved the assumed moment redistribution (20%) as can be seen in Fig. 8.6.

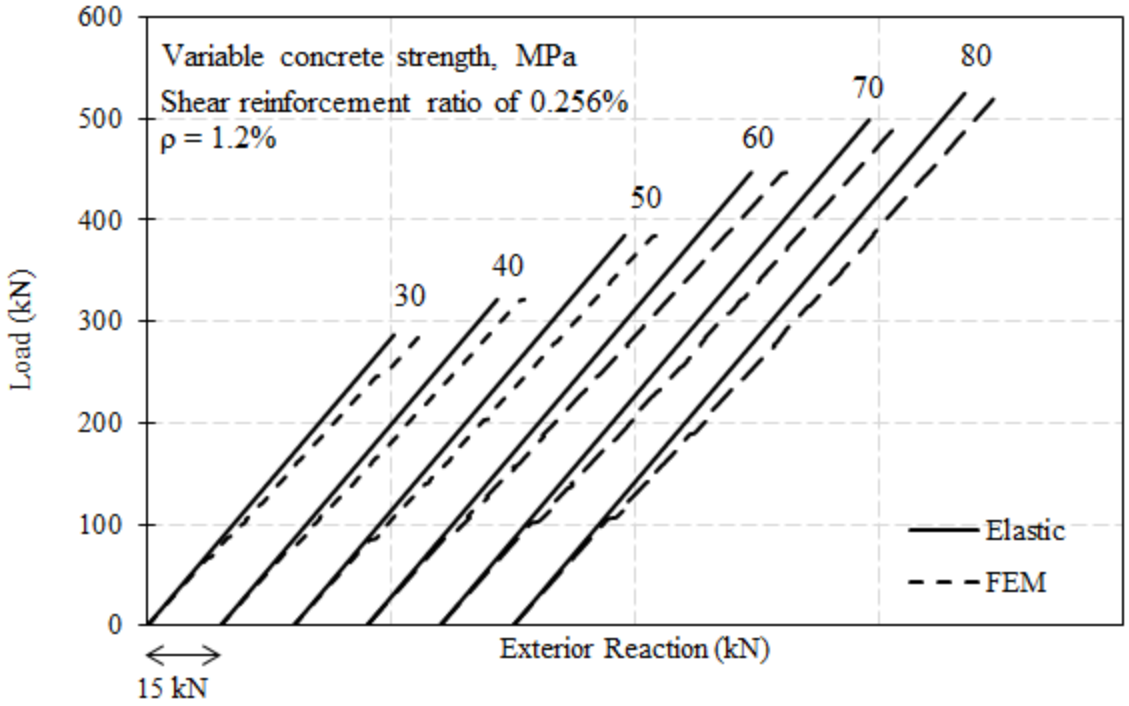

(a) Models with longitudinal reinforcement ratio of 1.2%

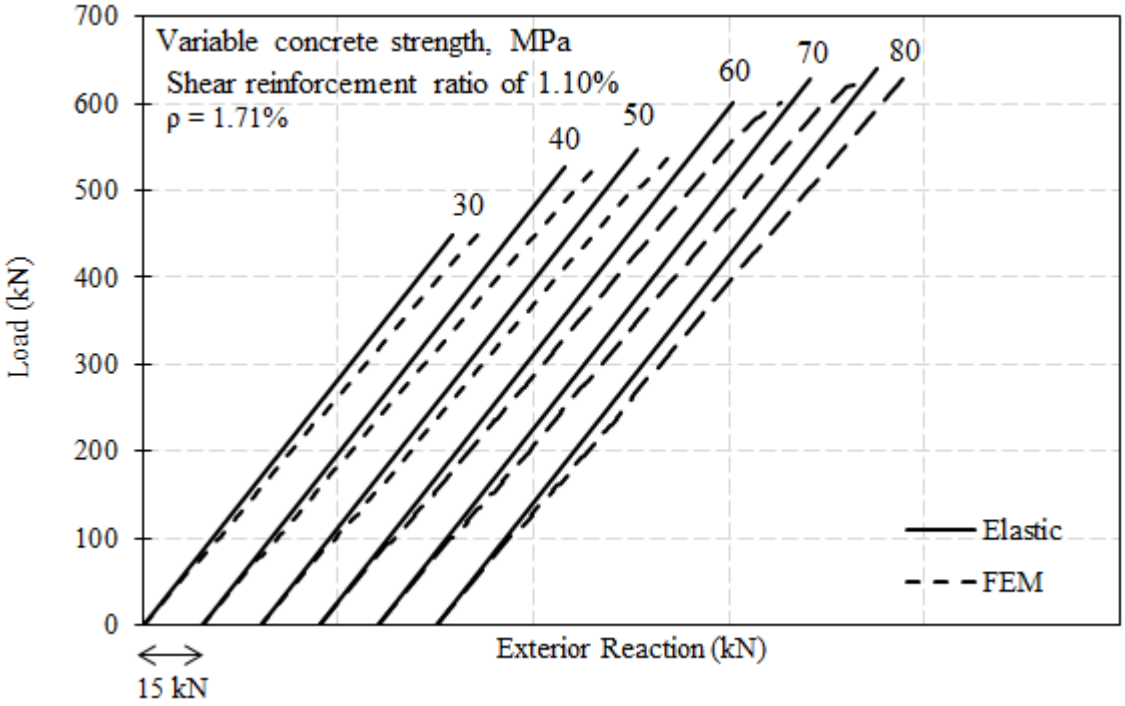

(b) Models with longitudinal reinforcement ratio of 1.71%

Figure 8.5: Load-exterior reaction relationship for beams with varying concrete strength (with shear reinforcement)

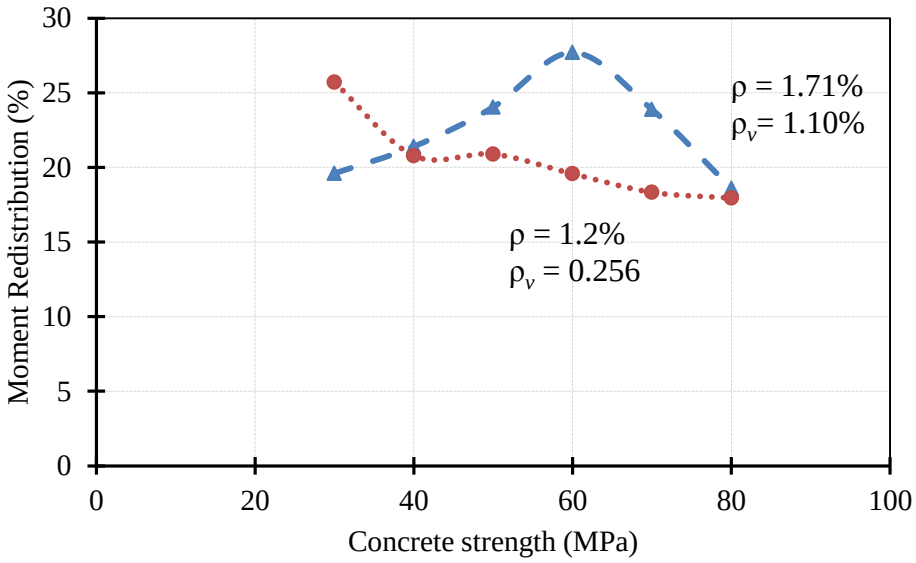

Figure 8.6: Variation of moment redistribution percentage with the concrete strength (beams with shear reinforcement)

8.2.3 Shear Strength

Figure 8.7 shows the variation of shear capacity with concrete strength for models with different longitudinal reinforcement ratio. Similar behaviour can be seen for the three different reinforcement ratios where the shear capacity increased with increasing the concrete strength. The increase in the shear strength was higher in models with high longitudinal reinforcement ratio (1.6%) than that of models with reinforcement ratio of 1.2 and 0.8%. This can be attributed to the fact that high reinforcement ratio provides better control of the shear crack width compared to low reinforcement ratio. Also, for concrete strength in the range of 30 to 60 MPa, the increase in the shear strength was steep while the shear capacity slightly increased when the concrete strength increased to 70 and 80 MPa. This is in good agreement with the well-established behaviour of high strength concrete where the crack surface is smoother than that in normal strength concrete. Smooth crack surface reduces the aggregate interlock which is a main

shear transfer mechanism. This results in a reduction in the increase in the shear strength in high concrete strengths.

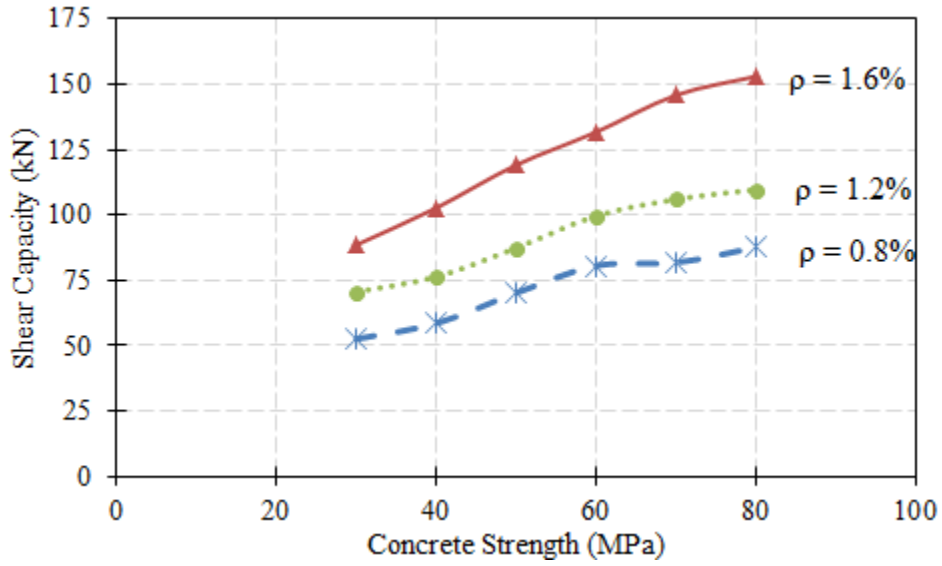

Figure 8.7: Variation of the shear capacity with the concrete strength in models without shear reinforcement

In beams with longitudinal reinforcement ratio of 0.8%, increasing the concrete strength from 30 to 80 MPa with increments of 10 MPa, increased the shear strength by 12.5, 18.4, 14.8, 1.5 and 7.2%, respectively. For the same incremental increase in the concrete strength, in models with longitudinal reinforcement ratio of 1.2%, the increase in the shear strength was 8.1, 14.4, 13.9, 6.4 and 3.5%, respectively, while this increase was 15.9, 16.0, 10.6, 10.7 and 4.9%, respectively, in models having a longitudinal reinforcement ratio of 1.6%.

Figure 8.8 shows the variation of the shear strength of the FEM and the concrete strength, in beams having transverse reinforcement, for different longitudinal reinforcement ratio (1.2% and 1.71%). In general, the shear capacity of the FEM increased with increasing the concrete strength for both longitudinal reinforcement ratios.

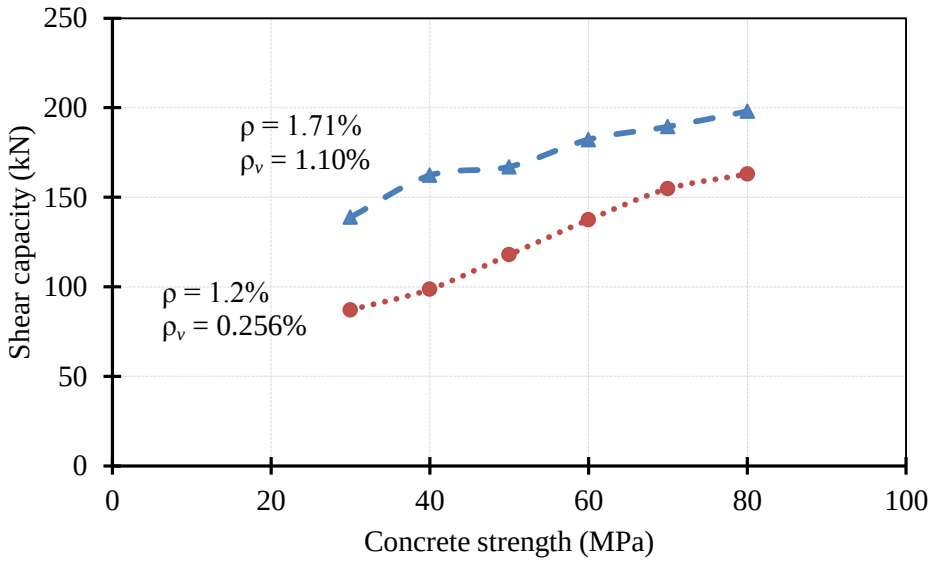

Figure 8.8: Shear capacity versus the concrete strength in models with shear reinforcement

In models having longitudinal reinforcement ratio of 1.2%, the shear capacity increased by 13.2, 19.5, 16.6, 12.6 and 5.3%, respectively, when the concrete strength increased incrementally, 10 MPa each increment, from 30 to 80 MPa. The small increase in the shear strength occurred when the concrete strength increased from 70 to 80 MPa. This could be due to that model with concrete strength of 80 MPa achieved the smallest moment redistribution and because of the nature of the high strength concrete that results in smoother crack surface compared to normal strength concrete. The smooth crack surface results in less aggregate interlock contribution to the shear strength compared to rough surface of normal strength concrete. models having longitudinal reinforcement ratio of 1.71% showed similar trend where increasing the concrete strength incrementally from 30 to 80 MPa increased the shear capacity by 16.9%, 3.0%, 9.1%, 3.95% and 4.5%, respectively. The small increase in the shear strength could be attributed to the same reasons mentioned above, in the case of beams without shear reinforcement.

8.3 EFFECT OF THE LONGITUDINAL REINFORCEMENT RATIO

In this section, the effect of the longitudinal reinforcement ratio on the shear behaviour GFRP-RC continuous beams without transverse reinforcement is investigated. The current design codes and guidelines for FRP-reinforced structures recommend compression failure mode rather than tension failure. To achieve compression failure in any concrete section reinforced with FRP bars, the reinforcement ratio should not be less than the balanced reinforcement ratio (ρ_b). In this study, the longitudinal reinforcement ratio ranged from 0.51 to 1.71% that represents 1.76 to 5.94 ρ_b in NSC of 40 MPa and 1.17 to 3.94 ρ_b in HSC of 70 MPa. The ratio between reinforcement at mid-span and middle support was kept constant at a value of 1.0 similar to the experimental program.

8.3.1 Load-Deflection Response

Figure 8.9 shows the load-deflection relationship at the mid-span of models having longitudinal reinforcement ratio in the range of 0.51 to 1.71%. It can be seen that the model with reinforcement ratio at middle support equal to 0.51% demonstrated the lowest post-cracking flexural stiffness and ultimate load capacity. As the reinforcement ratio at both critical sections was increased, significant improvement in the post-cracking flexural stiffness and ultimate load was observed. This reflects the effect of increasing the axial stiffness of the longitudinal reinforcement ratio. For example, increasing the reinforcement ratio from 0.8 to 1.2% reduced the deflection at mid-span by approximately 26 and 28% at a load level of 150 kN in NSC and HSC models, respectively. Also, the deflection at the same load level was reduced by 30 and 17% when the longitudinal reinforcement ratio increased from 1.2 to 1.7% in NSC and HSC models, respectively. At higher load levels, the difference in the deflection became high as the

models were close to failure. In model having a concrete strength of 40 MPa and a longitudinal reinforcement ratio of 0.51%, the reduction of the flexural stiffness was very rapid at approximately 90% of the failure load. However, for HSC model (70 MPa) with the same longitudinal reinforcement ratio (0.51%), the reduction in the flexural stiffness was gradual similar to models with higher longitudinal reinforcement ratio.

Moreover, it can be seen that increasing the reinforcement ratio had a positive impact on the ultimate load capacity. This might be attributed to the fact that increasing the reinforcement ratio increases the shear capacity of the beam and consequently the ultimate failure load. Increasing the reinforcement ratio from 0.51 to 0.8% increased the ultimate load capacity by approximately 74 and 26% in NSC and HSC models, respectively, while the load capacity increased by approximately 45% and 44% when the longitudinal reinforcement ratio increased from 1.2 to 1.7%.

Figure 8.10 shows the load-deflection relationship in beams with transverse reinforcement. It can be noticed that models having transverse reinforcement demonstrated similar load-deflection relationship to that of beams without shear reinforcement. The load-deflection relationship has the same two stages (pre-cracking and post-cracking stages). However, as expected, beam having transverse reinforcement showed significantly high failure load and post-cracking flexural stiffness compared to those of beam without shear reinforcement.

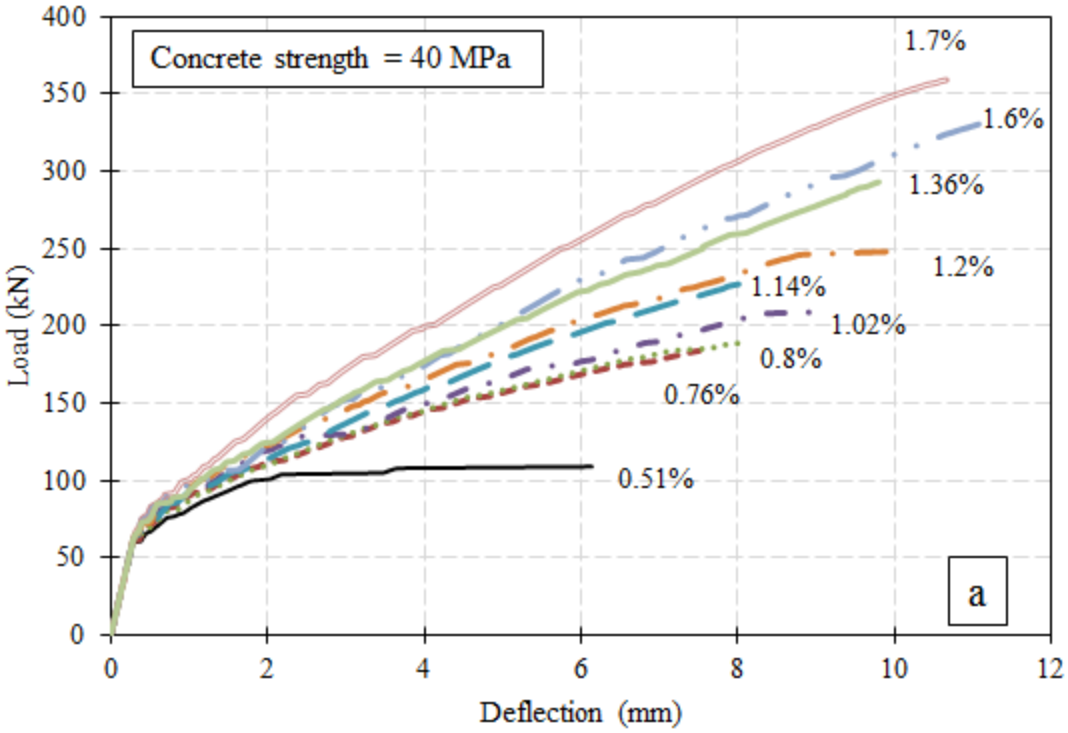

(a) Models with concrete strength of 40 MPa

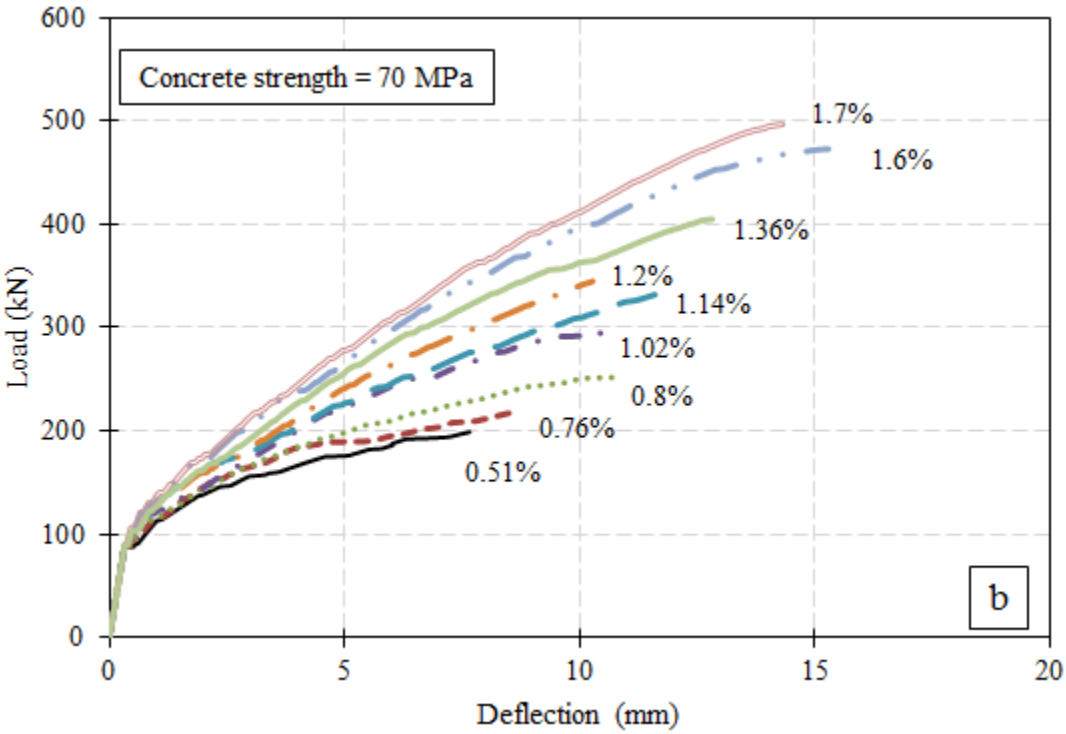

(b) Models with concrete strength of 70 MPa

Figure 8.9: Load-deflection relationship at mid-span of models with different longitudinal reinforcement ratio (without shear reinforcement)

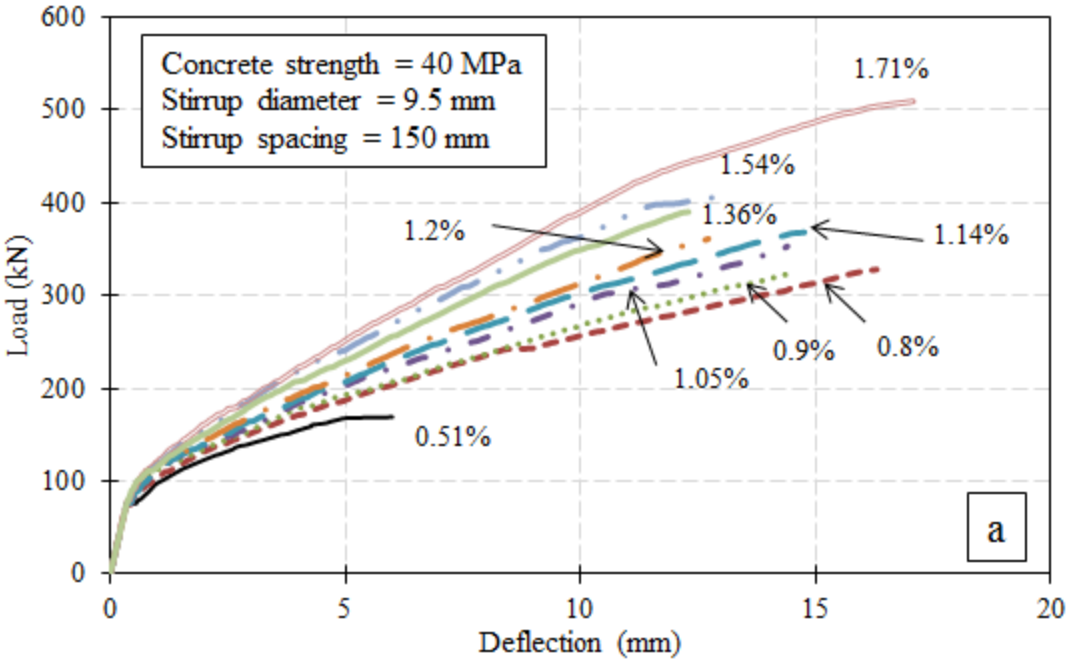

(a) Models with concrete strength of 40 MPa

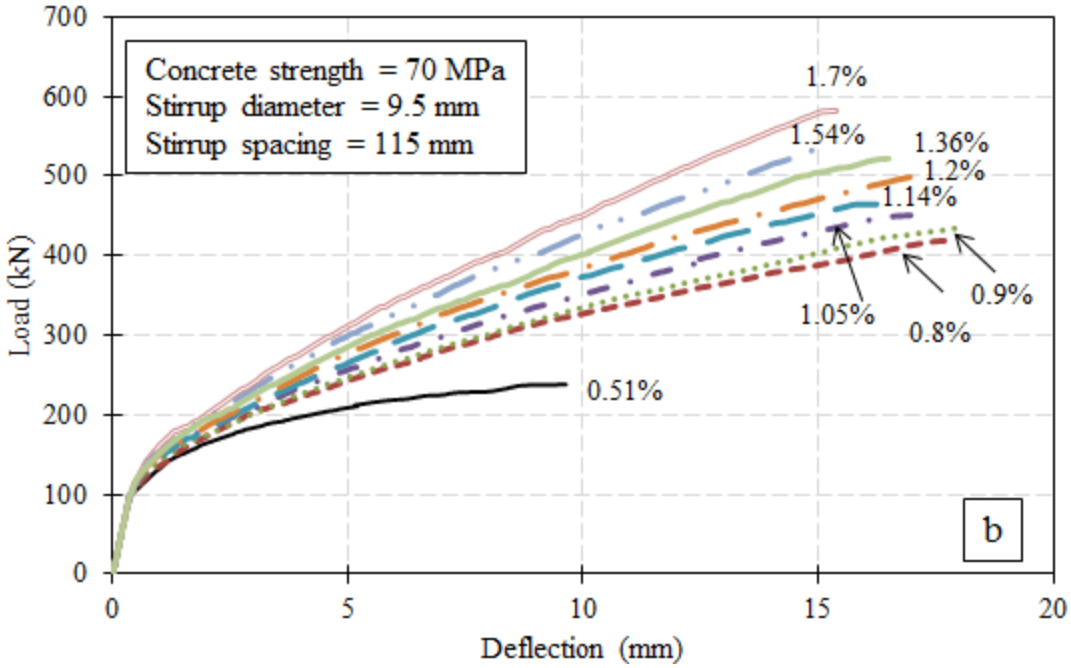

(a) Models with concrete strength of 70 MPa

Figure 8.10: Load-deflection relationship at mid-span point for models with different longitudinal reinforcement ratio (with shear reinforcement)

8.3.2 Moment Redistribution

The variation of exterior reactions with different longitudinal reinforcement ratios, for concrete strengths of 40 and 70 MPa, is shown in Fig. 8.11. It can be seen that the exterior reactions followed the elastic distribution until the formation of flexural cracks at the hogging moment region. Then, the exterior reaction had higher values compared to the elastic one all the way up to failure.

The exterior reactions at the last step were used to calculate the achieved moment redistribution at failure. Figure 8.12 shows the relationship between the longitudinal reinforcement ratio and the moment redistribution at middle support. It can be seen that there was no constant trend in both NSC and HSC models when the reinforcement ratio increased from 0.51 to 1.2%. However, further increase in the longitudinal reinforcement ratio resulted in a decrease in the moment redistribution percentage at failure in both NSC and HSC models. Increasing the longitudinal reinforcement ratio form 1.2 to 1.71% decreased the available moment redistribution by 8 and 7% in NSC and HSC models, respectively. This might be attributed to the fact that the higher the flexural reinforcement ratio, the better the control of the crack widths that, in turn, reduced the available rotation at the hogging moment sections. It can be seen also that all the models achieved moment redistribution percentage higher than that assumed in the design (20%). The highest moment redistribution was 30% in model with longitudinal reinforcement ratio of 1.14% in NSC while it was approximately 29% in model with longitudinal reinforcement ratio of 0.8% in HSC models.

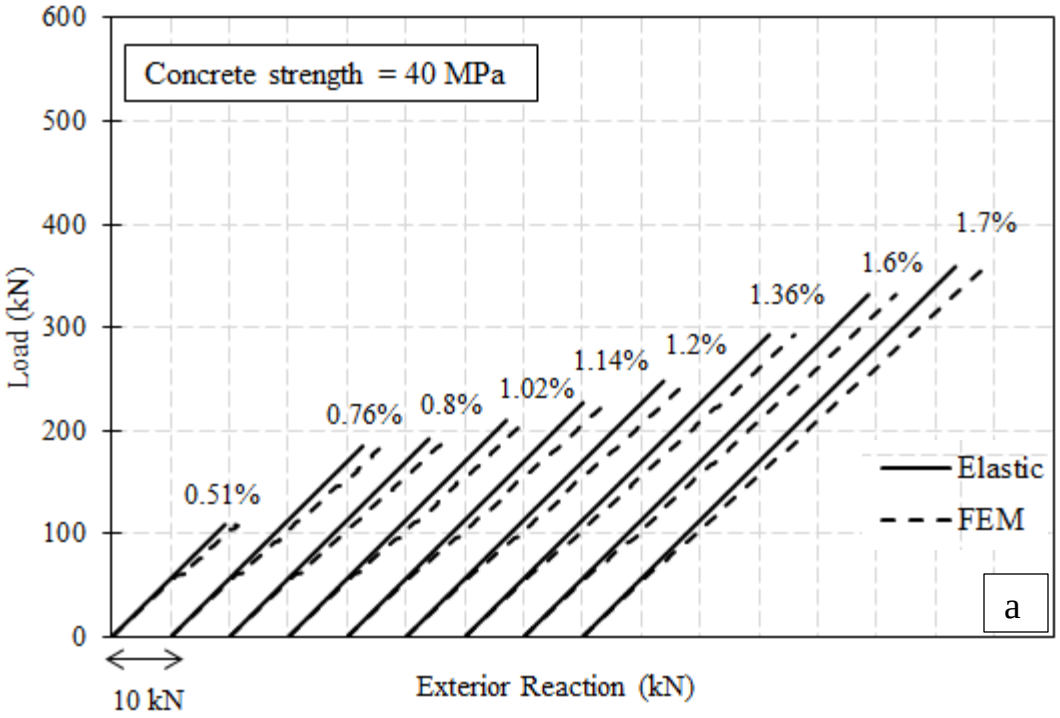

(a) Models with concrete strength of 40 MPa

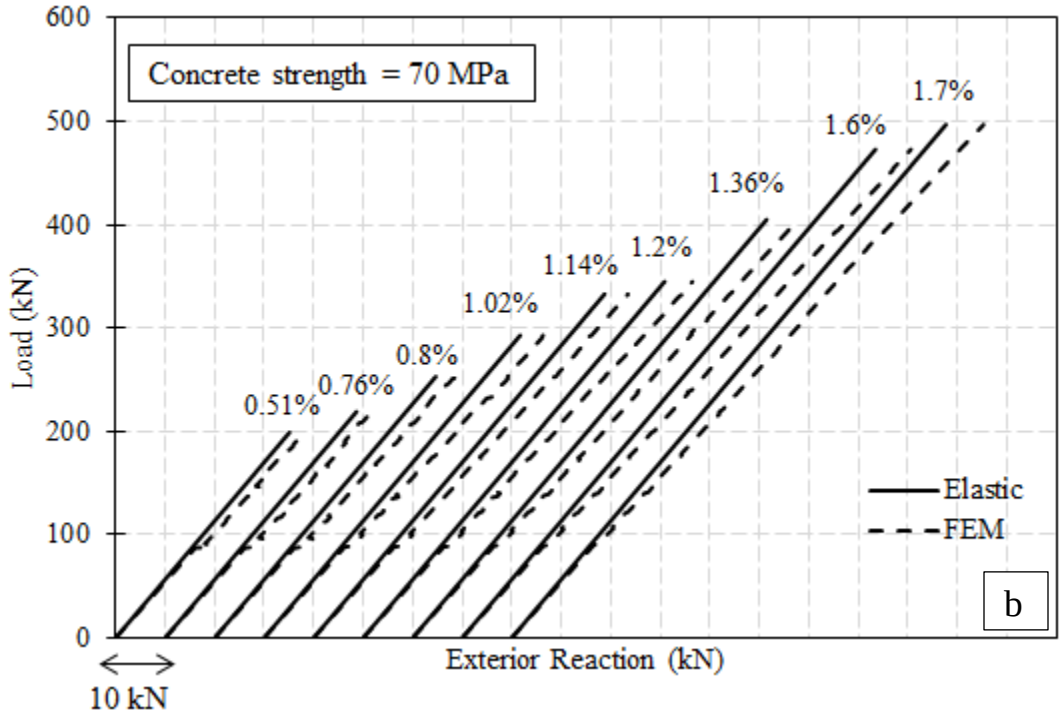

(b) Models with concrete strength of 70 MPa

Figure 8.11: Load-exterior reactions for models with different longitudinal reinforcement ratios (models without shear reinforcement)

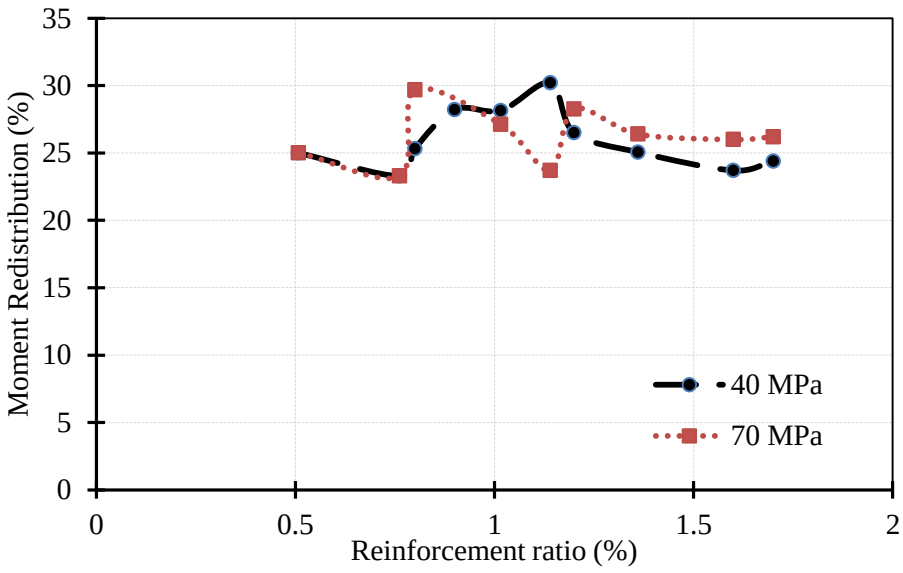

Figure 8.12: Moment redistribution at failure versus longitudinal reinforcement ratio (models without shear reinforcement)

In models having transverse reinforcement, the exterior reactions showed similar behaviour to that observed in models without shear reinforcement as can be seen in Fig. 8.13. However, the difference between the FEM exterior reaction and that calculated by the elastic theory is less than that in the case of models without shear reinforcement. As a result, the achieved moment redistribution at failure was smaller than that in models without shear reinforcement (Fig. 8.14). This can be attributed to that the presence of the stirrups better controlled the diagonal cracks near the middle support which, in turn, reduced the rotation at the middle support section.

The moment redistribution increased significantly when the reinforcement ratio increased from 0.51% to 0.8% while no significant change in the moment redistribution with further increase in the longitudinal reinforcement ratio (form 0.8% to 1.71%) in both NSC and HSC models. Also, models with 40 MPa concrete strength achieved moment redistribution higher than the assumed 20% while HSC models did not reach this ratio.

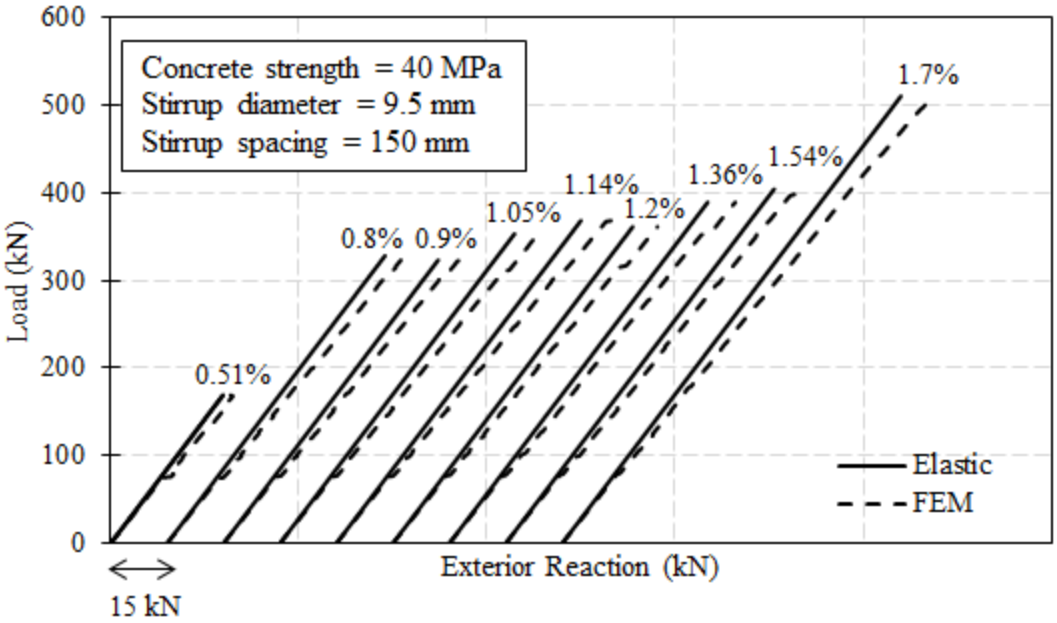

(a) Models with concrete strength of 40 MPa

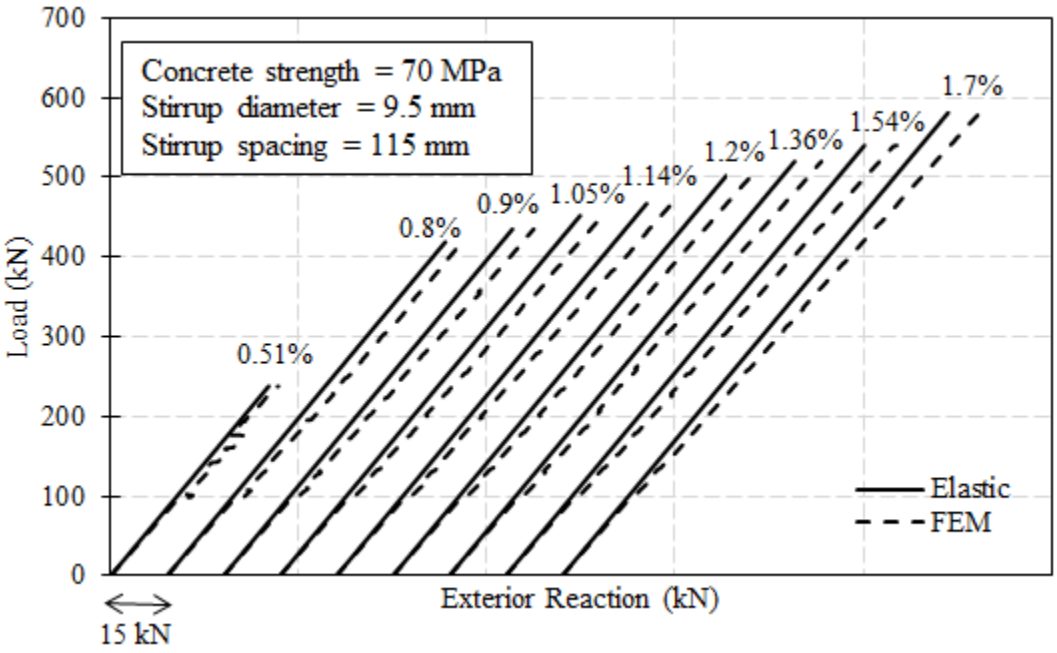

(b) Models with concrete strength of 70 MPa

Figure 8.13: Load-exterior reactions for models with different longitudinal reinforcement ratios (models with transverse reinforcement)

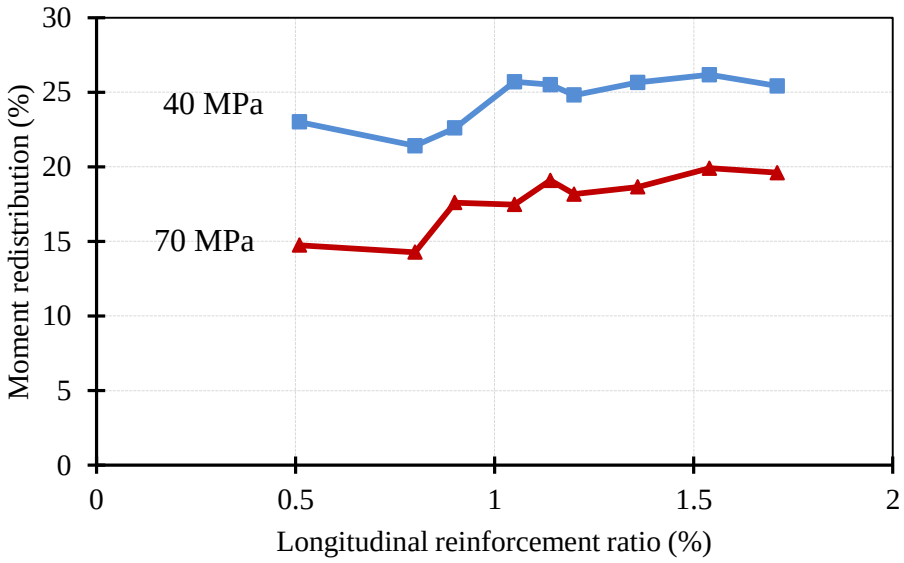

Figure 8.14: Moment redistribution at failure versus longitudinal reinforcement ratio (models with shear reinforcement)

8.3.3 Shear Strength

Figure 8.15 shows the variation of the shear capacity with the longitudinal reinforcement ratio for models with concrete strength of 40 and 70 MPa. In general, the shear capacity increased significantly by increasing the longitudinal reinforcement ratio in both NSC and HSC models. In models having concrete strength of 40 MPa, increasing the longitudinal reinforcement ratio from 0.51 to 0.8% increased the shear capacity by 74% while increasing the reinforcement ratio from 1.02 to 1.2% increased the shear capacity by only 10%. Further increase in the reinforcement ratio from 1.2 to 1.71% resulted in 45% increase in the shear capacity. Similar trend was observed in models having concrete strength of 70 MPa where the shear capacity increased by 26% when the reinforcement ratio increased from 0.51 to 0.8%. Also, increasing the reinforcement ratio from 1.02 to 1.2% increased the shear capacity by 17% while the shear capacity increased by 44% when the reinforcement ratio increased from 1.2 to 1.71%.

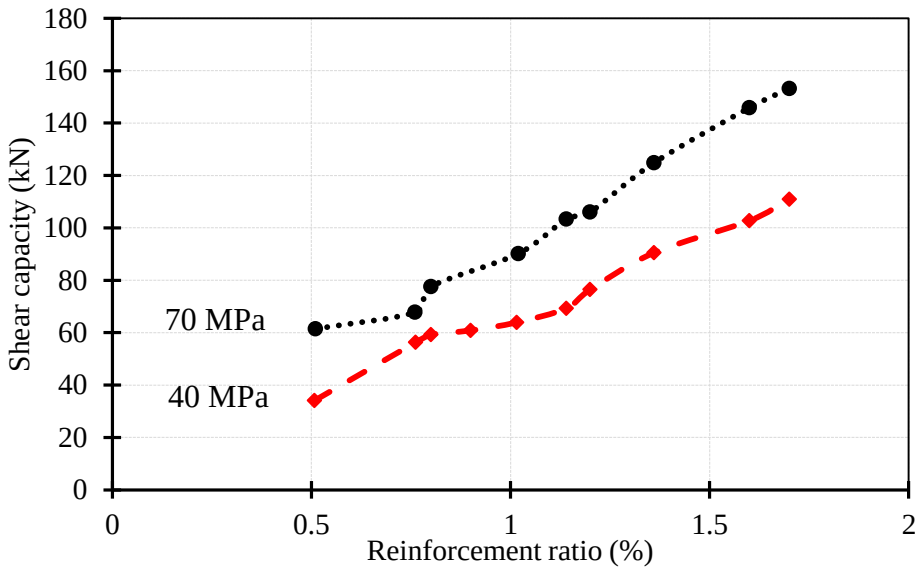

Figure 8.15: Shear capacity versus the longitudinal reinforcement ratio in models without shear reinforcement

NSC models (40 MPa) having transverse reinforcement showed significant increase in the shear strength (96%) when the reinforcement ratio increased from 0.51 to 0.8% while increasing the reinforcement ratio from 0.8 to 1.54% increased the shear strength slightly by 14%. Further increase in the longitudinal reinforcement ratio form 1.54 to 1.71% increased the shear strength by 27%. In the case of HSC (70 MPa), increasing the longitudinal reinforcement ratio from 0.51 to 0.8% resulted in 76% increase in the shear strength; then, there was slight increase in the shear strength (10%) when the reinforcement ratio increased from 0.8 to 1.14%. the shear strength continued to increase as the longitudinal reinforcement ratio increased from 1.2 to 1.71% where this increase in the reinforcement ratio increased the shear strength by 16%. It can be seen, form Figs. 8.15 and 8.16, that the presence of the stirrups had a pronounced impact on the shear strength of the models. In the case of NSC beams, the presence of the stirrups increased the shear strength by 48%, on average. This increase in the shear strength was 36% in HSC models.

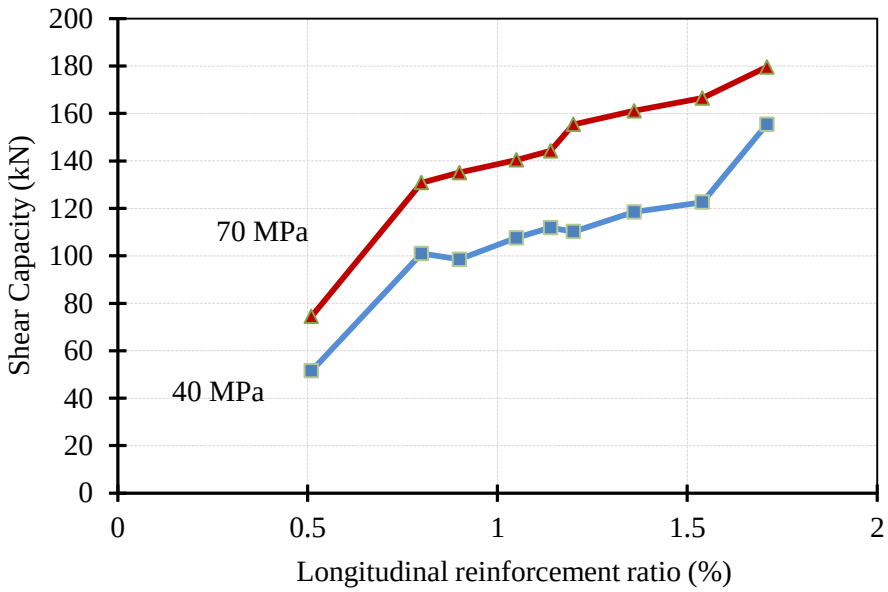

Figure 8.16: Shear capacity versus the longitudinal reinforcement ratio (models with shear reinforcement)

8.4 EFFECT OF SHEAR SPAN-TO-DEPTH RATIO

In this study, the shear span-to-depth ratio (*a/d*) ranged from 2.0 to 6.0. The main shear transfer mechanism in beams having *a/d* ratio of 2.0 is the arch action while beams with *a/d* ratio of 3.0 to 6.0 transfer the shear through a beam action. In this range of the shear span-to-depth ratio (2.0 to 6.0), the RC beams fail in shear before they attain their flexural capacities (Park and Paulay 1975). The effect of the *a/d* ratio was studied for different concrete strength, 30, 50 and 70 MPa, and for different longitudinal reinforcement ratio (0.8, 1.2 and 1.6%) as well.

8.4.1 Load-Deflection Response

Figures 8.17 to 19 show the load-deflection relationship at mid-span for selected models for different concrete strengths and longitudinal reinforcement ratios. The typical load-deflection

relationship has two stages, pre-cracking and post-cracking. It can be seen that both the pre-cracking and the post-cracking were affected by the *a/d* ratio where increasing the *a/d* ratio decreased the post-cracking flexural stiffness of the model and consequently the mid-span deflection increased. Also, the flexural stiffness showed significant increase as both the concrete strength and the reinforcement ratio increased.

At failure, the mid-span deflection of model having *a/d* ratio of 2.0 was approximately equal to or slightly less than that of model having *a/d* ratio of 3.0. This is because models having *a/d* of 2.0 failed at a load that is approximately 85% higher than that of models having *a/d* of 3.0. The mid-span deflection at failure increased as the *a/d* ratio increased from 3.0 to 6.0. For instance, in models having concrete strength of 30 MPa and 0.8% longitudinal reinforcement ratio, the deflection at failure increased by 28, 15 and 34% when the *a/d* ratio increased from 3.0 to 4.0, from 4.0 to 5.0 and from 5.0 to 6.0, respectively.

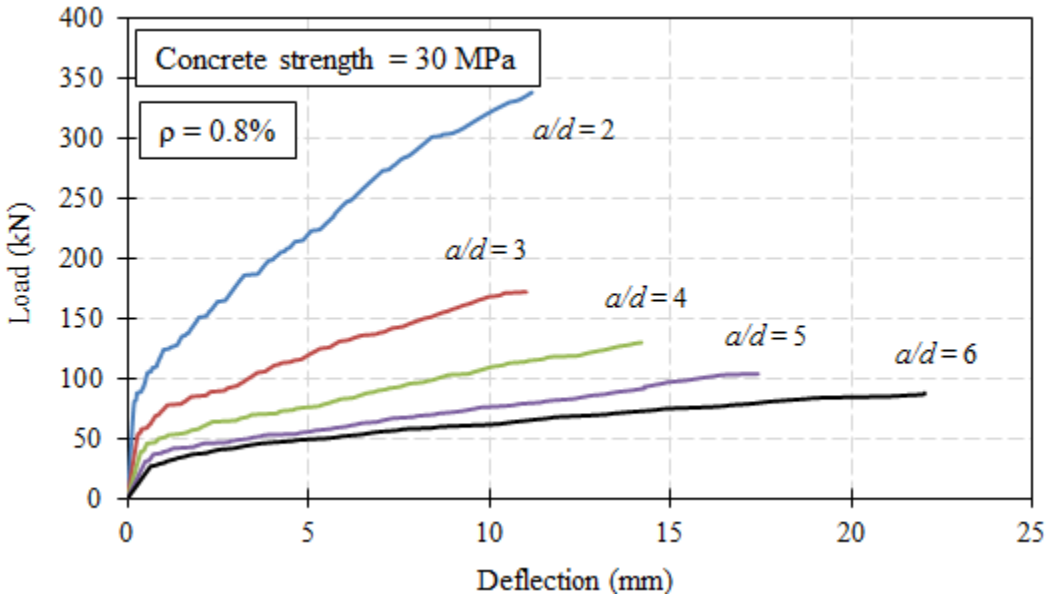

Figure 8.17: Load-deflection relationship for varying shear span-to-depth ratio in models with 0.8% and concrete strength of 30 MPa

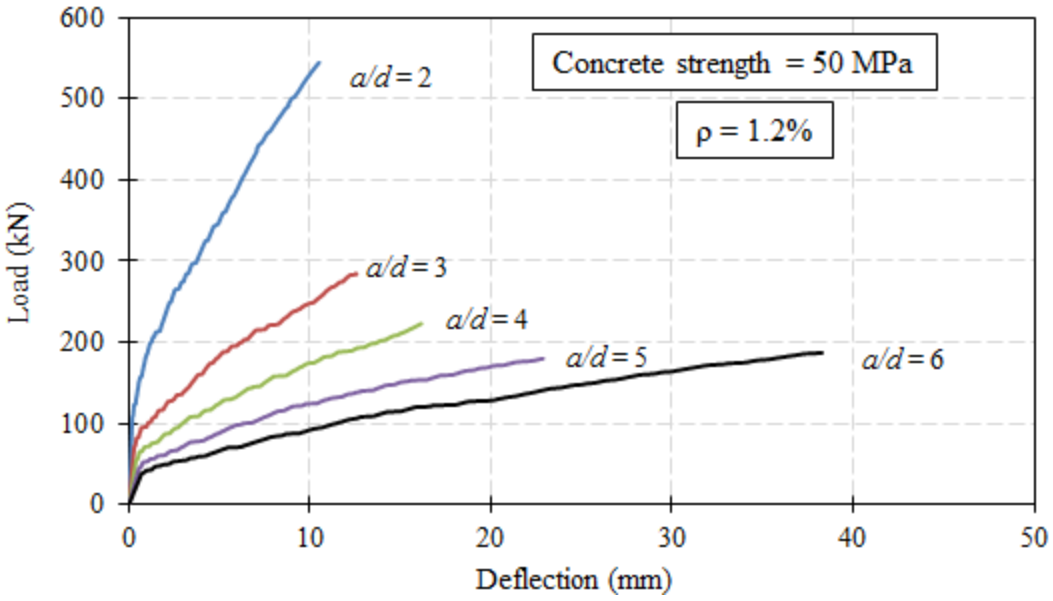

Figure 8.18: Load-deflection relationship for varying shear span-to-depth ratio in models with 1.2% and concrete strength of 50 MPa

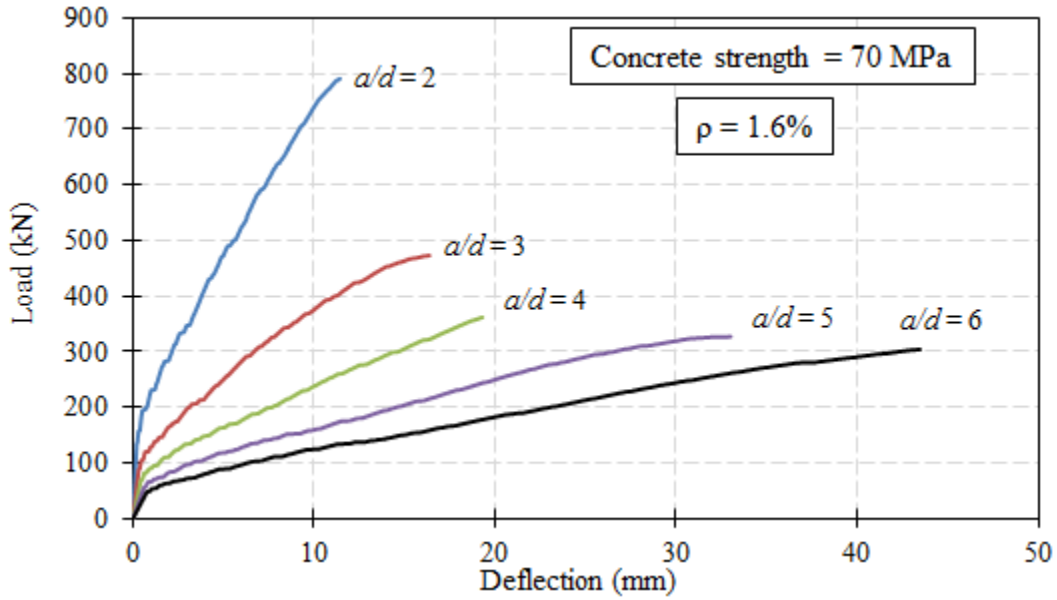

Figure 8.19: Load-deflection relationship for varying shear span-to-depth ratio in models with 1.6% and concrete strength of 70 MPa

8.4.2 Moment Redistribution

The applied load versus the monitored exterior reactions for selected models with varying shear span-to-depth ratio is shown in Figs. 8.20 to 8.22. In all models, the exterior reaction coincided with the elastic distribution until the formation of flexural cracks at the hogging moment region. Afterwards, the monitored exterior reaction diverged from the elastic one reflecting the beginning of the redistribution of the internal forces from the hogging moment region to the sagging moment regions. It can be seen that the difference between the numerical exterior reaction and elastic reaction decreases as the *a/d* ratio increases. Figure 8.23, also, shows the moment redistribution at the last step versus the shear span-to-depth ratio. As the shear span-to-depth ratio increases, the achieved moment redistribution form the hogging to the sagging moment decreased. This can be illustrated by the failure mode of the beams as follows: Beams with $3.0 < a/d < 6.0$ fail shortly after the initiation of the diagonal cracks before they reach their flexural capacity. This allows for small rotations at the middle support sections and consequently small moment redistribution. As the *a/d* ratio decreases (2.0 to 3.0) the beam can resist more loads (bending moments) which, in turn, results in high rotations and moment redistribution at the middle support section. Beams having *a/d* of 2.0 and 3.0 achieved moment redistribution more than the assumed one while beams having *a/d* equal to or greater than 4.0 could not achieve the assumed moment redistribution (20%).

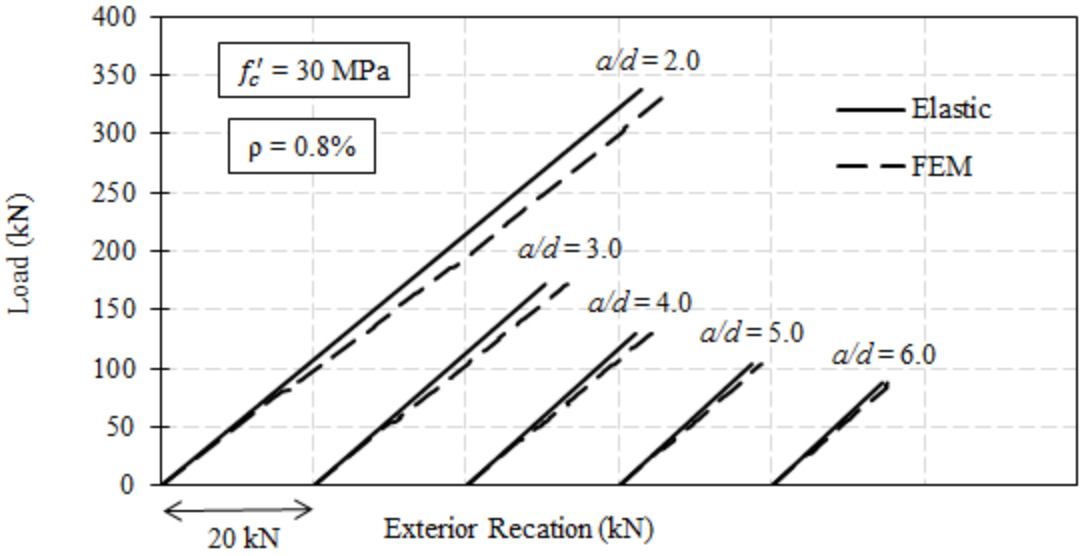

Figure 8.20: Load-exterior reaction relationship for varying shear span-to-depth ratio in models with 0.8% and concrete strength of 30 MPa

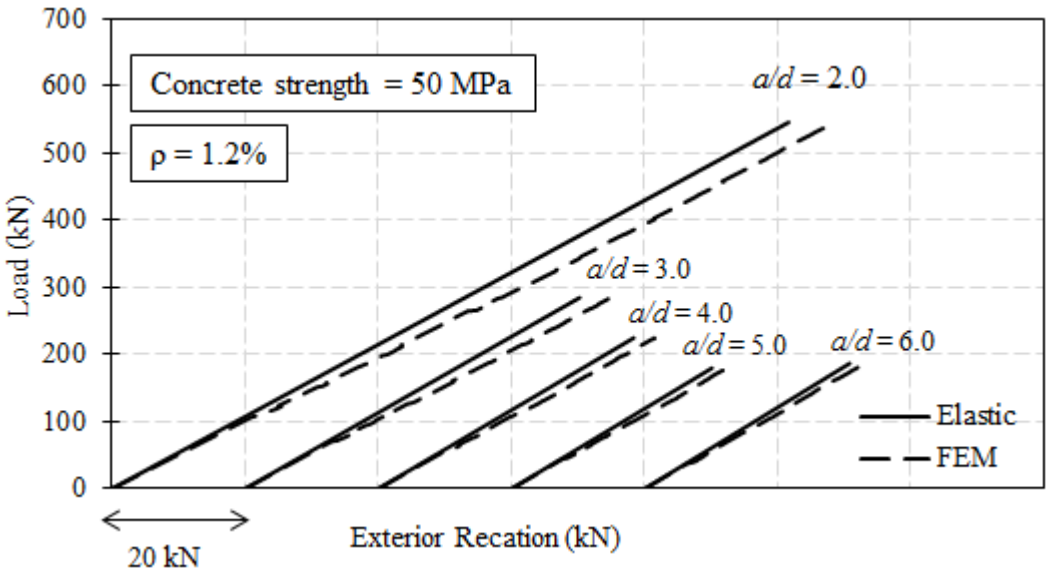

Figure 8.21: Load-exterior reaction relationship for varying shear span-to-depth ratio in models with longitudinal reinforcement ratio of 1.2% and concrete strength of 50 MPa

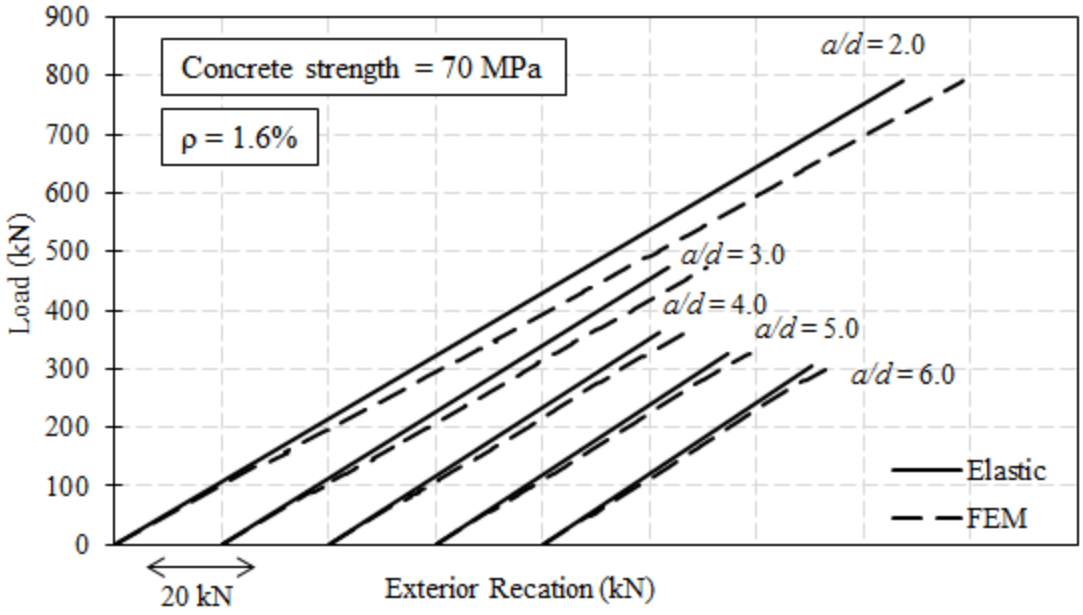

Figure 8.22: Load-exterior reaction relationship for varying shear span-to-depth ratio in models with longitudinal reinforcement ratio of 1.6% and concrete strength of 70 MPa

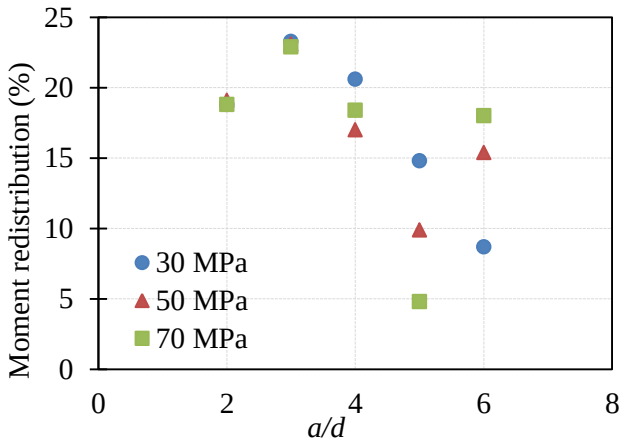

(a) Models with longitudinal reinforcement ratio of 0.8%

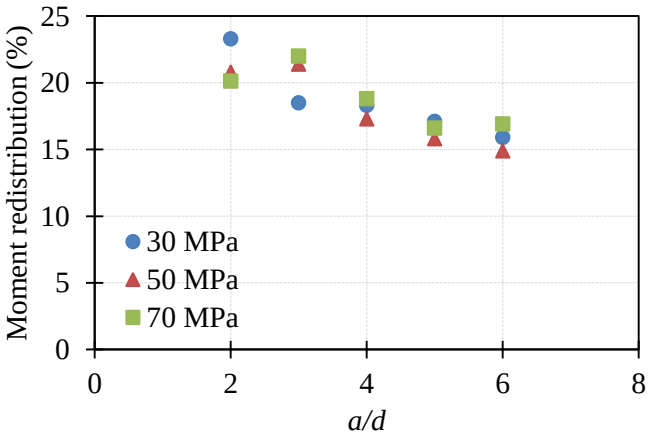

(b) Models with longitudinal reinforcement ratio of 1.2%

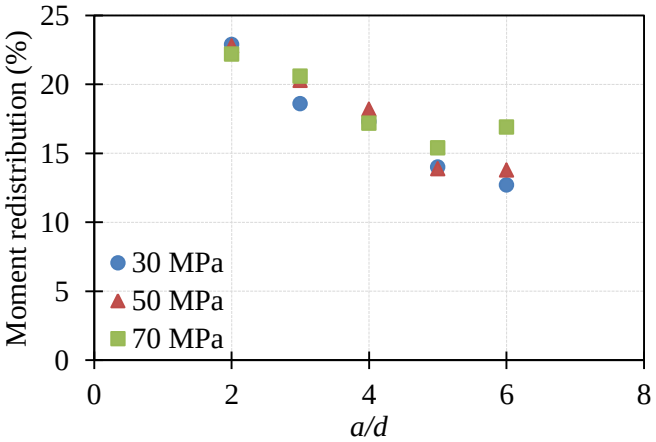

(c) Models with longitudinal reinforcement ratio of 1.6%

Figure 8.23: Moment redistribution percentage at failure versus span-to-depth ratio

8.4.3 Shear Strength

Figures 8.24 to 8.26 show the variation of the shear strength versus the shear span-to-depth ratio for different concrete strengths and longitudinal reinforcement ratios. It can be seen that the general behaviour of the shear strength is similar to that in simply supported beams where the shear strength decreases with increasing the *a/d* ratio. The shear strength is very high in beams having *a/d* = 2.0 compared to other beams having *a/d* ranged between 3.0 and 6.0. This is expected because beams having a*/d* = 2.0 is considered deep beams in which the load transfer mechanism between the loading point and the support is the arch action while beams having *a/d* equal to or greater than 3.0 or slender beams behave differently as discussed in Chapter 2.

In models having a longitudinal reinforcement ratio of 0.8%, increasing the *a/d* ratio from 2.0 to 3.0 decreased significantly the shear capacity by 48, 46 and 54% in models with 30, 50 and 70 MPa, respectively. The shear strength decreased by 23, 36 and 29% in models made of 30, 50 and 70 MPa, respectively, when the *a/d* ratio increased from 3.0 to 4.0. Further increase in the *a/d* ratio from 4.0 to 6.0 resulted in a reduction in the shear strength by 29, 22 and 30% for the three grades of the concrete strength, respectively. Similar behaviour can be seen in beams having 1.2 and 1.6% longitudinal reinforcement ratio.

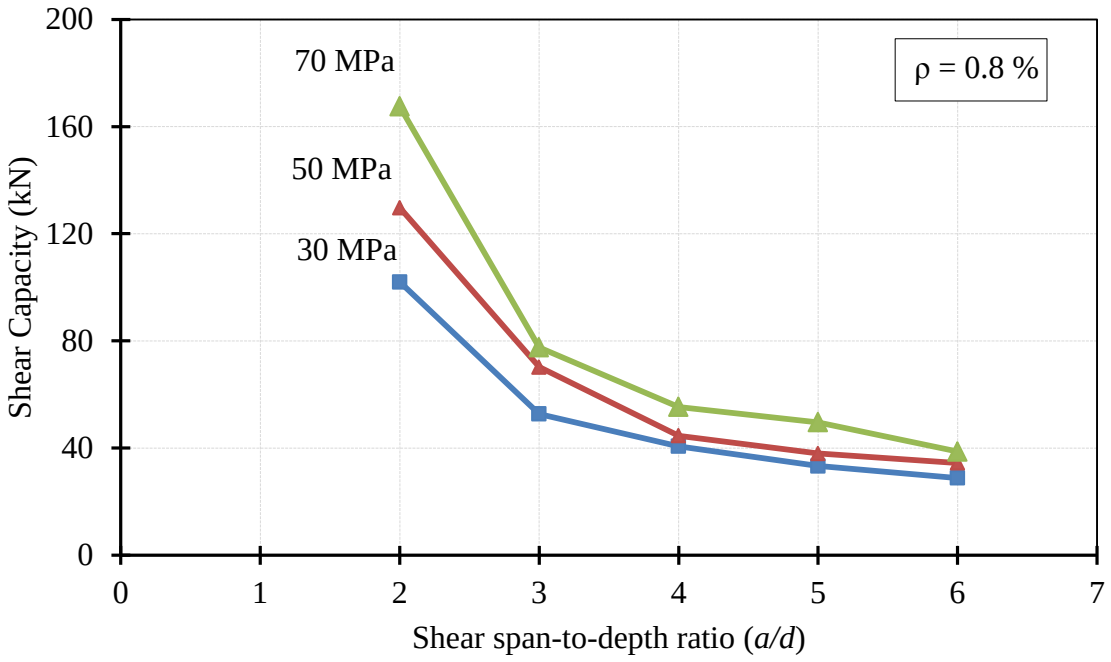

Figure 8.24: Variation of the shear strength with shear span-to-depth ratio in models with longitudinal reinforcement ratio of 0.8%

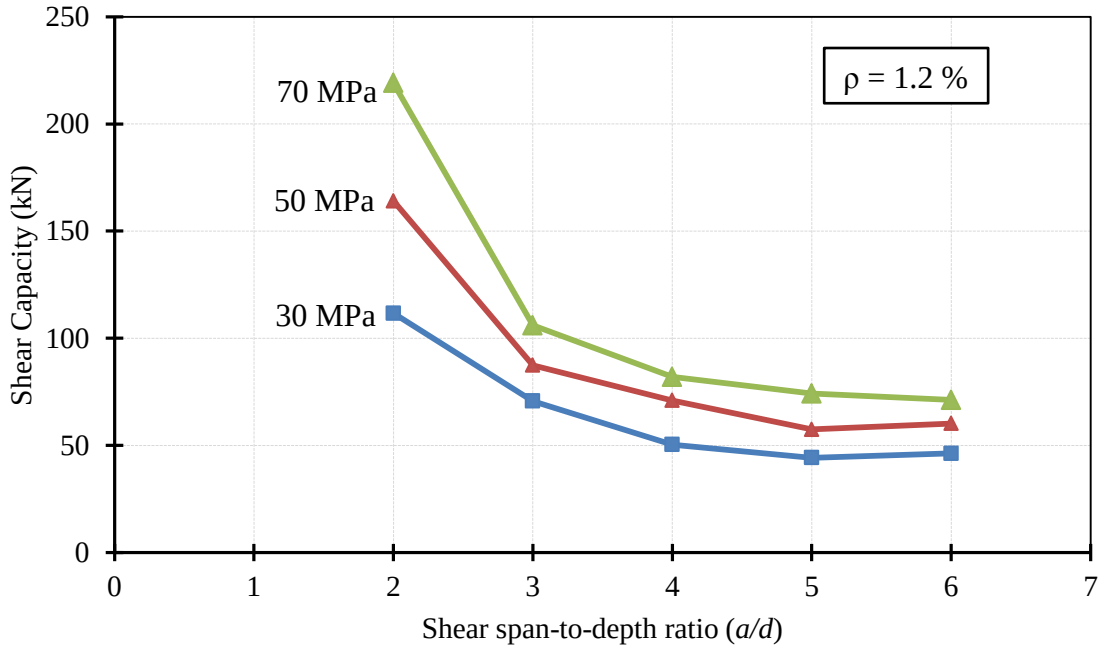

Figure 8.25: Variation of the shear strength with shear span-to-depth ratio in models with longitudinal reinforcement ratio of 1.2%

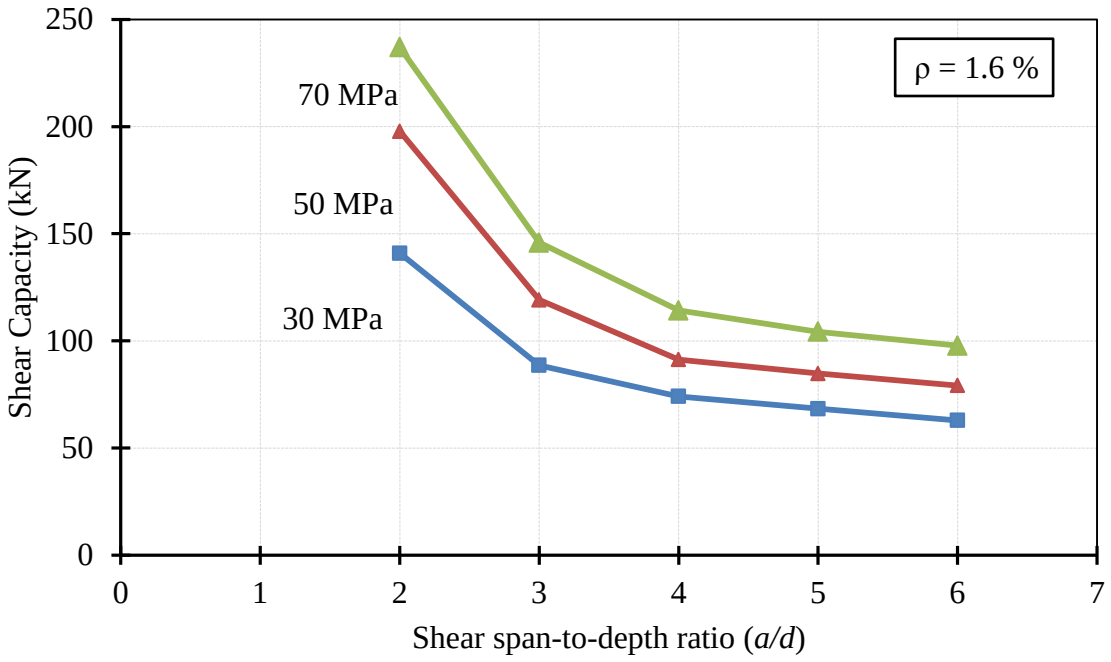

Figure 8.26: Variation of the shear strength with shear span-to-depth ratio in models with longitudinal reinforcement ratio of 1.6%

8.5 EFFECT OF TRANSVERSE REINFORCEMENT RATIO (SPACING OF STIRRUPS)

The presence of transverse reinforcement in beams improved the shear carrying capacity and also provided better confinement for the concrete in the compression regions. In the experimental phase of this study, the effect of transverse reinforcement ratio, using different stirrup diameter while keeping the spacing constant, on the shear strength of continuous GFRP-RC beams has been investigated. Using the FEM, this effect is examined; however, the reinforcement ratio is changed by changing the stirrup spacing for different concrete strengths and longitudinal reinforcement ratios. Also, the spacing is changed for the three different stirrups used in the experiments. The main spacing was the one used in the experiments (150 mm for NSC and 115 mm for HSC); then, the spacing is reduced to two-thirds and half that spacing.

8.5.1 Mid-Span Deflection

The load-deflection relationships for the FE modeled beams made of NSC (40 MPa) and HSC (75 MPa) are shown in Fig. 8.27. The models exhibited similar behaviour to the experiments. The slope of all curves was approximately the same because all beams had the same axial stiffness of the longitudinal reinforcement. The effect of the concrete strength on the load-deflection relationship is clear where high strength concrete showed steeper curves in both the pre-cracking and post-cracking stages. After the formation of the diagonal cracks, the shear reinforcement ratio affected the post-cracking flexural stiffness. Higher shear reinforcement ratio resulted in higher flexural stiffness. This can be attributed to that high shear reinforcement ratio results in a narrow diagonal crack width compared to that in the case of low shear reinforcement ratio.

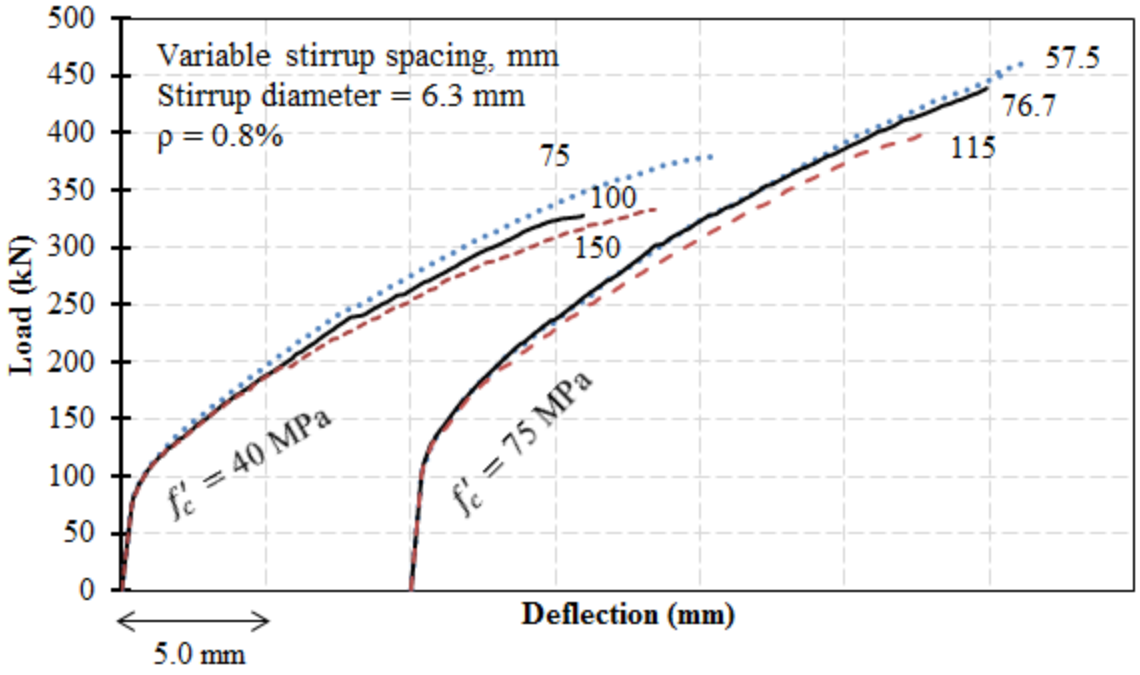

(a) Models with 0.8% longitudinal reinforcement ratio

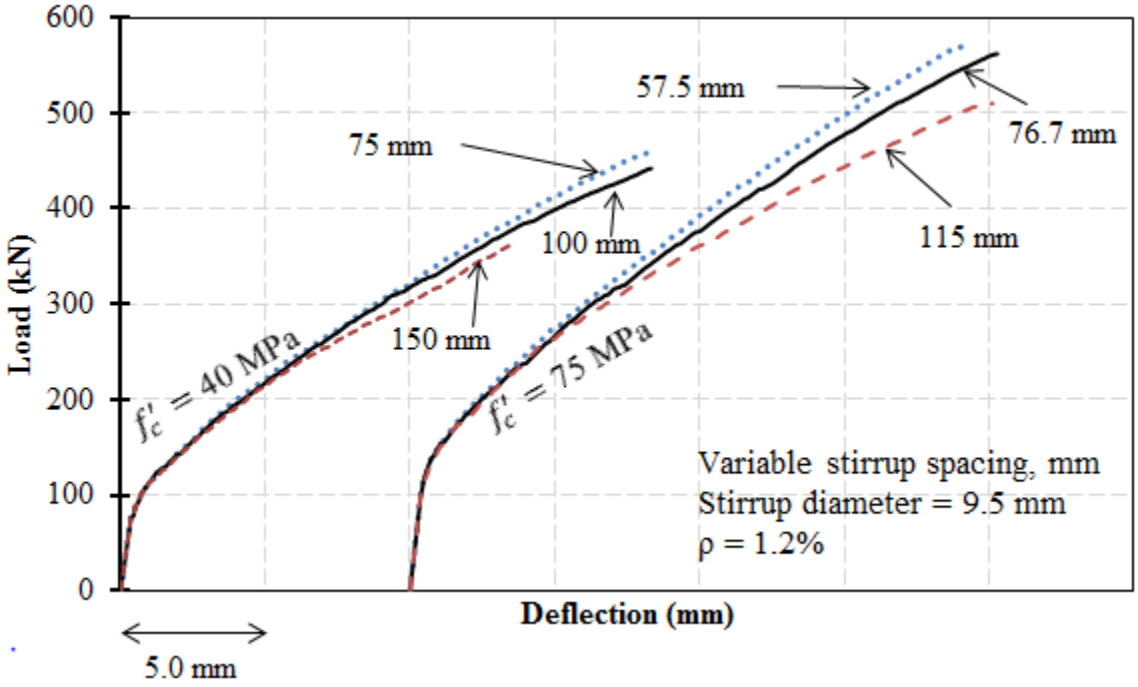

(b) Models with 1.2% longitudinal reinforcement ratio

Figure 8.27: Load-deflection relationship for representative models

8.5.2 Moment Redistribution

Figure 8.28 shows the load-exterior reaction relationship for representative models having different concrete strength, longitudinal reinforcement ratio and stirrup diameter. Similar to the experimental results, the exterior reactions followed the elastic distribution at early stages of loading. Once the flexural cracks initiated at the hogging moment region, the monitored exterior reaction diverged from the elastic one. The monitored exterior reaction had a greater value than the elastic exterior reaction and this continued until failure. These greater values mean that the internal forces (shear and bending moment) were redistributed form the hogging to the sagging moment region. The values of the monitored exterior reaction and the elastic one were used to calculate the percentage of moment redistribution for every model where 1% increase in the exterior reaction gives 2.25% moment redistribution form the hogging to the sagging moment region. The moment redistribution percentage at the last step is depicted in Fig. 8.29. In this figure, it can be observed that beams made of normal strength concrete achieved higher moment redistribution than those made of high strength concrete. This can be attributed to the brittleness of the high strength concrete. Also, beams having a longitudinal reinforcement ratio of 1.2% demonstrated higher moment redistribution percentage compared to those with longitudinal reinforcement ratio of 0.8%. This might be due to that beams having longitudinal reinforcement ratio of 1.2% sustained high loads and consequently shear and bending moment. This high shear and bending moment result in more deformations at the hogging moment region that, in turn, improve the rotation and moment redistribution at that region. Moreover, the reinforcement ratio had a slight effect on the moment redistribution where beams with higher transverse reinforcement ratio increased the moment redistribution and this could be attributed to the better

confinement provided with the high transverse reinforcement ratio compared to that of small transverse reinforcement ratio.

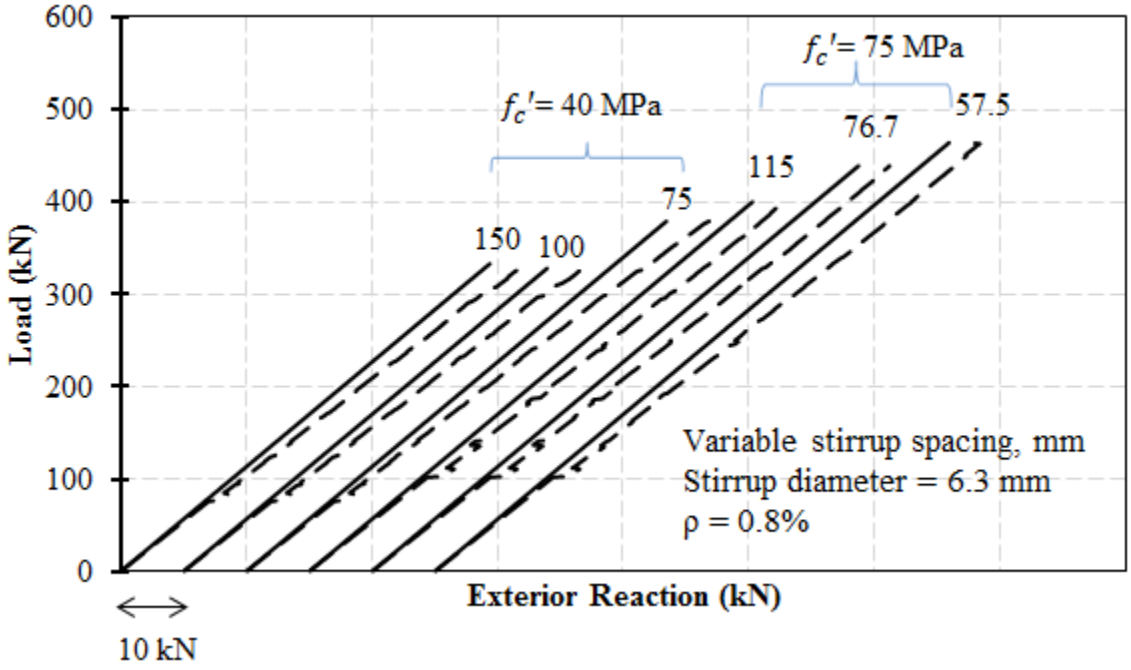

(a) Models with 0.8% longitudinal reinforcement ratio

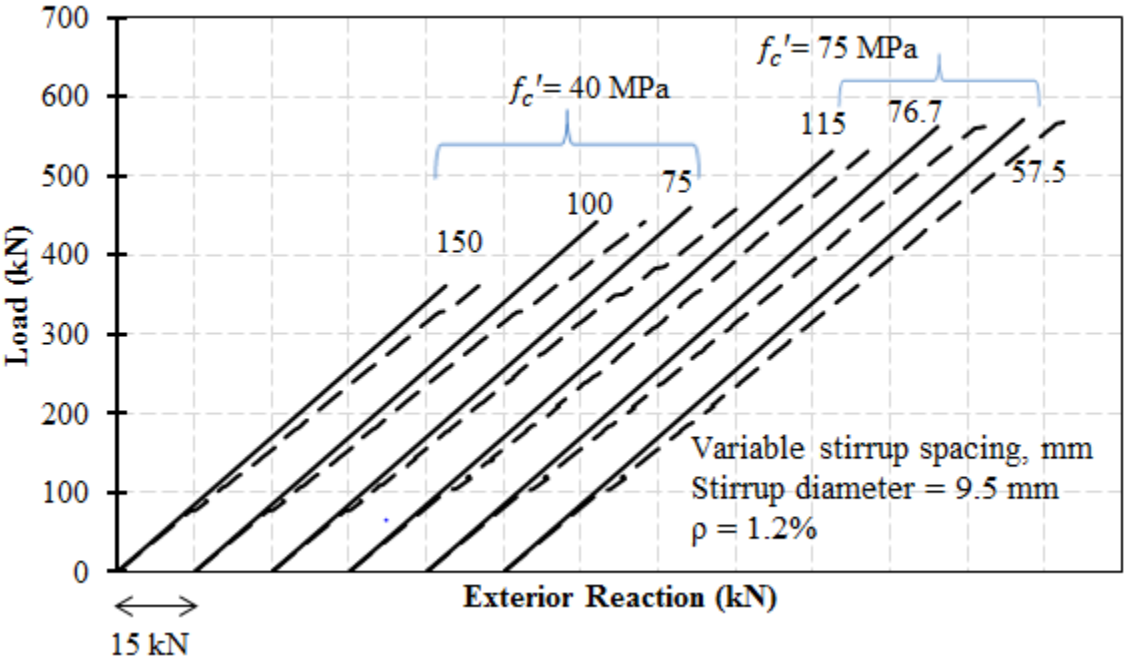

(b) Models with 1.2% longitudinal reinforcement ratio

Figure 8.28: Load-exterior reaction relationship for representative models

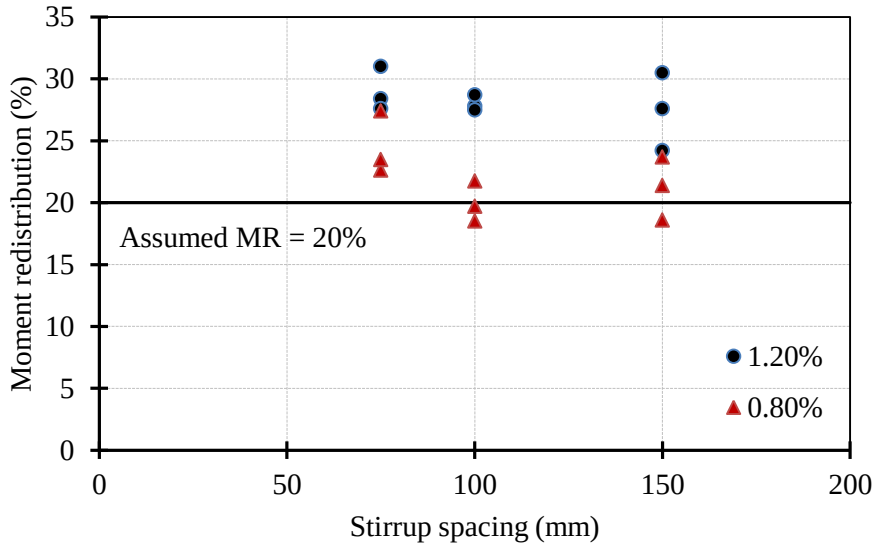

(a) Models with concrete strength of 40 MPa

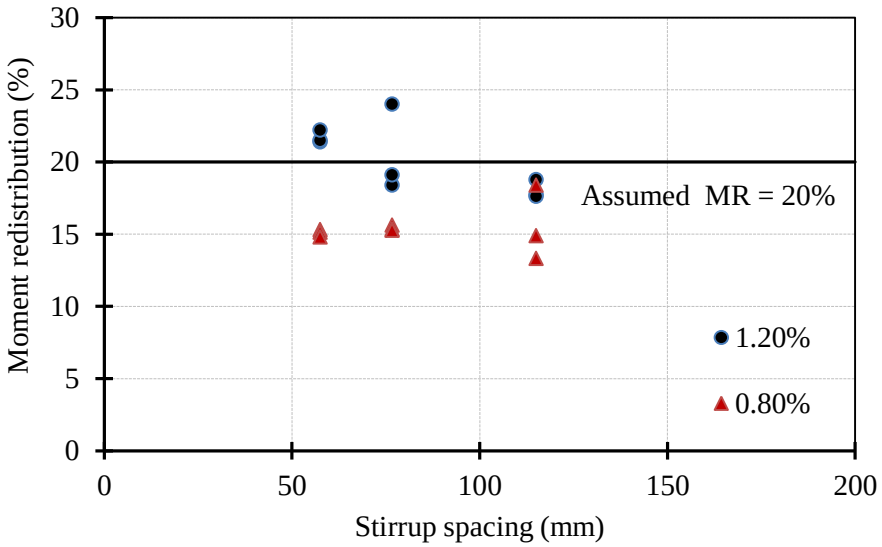

(b) Models with concrete strength of 75 MPa

Figure 8.29: Moment redistribution percentage at failure for models with varying stirrup spacing

8.5.3 Shear Strength

Increasing the shear reinforcement ratio, by decreasing the spacing between stirrups, increased the shear strength as shown in Figs. 8.30 and 8.31. This agrees well with the findings of Ahmed et al. (2010) and El-Mogy et al. (2011).

In NSC models ($f_c^{'}$ = 40 MPa) having longitudinal reinforcement ratio of 0.8%, decreasing the spacing of stirrups of 6.3 mm from 150 to 100 mm decreased the shear strength by 10%. This could be attributed to the moment redistribution achieved at failure (23.7% and 18.5%, respectively). However, decreasing the spacing from 100 to 75 mm increased the shear strength by 6.5%. Similar trend can be seen in models with 9.5 mm stirrup where the shear strength decreased by 7.0% then it increased by 15% when the spacing decreased from 150 to 100 mm and from 100 to 75 mm, respectively. In models having 12.7mm stirrups, the shear strength increased as the spacing decreased from 150 to 100 mm and from 100 to 75 mm.

HSC models (75 MPa) with 0.8% longitudinal reinforcement ratio, showed an increase in the shear strength with decreasing the spacing of the stirrups for all the three sizes of stirrups. the shear strength of models, with 6.3 mm stirrups, increased by 10.5 and 5.5% when the spacing decreased from 115 to 76.7 mm and from 76.7 to 57.5 mm, respectively. Also, in models with 9.5 mm stirrup, the same decrease in the spacing increased the shear strength by 23 and 3.0% respectively. for models having 12.7 mm stirrups, the shear strength increased by 3.0 and 9.0% for the same decrease in the stirrup spacing, respectively.

In models having a longitudinal reinforcement ratio of 1.2%, the shear capacity increased by 7, 20 and 3% when the spacing decreased from 150 to 100 mm in models of 40 MPa concrete strength with 6.3, 9.5 and 12.7-mm stirrup diameter, respectively. Further decrease in the spacing

of stirrups in these models, from 100 to 75 mm, resulted in an increase in the shear capacity by 6, 4.3 and 7.5%. In models of 75 MPa concrete strength, the shear capacity increased by 7.4, 9.0 and 10.2% when the spacing decreased from 115 to 76.7 mm in models with 6.3, 9.5, 12.7-mm stirrup diameter, respectively. However, decreasing the spacing of the stirrups from 76.7 to 57.5 mm increased the shear capacity by only 1% in models with 6.3-mm and 9.5-mm diameter, respectively. The same decrease in the spacing of 12.7-mm diameter stirrups resulted in a decrease in the shear strength by 4%.

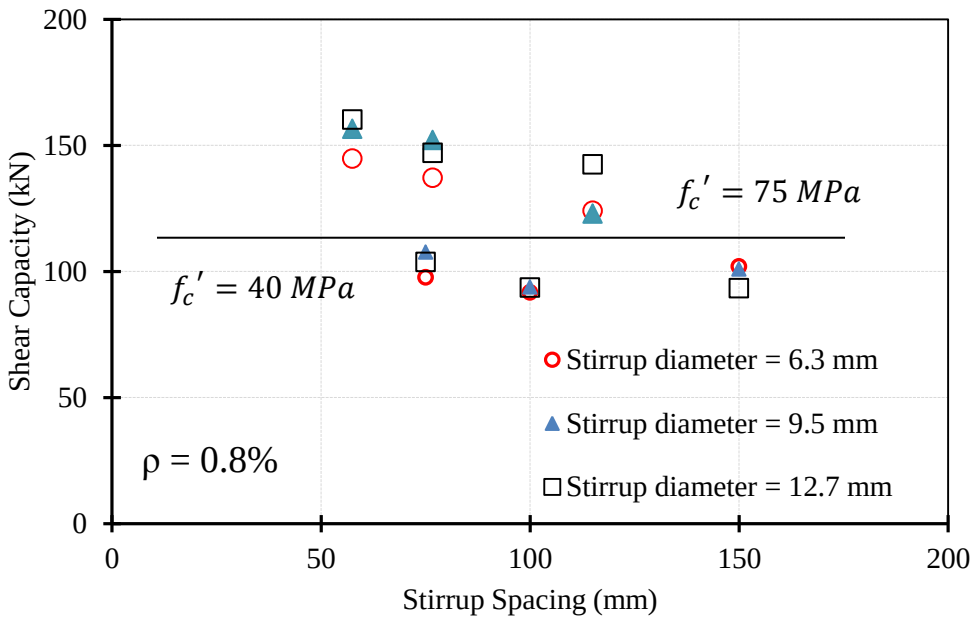

Figure 8.30: Shear capacity for NSC and HSC models with variable stirrup spacing in models with 0.8% longitudinal reinforcement ratio

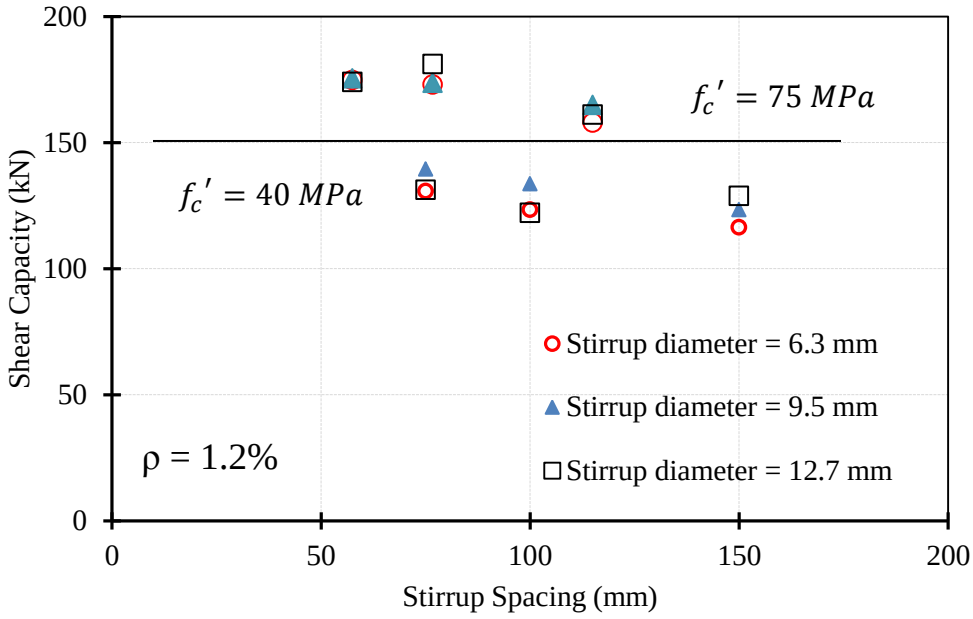

Figure 8.31: Shear capacity for NSC and HSC models with variable stirrup spacing in models with 1.2% longitudinal reinforcement ratio

CHAPTER 9: SUMMARY, CONCLUSIONS AND FUTURE WORK

9.1 SUMMARY

In this study, the shear behaviour of concrete continuous beams reinforced with GFRP bars and stirrups was investigated. The study consisted of two phases, experimental and numerical investigations. The study resulted in a number of findings on the effect of different parameters on the shear behaviour of FRP-RC continuous beams. In addition, a number of recommendations for future work were also presented.

The experimental phase included the construction and testing of twenty four full-scale concrete beams continuous over two-equal spans with rectangular cross-section. The tested beams were loaded to failure under a two-point monotonic loading system in each span. All the test beams had a constant shear span-to-depth ratio of 3.0. The tested variables were flexural reinforcement ratio and type, concrete strength, transverse reinforcement ratio and type, and depth of the beam.

The numerical phase started by constructing a finite element model (FEM) to simulate the shear behaviour of continuous concrete beams. The FEM was verified against results obtained from the experimental phase and validated against previous work found in the literature. Afterwards, a parametric study was conducted using the verified/validated model to investigate a wide range of parameters affecting the shear strength of continuous concrete beams reinforced with GFRP bars and stirrups such as concrete compressive strength, longitudinal reinforcement ratio, shear span-to-depth ratio, depth of the beam and the amount of transverse reinforcement.

9.2 CONCLUSIONS

Based on the experimental and numerical investigations carried out in this study, the following conclusion s can be drawn.

9.2.1 Conclusions based on the Experimental Results of Series I – Beams without Transverse Reinforcement

1. Moment redistribution was observed in GFRP-RC continuous beams without transverse reinforcement. This is in good agreement with the test results of the control steel-RC specimen and the findings of previous research on GFRP-RC continuous beams.
2. The shear failure location changed from the interior to the exterior shear span because of the moment and shear redistribution. Beams experienced high percentage of moment redistribution failed due to a diagonal tension crack in the exterior shear span. This was mainly due to the high sagging moment in the exterior shear span.
3. Increasing the longitudinal reinforcement ratio by 50% (from 0.8 to 1.2%) increased the shear strength of GFRP-RC continuous beams by 42% in NSC beams. While the same increase in the longitudinal reinforcement resulted in 20% increase in the shear strength of the HSC beams. Increasing the longitudinal reinforcement ratio from 0.8 to 1.6% increased the shear strength of the NSC beams by 95%. For HSC beams, the same increase in the longitudinal reinforcement ratio changed the failure location form the interior to the exterior shear span.
4. Increasing the reinforcement ratio from 1.2 to 1.6% changed the failure location from the interior to the exterior shear span in both NSC and HSC beams. This can be attributed to the high moment redistribution achieved in beams with 1.6% longitudinal reinforcement.
5. Increasing the concrete strength from 39 to 70 MPa resulted in an increase in the shear strength of 25 and 34% in beams with 0.8 and 1.6% longitudinal reinforcement ratio,

respectively. The same increase in the concrete strength, in beams with 1.2% longitudinal reinforcement ratio resulted in a slight increase of the shear capacity by approximately 5.7%. This can be attributed to the high moment redistribution in NSC beam compared to that in its counterpart HSC beam.

6. The comparison of the test results with the predictions of the relevant FRP design codes and guidelines showed that the current shear design expressions can be safely applied to the GFRP-RC continuous beams. However, the margin of safety in such continuous beams was less than that in simply-supported beams. Also, all the investigated codes and guidelines failed to predict the failure location for some beams where it was expected to occur in the interior shear span for all beams; however, failure was observed in the exterior shear span in several beams.
7. The Canadian standards CSA/S806-12 (CSA 2012) predicted well the shear strength of GFRP-RC continuous beams where the ratio of the experimental-to-predicted shear capacity was 1.02. However, this ratio was 1.16 1 in FRP-RC simply-supported beams (Yost et al. 2001; El-Sayed et al. 2005; El-Sayed et al. 2006a &b; Alam and Hussein 2012), which showed the effect of the continuity of such beams.
8. Both CSA/S6-06 (CSA 2009) and ACI 440.1R-06 (ACI Committee 440 2006) yielded very conservative predictions for the shear strength of the test beams. The ratio of the experimental-to-predicted shear strength was 2.26 and 2.23, respectively. Also, the continuity effect was obvious in this case since these ratios in simply-supported beams were 2.58 (Yost et al. 2001; El-Sayed et al. 2005; El-Sayed et al. 2006a &b; Alam and Hussein 2012) and 3.06 (Yost et al. 2001), respectively. However, the difference in the ratio of the experimental-to-predicted capacity between continuous beams and simply-

supported beams was smaller when CSA/S6-06 (CSA 2009) was used compared to that of the ACI 440.1R-06. This can be attributed to the fact that the CSA/S6-06 accounts for the straining actions at the section while the ACI 440.1R-06 does not.

9.2.2 Conclusions Based on the Experimental Results of Series II – Size Effect

1. All test beams showed moment and shear redistribution with different values and directions. The moment redistribution, from the hogging to the sagging moment regions, decreased or even became reversed redistribution (form the sagging to the hogging moment region) with increasing the effective depth for both NSC and HSC beams. This might be attributed to the fact that the sagging moment region was relatively weaker than the hogging moment region due to the development of more and wider cracks as the effective depth increased.
2. GFRP-RC continuous beams failed in the interior shear span showed adverse or no size effect on the shear strength of such beams. NSC beams showed an increase in the shear strength with increasing the effective depth while the shear strength of HSC beams approximately did not change as the effective depth increase.
3. Similar to simply-supported beams, size effect on the shear strength was observed in beams failed in the exterior shear span where the shear strength decreased significantly as the effective depth increased in both NSC and HSC beams. However, the high longitudinal reinforcement ratio and the modulus of elasticity of the used GFRP bars caused the size effect to be less pronounced compared to that in the previously tested simple beams.

4. The CSA/S806-12 (CSA 2012) yielded reasonable prediction for the shear strength of GFRP-RC continuous beams where all the tested beams failed at a shear stress greater than that predicted by this code. The average ratio of experimental-to-predicted shear strength, considering the shear stress in the interior shear span at failure was 1.23 with COV of 24.0%. However, it could not predict the failure location in such continuous beams.
5. The ACI 440.1R-06 (ACI 2006), CSA/S6-06 (CSA 2009) and the second order expression proposed by Hoult et al. (2008) yielded more conservative predictions for the shear strength of the test beams. The ratio of experimental-to-predicted shear strength ratio, calculated using the shear stress in the interior shear span at failure, was 2.87 (COV = 14.0%), 2.16 (COV = 23.0%) and 2.24 (COV = 25.5%), respectively. Again, they failed to predict the failure location in some beams.

9.2.3 Conclusions Based on the Experimental Results of Series III – Effect of Transverse Reinforcement Ratio

1. Shear-critical GFRP-RC continuous beams reinforced with GFRP bars and stirrups exhibited moment redistribution that was very similar to steel- RC reference beam. All the tested beams achieved moment redistribution percentage of approximately 20% or higher.
2. The shear strength of continuous beams reinforced with GFRP bars and stirrups depended on the amount of the shear reinforcement, the angle of inclination of the diagonal crack, the tensile strength of the stirrups, and the percentage of the moment redistribution.

3. Continuous beams with minimum shear reinforcement according to the CSA/S806-12 standard achieved adequate post-cracking shear strength where beams did not fail suddenly after the formation of diagonal cracks.
4. Beams with half the minimum and the minimum transverse reinforcement ratio specified in the CSA/S806-12 failed due to the rupture of the stirrups while using twice the minimum shear reinforcement ratio changed the mode of failure from the rupture of stirrups to crushing of the concrete of the web.
5. Increasing the concrete strength had a pronounced effect on increasing the shear strength of GFRP-RC continuous beams similar to simply-supported beams. However, this increase in the shear strength was a result of increasing both the concrete strength and the transverse reinforcement ratio.
6. The ACI 440.1R-06 yielded conservative predictions for the shear capacity where the average experimental-to-predicted shear capacity ratio was 1.81 (COV = 39%). This ratio was 1.43 (COV = 18.8%) for the CSA/S806-12. The better prediction by the CSA/S806-12 was mainly due to the fact that it accounts for the values of moment and shear at the shear critical section.

9.2.4 Conclusions Based on the Numerical Investigation

1. The constructed finite element model (FEM) using ATENA-3D program was able to analyse GFRP-RC continuous beams and predict the load capacity, the load-deflection relationship, the moment redistribution and the shear capacity with a reasonable degree of accuracy. Also, this FEM could capture the behaviour of GFRP-RC continuous beams tested under one-point load in each span found in literature.

2. The results of the analysis of the tested beams with the finite element model confirmed the occurrence of moment and shear redistribution in GFRP-RC beams. The NSC beams showed higher moment and shear redistribution compared to that in HSC beams. This agrees with the findings of El-Mogy et al. (2013).
3. Increasing the concrete compressive strength in the model increased significantly the shear strength of GFRP-RC beams. The same trend was observed in beams with and without shear reinforcement.
4. The shear strength of GFRP-RC continuous beams increased with increasing the longitudinal reinforcement ratio in models with and without shear reinforcement. Both NSC and HSC models showed this behaviour.
5. Similar to simply-supported beams, the shear strength of continuous beams reinforced with GFRP bars decreased with increasing the shear span-to-depth ratio. The reduction in the shear strength was very significant when the shear span-to-depth ratio changed from 2.0 to 3.0 while further increase in the shear span-to-depth ratio decreased the shear strength slightly.
6. The shear strength of GFRP-RC continuous beams increased with decreasing the spacing between the stirrups. This agrees with the results found in the literature (Ahmed et al. 2010 and El-Mogy et al. 2011).

9.3 RECOMMENDATIONS FOR FUTURE WORK

1. Further experimental and analytical studies are required to investigate the shear behaviour of FRP-RC continuous beams with a wider range of reinforcement ratios and different cross-sections, such as T-shaped sections.

2. The beams in this study were tested under two-point loading system in each span. A series of specimens should be tested under different loading configurations (one loading point in each span or uniformly distributed load).
3. Experimental and analytical studies should be conducted to verify the size effect on the shear strength of GFRP-RC continuous beams as the experimental results of this study showed no or adverse size effect in beams failed in the interior shear span.
4. Also, experimental investigation has to be carried out to verify the shear behaviour of the GFRP-RC continuous beams with different shear span-to-depth ratios observed in the FEM parametric study.
5. As the present study was carried out using mainly GFRP reinforcement, more experiments should be conducted on beams reinforced with CFRP bars. In addition, similar tests should be performed on concrete beams reinforced with different types of fibres (such as aramid and basalt) and surface texture (such as deformed surface).
6. Using the proposed FEM model, more variables need to be investigated such as the number of spans and the effect of unequal spans.

REFERENCES

ACI Committee 318. (2014). "Building code requirements for reinforced concrete." ACI 318-14, *American Concrete Institute*, Detroit, MI, 443 p.

ACI Committee 318. (2011). "Building code requirements for reinforced concrete." ACI 318-11, *American Concrete Institute*, Detroit, MI, 443 p.

ACI Committee 440. (2015). "Guide for the Design and Construction of Structural Concrete Reinforced with FRP Bars." ACI 440.1R-15, *American Concrete Institute*, Detroit, MI, 83 p.

ACI Committee 440. (2006). "Guide for the Design and Construction of Structural Concrete Reinforced with FRP Bars." ACI 440.1R-06, *American Concrete Institute*, Detroit, MI, 44 p.

Ahmed, E., El-Salakawy, E. and Benmokrane, B. (2010). "Performance Evaluation of Glass Fiber-Reinforced Polymer Shear Reinforcement for Concrete Beams." *ACI Structural Journal*, 107(1): 53-62.

Alam, M. and Hussein, A. (2013). "Size Effect on Shear Strength of FRP Reinforced Concrete Beams without Stirrups," ASCE, *Journal of Composites for Construction*, 17(4): 507-516.

Alam, M. and Hussein, A. (2012). "Effect of Member Depth on Shear Strength of High-Strength Fiber-Reinforced Polymer–Reinforced Concrete Beams." *Journal of Composites for Construction*, ASCE, 16(2): 119-126.

Arslan, G. (2008). "Cracking Shear Strength of RC Slender Beams without Stirrups." *Journal of Civil Engineering and Management*, 14(3):177-182.

ASCE-ACI Committee 445. (1999). "Recent Approaches to Shear Design of Structural Concrete (ACI 445R-99) (Reapproved 2009)." *American Concrete Institute*, Farmington Hills, MI, 55 pp.

Bažant, P. and Kazemi, M. (1991). "Size Effect on Diagonal Shear Failure of Beams without Stirrups." *ACI Structural Journal*, 88(3): 268-276.

Bentz, E., Massam, L. and Collins, M. (2010). "Shear Strength of Large Concrete Members with FRP Reinforcement." ASCE, *Journal of Composites for Construction*, 15(6): 637-646.

Bigaj, A.J. (1999). "Structural Dependence of Rotation Capacity of Plastic Hinges in RC Beams and Slabs." *PhD Thesis, Delft University of Technology*, ISBN 90-407-1926-8.

Bryant, R., Bianchini, A., Rodriguez, J. and Kesler, C. (1962). "Shear Strength of Two-Span Continuous Reinforced Concrete Beams with Multiple Point Loading." *ACI Structural Journal*, 1143-1177.

CEB (Comité Européen du béton). (1990). "CEB-FIP Model Code for Concrete Structures." Paris.

Cervenka, V., Jendele, L. and Cervenka, J. (2013). "ATENA Program Documentation Part I: Theory." *Cervenka Consulting Ltd*., Prague, Czech Republic.

Cladera, A. and Marí, A.R. (2005). "Experimental Study on High-Strength Concrete Beams Failing in Shear." *Engineering Structures*, 27:1519-1527.

Collins, M. P. and Kuchma, D. (1999). "How Safe Are Our Large, Lightly Reinforced Concrete Beams, Slabs, and Footings?" *ACI Structural Journal*, 96(4): 482-491.

CSA. (2014). "Code for the Design of Concrete Structures for Buildings." CSA/A23.3-14, *Canadian Standards Association*, Rexdale, ON, Canada.

CSA. (2012). "Code for the Design and Construction of Building Structures with Fibre-Reinforced Polymers." CSA/S806-12, *Canadian Standards Association*, Rexdale, ON, Canada.

CSA. (2009). "Canadian Highway Bridge Design Code-Addendum." CSA/S6-06, *Canadian Standards Association*, Rexdale, ON, Canada.

CSA. (2004). "Code for the Design of Concrete Structures for Buildings." CSA/A23.3-04, *Canadian Standards Association*, Rexdale, ON, Canada.

CSA. (2002). "Code for the Design and Construction of Building Components with Fibre-Reinforced Polymers." CSA/S806-02, *Canadian Standards Association*, Rexdale, ON, Canada.

Dawood, N., and Marzouk, H. (2012). "Cracking and Tension Stiffening of High-Strength Concrete Panels." *ACI Structural Journal*, 109(1): 21–30.

El-Mogy, M., El-Ragaby, A. and El-Salakawy, E. (2013). "Experimental Testing and Finite Element Modeling on Continuous Concrete Beams Reinforced with Fibre Reinforced Polymer Bars and Stirrups." *Canadian Journal of Civil Engineering*, 40(11), 1091–1102.

El-Mogy, M., El-Ragaby, A. and El-Salakawy, E. (2011). "Effect of Transverse Reinforcement on the Flexural Behavior of Continuous Concrete Beams Reinforced with FRP." ASCE, *Journal of Composites for Construction*, 15(5): 672-681.

El-Mogy, M., El-Ragaby, A. and El-Salakawy, E. (2010). "Flexural Behavior of Continuous FRP-reinforced Concrete Beams." ASCE, *Journal of Composites for Construction*, 14(6): 669-680.

El-Sayed, A., El-Salakawy, E.F. and Benmokrane, B. (2007). "Mechanical and Structural Characterization of New Carbon FRP Stirrups for Concrete Members." ASCE *Journal of Composites for Construction*, 11 (4): 352-362

El-Sayed, A., El-Salakawy, E. and Benmokrane, B. (2006a). "Shear Strength of FRP-Reinforced Concrete Beams without Transverse Reinforcement." *ACI Structural Journal*, 103(2): 235-243.

El-Sayed, A., El-Salakawy, E. and Benmokrane, B. (2006b). "Shear Capacity of High-Strength Concrete Beams Reinforced with FRP Bars." *ACI Structural Journal*, 103(3): 383-389.

El-Sayed, A., El-Salakawy, E. and Benmokrane, B. (2005). "Shear Strength of One-Way Concrete Slabs Reinforced with Fiber-Reinforced Polymer Composite Bars." ASCE, *Journal of Composites for Construction*, 9(2): 147-157.

Ernst, G.C. (1958). "Moment and Shear Redistribution in Two-Span Continuous Reinforced Concrete Beams." *ACI Structural Journal*, 30(5): 573-589.

Ghannoum, W. M. (1998). "Size Effect on Shear Strength of Reinforced Concrete Beams." Master Thesis, McGill University, Montréal, Canada.

Grace, N., Soliman, A. K., Abdel-Sayed, G. and Saleh, K. R. (1998). "Behaviour and Ductility of Simple and Continuous FRP reinforced Beams." ASCE, *Journal of Composites for Construction*, 2(4): 186-194.

Gravina, R. J. and Smith, S. T. (2008). "Flexural Behaviour of Indeterminate Concrete Beams Reinforced with FRP Bars." *Engineering Structures*, 30(9): 2370–2380.

Habeeb, M. N. and Ashour, A. F. (2008). "Flexural Behaviour of Continuous GFRP Reinforced Concrete Beams." ASCE, *Journal of Composites for Construction*, 12(2): 115-124.

Hordijk, D. A. (1991). "Local approach to fatigue of concrete." *Ph.D. dissertation, Delft University of Technology*, Delft, Netherlands.

Hoult, N. A., Sherwood, E. G., Bentz, E. C. and Collins, M. P. (2008). "Shear Behaviour of One Way Reinforced Concrete Slabs." ASCE, *Journal of Composites for Construction*, 12(2):125-133.

Johnson, M. K. and Ramirez, J. A. (1989). "Minimum Shear Reinforcement in Beams with Higher Strength Concrete." *ACI Structural Journal*, 86(4), 376–382.

Kani, G. N. J. (1967). "How Safe Are Our Large Concrete Beams?" *ACI Journal Proceedings*, 64(3):128–141.

Kara, I. F. and Ashour, A. F. (2013) "Moment Redistribution in Continuous FRP Reinforced Concrete Beams." *Construction and Building Materials*, V. 49, pp. 939–948.

Khaldoun N. and Al-Shaleh, K. (2004). "Minimum Transverse Reinforcement in 65 MPa Concrete Beams." *ACI Structural Journal*, 101(6): 872-878.

Kupfer, H., Hilsdorf, H. K. and Rüsch, H. (1969). "Behavior of Concrete under Biaxial Stress." *ACI Journal*, 66(8), 656–666.

Lee, J. and Kim, U. (2008). "Effect of Longitudinal Tensile Reinforcement Ratio and Shear Span-Depth Ratio on Minimum Shear Reinforcement in Beams." *ACI Structural Journal*, 105(2): 134-144.

Lin, C. and Chien, Y. (2000). "Effect of Section Ductility on Moment Redistribution of Continuous Concrete Beams." *Journal of the Chinese Institute of Engineers*, 23(2): 131-141.

Lubell, A., Sherwood, T., Bentz, E. and Collins, M.P. (2004). "Safe Shear Design of Large Wide Beams." *ACI Concrete International*, 26(1):67-78

Matta, F., El-Sayed, A., Nanni, A. and Benmokrane, B. (2013). "Size effect on concrete shear strength in beams reinforced with fiber-reinforced polymer bars." *ACI Structural Journal*, 110 (4), 617-628.

Mattock, A. H. (1959). "Redistribution of Design Bending Moments in Reinforced Concrete Continuous Beams." *The Institution of Civil Engineers Proceedings*, V.13: 35-46.

Maurizio, G., Pilakoutas, K. and Waldron, P. (2006). "Shear Resistance of FRP RC Beams: Experimental Study." ASCE, *Journal of Composites for Construction*, 10(6): 464-473.

Ozcebe, G., Ersoy, U. and Tankut, T. (1999). "Evaluation of Minimum Shear Reinforcement Requirements for Higher Strength Concrete." *ACI Structural Journal*, 96(3): 361-369.

Park, R. and Paulay, T. (1975). "Reinforced Concrete Structures." *John Wiley and Sons*, New York, NY.

Razaqpur, G., Shedid, M. and Isgor, B. (2011). "Shear Strength of Fiber- Reinforced Polymer Reinforced Concrete Beams Subject to Unsymmetric Loading." ASCE, *Journal of Composites for Construction*, 15(4):500-512.

Razaqpur, G. A., Isgor, B., Greenaway, S. and Selley, A. (2004). "Concrete Contribution to the Shear Resistance of Fiber Reinforced Polymer Reinforced Concrete Members." ASCE, *Journal of Composites for Construction*, 8(5): 452-460.

Razaqpur, G. A. and Mostofinejad, D. (1999). "Experimental Study of Shear Behaviour of Continuous Beams Reinforced with Carbon Fiber Reinforced Polymer." *ACI Special Publication*, SP-188-16, pp. 169-178.

Rebeiz, K., Fente, J. and Frabizzio, M.A. (2001). "Effect of Variables on Shear Strength of Concrete Beams." ASCE, *Journal of Materials in Civil Engineering*, 13(6): 467-470.

Rodriguez, J. J., Bianchini, A. C., Viest, I. M. and Kesler, C. E. (1959), "Shear Strength of Two-Span Continuous Reinforced Concrete Beams." *ACI Structural Journal,* 55(4): 1089-1130.

Santos, P., Laranja, G., França, P. and Correia, J. R. (2013) "Ductility and Moment Redistribution Capacity of Multi-Span T-Section Concrete Beams Reinforced with GFRP Bars," *Construction and Building Materials*, V. 49, pp. 949–961.

Shioya, T., Iguro, M., Nojiri, Y., Akiyama, H. and Okada, T. (1989). "Shear strength of large reinforced concrete beams, fracture mechanics: Application to concrete." *ACI Special Publication,* SP-118, ACI, Detroit, MI, 259-279.

Sneed, L.H. and Ramirez, J.A. (2010). "Influence of Effective Depth on Shear Strength of Concrete Beams-Experimental Study." *ACI Structural Journal,* 107(5): 554-562.

Tezuka, M., Ochiai, M., Tottori, S. and Sato, R. (1995). "Experimental Study on Moment Redistribution of Continuous Beams Reinforced or Pretensioned with Fibre Reinforced Plastic." *Non-Metallic (FRP) Reinforcement for Concrete Structures: Proceedings of the Second International RILEM Symposium*, London, UK, pp. 287-394.

Tureyen, A. and Forsch, R. (2003). "Concrete Shear Strength: Another Perspective." *ACI Structural Journal,* 100(5):609-615.

Tureyen A. and Forsch, R. (2002). "Shear Tests of FRP-Reinforced Concrete Beams without Stirrups." *ACI Structural Journal,* 99(4): 427-434.

Vecchio, F.J. and Collins, M.P. (1986). "Modified Compression-Field Theory for Reinforced Concrete Beams Subjected to Shear." *ACI Journal, Proc.* 83(2):219-231.

Whitehead, P.A. and Ibell, T. S. (2005). "Novel Shear Reinforcement for Fiber-Reinforced and Prestressed Concrete." *ACI Structural Journal,* 102(2), 286-294.

Wight, J. and MacGregor, J. (2011). "Reinforced Concrete: Mechanics and Design." Eighth Edition, *Pearson Education*, Inc., Upper Saddle River, New Jersey 07458.

Yoon, Y., William, D. and Mitchell, D. (1996). "Minimum Shear Reinforcement in Normal, Medium, and High-Strength Concrete Beams." *ACI Structural Journal*, 93(5): 576-584.

Yost, J. R., Gross, S. P. and Dinehart, D. W. (2001). "Shear Strength of Normal Strength Concrete Beams Reinforced with Deformed GFRP Bars." ASCE, *Journal of Composite for Construction*, 5(4):268–75.

APPENDICES

APPENDIX: A

DESIGN PROVISIONS

A.1. Code Provisions for Steel-RC Sections

In this section, the current design codes in North America for steel-RC structures are reviewed. Because of the well-established moment and shear redistribution in indeterminate structures, both the Canadian code CSA/A23.3-04 (CSA 2004) and the American code ACI 318-11 (ACI 2011) allow moment redistribution up to 20% and provide the same shear design provisions for both simple and indeterminate structures as will be shown below. It should be noted that there are no changes in the latest published versions of these codes (CSA 2014 and ACI 2015).

A.1.1. CSA/A23.3-04 Design Code

A.1.1.1. Flexural design:

According to Clause 8.6.1.1, used concrete compressive strength should not be less than 20 MPa or more than 80 MPa.

The modulus of elasticity of concrete with γ_c between 1500 and 2500 kg/m^3 can be calculated according to Clause 8.6.2.2 as follows:

$$E_c = (3300\sqrt{f_c'} + 6900)(\frac{\gamma_c}{2300})^{1.5}$$

For normal density concrete with compressive strength between 20 and 40 MPa, the modulus of elasticity can be determined according to Clause 8.6.2.3 as follows:

$$E_c = 4500\sqrt{f_c'}$$

In lieu of the formula above, concrete modulus of elasticity can be taken as the secant modulus for a stress of 0.4 f_c', Clause 8.6.2.1).

The modulus of rupture of concrete can be taken according to Clause 8.6.4:

$$f_r = 0.6\lambda\sqrt{f_c'}$$

The negative moments at supports of continuous flexural members calculated by elastic analysis may be reduced by a percentage equals to $(30-50\frac{c}{d})$ %, but not more than 20%, (Clause 9.2.4) and the modified negative moment shall be used to calculate the moments at sections within the span.

According to Clause 10.1.2, the strain in reinforcement and concrete shall be assumed to be directly proportional to the distance from neutral axis. In addition the maximum strain at the extreme concrete compression fibres can be assumed to be 0.0035, (Clause 10.1.3).

The equivalent rectangular concrete stress distribution in compression is defined according to Clause 10.1.7 as follows:

$$\alpha_1 = 0.85 - 0.0015 f_c^{'} \geq 0.67$$
$$\beta_1 = 0.97 - 0.0025 f_c^{'} \geq 0.67$$

A minimum reinforcement should be provided in beams calculated as in Clause 10.5.1.2 as follows:

$$A_{s,\min} = \frac{0.2\sqrt{f_c^{'}}}{f_y} b_t h$$

Where:

$f_c^{'}$: concrete compressive strength;

f_y : reinforcement yielding strength;

b_t : width of tension zone of section;

h : overall section height.

The tension reinforcement can be assumed to reach yield if $\frac{c}{d} \leq \frac{700}{700 + f_y}$, (Clause 10.5.2).

A.1.1.2. Shear design:

The factored shear resistance for a reinforced section can be calculated according to Clause 11.3.3 as follows:

$V_r = V_c + V_s$, and V_r shall not be taken more than $0.25\phi_c f_c' b_w d_v$

Where:

V_c : concrete shear resistance;

V_s : shear force resisted by stirrups;

d_v : effective shear depth taken as the greater of 0.9d or 0.72h

ϕ_c : factored concrete compressive strength = 0.65

According to Clauses 11.3.4 and 11.3.5, V_c and V_s can be calculated as follows:

$$V_c = \phi_c \lambda \beta \sqrt{f_c'} b_w d_v$$

$$V_S = \frac{\phi_S A_v f_y d_v \cot\theta}{S}$$

In lieu of more accurate calculations, and provided that the used yield strength of longitudinal steel does not exceed 400 MPa and concrete compressive strength is less than 60 MPa, θ can be taken as 35°. If the section contains the minimum transverse, the factor β can be taken as 0.18, (Clause 11.3.6.3).

For members subjected to significant axial tension, a more accurate method can be used to determine the factors β and θ according to Clause 11.3.6.4.

$$\beta = \frac{0.4}{(1+1500\varepsilon_x)} \frac{1300}{(1000+S_{ze})}$$

$$\theta = 29 + 7000\varepsilon_x$$

For sections containing the minimum shear reinforcement, the equivalent crack spacing parameter S_{ze} shall be taken as equal to 300 mm.

In lieu of more accurate calculations, the longitudinal strain at mid-depth of the member (ε_x) due to applied load can be calculated as follows:

$$\varepsilon_x = \frac{\frac{M_f}{d_v} + V_f + 0.5N_f}{2(E_s A_s)}$$

Where:

M_f: applied factored bending moment

V_f: factored shear force

N_f: applied factored axial force

d_v: effective shear depth taken as the greater of 0.9d or 0.72h

E_s: modulus of elasticity of reinforcement

A_s: area of longitudinal tension reinforcement

According to Clause 11.2.8.2, a minimum area of shear reinforcement should be provided if the applied shear force exceeds concrete shear resistance or overall section depth is greater than 750 mm. The minimum shear reinforcement is calculated as follows:

$$A_v = 0.06\sqrt{f_c'}\,\frac{b_w S}{f_y}$$

Where:

b_w: beam web width

s: spacing of transverse reinforcement

According to Clauses 11.3.8.1 and 11.3.8.3, the maximum transverse spacing should not exceed 600 mm or $0.7d_v$. If the applied shear force exceeds $0.125\phi_c\lambda f_c^{'}b_w d_v$, the maximum spacing should not exceed 300 mm or $0.35d_v$.

A.1.2. According to ACI 318-11 Code

A.1.2.1. Flexural design:

In indeterminate structures such as continuous beams, it is allowed that the bending moments calculated by elastic theory to be decreased by a percentage not more than the smallest of $1000\,\varepsilon_t$ or 20 %, (Clause 8.4.1). However, moment redistribution is only permitted if equals ε_t to or greater than 0.0075, where ε_t is the net tensile strain in longitudinal reinforcement.

For normal weight concrete, modulus of elasticity for concrete shall be taken as $4700\sqrt{f_c'}$, (Clause 8.5.1).

Concrete modulus of rupture can be calculated as follows: $f_r = 0.62\sqrt{f_c'}$

The maximum compressive strain in concrete is assumed to be 0.003 according to Clause 10.2.3.

Equivalent rectangular concrete compressive stress is defined by uniform stress of $0.85f_c'$ distributed over an equivalent compression zone with depth a = $\beta_1 c$, (Clause 10.2.7.1).

The factor β_1 shall be taken as 0.85 for f_c' between 17 and 28 MPa. β_1 shall be reduced linearly at a rate of 0.05 for each 7 MPa of strength in excess of 28 MPa, but β_1 should not be taken less than 0.65.

Sections are tension controlled if the net tensile strain in extreme tension steel equals to or greater than 0.005, (Clause 10.3.4).

The minimum reinforcement of flexural member can be calculated according to Clause 10.5.1 as follows:

$A_{s,min} = \frac{0.25\sqrt{f_c'}}{f_y} b_w d$, and not less than $1.4 b_w\, d/f_y$, where b_w is beam web width and d is the effective depth.

A.1.2.2. Shear design:

According to Clause 11.1.1, the ultimate shear force resistance of a RC section V_n can be calculated as follows:

$V_n = V_c + V_s$

Where:

V_c : concrete shear resistance;

V_s : shear forces resisted by transverse stirrups.

For members subjected to shear and flexure only, V_c can be calculated according to Clause 11.3.1.1 as follows:

$$V_c = 0.17 \sqrt{f_c'}\, b_w\, d$$

Where:

f_c': concrete compressive strength;

b_w: beam web width;

d: effective depth of section.

For members subjected to axial compression, V_c can be calculated according to Clause 11.3.1.2 as follows:

$$V_c = 0.17\left(1 + \frac{N_u}{14A_g}\right)\sqrt{f_c'}\, b_w\, d$$

Where:

N_u: factored axial normal force acting simultaneously with V_u, positive for compression;

A_g: gross area of concrete section.

Concrete shear resistance can also be calculated by a more detailed calculation according to Clause 11.3.2.1 as follows:

$$V_c = \left(0.16\sqrt{f_c'} + 17\,\rho_w\,\frac{V_u\, d}{M_u}\right)\, b_w\, d$$

However, V_c should not be taken greater than$0.29\sqrt{f_c'}\, b_w\, d$, and the term $V_u\, d/M_u$ should not be taken greater than 1.0.

Where:

ρ_w: ratio of reinforcement area to $b_w\, d$;

V_u: factored applied shear force;

M_u: factored applied bending moment.

According to Clause 11.5.2, the yield strength used in design for shear reinforcement should not be more than 420 MPa.

The maximum spacing of shear reinforcement should not exceed *d*/2 or 600 mm, (Clause 11.5.5.2). If the force resisted by stirrups V_s exceeds$0.33\sqrt{f_c'}\, b_w\, d$, maximum spacing should not be more than *d*/4 or 300 mm, (Clause 11.5.5.3).

If applied factored shear force exceeds $0.5\,\phi V_c$, minimum shear reinforcement has to be provided according to Clause 11.5.6.3 as follows:

$A_{v,min} = 0.062\sqrt{f_c'}\ b_w\ s/f_{yt}$, and should not be taken less than $0.35\ b_w\ s/f_{yt}$.

Where:

b_w: beam web width;

s : shear reinforcement spacing;

f_{yt}: yielding strength of shear reinforcement.

According to Clause 11.5.7.2, shear force resisted by stirrups V_s can be calculated as follows:

$$V_s = \frac{A_v f_{yt} d}{s}\ and\ should\ not\ be\ more\ than\ 0.66\sqrt{f_c'}\ b_w\ d$$

Where:

A_v: the area of shear reinforcement within spacing **s**;

f_{yt}: yielding strength of shear reinforcement;

s : shear reinforcement spacing;

d : effective section depth.

A.2. Code Provisions for FRP-RC Sections

A.2.1. According to CSA/S806-12

The Canadian code for design and construction of building structures with fibre-reinforced polymers CSA/S806-12 (CSA 2012) gives guidelines and recommendations as follows:

The concrete compressive strength used in design should not be less than 30 MPa and should not be more than 80 MPa, (Clause 8.5.1.1).

For normal weigh concrete with concrete compressive strength between 30 MPa and 40 MPa, concrete modulus of elasticity could be taken according to Clause 8.5.2.3 as follows:

$$E_c = 4500\sqrt{f_c'}$$

Concrete modulus of rupture could be taken as stated in Clause 8.5.4.

$$f_r = 0.6\,\lambda\sqrt{f_c'}$$

Where λ equals 1 for normal weight concrete

FRP bars properties should be determined by testing according to Clause 7.1.1. Pre-shaped FRP bars such as ties and hoops should be tested for strength development, (Clause 7.1.5.3).

A.2.1.1. Design for flexure:

According to CSA/S806-12, Clause 8.2.1, the failure of flexural element has to be due to concrete crushing rather than rupture of FRP bars. Failure by rupture of the FRP bars is only permitted if the factored resistance is greater than 1.6 times the effect of the factored loads.

The cracking moment M_{cr} should be calculated according to Clause 8.3.2.6 as follows:

$$M_{cr} = f_r \frac{I_g}{y_t}$$

Where:

f_r: Modulus of rupture of concrete,

I_g: Moment of inertia of gross concrete section, neglecting the reinforcement,

y_t: Distance from extreme fibres in tension to the centroidal axis of cross section.

The strain in concrete and reinforcement shall be assumed directly proportional in case of perfect bond, (Clause 8.4.1.1). The ultimate strain in concrete extreme compression fibres should be

taken equal to 0.0035 according to Clause 8.4.1.2. Concrete tensile strength shall be neglected for the ultimate flexure strength calculation of the section, (Clause 8.4.1.3).

Concrete strain at extreme fibres in compression shall be assumed to reach 0.0035 provided that the ratio $^{c}/_{d}$ satisfies Clause 8.4.1.4 as follows:

$$^{c}/_{d} \geq \frac{7}{7 + 2000\ \varepsilon_{Fu}}$$

Where:

c: Distance from extreme compression fibres to neutral axis,

d: Distance from extreme compression fibres to the centroid of longitudinal tension force,

ε_{Fu}: Ultimate strain for FRP reinforcement.

The concrete stress distribution is defined according to Clause 8.4.1.5. A uniform equivalent compressive strength of $\alpha_1\ \varphi_c\ f_c'$ is assumed to be distributed over distance $a = \beta_1 c$.

Where:

$$\alpha_1 = 0.85 - 0.0015\ f_c' \qquad \geq 0.67$$

$$\beta_1 = 0.97 - 0.0025\ f_c' \qquad \geq 0.67$$

In the calculation of ultimate flexural resistance the compressive strength of FRP bars shall be neglected according to Clause 8.4.1.8.

The minimum reinforcement provided in the section should satisfy Clause 8.4.2.1.

$$M_r\ > 1.5\ M_r$$

A.2.1.2. Design for shear:

The maximum acting shearing force used for design could be taken at a distance *d* from the face of support, (Clause 8.4.4.2).

The ultimate shear resistance for section reinforced with either FRP or steel stirrups should be calculated according to Clause 8.4.4.4 as follows:

$$V_r = V_c + V_{sF} \leq 0.22\phi_c f_c' b_w d_v + 0.5V_p + \left[(M_{dc} V_f) / \mathrm{M}_f \right], \text{ for FRP stirrups}$$

$$V_r = V_c + V_{ss} \leq 0.22\phi_c f_c' b_w d_v + 0.5V_p + \left[(M_{dc} V_f) / \mathrm{M}_f \right], \text{ for steel stirrups}$$

Where:

V_r: Nominal shear resistance,

V_c: Concrete shear resistance,

V_{sF}: FRP stirrups shear resistance,

V_{ss}: Steel stirrups shear resistance.

For sections having a depth not exceeding 300 mm and with no axial load acting on them, shear resistance provided by concrete V_c should be calculated, Clause 8.4.4.5, as follows:

$$V_c = 0.05\lambda\phi_c k_m k_r (f_c')^{\frac{1}{3}} b_w d_v$$

where $k_m = \sqrt{\frac{V_f d}{M_f}} \leq 1.0$ and $k_r = 1 + (E_f \rho_{Fw})^{\frac{1}{3}}$

Provided that V_c satisfies:

$$0.11\,\lambda\,\phi_c\,\sqrt{f_c'}\,b_w\,d_v \leq V_c \leq 0.22\,\lambda\,\phi_c\,\sqrt{f_c'}\,b_w\,d_v$$

Where:

ρ_{Fw}: Longitudinal reinforcement ratio

E_F: Modulus of elasticity of longitudinal FRP reinforcement

M_F: Ultimate bending moment at section under consideration

V_f: Corresponding ultimate shear force at section under consideration

For members with effective depth greater than 300 mm and with transverse reinforcement less than the minimum, the value of V_c should be multiplied by the size effect factor k_s which can be calculated, according to Clause 8.4.4.7, as

$$k_s = \frac{750}{450 + d} \leq 1.0$$

The shear resistance of FRP and steel stirrups V_{sF} and V_{ss}, respectively, should be calculated according to Clause 8.4.4.9 as follows:

$$V_{sF} = \frac{0.4\phi_F A_{Fv} f_{Fu} d_v}{s} \cot\theta \text{ and } V_{sF} = \frac{\phi_s A_v f_y d_v}{s} \cot\theta$$

Where:

A_v: Area of shear reinforcement,

f_{Fu}: Ultimate strength of FRP shear reinforcement. It should not be taken greater than 0.005 E_f.

f_y: Yield strength of reinforcement,

s: Spacing of shear reinforcement.

The angle θ of the compressive stress shall be calculated as follows:

$\theta = 30 + 7000\ \varepsilon_\ell$

where the longitudinal strain (ε_ℓ) at the mid-depth of the section shall be calculated as,

$$\varepsilon_l = \frac{\frac{M_f}{d_v} + (V_f - V_p) + 0.5N_f - A_p f_{po}}{2(E_F A_F + E_p A_p)}$$

According to Clauses 8.4.5.1 and 8.4.5.2, minimum shear reinforcement should be provided whenever $V_f > 0.5\ V_c$. The minimum are of shear reinforcement should be calculated as follows

$$A_{v,min} = 0.07\sqrt{f_c'}\frac{b_w s}{0.4\ f_{Fu}}$$

where f_{Fu} shall not be taken greater than 1200 MPa or $0.005E_f$

The maximum spacing between the transverse reinforcement shall not exceed 0.6 d_v or 400 mm (Clause 8.4.6.1).

A.2.1.3. Service conditions:

According to Clause 8.3.1.1, if the maximum strain in FRP tension reinforcement exceeds 0.0015 under service loads, cross-sections of maximum sagging and hogging moment should be proportioned as follows:

$$z = k_b \frac{E_s}{E_f} f_f \sqrt[3]{d_c A} \leq \begin{cases} 45\,000 & N/mm \quad for\ interior\ exposure \\ 38\,000 & N/mm \quad for\ exterior\ exposure \end{cases}$$

Where:

z: quantity limiting distribution of flexural FRP reinforcement bars;

k_b: coefficient dependent on the reinforcing bar bond characteristics;

E_s: modulus of elasticity of reinforcement;

E_f: modulus of elasticity of longitudinal FRP reinforcement;

f_f: stress in FRP reinforcement under specified loads;

d_c: distance from extreme tension fibre to the centre of the longitudinal bar;

A : effective tension area of concrete surrounding the flexural tension reinforcement and extending from the extreme tension fibre to the centroid of the flexural tension reinforcement and an equal distance past the centroid, divided by the number of bars.

In lieu of computing the stress in the steel reinforcement, f_f, it may be taken as 25% of the design ultimate stress of the GFRP bars. The value k_b may be taken as 1.2 for deformed rods and taken as 0.8 for sand-coated FRP bars. In calculating d_c and A, the clear cover should not be taken more than 50 mm.

A.2.1.4. Development length of bars in tension:

According to Clause 9.3.2, bars subjected to tension have to be embedded in concrete with development length, l_d, calculated as follows:

$$l_d = 1.15 \frac{k_1 k_2 k_3 k_4 k_5}{d_{cs}} \frac{f_f}{\sqrt{f_c'}} A_b$$

The factor d_{cs} should not be taken greater than 2.5 d_b and $\sqrt{f_c'}$ shall not be greater than 5.0 MPa. Provided that the clear cover and clear spacing of bars being developed are at least 1.5 d_b and 1.8 d_b, l_d can be computed as follows:

$$l_d = 0.5 k_1 k_2 k_3 k_4 k_5 \frac{f_f}{\sqrt{f_c'}} d_b$$

Where:

l_d: the development length of bars in tension;

f_f: design stress in FRP tension reinforcement at ultimate limit state;

d_{cs}: the smaller of (a) the distance from the closest concrete surface to the centre of the bar being developed; or (b) two-thirds of the centre-to-centre spacing of the bars being developed;

A_b: area of an individual bar;

d_b: nominal diameter of a circular bar.

The factors k_1 , k_2 , k_3 , k_4 and k_5 can be taken as follows:

k_1 = 1.3 for horizontal reinforcement placed so that more than 300 mm of fresh concrete is cast in the member below development length

= 1.0 for other cases

k_2 = 1.3 for structural low-density concrete

= 1.2 for structural semi-low-density concrete

= 1.0 for normal density concrete

k_3 = 0.8 for $A_b \leq 300$ mm^2

= 1.0 for $A_b > 300$ mm^2

k_4 = 1.0 for CFRP and GFRP

= 1.25 for AFRP

k_5 = 1.0 for surface-roughened or sand-coated surfaces

= 1.05 for spiral pattern surfaces

= 1.0 for braided surfaces

= 1.05 for ribbed surfaces

= 1.80 for indented surfaces

A.2.2. According to CSA/S6-06 (CSA 2009)

A.2.2.1. Design for deformability:

According to Clause 16.8.2.1 the overall performance factor J for FRP-RC beams or girders, should be at least 4.0 for rectangular sections and 6.0 for T-sections. The performance factor J can be calculated as follows:

$$J = \frac{M_{ult}\,\Psi_{ult}}{M_c\,\Psi_c}$$

Where:

M_{ult}: ultimate moment capacity of the section;

Ψ_{ult}: curvature at M_{ult}

M_c : moment corresponding to a maximum compressive concrete strain of 0.001 in the section;

Ψ_c : curvature at M_c.

A.2.2.2. Minimum flexural resistance:

The factored resistance M_r should be at least 50% greater than cracking moment M_{cr}. If the ultimate limit state design is governed by FRP rupture, M_r should be greater than 1.5 the factored applied moment M_f.

The maximum stress in GFRP bars at service load should not exceed 0.25 f_{FRPu}, where f_{FRPu} is the ultimate tensile strength of the bars.

A.2.2.3. Design for shear:

According to Clause 16.8.7, the nominal shear resistance should be calculated as follows:

$$V_r = V_c + V_{st} + V_{FRP}$$

Where:

V_r : ultimate shear resistance;

V_c : shear force resisted by concrete;

V_{st} : shear resistance provided by shear reinforcement V_s or V_{FRP};

V_s : shear resistance provided by steel stirrups;

V_{FRP}: shear resistance provided by FRP stirrups.

Shear force resisted by concrete V_c can be calculated as follows:

$$V_c = 2.5\,\beta\,\phi_c\,f_{cr}\,b_v\,d_{long}$$

Where:

β : the inclination angle of transverse reinforcement;

ϕ_c: resistance factor of concrete;

f_{cr}: cracking strength of concrete;

b_v: effective depth of beam web;

d_{long}: effective shear depth for longitudinal reinforcement;

E_{long}: modulus of elasticity of longitudinal reinforcement;

E_s : modulus of elasticity of steel.

$$\varepsilon_x = \frac{\frac{M_f}{d_{long}} + V_f + 0.5\,N_f}{2\,(E_s\,A_s + E_{FRP}\,A_{FRP})} \leq 0.003$$

Where:

ε_x: longitudinal strain at section mid height;

M_f: factored applied bending moment;

V_f: factored applied shear force;

N_f: factored applied normal force;

E_s: modulus of elasticity of steel;

A_s: cross-sectional area of steel or FRP;

E_{FRP}: modulus of elasticity of FRP bars;

A_{FRP}: cross-sectional area of FRP bars;

The factored shear resistance provided by FRP stirrups V_{FRP} can be calculated as follows:

$$V_{FRP} = \frac{\phi_{FRP}\, A_v\, \sigma_v\, d_{long} \cot\theta}{s}$$

Where $\sigma_v$is the smaller of $\begin{cases} \sigma_v = \frac{(0.05\, r/d_s + 0.3\,) f_{FRPbend}}{1.5} \\ \sigma_v = E_{vFRP}\ \varepsilon_v \end{cases}$

$$\varepsilon_v = 0.0001\,(\, f_c'\, \frac{\rho_s\, E_{FRP}}{\rho_{vFRP}\, E_{vFRPs}})^{0.5} \ \leq 0.0025$$

$$A_{v\,min} = 0.06\,\sqrt{f_c'}\,\frac{b_w\, s}{\sigma_v}$$

Where:

A_v: area of transverse shear reinforcement;

s : spacing of shear reinforcement;

r : radius of curvature of the bend or FRP stirrup;

d_s: diameter of FRP stirrup;

$f_{FRPbend}$: specified tensile strength of the straight portion of an FRP bent stirrup;

E_{vFRP}: modulus of elasticity of FRP stirrup;

ε_v: strain in FRP stirrup;

ρ_s : longitudinal FRP reinforcement ratio;

ρ_{vFRP}: FRP transverse reinforcement ratio;

$A_{v\,min}$: minimum required shear reinforcement;

b_w : beam web width.

A.2.3. According to ACI 440.1R-06

A.2.3.1. Design for flexure

The flexural capacity of FRP-reinforced member is dependent on the failure mode whether it is concrete-crushing failure or FRP-rupture failure. The mode of failure can be determined by comparing the FRP reinforcement ratio to the balanced reinforcement ratio ρ_{fb} as follows (Clause 8.2.1):

$$\rho_{fb} = 0.85\,\beta_1\,\frac{f_c'}{f_{fu}}\,\frac{E_f\,\varepsilon_{cu}}{E_f\,\varepsilon_{cu} + \varepsilon_{fu}}$$

Where:

ρ_{fb}: FRP reinforcement ratio producing balanced strain conditions;

f_{fu}: design tensile strength of FRP, considering reductions for service environment;

E_f : modulus of elasticity of FRP;

ε_{cu}: ultimate strain in concrete;

ε_{fu}: design rupture strain of FRP reinforcement.

The nominal flexural strength of FRP-reinforced section when the failure is initiated by concrete crushing can be calculated as follows (Clause 8.2.2):

$$M_n = A_f\,f_f\,(d - \frac{a}{2})$$

$$a = \frac{A_f\,f_f}{0.85\,f_c' b}$$

$$f_f = E_f\,\varepsilon_{cu}\frac{\beta_1 d - a}{a} \quad or \quad f_f = \left(\sqrt{\frac{(E_f\,\varepsilon_{cu})^2}{4} + \frac{0.85\,\beta_1\,f_c'}{\rho_f}E_f\,\varepsilon_{cu}} - 0.5\,E_f\,\varepsilon_{cu}\right) \leq f_{fu}$$

Where:

M_n: nominal moment capacity;

A_f: area of FRP reinforcement;

f_f: stress in FRP reinforcement in tension;

d: distance from extreme compression fibre to centroid of tension reinforcement;

a: depth of equivalent rectangular stress block.

In case of tension failure of FRP bars the equivalent concrete stress block used at ultimate is no more valid. A simple and conservative calculation for nominal flexural strength in this case can be as follows:

$$M_n = A_f f_{fu} \left(d - \frac{\beta_1 c_b}{2} \right)$$

$$c_b = \left(\frac{\varepsilon_{cu}}{\varepsilon_{cu} + \varepsilon_{fu}} \right) d$$

According to Clause 8.2.3, only if the failure of the member is controlled by FRP rupture, a minimum reinforcement should be provided to prevent failure upon cracking can be calculated as follows:

$$A_{f,min} = \frac{4.9\sqrt{f_c'}}{f_{fu}} b_w d \geq \frac{330}{f_{fu}} b_w d$$

A.2.3.2. Design for shear

According to Clause 9.2, the nominal shear capacity of RC cross-section can be calculated as follows:

$$V_r = V_c + V_F$$

V_r: ultimate shear strength;

V_c: nominal shear strength provided by concrete;

V_F: shear resistance provided by FRP stirrups.

The concrete shear capacity V_c of FRP-reinforced member can be calculated as follows:

$V_c = \frac{2}{5}\sqrt{f_c'}bc$

where $c = kd$ and $k = \sqrt{2\rho_{frp}n_{frp} + \left(\rho_{frp}n_{frp}\right)^2} - \rho_{frp}n_{frp}$

n_{frp}: ratio of modulus of elasticity of FRP bars to modulus of elasticity of concrete;

ρ_{frp}: FRP reinforcement ratio.

The shear resistance provided by FRP stirrups V_f can be calculated as follows:

$$V_f = \frac{A_v f_{fv} d}{s}$$

The stress level in the FRP shear reinforcement should be limited to control shear cracks. The stress level at ultimate used in design should be calculated as follows:

$$f_{fv} = 0.004\, E_{f,v} \leq f_{fb}$$

The required spacing and area of shear reinforcement can be computed as follows:

$$\frac{A_{fv}}{s} = \frac{V_u - \phi V_c}{\phi f_{fv}\, d}$$

According to Clause 9.2.2 a minimum amount of shear reinforcement should be provided when V_u exceeds $\phi V_c/2$. The minimum area of shear reinforcement can be computed as follows:

$$A_{v,min} = 0.35\frac{bs}{f_{fv}}$$

Where:

$A_{v,min}$: minimum amount of FRP shear reinforcement within spacing s;

f_{fv}: tensile strength of FRP for shear design, taken as smallest of design tensile strengthf_{fu}v strength of bent portion of FRP stirrups f_{fb}, or stress corresponding to $0.004E_f$.

The effective stress level in FRP stirrups should be governed by the allowable stress in the stirrup at the location of the bend which is computed as follows:

$$f_{fb} = \left(0.3 + 0.05\frac{r_b}{d_b}\right) f_{fu}$$

Where:

f_{fb}: strength of bent portion of FRP bar;

f_{fu}: design tensile strength of FRP, considering reductions for service environment;

r_b: internal radius of bend in FRP reinforcement;

d_b: diameter of reinforcing bar.

APPENDIX: B

DESIGN OF TEST BEAMS

B.1. Design Criteria for Beams without Transverse Reinforcement

The series of beams, without stirrups, were designed to fail in shear. The main objective was to investigate the concrete contribution to the shear strength in GFRP-RC continuous beams. For comparison purposes, one beam was reinforced with steel bars. The variables included in this series were the longitudinal reinforcement ratio at the critical sections, the concrete strength and the depth of the section (Size Effect). Loading configuration and the internal straining actions induced in beams, having different depths, are shown in Figures B.1 to B.3.

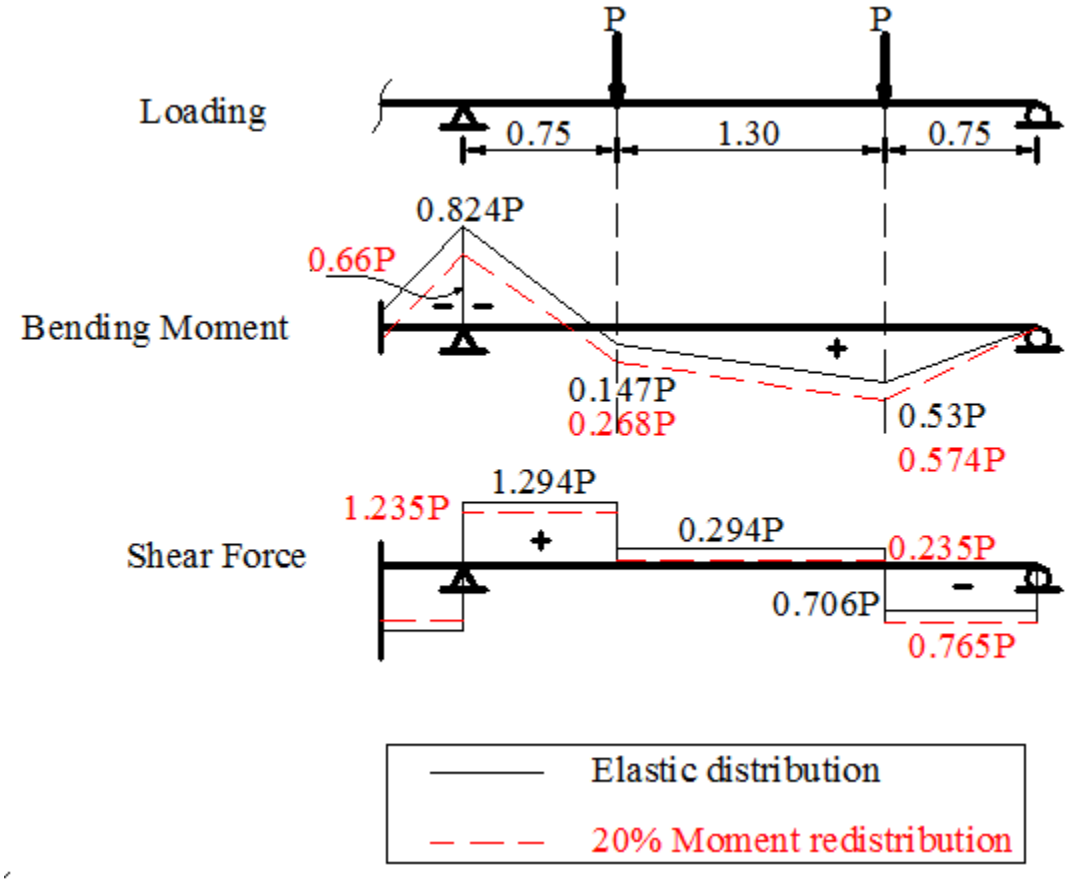

Figure B.1: Loading and internal straining actions for beams having depth of 250 mm

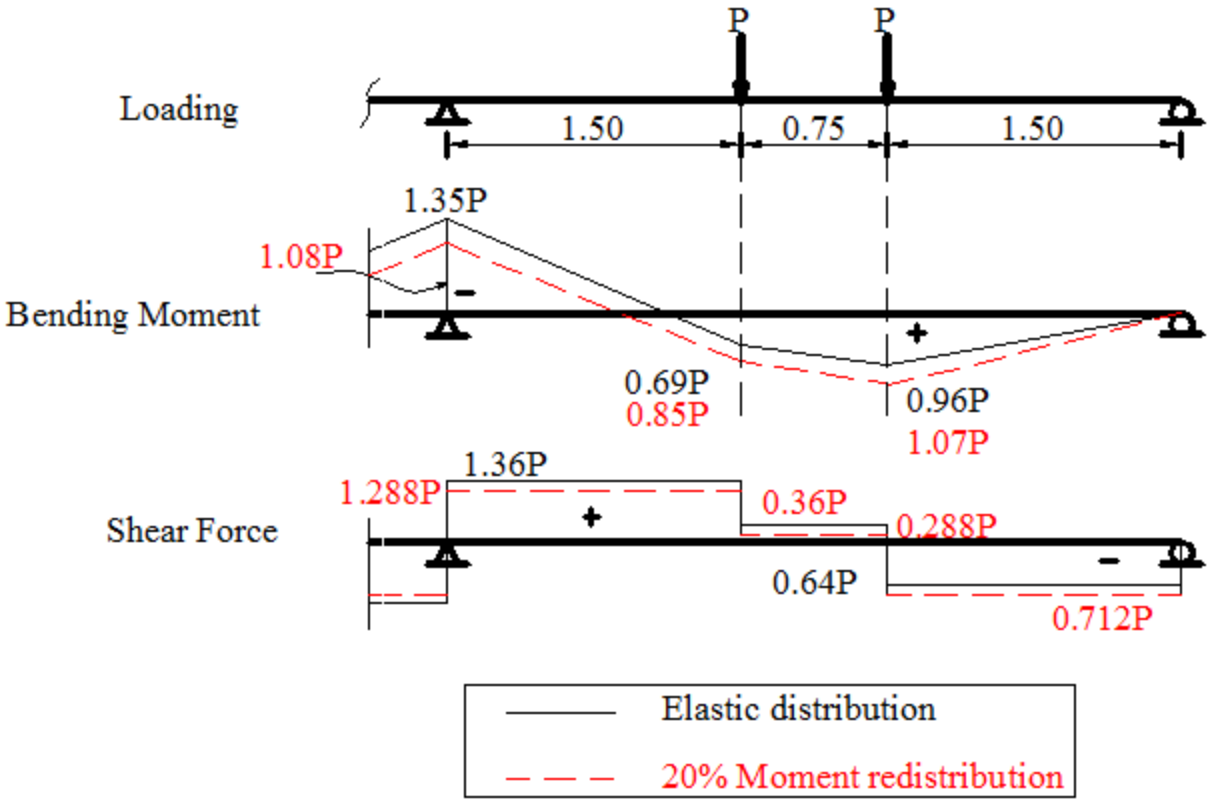

Figure B.2: Loading and internal straining actions for beams having depth of 500 mm

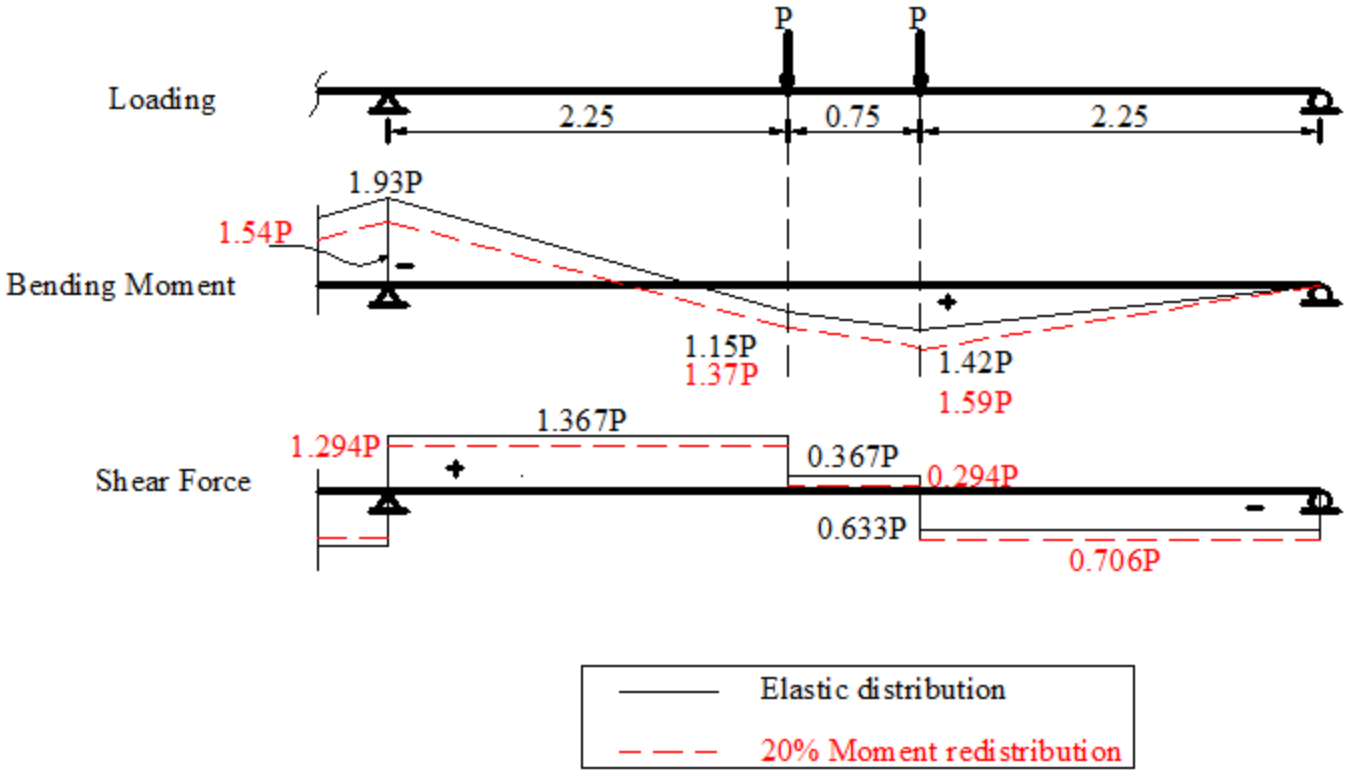

Figure B.3: Loading and internal straining actions for beams having depth of 750 mm

- b = 200 mm
- Target concrete strengths were $f_c^{'}$ = 35 MPa and $f_c^{'}$ = 70 MPa. The concrete strain before crushing was taken as 0.0035.
- Steel bars properties:
    - Size No.15M, nominal area = 200 mm^2, Yield strength f_y = 430 MPa, E = 200 GPa, and ε_y = 0.235 %
- GFRP bars properties:
    - Size No.16, nominal diameter = 15.9 mm, nominal area = 197.9 mm^2, tensile strength f_{frpu} = 1440 MPa, E_{frp} = 67.0 GPa, and ε_{frpu} = 2.1 %
    - Size No.19, nominal diameter = 19.5 mm, nominal area = 285 mm^2, tensile strength f_{frpu} = 1480 MPa, E_{frp} = 65.3 GPa, and ε_{frpu} = 2.3 %

All test beams were designed according the CSA standards (CSA/A23.3-04 for steel-RC beams and CSA/S806-12 for GFRP-RC beams). In designing the test beams, all material safety factors were taken equal to unity. Regarding the design for shear, it was found out that the critical shear section is located at a distance d_v form the face of the interior support; therefore, only this section is designed. Moreover, assuming 20% moment redistribution, the magnitude of the hogging and sagging moments were very similar, so the longitudinal reinforcement ratio at both sections are the same which, in turn, resulted in the same flexural capacity.

In this appendix, the design of selected beams from each series is presented.

B.1.1. Design of Beam GN-0.8-0.0-*d* (Series I)

Design for shear

The shear resistance of sections without shear reinforcement is calculated according to Clause 8.4.4.5.

$V_c = 0.05\lambda\phi_c k_m k_r (f_c')^{\frac{1}{3}} b_w d_v$ where $k_m = \sqrt{\frac{V_f d}{M_f}} \leq 1.0$ and $k_r = 1 + (E_f \rho_{Fw})^{\frac{1}{3}}$

Provided that $0.11\lambda \phi_c \sqrt{f_c'}\, b_w\, d_v \leq V_c \leq 0.22\, \lambda\, \phi_c \sqrt{f_c'}\, b_w\, d_v$

$0.11 \sqrt{f_c'}\, b_w\, d_v$ = $0.11\sqrt{35}$*200*225 = 29.28 kN

$0.22 \sqrt{f_c'}\, b_w\, d_v$ = $0.22\sqrt{35}$*200*225 = 58.56 kN

Critical section for shear is at distance d_v from the face of the middle support at which the values of shear and bending moment are 1.235*P* kN and 0.35*P* kN.m, respectively.

Using 2 No. 16 GFRP bars as longitudinal reinforcement, the diameter including the sand coating = 19 mm.

d = 300 – (40 + 19/2) = 250 mm.

ρ_f = 2 x 197.9 / (200 x 250) = 0.0079

k_r = 1+ (67000 x 0.0079)$^{1/3}$ = 9.07 ,

$k_m = \sqrt{1.235P \text{ x } 0.25/0.29\ P}$ = 1.03 ⟶ k_m = 1.0

V_c = 0.05 x 1x1x1.0x9.07x (35)$^{1/3}$ x200x225 = 66,754.3 N

V_c = 58.56 kN., governs the shear strength.

The value of load, *P*, corresponding to the calculated shear strength, is 47.42 kN.

Design for flexure

α_1 = 0.85 – 0.0015 x 35 = 0.8

β_1 = 0.97 – 0.0025 x 35 = 0.883

$$f_{frp} = 0.5\, E_{frp}\, \varepsilon_{cu} \left[\left(1 + \frac{4\, \alpha_1\, \beta_1\, f_c'}{\rho_{frp}\, E_{frp}\, \varepsilon_{cu}} \right)^{1/2} - 1 \right]$$

$$= 0.5 * 67000 * 0.0035 \left[\left(1 + \frac{4 * 0.8 * 0.883 * 35}{0.0079 * 67000 * 0.0035} \right)^{0.5} - 1 \right] = 747.4\, MPa$$

a = ($A_{sfrp}\, f_{frp}$) / ($\alpha_1\, f_c'\, b$) = 395.8* 747.4/ (0.8*35*200) = 52.83 mm

c = a / β_1 = 52.83/0.883 = 59.83 mm

Check concrete strain:

Concrete stain at extreme fibres in compression shall be assumed to reach 0.0035 provided that the ratio c/d satisfies Clause 8.4.1.4 as follows:

$$c/d \geq \frac{7}{7 + 2000\, \epsilon_{Fu}}$$

$$c/d = \frac{59.83}{250} = 0.24 > \frac{7}{7 + 2000 * 0.021} = 0.143$$

M_{ult} = T (d- a/2) = 295820.9* (250 -52.83/2) = **66.14** kN.m. The corresponding load, P, is 100.2 kN which is higher than the shear failure load (P = 47.42 kN).

Check if minimum reinforcement is provided:

The minimum reinforcement provided in the section should satisfy Clause 8.4.2.1.

$$M_r > 1.5\, M_{cr}$$

The cracking moment, M_{cr}, should be calculate according to Clause 8.3.2.6 as follows:

$$M_{cr} = f_r \frac{I_g}{y_t}$$

Concrete modulus of rupture could be taken as stated in Clause 8.5.4.

$$f_r = 0.6\, \lambda \sqrt{f_c'}$$

λ equals 1 for normal weight concrete.

$$M_{cr} = 0.6 * \sqrt{35}\ \frac{200 * 300^3}{12 * \frac{300}{2}} = 10.65\ kN.m$$

M_r = 66.14 kN.m > 1.5*10.65 = 15.97 kN.m (minimum reinforcement satisfied)

Development length

$\sum M = 0$ at distance x from middle support:

$1.235P*x - 0.66P = 0, \rightarrow x = 0.534\ m$

Point of zero moment = 534 mm from middle support

l_d = 534 + 40 x 15.9 = 1170 mm or

$l_d = 1.15\ \frac{k_1\ k_2\ k_3\ k_4\ k_5}{d_{cs}}\ \frac{f_f}{\sqrt{f_c'}} A_b$ (Clause 9.3.2)

For the longitudinal bars in that section, f_{frpu} = 747.4 MPa and $\sqrt{f_c'}$ should not be greater than 5 MPa.

$l_d = 1.15\ \frac{1*1*0.8*1*1}{40} * \frac{747.4}{\sqrt{35}} * 198 = 680.7\ mm$

Negative reinforcement cut-off length = 1170 mm (measured form interior support), take = **1500** mm to avoid bond slippage failure.

B.1.2. Design of Specimen GH-1.6-0.0-*d* (Series I)

Design for shear

The shear resistance of sections without shear reinforcement, according to Clause 8.4.4.5, is calculated as

$V_c = 0.05\lambda\phi_c k_m k_r (f_c')^{\frac{1}{3}} b_w d_v$ where $k_m = \sqrt{\frac{V_f d}{M_f}} \le 1.0$ and $k_r = 1 + (\mathrm{E}_f\ \rho_{Fw})^{\frac{1}{3}}$

Provided that $0.11\lambda\ \phi_c\ \sqrt{f_c'}\ b_w\ d_v\ \le\ V_c\ \le 0.22\ \lambda\ \phi_c\ \sqrt{f_c'}\ b_w\ d_v$

$0.11\sqrt{f_c'}\, b_w\ d_v$ = 0.11$\sqrt{60}$*200*225 = 38.34 kN

$0.22\sqrt{f_c'}\, b_w\ d_v$ = 0.22$\sqrt{60}$*200*225 = 76.68 kN

Critical section for shear is at distance d_v from the face of the middle support at which the values of shear and bending moment are 1.235*P* kN and 0.35*P* kN.m, respectively.

Using 4 No. 16 GFRP bars as longitudinal reinforcement, the diameter including the sand coating = 19 mm.

d = 300 – (40 + 19/2) = 250 mm.

ρ_f = 4 x 198 / (200 x 250) = 0.0158

k_r = 1+ (67000 x 0.0158)$^{1/3}$ = 11.2 ,

$k_m = \sqrt{1.235P \text{ x } 0.25/0.29\ P}$ = 1.03 ⟶ k_m = 1.0

V_c = 0.05 x 1.0x1.0x1.0x11.2x (60)$^{1/3}$ x200x225 = 98,653.3 N

V_c = 76.68 kN., governs the shear strength.

The value of load, *P*, corresponding to the calculated shear strength, is 62.1 kN.

Design for flexure

α_1 = 0.85 – 0.0015 x 70 = 0.745

β_1 = 0.97 – 0.0025 x 70 = 0.795

$$f_{frp} = 0.5\, E_{frp}\, \varepsilon_{cu} \left[\left(1 + \frac{4\, \alpha_1\, \beta_1\, f_c'}{\rho_{frp}\, E_{frp}\, \varepsilon_{cu}}\right)^{1/2} - 1\right]$$

$$= 0.5 * 67000 * 0.0035 \left[\left(1 + \frac{4 * 0.745\ * 0.795 * 70}{0.0158 * 67000 * 0.0035}\right)^{0.5} - 1\right] = 675.9\ MPa$$

a = ($A_{sfrp}\, f_{frp}$) / ($\alpha_1\, f_c'\, b$) = 792* 675.9/ (0.745*70*200) = 51.32 mm

c = a / β_1 = 51.32/0.795 = 64.56 mm

Check concrete strain:

Concrete stain at extreme fibres in compression shall be assumed to reach 0.0035 provided that the ratio $^{c}/_{d}$ satisfies Clause 8.4.1.4 as follows:

$$^{c}/_{d} \geq \frac{7}{7 + 2000\ \epsilon_{Fu}}$$

$$^{c}/_{d} = \frac{64.56}{250} = 0.258\ > \frac{7}{7 + 2000 * 0.021} = 0.143$$

M_{ult} = T (d- a/2) = 535307.5* (250 -51.32/2) = **120.1** kN.m.

The corresponding load, P, is 182 kN which is higher than the shear failure load (P= 62.1 kN).

Check if minimum reinforcement is provided:

The minimum reinforcement provided in the section should satisfy Clause 8.4.2.1.

$$M_r\ > 1.5\ M_{cr}$$

The cracking moment, M_{cr}, should be calculate according to Clause 8.3.2.6 as follows:

$$M_{cr} = f_r\ \frac{I_g}{y_t}$$

Concrete modulus of rupture could be taken as stated in Clause 8.5.4.

$$f_r = 0.6\ \lambda\ \sqrt{f_c'}$$

λ equals 1 for normal weight concrete.

$$M_{cr} = 0.6 * \sqrt{70}\ \frac{200 * 300^3}{12 * \frac{300}{2}} = 15.06\ kN.m$$

Mr = 120.1 kN.m > 1.5*15.06 = 22.59 kN.m (minimum reinforcement satisfied)

Development length

$\sum M$ = 0 at distance x from middle support:

1.235P*x – 0.66P = 0, $\rightarrow x = 0.534\ m$

Point of zero moment = 534 mm from middle support

l_d = 534 + 40 x 15.9 = 1170 mm or

$l_d = 1.15 \frac{k_1 k_2 k_3 k_4 k_5}{d_{cs}} \frac{f_f}{\sqrt{f_c'}} A_b$ (Clause 9.3.2)

For the longitudinal bars in that section, f_{frpu} = 675.9 MPa and $\sqrt{f_c'}$ should not be greater than 5 MPa.

$l_d = 1.15 \frac{1*1*0.8*1*1}{40} * \frac{675.9}{\sqrt{70}} * 198 = 615.6\, mm$

Negative reinforcement cut-off length = 1170 mm (measured form interior support), take = **1500** mm to avoid bond slippage failure.

B.1.3. Design of beam GN-0.8-0.0-2*d* (Series II)

Design for shear

The shear resistance of sections without shear reinforcement having depth greater than 300 mm is calculated according to Clauses 8.4.4.5 and 8.4.4.7.

$V_c = 0.05\lambda\phi_c k_s k_m k_r (f_c')^{\frac{1}{3}} b_w d_v$ where $k_m = \sqrt{\frac{V_f d}{M_f}} \leq 1.0$, $k_r = 1 + (\mathrm{E}_f \rho_{Fw})^{\frac{1}{3}}$ and $k_s = \frac{750}{450 + d} \leq 1.0$

Provided that $0.11\lambda\, \phi_c \sqrt{f_c'}\, b_w\, d_v \leq V_c \leq 0.22\, \lambda\, \phi_c \sqrt{f_c'}\, b_w\, d_v$

$0.11 \sqrt{f_c'}\, b_w\, d_v$ = 0.11$\sqrt{35}$*200*450 = 58.6 kN

$0.22 \sqrt{f_c'}\, b_w\, d_v$ = 0.22$\sqrt{35}$*200*450 = 117.2 kN

Critical section for shear is at distance d_v from the face of the middle support at which the values of shear and bending moment are 1.288*P* kN and 0.4038*P* kN.m, respectively.

Using 4 No. 16 GFRP bars as longitudinal reinforcement, the diameter including the sand coating = 19 mm.

d = 550 – (40 + 19/2) = 500 mm.

ρ_f = 4 x 198 / (200 x 500) = 0.0079

k_r = 1+ (67000 x 0.0079)$^{1/3}$ = 9.07 ,

$k_m = \sqrt{1.288P \text{ x } 0.5/0.4038\ P}$ = 1.22 ⟶ k_m = 1.0

k_s = 750/(450+500) = 0.789

V_c = 0.05 x 1 x 1 x 0.789 x 1.0 x 9.1 x (35)$^{1/3}$ x 200 x 450 = 105700N

V_c = 105.7 kN., governs the shear strength.

The value of load, *P*, corresponding to the calculated shear strength, is 82.06 kN.

Design for flexure

α_1 = 0.85 – 0.0015 x 35 = 0.8

β_1 = 0.97 – 0.0025 x 35 = 0.883

$$f_{frp} = 0.5\ E_{frp}\ \varepsilon_{cu} \left[\left(1 + \frac{4\ \alpha_1\ \beta_1\ f_c'}{\rho_{frp}\ E_{frp}\ \varepsilon_{cu}} \right)^{1/2} - 1 \right]$$

$$= 0.5 * 67000 * 0.0035 \left[\left(1 + \frac{4 * 0.8\ * 0.883 * 35}{0.0079 * 67000 * 0.0035} \right)^{0.5} - 1 \right] = 747.4\ MPa$$

a = ($A_{sfrp}\ f_{frp}$) / ($\alpha_1\ f_c$' b) = 792* 747.4/ (0.8*35*200) = 105.7 mm

c = a / β_1 = 105.7/0.883 = 119.71 mm

Check concrete strain:

Concrete stain at extreme fibres in compression shall be assumed to reach 0.0035 provided that the ratio c/d satisfies Clause 8.4.1.4 as follows:

$$c/d \geq \frac{7}{7 + 2000\ \epsilon_{Fu}}$$

$$c/d = \frac{119.7}{500} = 0.24\ > \frac{7}{7 + 2000 * 0.021} = 0.143$$

M_{ult} = T (*d*- a/2) = 591940.8* (500 -105.7/2) = **264.68** kN.m.

The corresponding load, *P*, is 245 kN which is higher than the shear failure load (*P*= 82.1 kN).

Check if minimum reinforcement is provided:

The minimum reinforcement provided in the section should satisfy Clause 8.4.2.1.

$$M_r > 1.5\, M_{cr}$$

The cracking moment, M_{cr}, should be calculate according to Clause 8.3.2.6 as follows:

$$M_{cr} = f_r \frac{I_g}{y_t}$$

Concrete modulus of rupture could be taken as stated in Clause 8.5.4.

$$f_r = 0.6\, \lambda \sqrt{f_c'}$$

λ equals 1 for normal weight concrete.

$$M_{cr} = 0.6 * \sqrt{35}\, \frac{200 * 550^3}{12 * \frac{550}{2}} = 35.8\, kN.m$$

Mr = 264.68 kN.m > 1.5*35.8 = 53.7 kN.m (minimum reinforcement satisfied)

Development length

$\sum M = 0$ at distance *x* from middle support:

$1.288P*x - 1.08P = 0, \rightarrow x = 0.8385\ m$

Point of zero moment = 838.5 mm from middle support

l_d = 838.5 + 40 x 15.9 = 1475 mm or

$l_d = 1.15\, \frac{k_1 k_2 k_3 k_4 k_5}{d_{cs}}\, \frac{f_f}{\sqrt{f_c'}} A_b$ (Clause 9.3.2)

For the longitudinal bars in that section, f_{frpu} = 747.4 MPa and $\sqrt{f_c'}$ should not be greater than 5 MPa.

$l_d = 1.15\ \frac{1*1*0.8*1*1}{40} * \frac{747.4}{\sqrt{35}} * 198 = 680.7\ mm$

Negative reinforcement cut-off length = 1475 mm (measured form interior support), take = **1875** mm to avoid bond slippage failure.

B.1.4. Design of beam GH-0.8-0.0-3*d* (Series II)

Design for shear

The shear resistance of sections without shear reinforcement having depth greater than 300 mm is calculated according to Clauses 8.4.4.5 and 8.4.4.7.

$V_c = 0.05\lambda\phi_c k_s k_m k_r (f_c')^{\frac{1}{3}} b_w d_v$ where $k_m = \sqrt{\frac{V_f d}{M_f}} \leq 1.0$, $k_r = 1 + (\mathrm{E}_f\ \rho_{Fw})^{\frac{1}{3}}$ and $k_s = \frac{750}{450 + d} \leq 1.0$

Provided that $0.11\lambda\ \phi_c\ \sqrt{f_c'}\ b_w\ d_v\ \leq\ V_c\ \leq 0.22\ \lambda\ \phi_c\ \sqrt{f_c'}\ b_w\ d_v$

$0.11\ \sqrt{f_c'}\ b_w\ d$ = $0.11\sqrt{60}$*200*750 = 127.8 kN

$0.22\ \sqrt{f_c'}\ b_w\ d$ = $0.22\sqrt{60}$*200*750 = 255.6 kN

Critical section for shear is at distance d_v from the face of the middle support at which the values of shear and bending moment are 1.294*P* kN and 0.5735*P* kN.m, respectively.

Using 4 No. 19 GFRP bars as longitudinal reinforcement distributed over two layers, the diameter of the bar including the sand coating = 22.5 mm.

d = depth to the centroid of the two layers = 757.5 mm.

ρ_f = 4 x 285 / (200 x 750) = 0.0076

k_r = 1+ (65000 x 0.0076)$^{1/3}$ = 8.91 ,

$k_m = \sqrt{1.294P \text{ x } 0.75/0.5735\ P}$ = 1.3 ⟶ k_m = 1.0

k_s = 750/(450+750) = 0.625

V_c = 0.05 x 1 x 1 x 0.625 x 1.0 x 8.91 x (60)$^{1/3}$ x 200 x 675 = 147156.2 N

V_c = 147.2 kN., governs the shear strength.

The value of load, *P*, corresponding to the calculated shear strength, is 114.2 kN.

Design for flexure

α_1 = 0.85 – 0.0015 x 70 = 0.745

β_1 = 0.97 – 0.0025 x 70 = 0.795

For doubly reinforced section,

C = T_1+ T_2 $\longrightarrow$ $\alpha_1 \beta_1 f_c' b$ c = $f_{frp1} A_{f1}$+ $f_{frp2} A_{f2}$

$$0.745*0.795*70*200*c = 2\times285\times65300\times0.0035\left(\frac{780-c}{c}\right)+2\times285\times65300\times0.0035\left(\frac{720-c}{c}\right)$$

c = 138.6 mm

a = c β_1 = 138.6*0.795 = 110.19 mm

Check concrete strain:

Concrete stain at extreme fibres in compression shall be assumed to reach 0.0035 provided that the ratio c/d satisfies Clause 8.4.1.4 as follows:

$$c/d \geq \frac{7}{7+2000\,\epsilon_{Fu}}$$

$$c/d = \frac{138.6}{750} = 0.185 > \frac{7}{7+2000*0.021} = 0.143$$

M_{ult} = T_1* (780- *a/2*) + T_2* (720- *a/2*)

= **602867.41*724.9+546471.95*664.9= 800.37** kN.m

Check if minimum reinforcement is provided:

The minimum reinforcement provided in the section should satisfy Clause 8.4.2.1.

$$M_r > 1.5\,M_{cr}$$

The cracking moment, M_{cr}, should be calculate according to Clause 8.3.2.6 as follows:

$$M_{cr} = f_r \frac{I_g}{y_t}$$

Concrete modulus of rupture could be taken as stated in Clause 8.5.4.

$$f_r = 0.6\,\lambda\sqrt{f_c'}$$

λ equals 1 for normal weight concrete.

$$M_{cr} = 0.6 * \sqrt{70}\,\frac{200 * 850^3}{12 * \frac{850}{2}} = 120.89\ kN.m$$

Mr = 800.37 kN.m > 1.5*120.89 = 181.33 kN.m (minimum reinforcement satisfied)

Development length

∑M = 0 at distance *x* from middle support:

1.294*P***x* – 1.544*P* = 0, $\rightarrow x = 0.838\ m$

Point of zero moment = 838 mm from middle support

l_d = 838.5 + 40 x 19 = 1598 mm or

$l_d = 1.15\,\frac{k_1 k_2 k_3 k_4 k_5}{d_{cs}}\,\frac{f_f}{\sqrt{f_c'}}A_b$ (Clause 9.3.2)

The tensile stress in the outer bars is f_{frpu} = 1057.66 MPa and $\sqrt{f_c'}$ should not be greater than 5 MPa.

$l_d = 1.15\,\frac{1*1*0.8*1*1}{40} * \frac{1057.66}{\sqrt{35}} * 285 = 1386.59\ mm$

Negative reinforcement cut-off length = 1598 mm (measured form interior support), take = **2625** mm to avoid bond slippage failure.

B.2. Design Criteria for Beams with Transverse Reinforcement

This series consists of nine beams designed to fail in shear. The variables in this group of beams are the concrete strength, longitudinal and transverse reinforcement ratio and type.

- b = 200 mm
- Target concrete strengths were $f_c^{'}$ = 35 MPa and $f_c^{'}$ = 70 MPa. The concrete strain before crushing was taken as 0.0035.
- Properties of reinforcing bars and stirrups

  The properties of steel and GFRP bars and stirrups are presented in Table B.1

Table B.1: Properties of the reinforcing bars and stirrups

Bar type	Diameter (mm)	Area (mm2)	Tensile strength (MPa)	Modulus of Elasticity (GPa)	Ultimate Strain (%)
GFRP					
Pultruded	15.9	198	1442	67	2.1
Stirrups*	6.3	32	1383	53	2.6
	9.5	72	1195	45	2.7
	12.7	127	1328	53	2.5
Steel					
Bar	16.0	200	fy = 430	200	εy = 0.23
Stirrup	4.8	18.1	fy = 460	165	εy = 0.28

*Provided properties are for the straight portion

All test beams were designed according the CSA standards (CSA/A23.3-04 for steel- RC beams and CSA/S806-12 for GFRP-RC beams). In designing the test beams, all material safety factors were taken equal to unity.

B.2.1. Design of beam GN-0.8-0.48-*d* (Series III)

Design for shear

According to Clause 8.4.4.4, the factored shear resistance of members with longitudinal and transverse FRP reinforcement is calculated as:

$V_r = V_c + V_{sF}$

Such that the shear resistance V_r shall not exceed

$$V_{r,\max} = 0.2\phi_c f_c' b_w d_v + 0.5V_p + \left[(M_{dc} V_f) / M_f \right]$$

- **Concrete contribution (*Vc*)**

This beam has the same longitudinal reinforcement ratio as beam GN-0.8-0.0-*d*; therefore, the concrete contribution to the shear strength (V_c) for this beams is of the same magnitude and is equal to V_c = **58.56 kN**

The provided shear reinforcement is the minimum and it was calculated as follows:

According to Clause 8.4.6.1., the maximum spacing between stirrups shall not exceed $0.6d_v \cot\theta$ or 400 mm.

The angle θ of the diagonal compressive stress shall be calculated according to Clause 8.4.4.9 ($\theta = 30 + 7000\varepsilon_l$). However, it will be assumed to be around 42^o based on the findings of Ahmed et al. (2010).

$\rightarrow 0.6d_v \cot\theta$ = 0.6x225x1.11= 150 mm

According to Clause 8.4.5.2.

f_{fu}= 0.005* E_f =0.005* 45000 = 225 MPa

$Av = 0.07\sqrt{f_c'} \frac{b_w\ s}{0.4 f_{FU}}$ = $Av = 0.07\sqrt{35} \frac{200*150}{0.4*.005*45000}$ =138.8 mm^2

Use No.10 GFRP @ 150, *A*= 72 mm^2, according to Clause 8.4.4.8

- **Shear reinforcement contribution (V_{sf})**

The contribution of the transverse reinforcement shall be calculated, according to Clause 8.4.4.9, as

$$V_{sF} = \frac{0.4\phi_F A_{Fv} f_{Fu} d_v}{S} \cot\theta$$

$$V_{sF} = \frac{0.4 \times 1.0 \times 144 \times 225 \times 225}{150} 1.11 = 21.58 \text{ kN}$$

$V_r = 58.56 + 21.58 = 80.14\ kN < Vr, \max = 0.2 * 35 * 200 * 225 * 10^{-3} = 315\ kN$

The value of load, *P*, corresponding to the calculated shear strength, is 64.9 kN.

Design for flexure

This beam (GN-0.8-0.48-*d*) has the same cross-section dimensions and longitudinal reinforcement ratio as beam GN-0.8-0.0-*d*.; therefore, it has the same flexural capacity.

***M*$_r$ = 66.14 kN.m,** the corresponding load *P* =100 kN which is higher than that corresponding to shear failure. So shear failure is expected to occur before flexural failure

B.2.2. Design of beam β1.2-0.21-*d*, GN-1.2-0.48-*d* and GN-1.2-0.85-*d* (Series III)

Design for shear

According to Clause 8.4.4.4, the factored shear resistance of members with longitudinal and transverse FRP reinforcement is calculated as:

$V_r = V_c + V_{sF}$

Such that the shear resistance V_r shall not exceed

$$V_{r,\max} = 0.2\phi_c f_c' b_w d_v + 0.5 V_p + \left[(M_{dc} V_f) / M_f \right]$$

- **Concrete contribution (V_c)**

Those beams have the same longitudinal reinforcement ratio as beam GN-1.2-0.0-*d*; therefore, the concrete contribution to the shear strength (V_c) for this beams is of the same magnitude and is equal to V_c = 58.56 kN

- **Shear reinforcement contribution (V_{sf})**

1) For beam GN-1.2-0.48-*d* (Series III)

In beam GN-1.2-0.48-*d*, the shear reinforcement ratio is the minimum; therefore, the transverse reinforcement contribution to the shear strength is the same as that of beam GN-0.8-0.48-*d*.

$$V_{sF} = \frac{0.4\phi_F A_{Fv} f_{Fu} d_v}{S} \cot\theta$$

$$V_{sF} = \frac{0.4 \times 1.0 \times 144 \times 225 \times 225}{150} 1.11 = 21.58 \text{ kN}$$

$V_r = 58.56 + 21.58 = 80.14\ kN < Vr, \max = 0.2 * 35 * 200 * 225 * 10^{-3} = 315\ kN$

The value of load, *P*, corresponding to the calculated shear strength, is 64.9 kN.

2) For beam GN-1.2-0.21-*d* (Series III)

In this beam, the used stirrup is No.6 and the spacing is 150 mm

$$V_{sF} = \frac{0.4\phi_F A_{Fv} f_{Fu} d_v}{S} \cot\theta$$

$$V_{sF} = \frac{0.4 \times 1.0 \times 62 \times 265 \times 225}{150} 1.11 = 10.94 \text{ kN}$$

$V_r = 58.56 + 10.94 = 69.5\ kN < Vr, \max = 0.2 * 35 * 200 * 225 * 10^{-3} = 315\ kN$

The value of load, *P*, corresponding to the calculated shear strength, is 56.3 kN.

3) For beam GN-1.2-0.85-d

In this beam, the used stirrup is No.13 and the spacing is 150 mm

$$V_{sF} = \frac{0.4\phi_F A_{Fv} f_{Fu} d_v}{S} \cot\theta$$

$$V_{sF} = \frac{0.4 \times 1.0 \times 254 \times 265 \times 225}{150} 1.11 = 44.83 \text{ kN}$$

$V_r = 58.56 + 44.83 = 103.4\ kN < Vr, \max = 0.2 * 35 * 200 * 225 * 10^{-3} = 315\ kN$

The value of load, *P*, corresponding to the calculated shear strength, is 83.7 kN.

Design for flexure

Those beams under consideration have the same cross-section dimensions and longitudinal reinforcement ratio as beam GN-1.2-0.0-*d*; therefore, they have the same flexural capacity.

***Mr* = 76.39 kN.m,** the corresponding load *P* =115.74 kN which is higher than that corresponding to shear failure. So shear failure is expected to occur before flexural failure

B.2.3. Design of beam GH-0.8-0.63-*d* (Series III)

Design for shear

According to Clause 8.4.4.4, the factored shear resistance of members with longitudinal and transverse FRP reinforcement is calculated as:

$V_r = V_c + V_{sF}$

Such that the shear resistance V_r shall not exceed

$$V_{r,\max} = 0.2\phi_c f_c' b_w d_v + 0.5 V_p + \left[(M_{dc} V_f) / M_f \right]$$

- **Concrete contribution (V_c)**

This beam has the same longitudinal reinforcement ratio as beam GH-0.8-0.0-*d*; therefore, the concrete contribution to the shear strength (V_c) for this beams is of the same magnitude and is equal to V_c = **75.25 kN**

The provided shear reinforcement is the minimum and it was calculated as follows:

According to Clause 8.4.6.1., the maximum spacing between stirrups shall not exceed $0.6d_v \cot\theta$ or 400 mm.

The angle θ of the diagonal compressive stress shall be calculated according to Clause 8.4.4.9 ($\theta = 30 + 7000\varepsilon_l$). However, it will be assumed to be around 42° based on the findings of Ahmed et al. (2010).

$\rightarrow 0.6d_v \cot\theta$ = 0.6x225x1.11= 150 mm

According to Clause 8.4.5.2,

f_{fu}= 0.005* E_f=0.005* 45000 = 225 *MPa*

$Av = 0.07\sqrt{f_c'}\ \frac{b_w\ s}{0.4 f_{FU}}$,

Using stirrup No. 10, the spacing between stirrups is

$144 = 0.07\sqrt{70}\ \frac{200 * S}{0.4 * .005 * 44750} \longrightarrow$ S = 115 mm

Use No.10 GFRP @ 115, according to Clause 8.4.4.8

- **Shear reinforcement contribution (V_{sf})**

The contribution of the transverse reinforcement shall be calculated, according to Clause 8.4.4.9, as

$$V_{sF} = \frac{0.4\phi_F A_{Fv} f_{Fu} d_v}{S}\cot\theta$$

$$V_{sF} = \frac{0.4\times 1.0\times 144\times 225\times 225}{115}1.11 = 28.15 \text{ kN}$$

$V_r = 75.25 + 28.15 = 103.4\ kN < Vr, \max = 0.2 * 60 * 200 * 225 * 10^{-3} = 540\ kN$

The value of load, *P*, corresponding to the calculated shear strength, is 83.7 kN.

Design for flexure

This beam (GH-0.8-0.63-*d*) has the same cross-section dimensions and longitudinal reinforcement ratio as beam GH-0.8-0.0-*d.*; therefore, it has the same flexural capacity.

***M_r* = 90.42 kN.m,** the corresponding load P =137 kN which is higher than that corresponding to shear failure. So shear failure is expected to occur before flexural failure

B.2.4. Design of beams SN-1.2-0.0-*d*, SN-1.2-0.12-*d* according to CSA/A23.3-04.

Design for flexure

Design of section at middle support:

α_1 = 0.85 – 0.0015 x 35 = 0.798

β_1 = 0.97 – 0.0025 x 35 = 0.883

The tension reinforcement can be assumed to reach yield if $c/d \leq \frac{700}{700+f_y}$, (Clause 10.5.2).

$\frac{c_b}{d} = \frac{700}{700+f_y} = 0.62$, using bars No.15M for which $f_y = 430\ MPa$.

d = (300- 40-16/2) = 250 mm

c_b = 0.62 x 250 = 154.0 mm

Using 3 No.15M, A_s = 3 x 200 = 600 mm^2

A minimum reinforcement should be provided in beams calculated as in Clause 10.5.1.2 as follows: $A_{s,min} = \frac{0.2\sqrt{f_c'}}{f_y} b_t h = \frac{0.2\sqrt{35}}{400}\ 200\ x\ 300$ = 177.48 mm^2 < 600 mm^2

Section at middle support:

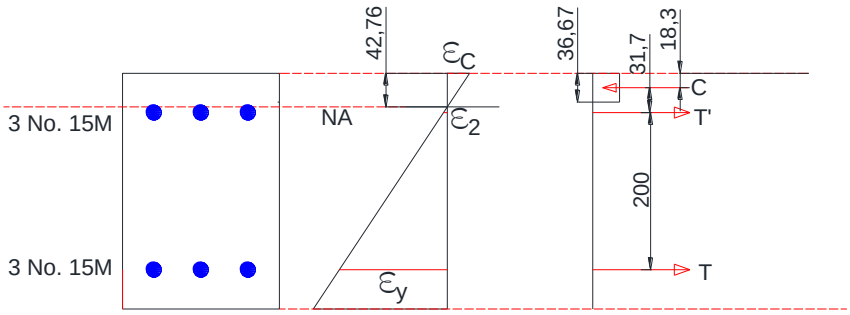

From the strain compatibility:

$$\frac{\varepsilon_2}{c-50}=\frac{\varepsilon_y}{250-c} \;\Rightarrow\; \varepsilon_2=\frac{\varepsilon_y(c-50)}{(250-c)}$$

From equilibrium of internal forces:

$$\alpha_1 f_c' a\, b + A_{s2} * E_s * \varepsilon_2 = A_s f_y$$

$$0.798 * 35 * a * 200 + 600 * 200 * \varepsilon_2 = 600 * 430$$

$$0.798 * 35 * 0.883\, c * 200 + 600 * 200 * \frac{\varepsilon_y(c-50)}{(250-c)} = 600 * 430$$

$$c = 42.76\,\text{mm}$$

Allowable moment redistribution (Clause 9.2.4) = (30-50 *c/d*) % = 21.45 % or 20%

$M_{u\text{-}ve}$ = 600*430*200+0.798*0.883*35*42.76*200*31.67

= **58.3** kN.m

Sagging moment section:

Use 3 No.15M, A_s = 4*200 = 800 mm^2,

$$a = \beta_1 c = \frac{A_s f_y}{\alpha_1 f_c' b}$$

a = 600*430/(0.798*35*200) = 46.19 mm

$M_{u+ve} = A_s f_y (d - a/2)$ = 600*430*(250-46.19/2) = **58.54** kN.m

A.1.1. Design for shear of beam SN-1.2-0.0-*d*

According to Clause 11.3.4 and Clause 11.3.5, V_c can be calculated as follows:

$V_c = \lambda \beta \sqrt{f_c'}\, b_w\, d_v < 0.25\, f_c'\, b_w\, d_v$

d_v = the greater of 0.9 d or 0.72h

= 0.9*250 = 225 mm or = 0.72*300 = 216 mm

d_v = 225 mm

$0.25\, f_c'\, b_w\, d_v$ = 0.25*35*200*225 = 393.8 kN

$V_c = \lambda \beta \sqrt{f_c'}\, b_w\, d_v$ = 1*0.18*$\sqrt{35}$*200*226.8 = 44.37 kN

The value of load, *P*, corresponding to the calculated shear strength, is 35.93 kN which is less than the load *P* corresponding to the flexural capacity.

A.1.2. Design for shear of beam SN-1.2-1.0-*d*

$V_r = V_c + V_s$, and V_r shall not be taken more than $0.25\, \phi_c\, f_c'\, b_w\, d_v$

$V_r = V_c + V_s < 0.25\, f_c'\, b_w\, d_v$

d_v = the greater of 0.9*d* or 0.72*h*

= 0.9*250 = 225 mm or = 0.72*300 = 216 mm

d_v = 225 mm

$0.25\, f_c'\, b_w\, d_v$ = 0.25*35*200*225 = 393.8 kN

According to CSA (2004) Clauses 11.3.8.1 and 11.3.8.3, the maximum transverse spacing should not exceed 600 mm or $0.7d_v$. If the applied shear force exceeds $0.125\, \phi_c\, \lambda\, f_c'\, b_w\, d_v$, the maximum spacing should not exceed 300 mm or $0.35d_v$.

$0.125\, \phi_c\, \lambda\, f_c'\, b_w\, d_v$ = 0.125*1*35*200*226.8 =196.9 kN

Max spacing of stirrups = 0.7d_v or 600mm = 0.7*225 = 157.5 mm

According to Clause 11.2.8.2, a minimum area of shear reinforcement should be provided if the applied shear force exceeds concrete shear resistance or overall section depth is greater than 750 mm. The minimum shear reinforcement is calculated as follows:

$$A_v = 0.06\sqrt{f_c'}\,\frac{b_w\,s}{f_y}$$

$A_{vmin} = 0.06\sqrt{f_c'}\,\frac{b_w\,s}{f_y}$ = 0.06*$\sqrt{35}$*200*150/450 = 24 mm^2

In lieu of more accurate calculations, and provided that used yield strength of longitudinal steel does not exceed 400 MPa and concrete compressive strength is less than 60 MPa, θ can be taken as 35°. If the section contains the minimum transverse, the factor β can be taken as 0.18, (Clause 11.3.6.3).

Clause 11.3.6.3, $\theta = 35°,\ \beta = 0.18$

According to Clauses 11.3.4 and 11.3.5, V_c and V_s can be calculated as follows:

$$V_c = \phi_c\,\lambda\,\beta\,\sqrt{f_c'}\,b_w\,d_v \quad and \quad V_s = \frac{\phi_c\,A_v\,f_y\,d_v\,\cot\theta}{s}$$

$V_c = \lambda\,\beta\,\sqrt{f_c'}\,b_w\,d_v$ = 1*0.18*$\sqrt{35}$*200*226.8 = 44.3 7kN

$V_s = \frac{A_v f_y d_v \cot\theta}{s}$, using Ø 4.9 with 150 mm spacing

V_s = 2*18.1*450*226.8*1.43/150 = 35.22 kN

V_r = 44.3 + 35.22 = **79.52** kN < 196.7 kN

The value of load, *P*, corresponding to the calculated shear strength, is 64.4 kN which is less than the load *P* corresponding to the flexural capacity.

End of the thesis